



Insights into membrane binding of PROPPINs  
and  
Reconstitution of mammalian autophagic  
conjugation systems

Dissertation  
for the award of the degree  
"Doctor rerum naturalium" (Dr. rer. nat.)  
of the Georg-August-Universität Göttingen

in the GGNB program of Biomolecules: Structure - Function - Dynamics  
of the Georg-August University School of Science (GAUSS)

submitted by  
**Ricarda Angela Busse**

from  
**Leinefelde, now Leinefelde-Worbis, Germany**

Göttingen, 2012



## **Members of the Thesis Committee:**

**Dr. Karin Kühnel (1<sup>st</sup> Reviewer)**

Department of Neurobiology, Max Planck Institute for Biophysical Chemistry

**Prof. Dr. Michael Thumm (2<sup>nd</sup> Reviewer)**

Department of Biochemistry II, University of Göttingen

**Prof. Dr. Nils Brose**

Department of Molecular Neurobiology, Max Planck Institute for Experimental Medicine

**Date of the oral examination:** January 08<sup>th</sup>, 2013



# Declaration of Authorship

## **Declaration of Authorship**

Hereby, I confirm that I have created this work *Insights into membrane binding of PROPPINs and Reconstitution of mammalian autophagic conjugation systems* entirely on my own and that I have only used the sources and materials cited.

Göttingen, November 14<sup>th</sup>, 2012

Ricarda Angela Busse



**For Patrick**





# Acknowledgements

First and foremost I would like to thank my advisor Dr. Karin Kühnel for giving me the opportunity to do the research in her lab. Without her supervision and training this thesis would not have been possible. Her door was always open for questions and discussions. Moreover, I would like to thank Prof. Dr. Reinhard Jahn for offering the generous financial support during my thesis and for the regular discussions we had about my work during the department seminars. Next, I would like to express my gratitude to my thesis committee formed by Prof. Dr. Nils Brose and Prof. Dr. Michael Thumm.

A special thanks goes to my close collaborator in Thumm lab, Dr. Roswitha Krick. In addition, I would like to thank Prof. Dr. Reinhard Lührmann for access to his insect cell culture laboratory and crystallization facility. In terms of insect cell culture expertise, my gratitude goes to Karine dos Santos and her excellent training. Moreover, I would like to thank Dr. Vladimir Pena and his group, especially Dr. Jana Schmitzova for access and guidance to their infrastructure such as the Thermofluor experiment. Furthermore, I would like to mention the help of Monika Raabe and He-Hsuan Hsiao from the department of Prof. Dr. Henning Urlaub for the assistance with the mass spectrometry analysis for which I am grateful.

I want to thank my colleagues and friends Andreea, Amanda and Caroline. They were all helpful with nice discussions about science and beyond. Especially, I would like to mention Andreea's help during the last period of my thesis that made it possible to finalize all the repetitive experiments in a very short time. Besides having a great colleague, I also won a wonderful friend in you.

Next I would like to express my appreciation of the Jahn department in which I have worked for three and a half years. It was a nice time both from the exciting scientific discussions and friendly atmosphere. First and foremost, I would like to thank Dr. Gottfried Mieskes for his assistance in everything ranging from machine maintenance to IT support. Heike, who has probably the most important but least appreciated tasks in the lab. Ursel and Matias for their assistance in the liposome related experiments:

DLS, MALLS, LUVs and phosphate determination. In addition, I am thankful to Esra and Angel for their helpful discussions related to ITC measurements. From Janina I had helpful insights into Cova PIP plates and the pH switch data analysis. I also want to say thank you to Michaela and Dagmar for their technical support.

I want to thank all the people in the Jahn department that touched my life over the period of my PhD thesis and for becoming so good friends: Beyenech, Julia, Hale, Sina, Dieter, Sabrina, Saskia, Momchil, Elisa, Zohreh, John, Yongsoo, Seichii, Dominika, Dragomir, Partho, Brigitte, Peter and Barbara.

Very important to me is my family and their love. First of course my husband Patrick, who is at my side since the time before I started to study. He supported me during my Diploma project and now we also managed the PhD thesis. Without him at my side I would not have been strong enough to succeed in all my tasks and plans. In addition, I thank my parents and parents-in-law, who provided all their possible support. I want to express my gratitude to my sister, my brothers and their partners for completing the supportive atmosphere of a family.

Finally, I want to say that I am proud of being a member of GGNB. This institution provides so many resources for a young scientist, from which I was able to take advantage and helped me in developing as a scientist.

There are many more people I have to thank!





# Abstract

Autophagy is a degradation pathway conserved in eukaryotes. Upon induction of autophagy a double layered membrane is formed *de novo* and engulfs the cytosolic content. After fusion of the membrane, an autophagosome vesicle is formed, which then fuses with the vacuole (or lysosome) where its content is degraded. PROPPINs,  $\beta$ -propeller proteins that bind polyphosphoinositides, play a role in autophagy and phosphoinositide binding depends on a conserved FRRG motif. The three yeast PROPPINs Atg18, Atg21 and Hsv2 are involved in different subtypes of autophagy.

In this study, I purified different Atg18, Atg21 and Hsv2 PROPPIN homologs and showed that they bind specifically to PI3P and PI(3,5)P<sub>2</sub> using protein-liposome co-floitation assays. Recently, we published the first structure of the PROPPIN Hsv2. Based on our structure I performed mutagenesis studies to probe phosphoinositide binding of Hsv2. I analyzed phosphoinositide binding of the alanine mutants with liposome floitation assays. I identified conserved residues essential for binding right and left of the FRRG motif, indicating the presence of two phosphoinositide binding sites, which was an unexpected finding. Using ITC measurements I then confirmed the binding stoichiometry of two phosphoinositides to one Hsv2 molecule and determined the binding affinities of PROPPINs to both PI3P and PI(3,5)P<sub>2</sub> incorporated in small unilamellar vesicles. Phosphoinositide binding of *S. cerevisiae* Hsv2 is pH dependent. Acidic environment increases and basic environment decreases the affinity. In addition, I showed the involvement of loop 6CD in membrane binding. Mutagenesis analysis of loop 6CD residues revealed that membrane insertion is dependent on both ionic and hydrophobic interactions.

Two ubiquitin-like conjugation systems modifying Atg8 (in mammals MAP1LC3) and Atg12 are essential for autophagy. Homologs of the canonical ubiquitin conjugation system, E1- and E2-like enzymes, are involved in the conjugation of Atg8 and Atg12 to their specific targets phosphatidylethanolamine and Atg5, respectively.

A *in vivo* reconstitution system for the two human ubiquitin-like conjugation systems Atg12 and MAP1LC3 was established using the MultiBac baculovirus expression system in insect cells. This allowed full length expression of the involved proteins and purification of the Atg5-Atg12 conjugate and lipidated MAP1LC3 in small yields.

# Contents

<b>1</b>	<b>General introduction</b>	<b>1</b>
1.1	Definition of autophagy . . . . .	1
1.2	Types of autophagy . . . . .	1
1.3	Molecular players in autophagy . . . . .	3
1.4	Structural characterization of autophagy proteins . . . . .	3
1.5	Involvement of autophagy in disease . . . . .	4
<b>2</b>	<b>Materials &amp; Methods</b>	<b>7</b>
2.1	Materials . . . . .	7
2.1.1	Chemicals . . . . .	7
2.1.2	Enzymes . . . . .	8
2.1.3	Lipids . . . . .	8
2.1.4	Kits . . . . .	9
2.1.5	Columns for chromatography . . . . .	10
2.1.6	Antibodies . . . . .	11
2.1.7	Buffers and media . . . . .	11
2.1.8	Antibiotics . . . . .	13
2.1.9	Insect cell lines and bacterial strains . . . . .	13
2.1.10	DNA constructs . . . . .	14
2.1.11	Oligonucleotides . . . . .	15
2.2	Methods . . . . .	20
2.2.1	Molecular cloning . . . . .	20
2.2.2	Methods for insect cell culture . . . . .	22
2.2.2.1	Insect cell culture . . . . .	22
2.2.2.2	Bacmid extraction from <i>E. coli</i> DH10 . . . . .	22
2.2.2.3	Transfection of insect cells . . . . .	23
2.2.2.4	Pull down of infected insect cells . . . . .	23
2.2.2.5	Measuring YFP in infected insect cells . . . . .	24

2.2.3	Purification protocols of protein complexes from insect cells . . . .	24
2.2.3.1	MAP1LC3 . . . . .	24
2.2.3.2	Atg5-Atg12 . . . . .	25
2.2.3.3	Increase of solubility of Atg5-Atg12 using a detergent screen . . . . .	26
2.2.4	Purification protocols for PROPPINs . . . . .	27
2.2.4.1	Batch purification for test expression . . . . .	27
2.2.4.2	Purification protocol for ScAtg18 . . . . .	27
2.2.4.3	Purification of PaAtg18, DmAtg18, CeAtg18, KlAtg21 and PaAtg21 . . . . .	28
2.2.4.4	Purification protocol for SpHsv2 . . . . .	30
2.2.4.5	Purification protocol for ScHsv2 and mutants . . . . .	32
2.2.4.6	GST SpinTrap purification of ScHsv2 and mutants . . . .	33
2.2.4.7	Purification protocol for KlHsv2 and mutants . . . . .	34
2.2.5	Purification protocol for PaAtg8 and KlAtg8 . . . . .	35
2.2.6	Biochemical methods . . . . .	36
2.2.6.1	SDS-PAGE and Western Blotting . . . . .	36
2.2.6.2	Protein stability assay . . . . .	37
2.2.6.3	Circular dichroism spectroscopy . . . . .	38
2.2.6.4	Limited proteolysis . . . . .	39
2.2.6.5	N-terminal protein sequencing . . . . .	39
2.2.6.6	Protein-lipid co-floitation assay and liposome preparation	40
2.2.6.7	Isothermal titration calorimetry . . . . .	42
2.2.6.8	Protein-lipid overlay assay (PIP strip, PIP array, membrane lipid strip) . . . . .	43
2.2.6.9	Cova PIP specificity plate . . . . .	43
2.2.6.10	Analytical gel filtration . . . . .	44
2.2.7	Crystallization and structure determination . . . . .	46
2.2.7.1	Crystallization screen setup . . . . .	46
2.2.7.2	Flash cooling of crystals . . . . .	47
<b>3</b>	<b>Project I: Reconstitution of mammalian Atg12 and MAP1LC3 conjugation pathways</b>	<b>49</b>
3.1	Introduction . . . . .	49
3.1.1	Ubiquitin-like conjugation systems in autophagy . . . . .	49
3.1.2	Structure and function of Atg12 . . . . .	51



3.1.3	Atg8 and its human homologs . . . . .	51
3.1.4	Aims . . . . .	52
3.2	Results . . . . .	53
3.2.1	Setting up the insect cell system for co-expression . . . . .	53
3.2.2	Expression and purification of modified human autophagy proteins	56
3.2.2.1	The Atg12-Atg5 conjugate . . . . .	56
3.2.2.2	Atg16 expression and purification from insect cells . . . . .	59
3.2.2.3	MAP1LC3II expression in insect cells . . . . .	61
3.2.3	Analyses of conjugated protein complexes . . . . .	63
3.2.4	Influence of Atg12-Atg5-Atg16 on MAP1LC3 lipidation . . . . .	64
3.3	Discussion . . . . .	65
3.4	Outlook . . . . .	67
<b>4</b>	<b>Project II: Insights into membrane binding of PROPPINs</b>	<b>69</b>
4.1	Introduction . . . . .	69
4.1.1	The autophagosomal membrane . . . . .	69
4.1.2	Phosphoinositide effectors . . . . .	70
4.1.3	Phosphoinositide effectors involved in autophagy . . . . .	72
4.1.4	PROPPINs and their role in autophagy . . . . .	72
4.1.5	WD40 repeat containing proteins in autophagy . . . . .	73
4.1.6	Structure of Hsv2 . . . . .	74
4.1.7	Aims . . . . .	76
4.2	Results . . . . .	76
4.2.1	Expression and purification of yeast PROPPINs . . . . .	76
4.2.1.1	Expression and purification of yeast PROPPINs in insect cells . . . . .	76
4.2.1.2	Bacterial expression and purification of yeast PROPPINs	81
4.2.1.3	Characterization of purified PROPPINs . . . . .	88
4.2.1.4	Crystallization of PROPPINs . . . . .	95
4.2.2	Functional analysis of PROPPINs . . . . .	99
4.2.2.1	Optimization of methods to analyze protein-lipid interaction . . . . .	99
4.2.2.2	PROPPINs binding specificity to phosphoinositides . . . . .	105
4.2.2.3	Characterization of Hsv2 membrane binding sites . . . . .	107
4.2.2.4	Determination of binding affinity and stoichiometry . . . . .	109
4.2.2.5	pH dependency of phosphoinositide binding for Hsv2 . . . . .	112

4.2.2.6	Role of loop 6CD for membrane binding . . . . .	116
4.2.2.7	Analysis of stability of Hsv2 mutants . . . . .	119
4.2.3	Co-expression and interaction studies of PROPPIN homologs with Atg8 . . . . .	120
4.2.3.1	Cloning, expression and purification using the ACEMBL system . . . . .	120
4.2.3.2	Purification of <i>K. lactis</i> and <i>P. angusta</i> Atg8 . . . . .	121
4.2.3.3	Biochemical analysis of interactions . . . . .	123
4.2.3.4	Co-expression of ScAtg21 and ScAtg8 in insect cells . . . . .	125
4.2.3.5	Crystal soaking for KIHsv2 with Atg8 peptide . . . . .	127
4.3	Discussion . . . . .	129
4.4	Outlook . . . . .	135
<b>5</b>	<b>Appendix</b>	<b>137</b>
5.1	Structures of autophagy-related proteins in the PDB . . . . .	137
5.2	Supplementary figures . . . . .	139
5.3	Sequence of synthetic genes . . . . .	152
	<b>References</b>	<b>165</b>
	<b>Curriculum Vitae</b>	<b>187</b>

# List of Figures

1.1	Scheme for autophagosome formation . . . . .	2
2.1	Standard curve for analytical gel filtration . . . . .	45
3.1	Ubiquitin-like conjugation systems involved in autophagy . . . . .	50
3.2	Structure of Atg12 from <i>A. thaliana</i> . . . . .	51
3.3	Structure of LC3 from <i>R. norvegicus</i> . . . . .	52
3.4	Ubiquitin, LC3 and Atg12 share a ubiquitin-fold region . . . . .	53
3.5	Cloning strategy for expression of complexes in insect cells . . . . .	54
3.6	Cloning strategy for expression of complexes in insect cells . . . . .	56
3.7	Expression of Atg5 and Atg12 in insect cells . . . . .	57
3.8	Purification of Atg5-Atg12 from insect cells . . . . .	58
3.9	Detergent test to increase Atg5-Atg12 solubility . . . . .	59
3.10	Expression of Atg16 in insect cells . . . . .	60
3.11	Expression of MAP1LC3 in insect cells . . . . .	62
3.12	Purification of MAP1LC3 from insect cells . . . . .	63
3.13	Thermofluor analysis of MAP1LC3 from <i>E. coli</i> BL21 (DE) cells . . .	64
3.14	Western blot analysis of the Atg5-Atg12 complex . . . . .	65
3.15	<i>In vitro</i> lipidation of LC3 . . . . .	66
4.1	Overview of phosphoinositide binding motifs and their structures . . .	71
4.2	Structure of the PROPPIN KIHsv2 . . . . .	75
4.3	Approach for the characterization of PROPPINs . . . . .	77
4.4	Expression of ScAtg18 and ScAtg21 from insect cells . . . . .	78
4.5	Purification of ScAtg18 from High5 insect cells . . . . .	80
4.6	Purification of PaAtg18 from <i>E. coli</i> BL21(DE3) cells . . . . .	83
4.7	Purification of KlAtg21 from <i>E. coli</i> BL21(DE3) cells . . . . .	84
4.8	Purification of SpHsv2 from <i>E. coli</i> BL21(DE3) cells . . . . .	85
4.9	Purification of ScHsv2 from <i>E. coli</i> BL21(DE3) cells . . . . .	86

4.10	Purification of KlHsv2 from <i>E. coli</i> BL21(DE3) cells . . . . .	87
4.11	Thermofluor analysis of PaAtg18 . . . . .	89
4.12	Thermofluor analysis of KlAtg21 . . . . .	90
4.13	Thermofluor analysis of PaAtg21 . . . . .	91
4.14	Limited proteolysis of PaAtg18 . . . . .	93
4.15	Limited proteolysis of KlAtg21 . . . . .	94
4.16	Analytical gel filtration analysis of SpHsv2 . . . . .	95
4.17	Spherulites resulting from PROPPIN crystallization . . . . .	97
4.18	Optimization of PIP strips and Cova PIP plate . . . . .	100
4.19	Optimization of lipid composition for flotation assay . . . . .	102
4.20	Optimization of ITC measurements . . . . .	104
4.21	Selective binding of PROPPINs to phosphoinositides . . . . .	106
4.22	Characterization of ScHsv2 membrane binding site I and II . . . . .	108
4.23	ITC measurements of PROPPINs with liposomes containing PI3P or PI(3,5)P <sub>2</sub> . . . . .	110
4.24	Local membrane concentration of phosphoinositides needed for Hsv2 binding . . . . .	111
4.25	Involvement of ScHsv2 histidines from binding sites 1 and 2 on phos- phoinositide binding . . . . .	113
4.26	ITC measurements of KlHsv2 and ScHsv2 with PI(3,5)P <sub>2</sub> liposomes in different pHs . . . . .	114
4.27	Stability of KlHsv2 and ScHsv2 in different pHs . . . . .	116
4.28	The impact of loop 6CD on membrane binding . . . . .	117
4.29	CD spectra of KlHsv2 and ScHsv2 mutants . . . . .	119
4.30	Purification of KlAtg8 and PaAtg8 from <i>E. coli</i> BL21(DE3) cells . . .	122
4.31	CD spectra and melting curve of KlAtg8 and PaAtg8 . . . . .	123
4.32	Interaction studies on KlHsv2 and KlAtg8 . . . . .	124
4.33	Co-expression of ScAtg21 and ScAtg8 in insect cells . . . . .	126
4.34	Gel filtration purification of KlHsv2 and KlAtg8 . . . . .	127
4.35	Thermofluor analysis of KlHsv2 in complex with KlAtg8 . . . . .	128
4.36	KlHsv2 crystals for Atg8 peptide soaking . . . . .	129
4.37	Proposed model of Hsv2 membrane binding . . . . .	134
5.1	Testexpression of CeAtg18, PaAtg18, PaAtg21 and KlAtg21 in <i>E. coli</i> BL21(DE3) cells . . . . .	139
5.2	Purification of CeAtg18 from <i>E. coli</i> BL21(DE3) cells . . . . .	140

5.3	Purification of DmAtg18 from <i>E. coli</i> BL21(DE3) cells . . . . .	141
5.4	Purification of PaAtg21 from <i>E. coli</i> BL21(DE3) cells . . . . .	142
5.5	Testexpression of SpHsv2 in <i>E. coli</i> BL21(DE3) cells . . . . .	142
5.6	Thermofluor analysis of CeAtg18 and DmAtg18 . . . . .	143
5.7	CD spectra and melting curves of yeast PROPPINs . . . . .	144
5.8	Limited proteolysis of PaAtg21 . . . . .	145
5.9	Buffer optimization for thrombin cleavage of ScHsv2 and Hsv2 anti- body test . . . . .	145
5.10	Analysis of ScHsv2 after thrombin treatment for stability using an analytical gel filtration . . . . .	146
5.11	GST SpinTrap purification of ScHsv2 homologs . . . . .	146
5.12	PIPstrip analysis of ScHsv2 binding site mutants . . . . .	147
5.13	Liposome floating analysis with SDS-PAGE . . . . .	148
5.14	Determination of liposome size distribution by FFF-MALLS . . . . .	148
5.15	Structure of KlHsv2 and homology model of ScHsv2 . . . . .	149
5.16	Alignment of the loop 6CD region of different Hsv2 homologs . . . . .	149
5.17	PIPstrip analysis of loop 6CD mutants . . . . .	150
5.18	Melting curves of KlHsv2 and ScHsv2 mutants . . . . .	150
5.19	Stability analysis of KlHsv2 and ScHsv2 mutants using Thermofluor .	151



# List of Tables

1.1	Structures of autophagy proteins in PDB . . . . .	4
2.1	Chemicals . . . . .	7
2.2	Enzymes . . . . .	8
2.3	Lipids . . . . .	9
2.4	Kits . . . . .	9
2.5	Chromatography columns . . . . .	10
2.6	Antibodies . . . . .	11
2.7	DNA constructs generated and used in this study . . . . .	14
2.8	Oligonucleotides ordered especially for this study . . . . .	15
2.9	PCR reaction . . . . .	20
2.10	Buffer and detergent stock solution volumes for screening . . . . .	26
2.11	Buffers for purification of ScAtg18 from insect cells . . . . .	28
2.12	Buffers for purification of PaAtg18, DmAtg18, CeAtg18, KlAtg21 and PaAtg21 . . . . .	30
2.13	Buffers for purification of SpHsv2 from <i>E. coli</i> BL21(DE3) cells . . . . .	31
2.14	Buffers for purification of ScHsv2 from <i>E. coli</i> BL21(DE3) cells . . . . .	32
2.15	Buffers for purification of KlHsv2 from <i>E. coli</i> BL21(DE3) cells . . . . .	35
2.16	Liposome lipid compositions . . . . .	40
2.17	Settings for isothermal calorimeters . . . . .	42
4.1	PROPPIN homologs analyzed by TarO . . . . .	82
4.2	Initial crystallization conditions for PROPPINs . . . . .	98
4.3	Binding affinities and stoichiometries of PROPPINs to phosphoinositides	112
4.4	Determination of binding affinity $K_D$ based on %-bound protein versus % phosphoinositide in liposomes . . . . .	112
4.5	Binding affinities and stoichiometries of Hsv2 in different pHs . . . . .	115
5.1	Structures of autophagy proteins in PDB (2) . . . . .	137

5.2 Sequence of synthetic genes used in this study . . . . . 152



# List of Abbreviations

(v/v) .....	Volume per volume
(w/v) .....	Weight per volume
aa .....	Amino acid
Atg .....	Autophagy-related gene
CD .....	Circular dichroism
CE .....	Whole cell extract
CV .....	Column volume
Cvt .....	Cytoplasm-to-vacuole-targeting
DPA .....	Day of proliferation arrest
FFF-MALLS .	Field-flow fractionation coupled to multi-angle laser light scattering
FT .....	Flow through
fwd .....	Forward
IPTG .....	Isopropyl $\beta$ -D-1-thiogalactopyranoside
ITC .....	Isothermal titration calorimetry
kb .....	Kilo base
LC3 .....	MAP1LC3 - microtubuli associated protein 1 light chain 3
LUV .....	Large unilamellar vesicles
min .....	Minute
MIP .....	Molecularly imprinted polymer
P .....	Pellet
PAS .....	Preautophagosomal structure
PAS .....	pre-autophagosomal structure
PBS .....	Phosphate buffered saline
PC .....	Phosphatidylcholine
PCR .....	Polymerase chain reaction
PD .....	Pull down
PDB .....	Protein DataBase

PE .....	Phosphatidylethanolamine
PIP .....	Phosphoinositol phosphate
PROPPIN ...	$\beta$ -propeller proteins that bind phosphoinositides
PS .....	Phosphatidylserine
rev .....	Reverse
rpm .....	Rounds per minute
RT .....	Room temperature, 22 – 25 °C
S .....	Supernatant
SDS-PAGE ..	Sodium dodecyl sulfate polyacrylamide gel electrophoresis
sec .....	Seconds
SEM .....	Standard error of mean
SUV .....	Small unilamellar vesicles
TBS .....	Tris buffered saline
T <sub>m</sub> .....	Melting temperature
TR-PE .....	Texas Red conjugated phosphatidylethanolamine
UV <sub>280</sub> .....	Ultraviolet absorbance at 280 nm
YFP .....	Yellow fluorescent protein





# 1 General introduction

## 1.1 Definition of autophagy

Metabolism is a widely studied field in the life sciences and of special interest because all chemical reactions described under metabolism are important for life. Metabolism is divided into two parts namely catabolism and anabolism. Anabolism includes all pathways that use energy to build up components of the cell e.g. proteins, lipids and storage substances. In contrast, catabolism generates energy through breakdown of cell compounds.

One important pathway to degrade cell components and to restore energy is autophagy (in greek 'self eating'). Autophagy is activated under nutrient starvation conditions or other stresses and serves as adaptation of the cell to new circumstances. Proteins, cytosolic material and even whole cell organelles are degraded through autophagy. During autophagy a growing isolation membrane (or phagophore) engulfs cytoplasmic content. The growing double layered membrane then fuses at its edges and forms an autophagosome. Finally, the autophagosomes fuse with the lysosome (in yeast: vacuole) and its content is degraded (see fig. 1.1) [1, 2].

This eukaryotic conserved pathway was discovered in 1950's [3] and the term autophagy was manifested by Christian De Duve, 1963. Yeast genetic screens in the 1990's led to the identification of the proteins involved in autophagy [4, 5, 6, 7]. Up to now 36 autophagy related (Atg) proteins have been described [8].

## 1.2 Types of autophagy

Different autophagic subtypes exist. Macroautophagy is a bulk degradation pathway, which delivers cytoplasmic content to the lysosome/vacuole [1, 2, 9]. Also or-

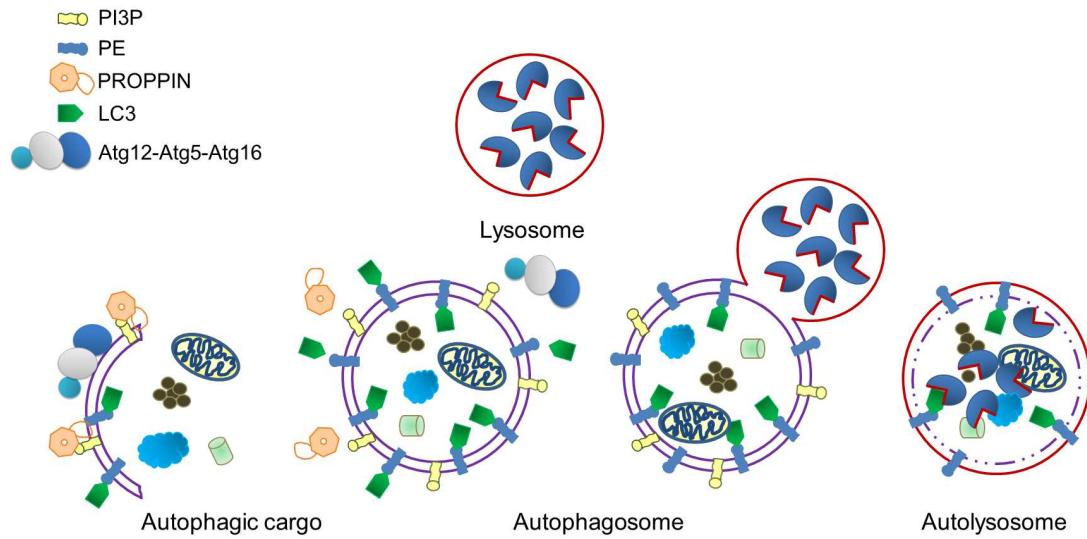


**Figure 1.1: Scheme for autophagosome formation**

During autophagosome formation a growing isolation membrane engulfs cytoplasmic content for degradation. The formed autophagosome fuses finally with the lysosome, where its content gets hydrolyzed in these so called autolysosomes. Different cargo like mitochondria, bacteria, etc. can be degraded in autophagy.

organelles can be degraded by macroautophagy. Specific autophagic subtypes where organelles are targeted for degradation are mitophagy [10], ribophagy [11] and pexophagy [12]. Another non selective autophagy subtype is microautophagy. Through protrusion, septation or incorporation of the membrane at the surface of the lysosome or vacuole, cytoplasmic content is taken up and degraded [9, 13].

The cytoplasm to vacuole targeting (Cvt) pathway is highly selective and a biosynthetic pathway. It delivers precursors of aminopeptidase I and  $\alpha$ -mannosidase to the vacuole where they are processed and activated. This process is restricted to yeast and involves Atg19 as receptor for aminopeptidase I and  $\alpha$ -mannosidase precursors [1, 14].

Chaperone mediated autophagy (CMA) has only been described in higher eukaryotes. The target molecules carrying a KFERQ motif is bound by a chaperone complex of Hsc70, Hsp90 and other co-chaperons in the cytoplasm. The protein is unfolded followed by direct delivery across the lysosomal membrane via the Lamp2A receptor [9, 15].

Autophagy plays also a role in defense against invading pathogens, which is then called xenophagy [16].

Most of the proteins of the core autophagy machinery are shared in these autophagic subtypes, but selective adapter proteins are employed to mediate cargo specificity [17].

### 1.3 Molecular players in autophagy

Initiation of macroautophagy (hereafter autophagy) is mediated by the Tor (target of rapamycin) kinase. During nutrient starvation Tor is inhibited and Atg13 is dephosphorylated. Dephosphorylation of Atg13 allows it to bind Atg1. The Atg1 complex (mammalian ULK1 complex) including Atg1, Atg11, Atg13, Atg17, Atg29 and Atg31 recruits downstream complexes to the PAS (pre-autophagosomal structure) [18]. One of the first complexes recruited is the class III PI3 kinase complex I Vps34 which generates phosphoinositol-3-phosphate (PI3P) at the PAS. This complex includes Vps34, Vps15, Vps30/Atg6 and Atg14 [19, 20].

PI3P is important as a signaling factor in autophagy and functions as an anchor for other proteins and protein complexes such as PROPPINs ( $\beta$ -propeller proteins that bind phosphoinositides). One of the three yeast PROPPIN homologs Atg18 forms a complex with Atg2 and is involved in the cycling of the only autophagic transmembrane protein Atg9 [21].

Two ubiquitin-like conjugation systems are involved in autophagy, namely Atg8 and Atg12 [22, 23]. Atg8 is the ubiquitin-like protein, which gets conjugated to its target phosphatidylethanolamine through action of the E1- and E2-like proteins Atg3 and Atg7, respectively. Atg7 is shared with the second conjugation system, where the ubiquitin-like protein Atg12 is conjugated to Atg5. The involved E1-like enzyme is Atg10. Atg5-Atg12 interacts via Atg5 with Atg16, which causes oligomerization of the whole complex. These two ubiquitin-like conjugation systems are important for membrane expansion (for review [1, 2]).

### 1.4 Structural characterization of autophagy proteins

Among the first determined structures of autophagy proteins were the two ubiquitin-like proteins Atg12 and MAP1LC3 (LC3, in yeast: Atg8) (see table 1.1). During the last years many other autophagy-related protein structures and structure improvements were published. More than 60 determined structures including homologs from different species can be found in the PDB (see suppl. table 5.1) .

Among the determined structures all the proteins part of the ubiquitin-like conjugation systems have been determined in the last years. Even some protein complexes using truncated proteins were described. However, full length protein complexes of the

conjugation systems are missing. In 2012, the first structure of a PROPPIN, namely Hsv2, was published by us and others [24, 25, 26].

Up to now a range of structures of the autophagic core machinery proteins are still missing. The determination of protein structures has become a growing field in autophagy. It is important to understand the interplay of these molecules on a molecular level which brings new insights into the understanding of the whole autophagy process.

**Table 1.1:** Structures of autophagy proteins in PDB

Protein	Organism	PDB entry	Structure type	Reference
MAP1A/1B	<i>R. norvegicus</i>	1UGM	X-ray, 2.05 Å	Sugawara <i>et al.</i> , <i>Genes Cell</i> (2004) [27]
LC3 (4-120)				
Atg4B	<i>H. sapiens</i>	2CY7	X-ray, 1.90 Å	Sugawara <i>et al.</i> , <i>JBC</i> (2005) [28]
Atg3	<i>S. cerevisiae</i>	2DYT	X-ray, 2.5 Å	Yamada <i>et al.</i> , <i>JBC</i> (2007) [29]
Atg7 (1-613)	<i>S. cerevisiae</i>	3VH2	X-ray, 3.30 Å	Noda <i>et al.</i> , <i>Mol Cell</i> (2011) [30]
Atg12 (10-93)	<i>A. thaliana</i>	1WZ3	X-ray, 1.80 Å	Suzuki <i>et al.</i> , <i>Autophagy</i> (2005) [31]
Atg5	<i>Kluyveromyces marxianus</i>	3VQI	X-ray, 2.50 Å	Yamaguchi <i>et al.</i> , <i>Structure</i> (2012) [32]
Atg16	<i>S. cerevisiae</i>	3A7P	X-ray, 2.80 Å	Fujioka <i>et al.</i> , <i>JBC</i> (2009) [33]
Atg10	<i>Kluyveromyces marxianus</i>	2LPU	solution NMR	Yamaguchi <i>et al.</i> , <i>Structure</i> (2012) [32]
Beclin 1 coiled coil domain (174-266)	<i>R. norvegicus</i>	3Q8T	X-ray, 1.90 Å	Li <i>et al.</i> , <i>Nat Commun</i> (2012) [34]
Beclin 1 evolutionary conserved domain (241-450)	<i>H. sapiens</i>	4DDP	X-ray, 1.55 Å	Huang <i>et al.</i> , <i>Cell Res</i> (2012) [35]
Vps34	<i>D. melanogaster</i>	2X6H	X-ray, 2.90 Å	Miller <i>et al.</i> , <i>Science</i> (2010) [36]
Hsv2	<i>Kluyveromyces lactis</i>	4AV9	X-ray, 3.00 Å	Krick <i>et al.</i> , <i>PNAS</i> (2012) [24]
		4EXV	X-ray, 3.00 Å	Baskaran <i>et al.</i> , <i>Mol Cell</i> (2012) [25]

## 1.5 Involvement of autophagy in disease

Autophagy most likely evolved out of two reasons. First, to regain nutrients by degradation of macromolecules and second to guard the cell against toxic or invading components similar to a checkpoint of quality control. Therefore, impaired autophagy is linked to diseases such as neurodegenerative diseases, Crohn's disease, type II diabetes, cancer, heart disease and others. Autophagy is also linked to longevity and involved in



cellular defense against pathogens [37, 38, 39, 40]. Neurodegenerative diseases such as Parkinson, Alzheimer and Huntington's disease are caused by accumulation of protein aggregates in the cell, which are usually degraded via the autophagy pathway.

Deciphering the role of autophagy in disease is still at an early stage. Understanding autophagy on a molecular level might provide novel targets to fight against diseases.



## 2 Materials & Methods

### 2.1 Materials

#### 2.1.1 Chemicals

For this study I used reagent grade chemicals from the following companies: Fluka (Buchs, Switzerland), Merck (Darmstadt, Germany), Sigma-Aldrich (Steinheim/Seelze, Germany), Roth (Karlsruhe, Germany), Serva (Heidelberg, Germany), Roche (Basel, Switzerland). Chemicals used were of analytical purity and chemicals for crystallization were ultrapure quality. Further chemicals are listed in table 2.1.

**Table 2.1:** Chemicals

Chemical	Company
Pefabloc	Roche
complete EDTA-free, Protease inhibitor tablet	Roche
IPTG	
Ni-NTA Sepharose	GE Healthcare
Streptactin Sepharose	IBA
Sephadex G-50	Sigma
Fugene	Roche
Gibco Sf900 III SFM (1x), Liquid	Invitrogen
Gibco Express Five SFM (1x), Liquid	Invitrogen
L-glutamine 100x	Invitrogen
TMB substrate solution (3,3',5,5' - tetramethylbenzidine)	Thermo Fisher Scientific
ADDit - Additive Screen	Emerald BioSystems
pHat Buffer Block	Hampton Research

Chemical	Company
SYPRO Orange	Sigma
Blue-Gal	Invitrogen
I-PER Insect cell protein extraction reagent	Thermo Fisher Scientific
Nycodenz	Progen
Na-cholate	Sigma

### 2.1.2 Enzymes

Enzymes were ordered from the companies stated in table 2.2. Enzymes were used with their supplied buffers following the manufacturers manuals.

**Table 2.2:** Enzymes

Enzyme	Company
Restriction enzymes	NEB
T4 DNA Ligase	NEB
Cre Recombinase	NEB
Thrombin	MP Biomedical
DNaseI	Applichem
Lysozyme	Roth

99 mg of Trombin was prepared in 7.5 ml Tris/EDTA buffer (10 mM Tris pH 7.4, 1 mM EDTA) and mixed with 7.5 ml glycerol.

### 2.1.3 Lipids

Lipids were ordered from the companies stated in table 2.3. Most lipids were shipped as powder and were dissolved in chloroform to the stated concentration and stored at -20°C.

**Table 2.3:** Lipids

Lipid	Concentration	Order No.	Company
<b>PC:</b> L- $\alpha$ -phosphatidylcholine from egg, chicken	10/25 mg/ml	840051C/P	Avanti Polar Lipids, Inc.
<b>PE:</b> L- $\alpha$ -phosphatidylethanolamine from brain, porcine	25 mg/ml	840022P	Avanti Polar Lipids, Inc.
<b>PS:</b> L- $\alpha$ -phosphatidylserine from brain, porcine	25 mg/ml	840032P	Avanti Polar Lipids, Inc.
18:1 <b>PI(3)P:</b> 1,2-dioleoyl-sn-glycero-3-phospho-(1'-myo-inositol-3'-phosphate)	1 mg/ml	850150P	Avanti Polar Lipids, Inc.
<b>PI(4)P:</b> L- $\alpha$ -phosphatidylinositol-4-phosphate ammonium salt from brain, porcine	1 mg/ml	840045P	Avanti Polar Lipids, Inc.
18:1 <b>PI(5)P:</b> 1,2-dioleoyl-sn-glycero-3-phospho-(1'-myo-inositol-5'-phosphate) ammonium salt	1 mg/ml	850152P	Avanti Polar Lipids, Inc.
18:1 <b>PI(3,5)P2:</b> 1,2-dioleoyl-sn-glycero-3-phospho-(1'-myo-inositol-3',5'-bisphosphate) ammonium salt	1 mg/ml	850154P	Avanti Polar Lipids, Inc.
18:1 <b>PI(4,5)P2:</b> 1,2-dioleoyl-sn-glycero-3-phospho-(1'-myo-inositol-4',5'-bisphosphate) ammonium salt	1 mg/ml	850155P	Avanti Polar Lipids, Inc.
18:1 <b>PI(3,5)P2:</b> 1,2-dioleoyl-sn-glycero-3-phospho-(1'-myo-inositol-3',5'-bisphosphate) ammonium salt	1 mg/ml	850154P	Avanti Polar Lipids, Inc.
18:1 <b>PI(3,4,5)P3:</b> 1,2-dioleoyl-sn-glycero-3-phospho-(1'-myo-inositol-3',4',5'-trisphosphate) ammonium salt	1 mg/ml	850156P	Avanti Polar Lipids, Inc.
<b>TR-PE:</b> 1,2-dihexadecanoyl-sn-glycero-3-phosphoethanolamine, triethylammonium salt	1 mg/ml	T-1395MP	Invitrogen
<b>PI3P-diC4:</b> dibutanoyl phosphatidylinositol-3-phosphate		P3004-EC	MoBiTec

### 2.1.4 Kits

All kits used in this study are summarized in table 2.4. All kits were used with the supplied buffers following the manufacturers recommendation.

**Table 2.4:** Kits used in this study

Kit	Company
Phusion High-Fidelity PCR Kit	NEB
Gateway pENTR/D-TOPO cloning	Invitrogen
Gateway LR Clonase enzyme mix, and reaction buffer	Invitrogen
CloneJET PCR Cloning Kit	Fermentas

Kit	Company
NucleoSpin Plasmid kit	Macherey & Nagel
NucleoSpin Extract II kit	Macherey & Nagel
NucleoBond PC100	Macherey & Nagel
NucleoBond Xtra	Macherey & Nagel
QuickChange II Site-Directed Mutagenesis kit	Agilent Technologies (Stratagene)
QuickChange Lightning Site-Directed Mutagenesis kit	Agilent Technologies (Stratagene)
Western Lightening <i>Plus</i> -ECL	Perkin Elmer
GST Spin Trap	GE Healthcare
Proti-Ace	Hampton Research
Proti-Ace II	Hampton Research
Gel filtration molecular weight markers (12,400 - 200,000)	Sigma
Ni-NTA Membrane Protein Kit	Qiagen

### 2.1.5 Columns for chromatography

All columns listed below in table 2.5 were used in combination with an Äkta Purifier FPLC system (RT) or with the Äkta Prime FPLC (4°C). The manufacturers recommendations were followed for handling of the columns, including storage, cleaning and equilibration.

**Table 2.5:** Chromatography columns

Column	Company
5 ml HiTrap SP FF column	GE Healthcare
5 ml HiTrap Q FF column	GE Healthcare
1 ml/5 ml His-Trap FF column	GE Healthcare
5 ml Strep-Trap column	GE Healthcare
5 ml GSTrap column	GE Healthcare
Superdex 200 10/300 GL	GE Healthcare

Column	Company
HiLoad 16/60 Superdex 200 prep grade	GE Healthcare
HiLoad 16/60 Superdex 75 prep grade	GE Healthcare

### 2.1.6 Antibodies

All antibodies used in this study are listed in table 2.6.

**Table 2.6:** Antibodies

Antibody	Company
monoclonal GST	Clontech
Ms mAb to GST	Abcam
Hsv2 (CGEPTRWELVRESWREL)	gift from Prof. M. Thumm
Hexa-Histidine tag (DIA900)	Dianova
murine Strep-tag II	IBA GmbH
Ubiquitin antibody [10C2-2]	Abcam
Penta His HRP conjugate	Qiagen GmbH
<i>Strep</i> MAB-Classic HRP conjugate	IBA GmbH
goat polyclonal mouse IgG (HRP labeled)	BioRad Laboratories GmbH
goat polyclonal rabbit IgG (HRP labeled)	BioRad Laboratories GmbH

### 2.1.7 Buffers and media

#### Luria Bertani (LB) media and plates

10 g/l (w/v) tryptone, 5 g/l (w/v) yeast extract, 10 g/l (w/v) NaCl  
for plates: 18 g/l (w/v) Agar were added

#### TYE low salt plates

15 g/l (w/v) Agar, 10 g/l (w/v) tryptone, 5 g/l (w/v) yeast extract

**SOB/SOC-media**

2 % tryptone, 0.5 % yeast extract, 10 mM NaCl, 2.5 mM KCl,  
after autoclaving 10 mM MgCl<sub>2</sub>, 10 mM Mg<sub>2</sub>SO<sub>4</sub> were added  
SOC: + 20 mM glucose

**ZYM-5052 media (Autoinducible media) [41]**

950 ml ZY (10 g/l (w/v) N-Z-Amine AS (Sigma) and 5 g/l (w/v) yeast extract-B (QBIogene))  
20 ml 50x5052 (250 g/l (w/v) glycerol, 25 g/l (w/v) glucose, 100 g/l (w/v)  $\alpha$ -lactose monohydrate, 730 ml H<sub>2</sub>O)  
20 ml 50xM (222.5 g/l (w/v) Na<sub>2</sub>HPO<sub>4</sub> x 2 H<sub>2</sub>O, 170 g/l (w/v) KH<sub>2</sub>PO<sub>4</sub>, 134 g/l (w/v) NH<sub>4</sub>Cl, 35.5 g/l (w/v) Na<sub>2</sub>SO<sub>4</sub>, 800 ml H<sub>2</sub>O)  
1 ml 2 M MgSO<sub>4</sub>  
200  $\mu$ l 1000x trace metals mixture (50 mM Fe, 20 mM Ca, 10 mM Mn, 10 mM Zn, 2 mM Co, 2 mM Cu, 2 mM Ni, 2 mM Mo, 2 mM Se, 2 mM B; further details in [41])

**Terrific broth (TB) media**

12 g/l (w/v) tryptone, 24 g/l (w/v) yeast extract, 0.4 % (v/v) glycerol, 2.31 g/l (w/v) KH<sub>2</sub>PO<sub>4</sub>, 12.54 g/l (w/v) K<sub>2</sub>HPO<sub>4</sub>

**Minimal media with selenomethionine**

1 l culture consists of:

200 ml 5x M9 stock solution (15 g/l (w/v) KH<sub>2</sub>PO<sub>4</sub>, 5 g/l (w/v) NH<sub>4</sub>Cl, 2.5 g/l (w/v) NaCl)  
800 ml autoclaved water  
1 ml of 1 M MgSO<sub>4</sub> (autoclaved)  
20 ml 20 % glucose (w/v) (sterile filtered)  
100  $\mu$ l of 0.5 % (w/v) thiamine vitamin (sterile filtered)  
1 ml of 4.2 g/l (w/v) FeIISO<sub>4</sub> (sterile filtered)

For inoculation an over night culture was harvested and spun down at low speed and washed with in M9 media to remove all full media components. The culture in minimal media was grown until an OD of 0.3 at 600 nm. At this point solid amino acids were added:

100 mg/l (w/v) L-Lysine  
100 mg/l (w/v) L-Phenylalanine  
100 mg/l (w/v) L-Threonine



50 mg/l (w/v) L-Isoleucine

50 mg/l (w/v) L-Leucine

50 mg/l (w/v) L-Valine

50 mg/l (w/v) L-Selenomethionine

About 15 min after amino acid addition the expression was started with 1 mM IPTG.

This protocol was adopted from [42].

#### **1x PBS**

150 mM NaCl, 20 mM Na<sub>2</sub>PO<sub>4</sub> pH 7.4

for PBS-T add 0.1 % (v/v) Tween 20

#### **1x TBS**

50 mM Tris, 150 mM NaCl, pH 7.5

for TBS-T add 0.1 % (v/v) Tween 20

### **2.1.8 Antibiotics**

The following antibiotics were prepared as 1000x stock solutions. Ampicillin, gentamycin and kanamycin were prepared in deionized water, tetracyclin powder was resuspended in 70 % ethanol. All solutions were filter sterilized and stored at -20 °C.

Ampicillin (100 µg/ml (w/v))

Gentamycin (7 µg/ml (w/v))

Kanamycin (30 µg/ml (w/v))

Streptomycin sulfate salt (2 % (w/v))

Tetracycline (10 µg/ml (w/v))

### **2.1.9 Insect cell lines and bacterial strains**

Sf9 insect cells (Invitrogen) - virus generation

Sf21 insect cells (Invitrogen) - virus generation

High5 insect cells (Invitrogen) - expression cell line

*E. coli* DH10MultiBac (Imre Berger) - generation of bacmid with genes of interest

*E. coli* BW23474 - cloning strain for plasmids with R6Kγ origin

*E. coli* DH5α - standard cloning strain

*E. coli* XL1-blue - standard cloning strain

*E. coli* BL21(DE3) - expression strain

*E. coli* Rosetta(DE3) - expression strain

## 2.1.10 DNA constructs

In the following table 2.7 all plasmids are stated, which were used in this study.

**Table 2.7:** DNA constructs generated and used in this study

Vector	Gene	Affinity tag	Cleavage sites	Cloning sites	Resistance	Source
pFL					Amp <sup>R</sup> , Genta <sup>R</sup>	I. Berger
pFL	MAP1LC3	10x His	TEV	<i>XmaI/NheI</i>	Amp <sup>R</sup> , Genta <sup>R</sup>	R. Busse
pFL	MAP1LC3/ <i>hatg3/hatg7</i>	10x His	TEV	<i>Cre/loxP</i>	Amp <sup>R</sup> , Genta <sup>R</sup>	R. Busse
pFL	<i>hatg5</i>	StrepII	TEV	<i>XmaI/NheI</i>	Amp <sup>R</sup> , Genta <sup>R</sup>	R. Busse
pFL	<i>hatg5/hatg12</i>	10x His	TEV	<i>BamHI/SalI</i>	Amp <sup>R</sup> , Genta <sup>R</sup>	R. Busse
pFL	<i>hatg5/hatg12/hatg10/hatg7</i>	10x His, StrepII	TEV	<i>Cre/loxP</i>	Amp <sup>R</sup> , Genta <sup>R</sup>	R. Busse
pFL-His		6x His	TEV		Amp <sup>R</sup> , Genta <sup>R</sup>	K. dos Santos
pFL-His	<i>Scatg18</i>	6x His	TEV	<i>EcoRI/HindIII</i>	Amp <sup>R</sup> , Genta <sup>R</sup>	R. Busse
pFL-His	<i>Scatg18/Schsv2</i>	StrepII	TEV	<i>XmaI/XhoI</i>	Amp <sup>R</sup> , Genta <sup>R</sup>	R. Busse
pFL-His	<i>Scatg21</i>	6x His	TEV	<i>SalI/HindIII</i>	Amp <sup>R</sup> , Genta <sup>R</sup>	R. Busse
pFL-His	<i>Scatg21/Schsv2</i>	StrepII	TEV	<i>XmaI/XhoI</i>	Amp <sup>R</sup> , Genta <sup>R</sup>	R. Busse
pFL-His	<i>Scatg21/Scatg8</i>	StrepII	TEV	<i>XmaI/NcoI</i>	Amp <sup>R</sup> , Genta <sup>R</sup>	R. Busse
pFL-His	<i>Scatg21/Scatg8</i>	StrepII	TEV	<i>XmaI/NcoI</i>	Amp <sup>R</sup> , Genta <sup>R</sup>	R. Busse
pFL-His	<i>hatg16</i>	6x His	TEV	<i>EcoRI/SalI</i>	Amp <sup>R</sup> , Genta <sup>R</sup>	R. Busse
pFL-Strep		StrepII	TEV		Amp <sup>R</sup> , Genta <sup>R</sup>	K. dos Santos
pFL-Strep	<i>Scatg18</i>	6x StrepII	TEV	<i>EcoRI/HindIII</i>	Amp <sup>R</sup> , Genta <sup>R</sup>	R. Busse
pFL-Strep	<i>Scatg21</i>	6x StrepII	TEV	<i>SalI/HindIII</i>	Amp <sup>R</sup> , Genta <sup>R</sup>	R. Busse
pFL-Strep	<i>hatg16</i>	6x StrepII	TEV	<i>EcoRI/SalI</i>	Amp <sup>R</sup> , Genta <sup>R</sup>	R. Busse
pUCDM					Cm <sup>R</sup>	I. Berger
pUCDM	<i>hatg3</i>			<i>BamHI/SalI</i>	Cm <sup>R</sup>	R. Busse
pUCDM	<i>hatg3/hatg7</i>			<i>XmaI/NheI</i>	Cm <sup>R</sup>	M. Druminski
pUCDM	<i>hatg10</i>			<i>BamHI/SalI</i>	Cm <sup>R</sup>	R. Busse
pUCDM	<i>hatg10/hatg7</i>			<i>XmaI/NheI</i>	Cm <sup>R</sup>	M. Druminski
pENTR				<i>attL1/attL2</i>	Kan <sup>R</sup>	Invitrogen
pENTR	<i>Scatg18</i>	10x His	TEV	<i>attL1/attL2</i>	Kan <sup>R</sup>	R. Busse
pENTR	<i>Scatg21</i>	10x His	TEV	<i>attL1/attL2</i>	Kan <sup>R</sup>	R. Busse
pDEST8				<i>attR1/attR2</i>	Amp <sup>R</sup> , Genta <sup>R</sup>	Invitrogen
pDEST8	<i>Scatg18</i>	10x His	TEV	<i>attR1/attR2</i>	Amp <sup>R</sup> , Genta <sup>R</sup>	R. Busse
pDEST8	<i>Scatg21</i>	10x His	TEV	<i>attR1/attR2</i>	Amp <sup>R</sup> , Genta <sup>R</sup>	R. Busse
pETDuet-1		6x His, S-Tag			Amp <sup>R</sup>	Novagen
pETDuet-1	SpHsv2/SpAtg18	StrepII	TEV		Amp <sup>R</sup>	R. Busse
pETDuet-1	SpAtg18/SpAtg21	StrepII	TEV		Amp <sup>R</sup>	R. Busse
pETDuet-1	SpHsv2/SpAtg21	StrepII	TEV		Amp <sup>R</sup>	R. Busse
pET-28a		6x His, T7			Kan <sup>R</sup>	Novagen
pET-28a	<i>Spatg18</i>	6x His		<i>NdeI/XhoI</i>	Kan <sup>R</sup>	R. Busse
pET-28a	<i>Spatg21</i>	6x His		<i>NdeI/XhoI</i>	Kan <sup>R</sup>	R. Busse
pET-28a	<i>Paatg18</i>	6x His		<i>NdeI/XhoI</i>	Kan <sup>R</sup>	R. Busse
pET-28a	<i>Ceatg18</i>	6x His		<i>NdeI/XhoI</i>	Kan <sup>R</sup>	R. Busse
pET-28a	<i>Dmatg18</i>	6x His		<i>NdeI/XhoI</i>	Kan <sup>R</sup>	R. Busse
pET-28a	<i>Paatg21</i>	6x His		<i>NdeI/XhoI</i>	Kan <sup>R</sup>	R. Busse
pET-28a	<i>Klatg21</i>	6x His		<i>NdeI/XhoI</i>	Kan <sup>R</sup>	R. Busse
pET-28a	<i>KlHsv2</i>	6x His		<i>NdeI/XhoI</i>	Kan <sup>R</sup>	K. Kühnel
pET-28a	<i>KlHsv2</i> GS linker	6x His		<i>NdeI/XhoI</i>	Kan <sup>R</sup>	K. Kühnel
pET-28a	<i>KlHsv2</i> 272A/273A	6x His		<i>NdeI/XhoI</i>	Kan <sup>R</sup>	K. Kühnel
pET-28a	<i>KlHsv2</i> K260E/R261D/H262D	6x His		<i>NdeI/XhoI</i>	Kan <sup>R</sup>	R. Busse
pET-28a	<i>KlHsv2</i> loop chimera	6x His		<i>NdeI/XhoI</i>	Kan <sup>R</sup>	R. Busse
pET-28a	<i>Schsv2</i> loop chimera	6x His		<i>NdeI/XhoI</i>	Kan <sup>R</sup>	R. Busse
pACE					Amp <sup>R</sup>	I. Berger

Vector	Gene	Affinity tag	Cleavage sites	Cloning sites	Resistance	Source
pACE-His					Amp <sup>R</sup>	A. Scacioc
pACE-His	<i>KlHSV2</i>	10x His		<i>NdeI/XhoI</i>	Amp <sup>R</sup>	R. Busse
pACE-His	<i>KlHSV2</i> FTTG	10x His		<i>NdeI/XhoI</i>	Amp <sup>R</sup>	R. Busse
pACE-His	<i>KlHSV2</i> K260E/R261D/H262D	10x His		<i>NdeI/XhoI</i>	Amp <sup>R</sup>	R. Busse
pACE-His	<i>KlHSV2</i> Y272D/F273D	10x His		<i>NdeI/XhoI</i>	Amp <sup>R</sup>	R. Busse
pACE-His	<i>KlHSV2</i> Y272D	10x His		<i>NdeI/XhoI</i>	Amp <sup>R</sup>	R. Busse
pACE-His	<i>KlHSV2</i> F273D	10x His		<i>NdeI/XhoI</i>	Amp <sup>R</sup>	R. Busse
pACE-His	<i>KlHSV2</i> loop chimera	10x His		<i>NdeI/XhoI</i>	Amp <sup>R</sup>	R. Busse
pACE-His	<i>Schsv2</i> loop chimera	10x His		<i>NdeI/XhoI</i>	Amp <sup>R</sup>	R. Busse
pACE-His	<i>Paatg18</i>	10x His		<i>NdeI/XhoI</i>	Amp <sup>R</sup>	R. Busse
pACE-His	<i>Klatg21</i>	10x His		<i>NdeI/XhoI</i>	Amp <sup>R</sup>	R. Busse
pACE-His	<i>KlHSV2/Klatg8</i>	10x His, OneStrEP		<i>Cre/loxP</i>	Amp <sup>R</sup>	R. Busse
pACE-His	<i>Klatg21/Klatg8</i>	10x His, OneStrEP		<i>Cre/loxP</i>	Amp <sup>R</sup>	R. Busse
pACE-His	<i>Paatg18/Paatg8</i>	10x His, OneStrEP		<i>Cre/loxP</i>	Amp <sup>R</sup>	R. Busse
pDK					Cm <sup>R</sup>	I. Berger
pDK	<i>Klatg8</i>	OneStrEP		<i>NdeI/XhoI</i>	Cm <sup>R</sup>	R. Busse
pDK	<i>Paatg8</i>	OneStrEP		<i>NdeI/XhoI</i>	Cm <sup>R</sup>	R. Busse
pGEX-4T3	<i>Schsv2</i>	GST	Thrombin		Amp <sup>R</sup>	R. Krick
pGEX-4T3	<i>Schsv2</i> FTTG	GST	Thrombin		Amp <sup>R</sup>	R. Busse
pGEX-4T3	<i>Schsv2</i> FAAG	GST	Thrombin		Amp <sup>R</sup>	R. Busse
pGEX-4T3	<i>Schsv2</i> R123A	GST	Thrombin		Amp <sup>R</sup>	R. Busse
pGEX-4T3	<i>Schsv2</i> H223A	GST	Thrombin		Amp <sup>R</sup>	R. Busse
pGEX-4T3	<i>Schsv2</i> S243A	GST	Thrombin		Amp <sup>R</sup>	R. Busse
pGEX-4T3	<i>Schsv2</i> T247A	GST	Thrombin		Amp <sup>R</sup>	R. Busse
pGEX-4T3	<i>Schsv2</i> R250A	GST	Thrombin		Amp <sup>R</sup>	R. Busse
pGEX-4T3	<i>Schsv2</i> E262A	GST	Thrombin		Amp <sup>R</sup>	R. Busse
pGEX-4T3	<i>Schsv2</i> R264A	GST	Thrombin		Amp <sup>R</sup>	R. Busse
pGEX-4T3	<i>Schsv2</i> R265A	GST	Thrombin		Amp <sup>R</sup>	R. Busse
pGEX-4T3	<i>Schsv2</i> K290A	GST	Thrombin		Amp <sup>R</sup>	R. Busse
pGEX-4T3	<i>Schsv2</i> T292A	GST	Thrombin		Amp <sup>R</sup>	R. Busse
pGEX-4T3	<i>Schsv2</i> H294A	GST	Thrombin		Amp <sup>R</sup>	R. Busse
pGEX-4T3	<i>Schsv2</i> K269A	GST	Thrombin		Amp <sup>R</sup>	R. Busse

### 2.1.11 Oligonucleotides

Oligonucleotides were ordered from Sigma-Genosys and purchased through Sigma Aldrich Chemie GmbH (Steinheim, Germany). Mutagenesis primers were designed with the software QuickChange primer design from Agilent Technologies (<https://www.genomics.agilent.com>). All oligonucleotides used in this study are listed in table 2.8.

**Table 2.8:** Oligonucleotides ordered especially for this study

Name	Sequence 5'-3'	Properties	Tm	Aim
RB1	CACCATGTCGTA CTACTACCATCACCATCACCA TCACCATCACCATCACGATTACGATATCCC AACGACCGAAAACCTGTATTTTCAGGGCA TCACAATGCTGTGATTCATCACCTACTAT	Kozak, 10x His tag, TEV cleavage site	52 °C	forward primer to amplify ScAtg18 for pENTR/pDEST8 cloning
RB2	TCAATCCATCAAGATGGAATACT	stop codon	52 °C	reverse primer for RB1
RB3	CACCATGTCGTA CTACTACCATCACCATCACCA TCACCATCACCATCACGATTACGATATCCC AACGACCGAAAACCTGTATTTTCAGGGCA TCACAATGAAAAGTATTACAATTC AATCAAG	Kozak, 10x His tag, TEV cleavage site	52 °C	forward primer to amplify ScAtg21 for pENTR/pDEST8 cloning

Name	Sequence 5'-3'	Properties	Tm	Aim
RB4	TTATGTAAATTTATTATTTTGTAGTCAG	stop codon	52 °C	reverse primer for RB3
RB5	ATTGTCAAATGCCAGGCTGACGGGAAGGA CATATCAAACCGTGAAAGAAATCCCCGGA TCTGGTGAGGCACAAGCCCAAGA		60 °C	generation of <i>hatg7</i> isoform 1, include 27 missing aa, bp 1-61
RB6	CGTCAGCCTGGCATTTGACAAATGTACAGC TTGTTCTTCCAAAGTTCTTGATCAATATGA ACGAGAAGG		62 °C	generation of <i>hatg7</i> isoform 1, include 27 missing aa, bp 38-81
RB7	GTGGCCTTATGGCTATGTCTCCT		60 °C	sequencing primer for <i>Scatg18</i> , aligns at position 450 bp, fwd
RB8	GATAGCCAGTACTTGGCGGTAC		60 °C	sequencing primer for <i>Scatg18</i> , aligns at position 900 bp, fwd
RB9	CTATTTGTGAAATAGTTTCCACAT		58 °C	sequencing primer for <i>Scatg21</i> , aligns at position 450 bp, fwd
RB10	TGTTTAGCAGTAAGTCACGATGGTA		60 °C	sequencing primer for <i>Scatg21</i> , aligns at position 900 bp, fwd
RB11	tataaCCCGGGATGCATCACCATCACCATCAC CATCACCATCAGATTACGATATCCCAACGA CCGAAAACCTGTATTTTCAGGGCATCACAA TGCCCTCAGACCGGCCTTTCA	<i>Xma</i> I, 10x His tag, TEV cleavage site	59 °C	fwd primer to amplify MAP1LC3
RB12	tataaGCTAGCTCAGCCGAAGGTTTCCTGGGAG	<i>Nhe</i> I, C-terminal Gly, stop codon	60 °C	reverse primer for RB11
RB13	tataaCCCGGGATGGCGGCAGCTACGGGGAT	<i>Xma</i> I	60 °C	fwd primer to amplify <i>hatg7</i>
RB14	tataaGCTAGCTCAGATGGTCTCATCATCGCT CATGT C	<i>Nhe</i> I, stop codon	60 °C	rev primer for RB13
RB15	tataaGGATCCATGCAGAATGTGATTAATACT GTGAAGGGAAG	<i>Bam</i> HI,	59 °C	fwd primer to amplify <i>hatg3</i>
RB16	tataaGTGACTTACATTGTGAAGTGTCTTGT GTAGTCATATTC	<i>Sal</i> I, stop codon	58 °C	rev primer for RB15
RB17	tataaGGATCCATGCATCACCATCACCATCAC CATCACCATCAGATTACGATATCCCAACGA CCGAAAACCTGTATTTTCAGGGCATCACAA TGA TAGCCGGGAACACCAAGTTTC	<i>Bam</i> HI, 10x His tag, TEV cleavage site	60 °C	fwd primer to amplify <i>hatg12</i>
RB18	tataaGTGACTCATCCCCACGCTGAGACTTG	<i>Sal</i> I, stop codon	59 °C	rev primer for RB17
RB19	tataaCCCGGGATGTGGAGCCACCCGAGTT CGAAAAAGATTACGATATCCCAACGACCGA AAACCTGTATTTTCAGGGCATCACAATGAC AGATGACAAAGATGTGCTTCGAGATG	<i>Xma</i> I, StrepII tag, TEV	60 °C	fwd primer to amplify <i>hatg5</i>
RB20	tataaGCTAGCTCAATCTGTTGGCTGTGGGAT GATACTAATATG	<i>Nhe</i> I, stop codon	61 °C	rev primer for RB19
RB21	tataaGGATCCATGGAAGAAGATGAGTTCATT GGAGAAAAACATTC	<i>Bam</i> HI	60 °C	fwd primer to amplify <i>hatg10</i>
RB22	tataaGTGACTTAAAGGACATTCGTTTCATC CTGAGACG	<i>Sal</i> I, stop codon	60 °C	rev primer for RB21

Name	Sequence 5'-3'	Properties	Tm	Aim
RB30	ttatGAATTCATGTCTGATTCATCACCTACTAT CAACTTTATTAATTTCAAT	<i>EcoRI</i>	60 °C	fwd primer to amplify <i>Scatg18</i>
RB31	ataaAAGCTTTCATCCATCAAGATGGAAT ACTGTGACAATATTAAG	<i>HindIII</i> , stop codon	60 °C	rev primer for RB30
RB33	ataaAAGCTTTTATGTAAATTTATTATTTT TAGTCAGCACACATTCACCAG	<i>HindIII</i>	60 °C	rev primer for RB49, amplifies <i>Scatg21</i>
RB39	AACGCCATATCAGTGAACAACGCGCCGTC GTGATCGTCTGCAGAGACAGGCGTTCGAGG AGATC		61 °C	generation of full length <i>hatg16</i> , include missing N-terminus, fwd primer 1
RB40	ATGAGTAGCGGCCTGCGTGCTGCTGATTTT CCTCGCTGGAAACGCCATATCAGTGAACAA CTGCGCC		61 °C	generation of full length <i>hatg16</i> , include missing N-terminus, fwd primer 2
RB41	TCAGTACTGTGCCCCACAGCACAGC		61 °C	rev primer for RB39 and RB40
RB42	ACTCTCGCAGCCTGCTGGAGG		60 °C	sequencing primer for hAtg16, anneals at position 801-821 bp
RB43	GCATTACTGCCAGATAGGGAACCCTT		60 °C	rev sequencing primer for hAtg16, anneals at position 1100-1057 bp
RB49	ttatGTCGACaaATGAAAGTATTACAATTCAAT CAAGATGCAACGTGCT	<i>SalI</i>	60 °C	fwd primer to amplify <i>Scatg21</i>
RB57	cttattGAATTCATGAGTAGCGGCCTGCGT GCTG	<i>EcoRI</i>	60 °C	fwd primer to amplify <i>hatg16</i>
RB58	cttattGTCGACTCAGTACTGTGCCCCACAG CACAG	<i>SalI</i> , stop codon	59 °C	rev primer for RB57
RB65	CATATGTGGAGCCACCCGCAGTTCGAAAAA GATTACGATATCCCAACGACCGAAAACCTG TATTTTCAGGGCATCACAATGAGCACGATC AACACAGTTTCCCTG	<i>NdeI</i> , StrepII tag, TEV cleavage site	60 °C	fwd primer to amplify <i>Sphsv2</i>
RB66	CTCGAGTTAACACAGACTTCCGTCGGCCTCC	<i>XhoI</i> , stop codon	60 °C	rev primer for RB65
RB67	CATATGTGGAGCCACCCGCAGTTCGAAAAA GATTACGATATCCCAACGACCGAAAACCTG ATTTTCAGGGCATCACAATGCCGTCGATC ATCCTGTATTGCTC	<i>NdeI</i> , StrepII tag, TEV cleavage site	60 °C	fwd primer to amplify <i>Spatg21</i>
RB68	CTCGAGTTAGTCATCGAAGATATAACGCTC CAGCAG	<i>XhoI</i> , stop codon	60 °C	rev primer for RB67
RB69	CCATTAAAGACGTGTTTTATCTgcGATTC ATATTGTGGTAGTCCTGG		78.65 °C	mutagenesis primer, <i>Schsv2</i> R123A
RB70	CCAGGACTACCACAATATGAATCgcAGATA AAAACACGTCTTTAATGG		78.65 °C	mutagenesis primer, <i>Schsv2</i> R123A
RB71	GCCCACTCCATCATTTAAAGCagcTAAAAATC CCATCAAACCTGGTT		78.52 °C	mutagenesis primer, <i>Schsv2</i> H223A
RB72	AACCAGTTTGTATGGGATTTTAgcTGCTTT AATGATGGAAGTGGGC		78.52 °C	mutagenesis primer, <i>Schsv2</i> H223A
RB73	CACCATGGTAGCAACATGTgCCGTCCAGGG		78.9 °C	mutagenesis primer, <i>Schsv2</i> S243A

Name	Sequence 5'-3'	Properties	Tm	Aim
RB74	CCCTGGACGGcACATGTTGCTACCATGGTG		78.9 °C	mutagenesis primer, <i>Schsv2</i> S243A
RB75	ACATGTTCCGTCCAGGGTgCACTTATAAGA ATCTTCAG		78.37 °C	mutagenesis primer, <i>Schsv2</i> T247A
RB76	CTGAAGATTCTTATAAGTGcACCCTGGACG GAACATGT		78.37 °C	mutagenesis primer, <i>Schsv2</i> T247A
RB77	GTTCCGTCCAGGGTACACTTATAgcAATCT TCAGTACGCATA		78.24 °C	mutagenesis primer, <i>Schsv2</i> R250A
RB78	TATGCGTACTGAAGATTgcTATAAGTG TAC CCTGGACGGAAC		78.24 °C	mutagenesis primer, <i>Schsv2</i> R250A
RB79	CATAACGGTACTTTAATCAAAGcATT TAGA AGAGGGGTGGACAAG		79.77 °C	mutagenesis primer, <i>Schsv2</i> E262A
RB80	CTTGTCACCCCTCTTCTAAATgCTTTGAT TAAAGTACCGTTATG		79.77 °C	mutagenesis primer, <i>Schsv2</i> E262A
RB81	ACGCATAACGGTACTTTAATCAAAGAATTT gcAAGAGGGGTGGACAAG		79.5 °C	mutagenesis primer, <i>Schsv2</i> R264A
RB82	CTTGTCACCCCTCTTgcAAATCTTTGAT TAAAGTACCGTTATGCGT		79.5 °C	mutagenesis primer, <i>Schsv2</i> R264A
RB83	ATAACGGTACTTTAATCAAAGAATTTAGAgc AGGGGTGGACAAGGC		78.52 °C	mutagenesis primer, <i>Schsv2</i> R265A
RB84	GCCTGTCCACCCCTgcTCTAAATCTTTGAT TAAAGTACCGTTAT		78.52 °C	mutagenesis primer, <i>Schsv2</i> R265A
RB85	GGTAGTAAGTTGGCCGTATTGTCAAATgcG CAAACATTGCATATTTTCCAAA		78.87 °C	mutagenesis primer, <i>Schsv2</i> K290A
RB86	TTTGAAAATATGCAATGTTTGCgcATTTG ACAATACGGCCAACCTACTACC		78.87 °C	mutagenesis primer, <i>Schsv2</i> K290A
RB87	TTGGCCGTATTGTCAAATAAGCAAgCATTG CATATTTTCCAAATTTTGA		78.3 °C	mutagenesis primer, <i>Schsv2</i> T292A
RB88	TCAAAAATTTGAAAATATGCAATGcTTGC TTATTTGACAATACGGCAA		78.3 °C	mutagenesis primer, <i>Schsv2</i> T292A
RB89	GCCGTATTGTCAAATAAGCAAACATTgcT ATTTTCCAAATTTTGAACAACCAA		78.32 °C	mutagenesis primer, <i>Schsv2</i> H294A
RB90	TTGGTTGTTTCAAAAATTTGAAAATAgcC AATGTTTGCTTATTTGACAATACGGC		78.32 °C	mutagenesis primer, <i>Schsv2</i> H294A
RB91	ATTTAGAAGAGGGGTGGACgcGGCGGATAT TTACGAGATG		78.08 °C	mutagenesis primer, <i>Schsv2</i> K269A
RB92	CATCTCGTAAATATCCGCCgcGTCCACCCC TCTTCTAAAT		78.08 °C	mutagenesis primer, <i>Schsv2</i> K269A
RB93	CAAGCATCGCAGTCACAGTCTAAATCTTAG			sequencing primer for <i>ScHsv2</i> mutants
RB94	GCATAACGGTACTTTAATCAAAGAATTTAc AAcAGGGGTGGACAAGGC		80.35 °C	mutagenesis primer, <i>Schsv2</i> FTTG
RB95	GCCTGTCCACCCCTgTTgTAAATCTTTGAT TAAAGTACCGTTATGC		80.35 °C	mutagenesis primer, <i>Schsv2</i> FTTG
RB96	AACGGTACTTTAATCAAAGAATTTGCAgcA GGGGTGGACAAGG		78.31 °C	mutagenesis primer, <i>Schsv2</i> FAAG

Name	Sequence 5'-3'	Properties	Tm	Aim
RB97	CCTTGTCACCCCTgcTGCAAATCTTTGA TTAAAGTACCGTT		78.31 °C	mutagenesis primer, <i>Schsv2</i> FAAG
RB98	attggtCCCGGGATGAAGTCTACATTTAAGTCT GAATATCCATTTGAAAAAAGG	<i>XmaI</i>	61 °C	fwd primer to amplify <i>Scatg8</i>
RB99	aacaatCCATGGTTATTTTTCGAACTGCGGGT GGCTCCAGGTCGTTGGGATATCGTAATCGC CCTGAAAATACAGG	<i>NcoI</i> , StrepII tag, TEV cleavage site	61 °C	rev primer for RB98, second PCR primer with RB98
RB100	GGATATCGTAATCGCCCTGAAAATACAGGT TTTCTGTGATGCCAAATGTATTTTCTCCTG AGTAAGTGACATAC		60 °C	rev primer for RB98, first PCR primer with RB98
RB101	aacaatCCATGGTTATTTTTCGAACTGCGGGTG GCTCCATGTGATGCCAAATGTATTTTCTCCT GAGTAAGTGACATAC	<i>NcoI</i> , StrepII tag	61 °C	rev primer for RB98
RB104	attggtCCCGGGATGTGGAGCCACCCGACGT TCGAAAAAGATTACGATATCCCAACGACCG AAAACCTGTATTTTC	<i>XmaI</i> , StrepII tag, TEV cleavage site	60 °C	fwd primer to amplify <i>Schsv2</i> , second PCR primer with RB106
RB105	GATATCCCAACGACCGAAAACCTGTATTTT CAGGGCATCACAATGGATGTTTCGTCGACCT ATAAGGGAG		60 °C	fwd primer to amplify <i>Schsv2</i> , first PCR primer with RB106
RB106	attggtCTCGAGTTAAAGCTCTCTCCATGAT TCTCTCACC	<i>XhoI</i>	60 °C	rev primer for RB104 and RB105
RB109	ttaggatCATATGATGAGCCTGCTCGGGCGC	<i>NdeI</i>	60 °C	fwd primer to amplify <i>Dmatg18</i>
RB110	ttaggatCTCGAGTTAAGCACCTTTGATATCC ATGGCATAGTGG	<i>XhoI</i>	60 °C	rev primer for RB109
RB117	ACGGAGTACTGGTCCGTGAATTTGCTGCTG GACTGGACCG		78.20 °C	mutagenesis primer for <i>KlHSV2</i> FAAG
RB118	CGGTCCAGTCCAGCAGCAAATTCACGGACC AGTACTCCGT		78.20 °C	mutagenesis primer for <i>KlHSV2</i> FAAG
RB119	GACAACGGAGTACTGGTCCGTGAATTTACT ACTGGACTGGACCGTA		78.63 °C	mutagenesis primer for <i>KlHSV2</i> FTTG
RB120	TACGGTCCAGTCCAGTAGTAAATTCACGGA CCAGTACTCCGTTGTC		78.63 °C	mutagenesis primer for <i>KlHSV2</i> FTTG
RB121	GAAGTGTTCAATGACGCCGAGAATGAAGAC GATGTGCTGAAAGATTGGATCAAC		79.06 °C	mutagenesis primer for <i>KlHSV2</i> K260E/R261D/H262D
RB122	GTTGATCCAATCTTTCAGCACATCGTCTTC ATTCTCGGGTCAATTGAACACTTC		79.06 °C	mutagenesis primer for <i>KlHSV2</i> K260E/R261D/H262D
RB123	CCATGTGCTGAAAGATTGGATCAACATCAA AGATGACCAAAGTGAATGGAGC		78.52 °C	mutagenesis primer for <i>KlHSV2</i> Y272D/F273D
RB124	GCTCCATTCACCTTGGTCATCTTTGATGTT GATCCAATCTTTCAGCACATGG		78.52 °C	mutagenesis primer for <i>KlHSV2</i> Y272D/F273D
RB125	TGAAAGATTGGATCAACATCAAAGATTTC AAAGTGAATGGAGCATC		78.97 °C	mutagenesis primer for <i>KlHSV2</i> Y272D
RB126	GATGCTCCATTCACCTTGGAAATCTTTGAT GTTGATCCAATCTTTC		78.97 °C	mutagenesis primer for <i>KlHSV2</i> Y272D

Name	Sequence 5'-3'	Properties	Tm	Aim
RB127	GTGCTGAAAGATTGGATCAACATCAAATAT GACCAAAGTGAATGGAGC		78.65 °C	mutagenesis primer for <i>Kl<sub>hsv2</sub></i> F273D
RB128	GCTCCATTCACTTTGGTCATATTTGATGTT GATCCAATCTTTCAGCAC		78.65 °C	mutagenesis primer for <i>Kl<sub>hsv2</sub></i> F273D
pFL fwd	GGTCCGTATACTAGTATCGATTCCGCGACC			sequencing primer for pFL cloning
pFL rev	CAATTGCATTCAATTTTATGTTTCAGGTTC AGGGG			sequencing primer for pFL cloning

## 2.2 Methods

### 2.2.1 Molecular cloning

Standard methods were used for molecular cloning. **PCR**'s were done with the Phusion High-Fidelity PCR kit and the provided manual was followed. Elongation time was adjusted to template length (30 sec per 1 kb). Furthermore the annealing temperature was chosen according to the melting temperature of the primers (see table 2.9).

**Table 2.9:** PCR reaction

Master Mix		PCR program	
Component	50 $\mu$ l reaction	Cycle step	Settings
water	36.5 $\mu$ l	1 - initial denaturation	95 °C, 30 sec
5x HF or GC buffer	10 $\mu$ l	2 - denaturation	95 °C, 30 sec
10 mM dNTP	1 $\mu$ l	3 - annealing	55 – 60 °C, 30 sec
10 $\mu$ M P fwd	0.5 $\mu$ l	4 - elongation	72 °C, 30 sec/kb
10 $\mu$ M Prev	0.5 $\mu$ l	jump to step 2	for 30 cycles
template DNA	1 $\mu$ l (10 ng)	5 - final extension	72 °C, 10 min
Phusion DNA polymerase	0.5 $\mu$ l	6 - hold	4 °C, $\infty$

PCR products were extracted from 1 % (w/v) **agarose gels** using the NucleoSpin Extract II kit. Agarose gel check of Bacmids prior transfection was done on 0.8 %



(w/v) agarose gels. Before loading, samples for agarose gels were supplemented with reasonable amounts of 6x loading dye (0.25 % (w/v) bromphenol blue, 0.25 % (w/v) xylene cyano, 30 % (v/v) glycerol in H<sub>2</sub>O). TBE (10x: 108 g/l (w/v) Tris, 55 g/l (w/v) boric acid, 40 ml/l (v/v) of a 5.5 M EDTA stock) or TAE (50x: 242 g/l (w/v) Tris, 57,1 ml/l (v/v) glacial acetic acid, 100 ml/l (v/v) of a 0.5 M EDTA stock) buffer was used for agarose gel electrophoresis.

In a next step, **restriction digestion** was carried out with restriction enzymes from NEB. PCR products were usually resuspended in a total of 50  $\mu$ l. To this 5  $\mu$ l buffer (0.5  $\mu$ l BSA) and 1  $\mu$ l of each enzyme were added. For control digestions after cloning a reaction of 30  $\mu$ l volume were set up containing 5  $\mu$ l purified plasmid, 3  $\mu$ l buffer, 1  $\mu$ l of each enzyme, 0.3  $\mu$ l BSA, if required, and 25  $\mu$ l water.

T4 DNA ligase was used for **ligation** reactions. For this purpose, usually 50 ng of vector was used. Amount of insert was calculated in a way that insert was available in a three times molar excess. A final volume of 20  $\mu$ l was set up with 2  $\mu$ l 10x buffer and 1  $\mu$ l T4 DNA ligase. The reaction was incubated for 30 min at RT.

**Mutagenesis** of ScHsv2 was done using the QuickChange II site-directed mutagenesis kit and for KIHsv2 the QuickChange Lightning site-directed mutagenesis kit was used. The PCR mix contained 5  $\mu$ l 10x reaction buffer, 2  $\mu$ l of 10 ng/ $\mu$ l dsDNA template, 1  $\mu$ l oligonucleotide primer 1 (125 ng), 1  $\mu$ l oligonucleotide primer 2 (125 ng), 1  $\mu$ l dNTP mix, 40  $\mu$ l H<sub>2</sub>O and 1  $\mu$ l PfuUltra HF DNA polymerase (2.5 U/ $\mu$ l). The PCR reaction was run with the following program 95 °C for 30 sec as initial denaturation step, then 16 cycles of 95 °C for 30 sec, 55 °C for 1 min and 68 °C for 6 min and 30 sec (1 min/kb) was done. The temperature was held at 16 °C. Afterwards, template DNA was degraded by *DpnI*-treatment. Finally the PCR product was transformed with *E. coli* XL1-blue supercompetent cells.

**Recombination** was used for insect cell vectors like pFL and pUCDM as well as ACEMBL vectors (pACE, pDK) contain a loxP site. Here, a total of 2  $\mu$ g per vector was mixed with 1  $\mu$ l **Cre recombinase** and 2  $\mu$ l of its supplied buffer. The total volume of these reactions were 20  $\mu$ l and they were incubated for 2 hours at 37 °C.

**Heat shock transformation** was done with 100  $\mu$ l chemocompetent *E. coli* XL1-blue or DH5 $\alpha$  cells. They were incubated with plasmid for 20 min on ice, then heat shock was done at 42 °C for 1 min. Cells were incubated for a few minutes on ice again, before 900  $\mu$ l of pre-warmed LB or SOC media was added and the culture was incubated at 37 °C for 1 hour. After this the culture was centrifuged for 3 min at 7,000 rpm and plated on LB plates with the appropriate antibiotics. Heat competent *E. coli* cells were

prepared according to Hanahan [43] and high efficiency electro competent *E. coli* DH10 MultiBac were prepared following the protocol from Dower [44].

**Plasmid preparation** was done using the NucleoSpin Plasmid kit. Afterwards a control restriction digestion or colony-PCR was performed. For colony-PCR a PCR reaction as described in table 2.9 was pipetted and then a colony was touched with a pipette tip and swirled in the PCR reaction.

## 2.2.2 Methods for insect cell culture

### 2.2.2.1 Insect cell culture

Insect cells were cultured in a room kept at a constant temperature of 27 °C since insect cells are highly sensitive to temperature changes. These cells can be cultured as suspension culture in autoclaved glass flasks with screw cap or as adherent culture in 6-well plates. When the insect cells are cultivated in flasks their densities should be kept at  $1 \times 10^6$  cells/ml.

For this study *Spodoptera frugiperda* (Sf21 and Sf9) cells were used to generate virus (virus generation  $v_0$ ) through transfection with bacmid (2.2.2.3) and to increase virus titer (virus generations  $v_1$  and  $v_2$ ). These cells were cultivated in Sf900 media. *Trichoplusia ni* (High5) cells were used for protein expression and cultured in ExpressFive media supplemented with 20 mM final concentration of glutamine.

Media containing the budded virus can be stored in sterile plastic bottles for a few weeks at 4 °C. For insect cell culture no antibiotics are used therefore special care and sterile handling is necessary and all work was done in a sterile hood.

### 2.2.2.2 Bacmid extraction from *E. coli* DH10

In order to prepare bacmid for transfection of insect cells, 7 ml LB media supplemented with kanamycin, tetracyclin and gentamycin were inoculated with *E. coli* DH10 MultiBac and incubated over night. Cells were harvested by spinning the culture at 4,500 rpm for 10 min at 4 °C. Pellet was resuspended in 250  $\mu$ l buffer A1 from Nucleospin plasmid kit. 250  $\mu$ l buffer A2 were added and the tubes inverted for mixing. After adding 300  $\mu$ l buffer A3 tubes were inverted again and centrifuged at 4,500 rpm for 10 min at 4 °C. Supernatant is transferred into a new 2 ml tube and spun again at 13,000 rpm for 10 min at 4 °C. For precipitation of the bacmid the supernatant is again transferred into a new 2 ml test tube, 800  $\mu$ l 2-propanol are added to the supernatant and

mixed very well by inverting. Precipitated bacmid is pelleted through centrifugation at 13,000 rpm for 30 min at 4 °C. Pellet is washed twice with 1 ml of 70 % ethanol. Dry the pellet with open lid at room temperature. The dried pellet is resuspended in 20  $\mu$ l sterile MilliQ water. The bacmid can be stored at 4 °C for a few days [45].

### 2.2.2.3 Transfection of insect cells

Cells were plated into a 6-well plate at a concentration of  $0.25 \times 10^6$  cells per ml in a total of 3 ml and kept for 30 min until cells settled. In the mean time, 18  $\mu$ l bacmid was mixed with 200  $\mu$ l Sf900 media through gentle bubble generation with pipette (no up and down pipetting). In an additional test tube 20  $\mu$ l Fugene was mixed in the same way with 200  $\mu$ l media. Both test tubes were incubated for 5 min at RT (here: RT = 27 °C). Afterwards Fugene-mix was added to the bacmid-mix by slowly releasing the mix starting at the bottom and go up in circles with the pipette. Additional bubbles can be created for mixing. After 1 hour 200  $\mu$ l of this mix can be added per well to the insect cells. Usually as control one well was not transfected and in a second well only media was plated as contamination control.

### 2.2.2.4 Pull down of infected insect cells

A pull down of infected insect cells was routinely performed after transfection of insect cells, when the first virus generation ( $v_0$ ) was harvested. This method was used as first to test the expression level of the protein and its solubility.

Therefore adherent insect cells were washed with PBS and resuspended in 0.5 ml PBS per well. Supernatant of wells with same conditions were pooled to increase protein amounts. Then cells were lysed using a Branson Sonifier 450 sonicator with an amplitude of 20 % for some seconds. From this whole cell extract 50  $\mu$ l were taken for SDS-PAGE analysis. Whole cell extract was centrifuged for 3 min at full speed and from the supernatant another 50  $\mu$ l were taken for analysis.

In order to perform the pull down 20  $\mu$ l Ni-NTA beads are taken and washed with water and buffer (spin 1 - 2 min, 2,000 rpm). Afterwards the supernatant is put on the beads and incubated for 30 min at 4 °C. Unbound protein in the supernatant is removed by spinning at low speed.

The samples with whole cell extract, supernatant and bead fraction are supplemented with 25  $\mu$ l 3x sample buffer, heated for 3 min at 95 °C and analyzed on SDS-PAGE (2.2.6.1).

The same procedure applies for streptactin beads.

### 2.2.2.5 Measuring YFP in infected insect cells

YFP is encoded by the bacmid and is therefore expressed at the same time as protein necessary for virus budding. Comparable to YFP expression is the expression of the gene of interest, since both are regulated by a late stage virus expression promoter. Therefore YFP levels are a direct indicator for virus gene expression and is generally measured from infected High5 insect cells in order to determine the maximum protein level.

Supernatant from  $1 \times 10^6$  insect cells was prepared in the same way as described in 2.2.2.4. From this a dilution series of 200  $\mu$ l undiluted supernatant, 1:5 dilution and 1:25 dilution was prepared in a black flat bottom 96-well plate (Greiner). As a control 200  $\mu$ l PBS was used. Fluorescence was measured with a Victor 3V (Perkin Elmer) at 495 nm excitation and 520 nm emission wavelength.

## 2.2.3 Purification protocols of protein complexes from insect cells

### 2.2.3.1 MAP1LC3

Human MAP1LC3 (1-120) was expressed together with full length human Atg3 and Atg7 in insect cells. Sf21 and Sf9 cells were used for virus generation, High5 insect cells were infected for large scale expression of 1 l culture divided into 5 flasks.

Best purification results were achieved for LC3 purification, when freshly harvested High5 insect cells were used, harvested 48 hours after day of proliferation arrest (DPA). Cells were harvested by centrifugation at 1,000 rpm for 20 min, 4 °C and resuspended in buffer (50 mM  $\text{NaH}_2\text{PO}_4$  pH 8.0, 300 mM NaCl, 30 mM imidazole). Cell lysis was induced using a Branson Sonifier 450 sonicator with an amplitude of 20 % for 30 sec, followed by addition of 1 mM final concentration of  $\text{MgCl}_2$ , a protease inhibitor pill, lysozyme, DNaseI and 2 % Triton X-100. The sample was incubated for 20 min on a head-over rotator, 4 °C and then spun in a Sigma centrifuge at 4,000 rpm, 30 min, 4 °C.

In the mean time  $\text{Ni}^{2+}$ -sepharose beads were prepared by washing two times with water and equilibration twice with buffer. Beads were only spun at low speed (2,000

rpm, 1 min). 1 ml Ni<sup>2+</sup>-sepharose beads were added to the supernatant and incubated for 2 hours, rotating at 4 °C. 5 ml resuspension buffer was used for washing the beads and this step was four times repeated. For elution of the protein the same buffer with 500 mM imidazole was used. Four times 1 ml elution buffer was subjected onto the beads. Elution fractions were snap frozen and stored at -80 °C.

The purification efficiency was analyzed by SDS-PAGE of whole cell extract, supernatant, pellet, flow through, washing steps and elution fractions.

### 2.2.3.2 Atg5-Atg12

Full length Atg5, Atg12, Atg7 and Atg10 from human were co-expressed using the MultiBac baculovirus system. Sf9 and Sf21 insect cells were used for virus production. High5 insect cells were infected for large scale protein expression. Usually a 1 l culture was grown subdivided into five 2 l flasks.

Atg5-Atg12 conjugate was purified from freshly harvested High5 insect cells, 48 hours after DPA. After centrifugation of these cells at 1,000 rpm for 20 min, 4 °C, the pellet was resuspended in buffer (50 mM NaH<sub>2</sub>PO<sub>4</sub> pH 8.0, 300 mM NaCl, 30 mM imidazole). Insect cells were lysed using a Branson Sonifier 450 sonicator with an amplitude of 20 % for 30 sec. Then one tablet of protease inhibitors, 1 mM final concentration of MgCl<sub>2</sub>, lysozyme and DNaseI as well as 2 % Triton X-100 were added. The cell suspension was incubated for 20 min, 4 °C in a head-over rotating wheel. Then soluble and insoluble fractions were divided by centrifugation in a Sigma centrifuge at 4,000 rpm, 30 min, 4 °C.

The obtained supernatant was incubated with 1 ml Ni<sup>2+</sup>-sepharose beads for 2 hours on a rotator, 4 °C. Preparation of Ni<sup>2+</sup>-sepharose beads was done by washing first twice with water and then twice with buffer. In between beads were spun at 2,000 rpm for 1 min. After the incubation time the bead-supernatant suspension was spun at 2,000 rpm, for 2 min, 4 °C. Thereafter beads were washed four times with 5 ml buffer, followed by protein elution in buffer supplemented with 500 mM imidazole. Five times 1 ml elution buffer was added. Afterwards elution fractions were snap frozen in liquid nitrogen and stored at -80 °C.

Samples taken during the purification process were analyzed by SDS-PAGE.

### 2.2.3.3 Increase of solubility of Atg5-Atg12 using a detergent screen

A Ni-NTA membrane protein kit (Qiagen) containing seven different detergents was employed to test if higher amounts of soluble protein can be obtained. This kit comprises the detergents octyl- $\beta$ -D-glucopyranoside (DG), n-dodecyl- $\beta$ -D-maltopyranoside (DM), N, N-Dimethyldodecylamine-N-oxide (lauryldimethylamine-N-oxide, LDAO), n-dodecyl- $\beta$ -D-maltoside (DDM), Cymal 6 (Cy6), n-Nonyl- $\beta$ -D-glucopyranoside (NG) and FOS-choline-16 (FOS).

High5 insect cells expressing Atg5-Atg12 were prepared by resuspension of the cells in TS-buffer provided in the kit and incubated on ice for 30 min with DNaseI. Cell extract was divided into seven 200  $\mu$ l aliquots and spun (Fresco centrifuge, maximum speed, 1 hour, 4°C) to obtain the insoluble membrane fraction (pellet). The obtained pellet was resuspended in the provided NTI-10-G-buffer (volumes can be taken from table 2.10) and detergent was added. The samples were incubated in an end-over-end shaker for 1 hour at RT. Afterwards 10  $\mu$ l samples were taken for immunoblotting. Another sample was taken after centrifugation for 1 hour, full speed, at 4°C in a fresco centrifuge.

Samples of cell extract and supernatant were analyzed by SDS-PAGE and Western blotting.

**Table 2.10:** Buffer and detergent stock solution volumes for screening

Detergent	Vol. Buffer NTI-10-G	Vol. detergent	Final detergent concentration
OG	457 $\mu$ l	43 $\mu$ l	51 mM
DM	430 $\mu$ l	70 $\mu$ l	21 mM
LDAO	432 $\mu$ l	68 $\mu$ l	30 mM
DDM	421 $\mu$ l	79 $\mu$ l	20 mM
Cy6	424 $\mu$ l	76 $\mu$ l	20 mM
NG	441 $\mu$ l	59 $\mu$ l	33 mM
FOS	421 $\mu$ l	79 $\mu$ l	1.3 mM

## 2.2.4 Purification protocols for PROPPINs

### 2.2.4.1 Batch purification for test expression

For this purpose, 2 ml of expression culture were spun in a centrifuge for 2 min at 13,000 rpm. The pellet was resuspended in buffer (50 mM NaH<sub>2</sub>PO<sub>4</sub> pH 7.5, 300 mM NaCl, 30 mM imidazole). Then cells were lysed using a sonicator at low intensity for a few seconds. Afterwards soluble and insoluble fractions were separated by centrifugation for 10 min at 13,000 rpm. The supernatant was transferred into a new Eppendorf tube. 20  $\mu$ l beads per sample were prepared by spinning at low speed (2,000 rpm, 1 min). Then beads were washed with water and equilibrated with buffer. Supernatant was added to beads and incubated for 30 min on a rotating wheel at 4 °C. Afterwards beads were washed two times with buffer. Finally 20  $\mu$ l of 3x sample buffer were added and heated for 3 min at 95 °C. SDS-PAGE was performed with cell extract, supernatant, pellet and bead fraction.

### 2.2.4.2 Purification protocol for ScAtg18

Synthetic genes for ScAtg18 and ScAtg21 were ordered from Mr. Gene GmbH and codon usage was optimized for insect cell expression. As transfer vector for bacmid integration pFL was used. Virus was generated using Sf21 insect cells, protein expression and purification was done using High5 insect cells. After infection of High5 cells it took 48 hours for optimal protein expression (see also 4.2.1.1). At this time point High5 insect cells were harvested.

After harvesting through spinning of the cell suspension at 1,000 rpm for 20 min, 4 °C, the pellet is resuspended in 80 ml buffer A (see table 2.11). One protease inhibitor tablet, 1 mM final concentration of MgCl<sub>2</sub> and DNaseI was added to the resuspended cells. Cells were opened by sonication with a Biorupter for 3 times 5 min at a duration of 30 sec ultrasound and 30 sec pause. After sonication 1 % final concentration of Triton X-100 was added and everything incubated stirring for 25 min, at 4 °C. Cell extract was spun for 1 hour at 14,000 rpm, 4 °C in a Du Pont Sorvall centrifuge with a SS-34 rotor. Phytic acid powder at a final concentration of 2 mM was added to the supernatant.

In the same time 4 ml Ni<sup>2+</sup>-sepharose beads were prepared by washing once with water and twice with buffer A for equilibration. Beads were spun at 2,000 rpm for 1 min at RT. Supernatant was incubated with beads for 2 hours at 4 °C, rotating. Then beads were separated from unbound solution by spinning in a Sigma centrifuge for 10 min,

2,000 rpm at 4 °C. Using 3 times 30 ml buffer A the beads were washed, incubated for 10 min at 4 °C, rotating in between and then spun in the centrifuge. Next, beads were resuspended with 5 ml buffer A and put in a membrane column. For elution 3 times 5 ml buffer B (see table 2.11) were applied onto the beads and carefully resuspended. After beads settled again, the column was opened for buffer B to run through. Fractions were checked with SDS-PAGE.

**Table 2.11:** Buffers for purification of ScAtg18 from insect cells

His-Trap purification		gel filtration
Buffer A	Buffer B	
50 mM NaH <sub>2</sub> PO <sub>4</sub>	50 mM	50 mM NaH <sub>2</sub> PO <sub>4</sub>
500 mM NaCl	500 mM NaCl	500 mM NaCl
30 mM imidazole	500 mM imidazole	
pH 8.5	pH 8.5	pH 8.5

Buffers used for protein purification were filtered and degased.

Elution fractions 1 to 3 were pooled and diluted in gel filtration buffer to decrease the imidazole concentration. Then batch purified protein was loaded on an 1 ml His-Trap FF column (GE Healthcare) for further purification. Protein was loaded with a 50 ml Superloop and then the column was washed with buffer A for 10 CV before protein was eluted with an imidazole gradient over 10 CV to a final concentration of 100 % B. Column was run at 1 ml/min.

After another SDS-PAGE check fractions containing the protein were pooled and concentrated to 500  $\mu$ l final volume. The sample was loaded on a Superdex 200 10/300 GL (GE Healthcare) column. Size exclusion chromatography was done at 0.5 ml/min and 500  $\mu$ l fractions were collected. Afterwards SDS-PAGE check was performed.

His-tagged ScHsv2 was concentrated with a Vivaspin 2, 30,000 MWCO (Sartorius) concentrator to a final concentration of 5 mg/ml and directly subjected to crystallization screens.

#### 2.2.4.3 Purification of PaAtg18, DmAtg18, CeAtg18, KlAtg21 and PaAtg21

DmAtg18 was ordered from the Drosophila Genomics Resource Center (No. CG7986) and cloned into pET-28a vector. The other proteins were ordered from GeneArt (In-



vitrogen) as synthetic genes and the codon sequence was optimized for expression in bacteria. The genes were cloned into pET-28a vector for expression with a 6x His-tag. Additionally PaAtg18, PaAtg21 and KlAtg21 were cloned into pACE-His vector for later co-expression experiments with PaAtg8 and KlAtg8 [46].

For each construct 9 l autoinducible media were inoculated from a LB over night culture and incubated for 3 hours at 37 °C. Afterwards the temperature was shifted to 22 °C for 20 to 24 hours. The culture was harvested using the JS-4.2 rotor in a Beckman J6-MI centrifuge for 20 min at 4,000 rpm at 4 °C. Resuspension of the cell pellet was done in 150 ml buffer A (see table 2.12) on a horizontal shaker. After this 1 mM final concentration MgCl<sub>2</sub>, a protease inhibitor tablet, DNaseI and lysozyme were added. The cell suspension was incubated with a stir bar on a magnetic-stirrer device. Then sonication with a Branson Sonifier 450 sonicator using a duty cycle of 70, the output control set to the microtip limit which yielded an output of 20 - 30 % for 5 cycles of 30 sec sonication and 30 sec break on ice was performed. Or a microfluidizer M-110L (Microfluidics Corporation) was used with 3 repetitions. Afterwards 1 % Triton X-100 was added to DmAtg18 and CeAtg18 cell lysate. Lyzed cells were incubated stirring for another 10 min and then spun at 14,000 rpm for 1 h at 4 °C in a SS-34 rotor in a Du Pont Survall centrifuge to remove cell debris.

Cleared cell lysate was subjected to a 5 ml His-Trap FF column (GE Healthcare) with 1 ml/min. Loading the supernatant was done with a 150 ml Superloop (GE Healthcare), then the column was washed with buffer A for 20 CV with 2 ml/min, followed by an elution gradient over 20 CV with 1 ml/min from buffer A to buffer B. A final elution step with 5 CV buffer B was applied. Elution fractions were checked with SDS-PAGE and purified protein containing fractions were pooled. Over night the protein was dialyzed with gel filtration buffer (see table 2.12). The purified protein sample was concentrated to a final volume of 5 ml with Vivaspin 20, 30,000 MWCO (Sartorius) concentrators.

In addition to the affinity purification of this proteins size exclusion chromatography was done. For this a HiLoad 16/60 Superdex 200 prep grade or HiLoad 16/60 Superdex 75 prep grade was employed connected to an Äkta Prime or Äkta Purifier FPLC system. Here dialyzed protein was loaded with a 5 ml loop and the gel filtration run was done for 1.1 CV at 1 ml/min. After 0.3 CV the fraction collector was started and 2 ml fractions were collected. Fractions containing protein indicated by UV<sub>280</sub> detection were checked with SDS-PAGE. Fractions containing the protein of interest were pooled and concentrated to a concentration of approximately 30 mg/ml, then aliquoted, snap frozen in liquid nitrogen and stored at -80 °C.

**Table 2.12:** Buffers for purification of PaAtg18, DmAtg18, CeAtg18, KlAtg21 and PaAtg21

PROPPIN	His-Trap purification		gel filtration
	Buffer A	Buffer B	
PaAtg18	30 mM Hepes 300 mM NaCl 30 mM imidazole pH 7.0	30 mM Hepes 300 mM NaCl 500 mM imidazole pH 7.0	30 mM Na-lactate 300 mM NaCl 1 mM DTT pH 4.0
DmAtg18	30 mM MES 300 mM NaCl 30 mM imidazole pH 5.8	30 mM MES 300 mM NaCl 500 mM imidazole pH 5.8	30 mM Na-lactate 300 mM NaCl 1 mM DTT pH 5.2
CeAtg18	30 mM Tris 300 mM NaCl 30 mM imidazole pH 8.0	30 mM Tris 300 mM NaCl 500 mM imidazole pH 8.0	30 CHES 300 mM NaCl 1 mM DTT pH 8.0
KlAtg21	30 mM MES 300 mM NaCl 30 mM imidazole pH 5.8	30 mM MES 300 mM NaCl 500 mM imidazole pH 5.8	30 mM MES 300 mM NaCl 1 mM DTT pH 5.8
PaAtg21	30 mM MES 300 mM NaCl 30 mM imidazole pH 5.8	30 mM MES 300 mM NaCl 500 mM imidazole pH 5.8	30 mM MES 300 mM NaCl 1 mM DTT pH 5.8

Buffers used for protein purification were filtered and degased.

#### 2.2.4.4 Purification protocol for SpHsv2

SpHsv2 was expressed with an N-terminal 6x His-tag from the pET-28a expression vector in *E. coli* BL21(DE3). 9 l culture of LB media with kanamycin was inoculated 1:100 with an over night pre-culture. The culture was incubated at 37 °C, shaking until it reached an OD of 0.6. At this time point 1 mM final concentration of IPTG was added to induce expression of *SpHsv2* from the vector. IPTG is a molecular mimic of allolactose and activates the lac-UV promoter of T7-RNA polymerase which then activates the T7

promoter present in pET-28a vector. When IPTG was added temperature was shifted to 25 °C and the culture was incubated over night.

After approximately 20 hours the culture was harvested using the JS-4.2 rotor in a Beckman J6-MI centrifuge for 20 min at 4,000 rpm, 4 °C. The pellet was resuspended in 90 ml buffer A (see table 2.13). Then 1 mM final concentration of MgCl<sub>2</sub>, DNaseI powder, lysozyme powder and a protease inhibitor tablet were added and mixed on a stirring device for 15 min. Cells were lysed using the Branson Sonifier 450 with the same settings as above mentioned for 5 times 30 sec sonication and 30 sec break in between. The lysate was kept on ice during sonication. Further incubation of the lysate provided time for DNaseI and lysozyme activity. Finally, cell debris and soluble protein fraction were separated during centrifugation using the SS-34 rotor.

**Table 2.13:** Buffers for purification of SpHsv2 from *E. coli* BL21(DE3) cells

His-Trap purification		gel filtration
Buffer A	Buffer B	
50 mM NaH <sub>2</sub> PO <sub>4</sub>	50 mM NaH <sub>2</sub> PO <sub>4</sub>	30 mM Citric acid
500 mM NaCl	500 mM NaCl	500 mM NaCl
30 mM imidazole	500 mM imidazole	
pH 7.5	pH 7.5	pH 5.5

Buffers used for protein purification were filtered and degased.

In a next step, supernatant was applied to a 5 ml His-Trap FF column (GE Healthcare) using a 150 ml Superloop. After loading the column was washed with buffer A for 20 CV to remove unspecific bound protein. Then a gradient of imidazole for elution was run over the column using buffer A and B (see table 2.13). A final elution step of 5 CV 100 % buffer B was applied to remove all remaining protein from the column. All steps were done at a flow rate of 1 ml/min.

The protein was then dialyzed over night into gel filtration buffer and concentrated (Vivaspin 20, cut off 30,000 MW; Sartorius) to a final volume of 5 ml. Either of the two HiLoad Superdex 200 or 75 prep grade columns were used and run at 1 ml/min for 1.1 CV, 0.3 CV without fraction collection and 0.8 CV with collection of 2 ml fractions. Fractions containing protein were pooled and concentrated to 30 mg/ml, then aliquoted, snap frozen in liquid nitrogen and stored at -80 °C.

DTT was added to the gel filtration buffer to avoid dimerization of the protein (compare section 4.2.1.3).

#### 2.2.4.5 Purification protocol for ScHsv2 and mutants

ScHsv2 and mutants were expressed from the pGEX-4T3 vector with an N-terminal GST-tag and a thrombin cleavage site between the tag and ScHsv2. *E. coli* BL21(DE3) carrying the respective vector was cultivated in 1.5 l autoinducible media and inoculated with 10 ml from an over night LB pre-culture. The culture was incubated for 3 hours at 37 °C and then shifted for 20 to 24 hours to 22 °C. Harvesting was done for 20 min at 4,000 rpm at 4 °C using the JS-4.2 rotor in a Beckman J6-MI centrifuge.

Pellets were resuspended each in 15 ml buffer A (see table 2.14) by incubation on a horizontal shaker for 20 min. Afterwards DNaseI, lysozyme, a protease inhibitor tablet and MgCl<sub>2</sub> at a final concentration of 1 mM were added and everything incubated stirring for 15 min. Then a Branson Sonifier 450 sonicator using a duty cycle of 70 and the output control set to the microtip limit which yielded an output of 20 - 30 % was used for cell opening, while cells were kept on ice during sonication. Or a microfluidizer M-110L (Microfluidics Corporation) was used with 3 repetitions. The lysed cells were incubated on a stirrer for 10 min. Following this the cell lysate was spun in a centrifuge (Du Pont Sorvall) with a SS-34 rotor for 1 hour, 14,000 rpm, at 4 °C.

**Table 2.14:** Buffers for purification of ScHsv2 from *E. coli* BL21(DE3) cells

GSTrap purification		gel filtration
Buffer A	Buffer B	
30 mM Hepes	30 mM Hepes	30 mM Hepes
300 mM NaCl	300 mM NaCl	300 mM NaCl
	20 mM Glutathione	
pH 7.0	pH 7.0	pH 7.0

Buffers used for protein purification were filtered and degased.

Using a 50 ml Superloop (GE Healthcare) the supernatant was applied to a 5 ml GSTrap FF column (GE Healthcare) connected to the Äkta Prime FPLC system or Äkta Purifier FPLC system. After loading the supernatant with 2 ml/min, the column was washed with 20 CV buffer A and then bound protein was eluted with 5 CV buffer

B containing glutathione (see table 2.14) with 2 ml/min. Elution fractions containing the protein were collected and pooled.

Over night the affinity purified protein was dialyzed with buffer A and 200  $\mu$ l thrombin (1 U/ $\mu$ l) were added for cleavage of the GST-tag. On the next day thrombin activity was blocked by adding Pefabloc (0.4 mM final concentration), the protein was loaded on the GSTrap column and flow through was collected, which contained the cleaved protein. Uncleaved protein and free GST bound to the column. Flowthrough fractions were pooled and concentrated to a final volume of 5 ml (Vivaspin 20, cut off 30,000 MW; Sartorius).

An additional purification step was implemented. Here, size exclusion chromatography (HiLoad 16/60 Superdex S200 or S75 prep grade) was used to improve purity. For this, the same buffer as buffer A was used at 1 ml/min. After each purification step the protein fractions were checked with SDS-PAGE. Finally purified protein fractions were pooled, aliquoted and snap frozen in liquid nitrogen. The purified protein was stored at  $-80^{\circ}\text{C}$ .

#### 2.2.4.6 GST SpinTrap purification of ScHsv2 and mutants

GST SpinTrap purification was performed for wild type ScHsv2 and ScHsv2 mutants in order to obtain freshly purified protein for PIPstrip analyses.

20 ml cultures of *E. coli* BL21(DE3) carrying the respective plasmids were grown in 50 ml autoinducable media. Cultures were incubated 3 hours at  $37^{\circ}\text{C}$  and then for another 20 hours at  $22^{\circ}\text{C}$ . From each culture 12 ml were harvested in a Sigma centrifuge at 4,000 rpm, 10 min,  $4^{\circ}\text{C}$ . Then the pellet was resuspended in 2 ml Hepes buffer (20 mM Hepes pH 7.0, 300 mM NaCl). Since the same buffer was used for several cultures at a time it was supplemented with a protease inhibitor tablet, 1 mM  $\text{MgCl}_2$ , DNaseI and lysozyme before resuspension. After 10 min incubation cells were sonicated using a Branson Sonifier 450 sonicator with a duty cycle of 70, the output control set to the microtip limit which yielded an output of 20 - 30 % for one cycle of 30 sec sonication on ice. After another 10 min incubation on ice cells were spun in a Du Pont Sorvall centrifuge with a SS-34 rotor for 30 min at 14,000 rpm,  $4^{\circ}\text{C}$ .

In the mean time GST SpinTrap columns were prepared by first shaking the column to resuspend the resin. Then the column was opened at the bottom and spun to remove the storage liquid (1500 rpm, 30 sec). Afterwards the top cap was removed and the column equilibrated with 600  $\mu$ l Hepes buffer. Column was spun at 1,500 rpm for 30

sec. Then in three steps of 600  $\mu$ l supernatant was subjected onto the column and spun in between. Two washing steps were performed with 600  $\mu$ l Hepes buffer. Bound protein was then eluted in two steps with Hepes buffer containing 20 mM glutathione.

Elution fractions were pooled for each protein and 5  $\mu$ l thrombin was added. The purified protein was transferred into a Slide-A-Lyzer G2 Dialysis Cassette 3.5K MWCO (Pierce Protein Biology Products; Thermo Fischer Scientific) for dialysis with Hepes buffer over night at 4 °C.

Next day a second GST SpinTrap purification was performed for each protein to remove uncleaved protein and free GST. Thrombin activity was blocked by adding 5  $\mu$ l Pefabloc.

#### 2.2.4.7 Purification protocol for KIHsv2 and mutants

The pET-28a or pACE-His expression vector was used for expression of KIHsv2 and mutants in *E. coli* BL21(DE3) (see table of plasmids 2.7). Particularly, KIHsv2<sup>loopchimera</sup> construct and KIHsv2<sup>EDD</sup> mutant could only be purified, when expressed from pET-28a vector. pACE is lacking the *lacI* gene in its vector, the repressor of IPTG/allolactose activated promoters. The expression of the gene in the molecular cloning site is therefore active in low amounts all the time from this vector.

10 ml over night culture in LB was used to inoculate 1.5 l of autoinducible media. The culture was incubated, shaking for 3 hours at 37 °C and then shifted to 22 °C for 20 hours. To harvest the culture it was spun in a Beckman J6-MI centrifuge with the JS-4.2 rotor, for 20 min, 4,000 rpm and at 4 °C. Resuspension of the pellet was done with 15 ml buffer A (see table 2.15). Next, a protease inhibitor tablet was added, as well as DNaseI, lysozyme and MgCl<sub>2</sub> to a final concentration of 1 mM. The mixture was incubated with a magnetic stir bar on an electric device for 10 min. Afterwards cells were opened with a microfluidizer M-110L (Microfluidics Corporation) with 3 repetitions. During sonication the cell lysate was kept on ice. Another incubation for 10 min on a stirring device followed before soluble and insoluble cell components were separated while spinning in a Du Pont Sorvall centrifuge with a SS-34 rotor for 1 hour at 14,000 rpm, 4 °C.

The clear lysate was then loaded onto an 1 ml His-Trap FF column (GE Healthcare) applying 1 ml/min on the column in all steps. When supernatant has passed the column it was washed with 20 CV buffer A. After this an imidazole gradient was created on the

column from 0 % to 100 % buffer B for elution (see table 2.15). A final elution step of 5 CV buffer B was applied.

**Table 2.15:** Buffers for purification of KIHsv2 from *E. coli* BL21(DE3) cells

His-Trap purification		gel filtration
Buffer A	Buffer B	
30 mM Hepes	30 mM Hepes	30 mM Hepes
300 mM NaCl	300 mM NaCl	300 mM NaCl
30 mM imidazole	300 mM imidazole	
pH 7.0	pH 7.0	pH 7.0

Buffers used for protein purification were filtered and degased.

After SDS-PAGE for checking elution fractions, fractions containing the protein were pooled and concentrated to a final volume of 5 ml. Then the affinity purified protein was loaded on a HiLoad 16/60 Superdex column with a flow rate of 1 ml/min. The first 0.3 CV representing the void volume of the column were run without fraction collection followed by 0.8 CV with collecting 2 ml fractions. An additional SDS-PAGE check was done to check purity. Fractions with pure protein were pooled, aliquoted and snap frozen in liquid nitrogen. The purified protein was stored at  $-80^{\circ}\text{C}$ .

### 2.2.5 Purification protocol for PaAtg8 and KlAtg8

Synthetic genes of PaAtg8 and KlAtg8 were ordered from Gene Art (Invitrogen). The codon usage was optimized for bacterial expression and a C-terminal OneSTrEP-tag was added to the gene. The genes were cloned into the pACE expression vector and expressed in *E. coli* BL21(DE3). *E. coli* cells containing the plasmid were grown in 3 l autoinducible media for 3 hours at  $37^{\circ}\text{C}$  and then shifted for additional 20 hours to  $22^{\circ}\text{C}$ . The cells were harvested in a Beckman J6-MI centrifuge with the JS-4.2 rotor, for 20 min, 4,000 rpm and at  $4^{\circ}\text{C}$ . The cell pellet was resuspended in 30 mM Hepes pH 7.0 and 300 mM NaCl. After addition of a protease inhibitor tablet, 1 mM  $\text{MgCl}_2$ , DNaseI and lysozyme the cells were incubated for 10 min stirring and then a microfluidizer M-110L (Microfluidics Corporation) was used for lysis with 3 repetitions. Another incubation of 10 min was performed followed by centrifugation with a SS-34 rotor in a Du Pont Sorvall centrifuge for 1 hour at 14,000 rpm,  $4^{\circ}\text{C}$ . The obtained supernatant

was loaded to a 5 ml Strep-Trap column (GE Healthcare). Loading and washing of the column was done with the Hepes buffer, for elution 2.5 mM desthiobiotin was added to the Hepes buffer. Washing was done for 10 CV, elution for 3 CV. Samples were taken from cell extract, supernatant, pellet, flow through and peak fractions and analyzed with SDS-PAGE. The protein containing peak fractions were pooled, concentrated and subjected to a Superdex S75 gel filtration column using Hepes buffer. With SDS gels protein purity was confirmed. The peak fractions were pooled, concentrated if necessary, aliquoted, snap frozen in liquid nitrogen and stored at  $-80^{\circ}\text{C}$ .

## 2.2.6 Biochemical methods

### 2.2.6.1 SDS-PAGE and Western Blotting

Denaturing protein gels for **SDS-PAGE** were done using an adapted protocol from Laemmli [47]. The gels generally consist of resolving and separation parts. Samples were mixed with 3x SDS sample buffer (9 g SDS, 30 g glycerol, 0.02 g bromphenol blue, 18.75 ml of 1 M Tris pH 6.8, 90 ml water; for use mix: 9 parts of premix and 1 part beta-mercaptoethanol (end concentration 3.3 %)) and heated for 3 to 5 min at  $95^{\circ}\text{C}$ . A 10x protein running buffer (2 l: 60.6 g Tris, 285.2 g Glycine, 20 g SDS, pH 8.4) was diluted to 1x concentration and gels were applied to a current of 120 V until the blue protein running front completely run through.

For **Coomassie staining** the SDS gel is placed in a microwave container, overlaid with staining solution A (500 mg Coomassie R, 650 ml  $\text{H}_2\text{O}$ , 250 ml 2-propanol, 100 ml acetic acid) and heated for one minute at maximum temperature in the microwave. Afterwards the staining solution was drained and the procedure was repeated with solution B (50 mg Coomassie R, 800 ml  $\text{H}_2\text{O}$ , 100 ml 2-propanol, 100 ml acetic acid), solution C (20 mg Coomassie R, 900 ml  $\text{H}_2\text{O}$ , 100 ml acetic acid) and with destaining solution D (900 ml  $\text{H}_2\text{O}$ , 100 ml acetic acid). If necessary solution D was replaced again for further destaining.

In another Coomassie staining method applied in this study gels were stained in Coomassie Brilliant Blue solution (0.1 % (w/v) Coomassie R250 Brilliant Blue, 10 % (v/v) acetic acid, 40 % (v/v) ethanol) for 20 - 30 min and then left in destaining solution (10 % (v/v) acetic acid, 40 % (v/v) ethanol) until bands became visible.

Analysis of SDS gels by **Western blotting** [48, 49] was performed by blotting the gel on either Immobilon-FL Transfer PVDF membrane (Millipore) (generally used for protein-lipid co-floitation assays, section 2.2.6.6) or nitrocellulose (Whatman, Schleicher



& Schüll). The blotting was performed on a semi-dry apparatus. For this purpose, the gel, Whatman paper (Whatman) and nitrocellulose membrane were preincubated in transfer buffer (2.9 g/l (w/v) Glycine, 5.8 g/l (w/v) Tris, 0.37 g/l (w/v) SDS, 20 % (v/v) Methanol). When a PVDF membrane was used it was first incubated in methanol for approx. 15 - 20 sec and then put into transfer buffer. The transfer was performed at 45 mA per gel for nitrocellulose membranes in the apparatus for 45 min and for PVDF membranes at 25 V for 90 - 120 min at RT. After blotting the membrane was blocked in blocking solution (PBS-T or TBS-T supplemented with 1 % (w/v) milk powder) for 30 min. Next, the membrane was incubated with a primary antibody for 1 hour at RT or over night at 4 °C. When an antibody labeled with HRP was used incubation time was 1 hour. Unbound antibody was washed off in three repeated steps with PBS-T or TBS-T. Subsequently a secondary antibody was added on the membrane for 1 hour at RT. Washing the membrane was repeated before detection using the ECL solution (Perkin Elmer) with a Imageready LAS-1000 CCD camera (Fujifilm). Visualization and editing of the images was performed with the AIDA software (Fujifilm).

#### 2.2.6.2 Protein stability assay

Thermofluor experiments were performed to test protein stability after the first purification of a protein [50]. The influence of buffers on protein stability were tested. A first run of Thermofluor experiment was done after affinity purification of the protein. The found optimal buffer conditions were used to run the size exclusion column.

In order to perform this assay, purified protein was diluted to 3 - 10  $\mu$ M in affinity purification buffer without imidazole. 16  $\mu$ l of protein were pipetted per well in a white 96-well plate (Biozym Scientific GmbH) leaving out the last four rows of column 12 for controls. Column 12, row E+F were filled with 18  $\mu$ l buffer and row G+H with 18  $\mu$ l water. In addition, 2  $\mu$ l of buffer from the pHat screen (Hampton Research) were added to the protein in columns 1 - 11. On top, 2  $\mu$ l of 50x diluted Sypro Orange (5000x stock solution, Invitrogen) were added to all wells. The plate was closed with transparent caps (Biozym Scientific GmbH) and then spun at 1,000 rpm, for 1 min, at 4 °C.

For the thermal shift and read out of Sypro Orange fluorescence a CFX96 Real-Time System (C1000 Thermal Cycler, BioRad) was used. Here the plate was heated starting from 25 °C up to 95 °C. At the beginning of the thermal shift protein is folded and Sypro Orange in aqueous environment is quenched. Therefore the measured fluorescence signal is low. While temperature is increasing the protein unfolds and presents

hydrophobic patches, which Sypro Orange binds and becomes dequenched. Sypro Orange fluorescence increases until it reaches a plateau. The melting temperature  $T_m$  of a protein is defined as half way of the linear increase of the Sypro Orange fluorescence.

A second thermofluor run using the ADDit screen (Emerald BioSystems) was carried out after gel filtration. In the same way as described for the pHat screen.

Analysis of Thermofluor experiments were done using the DSF analysis sheet, version 2.5 (available from: <ftp://ftp.sgc.ox.ac.uk/pub/biophysics>). Before, data of the HEX channel were exported from the Real-Time System to an excel-sheet. After including the data into the DSF analysis sheet a special Excel-file containing macros (minNormMacro.xlsm) was run.

### 2.2.6.3 Circular dichroism spectroscopy

Circular dichroism spectroscopy (CD) was used to analyse the secondary structure of a protein. In order to get good CD spectra with a low background purified protein was dialyzed in NaF buffer (30 mM  $\text{NaH}_2\text{PO}_4$  pH 7.5, 300 mM NaF), because NaF shows no absorbance in far UV (for summary read [51]). Chloride ions and imidazole should be avoided, since they show a high absorbance in the far UV region. Dialyzed protein was used at a concentration of 40  $\mu\text{M}$  and pipetted into a 1 mm glas cuvette. For measuring CD spectra a Chirascan Circular Dichroism Spectrometer (Applied Photophysics) was used and set to 20 °C. CD spectra were recorded from 190 nm to 260 nm with a bandwidth of 2 nm and in 0.5 nm steps. Each time point was recorded for 3 sec and a total of 3 repetitions were measured. First a buffer run was taken as baseline.

The minimum at 216 nm characteristic for  $\beta$ -strands was used to measure the melting temperature of the protein. For this purpose, the wavelength was set to 216 nm and a temperature shift from 20 °C to 90 °C was applied to the sample chamber. Here, 4 sec per time point were recorded, for 3 repetitions with a bandwidth of 1.5 nm. The temperature was increased in steps of 0.5 °C and at a rate of 0.25 °C/min.

For analysis data were exported. Therefore, the three repetitions of baseline and protein run were each averaged, baseline subtracted from the protein spectrum and the resulting curve smoothed. CD spectra data were converted to mean residual molar ellipticity by including concentration, molecular weight and path length. Final figures were prepared with the software Kaleidagraph.

#### 2.2.6.4 Limited proteolysis

Generation of stable protein fragments for crystallization was done with limited proteolysis [52] using the Proti-Ace kit I + II (Hampton Research). Each of these kits provides a set of 6 commonly used proteases.

- Kit I:  $\alpha$ -Chymotrypsin, Trypsin, Elastase, Papain, Subtilisin, Endoproteinase Glu-C
- Kit II: Proteinase K, Endoproteinase Arg-C, Pepsin, Thermolysin, Bromelain, Actinase

Proteases were prepared at a concentration of 1 mg/ml by resuspending the powder in 100  $\mu$ l deionized water. These were further diluted 1:100 with supplied dilution buffer (10 mM Hepes pH 7.5, 500 mM NaCl). From this 10  $\mu$ l were mixed with 10  $\mu$ l of protein (approximately 10 mg/ml). Samples were incubated at 37°C and the reaction was stopped at defined time points by adding 3x SDS sample buffer (9 g (w/v) SDS, 30 g (w/v) glycerol, 0.02 g (w/v) bromphenol blue, 18.75 ml of 1 M Tris pH 6.8, 90 ml water; for use mix: 9 parts of premix and 1 part beta-mercaptothanol (end concentration 3.3 %)) and heated for 3 to 5 min at 95°C. Afterwards samples were checked with SDS-PAGE.

Identified stable fragments were analyzed by N-terminal sequencing or mass spectrometry.

#### 2.2.6.5 N-terminal protein sequencing

Samples for N-terminal sequencing of the first five amino acids were sent to SeqLab (Sequence Laboratories Göttingen GmbH). Sequencing results were used to identify the cleavage site of stable fragments. SeqLab provides this service according to Edman's degradation [53]. Sample preparation was performed analog to the protocol given by SeqLab.

This requires SDS-PAGE separation and immobilization of the fragment on a PVDF-membrane (see caption 2.2.6.1). For transfer to the membrane a special CAPS buffer (10 mM CAPS pH 11, 10 % (v/v) methanol) was used.

Then the membrane was washed with water, moistened in 100 % (v/v) methanol, stained with Coomassie Brilliant Blue (0.1 % (w/v) Coomassie Blue R-250 in 1 % (v/v) acetic acid and 40 % (v/v) methanol) and destained in 50 % (v/v) methanol. Again the membrane was washed with water, dried and the protein band cut with a clean razor blade.

Finally the membrane was transferred in a polypropylen cup for shipping.

### 2.2.6.6 Protein-lipid co-flotation assay and liposome preparation

Flotation assays with small unilamellar vesicles (SUV) were used to study membrane binding and lipid binding specificity of proteins.

**Liposome preparation** was done with lipids stated in table 2.3, which were dissolved in chloroform at indicated concentrations. Lipids were added in their respective (w/w) volumes to a total of 1 mg lipids in 2 ml test tubes and dried. Addition of Texas-Red conjugated PE served as visible marker of dried lipids and later liposomes. After chloroform evaporation the lipids were resuspended in HP150 buffer (20 mM Hepes pH 7.4, 150 mM KCl) supplemented with 3 % cholate. Liposome formation and cholate removal was done by size exclusion chromatography on a column of 0.7 cm in diameter and 15 cm in length (BioRad) containing Sephadex G-50 as matrix. The purple colored fraction was collected. Typical liposome compositions are listed in table 2.16.

**Table 2.16:** Liposome lipid compositions

Control	2 % PIP	1 % PIP	20 % PS	10 % PS
75 % (w/w) PC	73 % (w/w) PC	74 % (w/w) PC	55 % (w/w) PC	65 % (w/w) PC
23 % (w/w) PE	23 % (w/w) PE	23 % (w/w) PE	23 % (w/w) PE	23 % (w/w) PE
2 % (w/w) TR-PE	2 % (w/w) TR-PE	2 % (w/w) TR-PE	2 % (w/w) TR-PE	2 % (w/w) TR-PE
	2 % (w/w) PIP	1 % (w/w) PIP	20 % (w/w) PS	10 % (w/w) PS

Large unilamellar vesicles (LUV) were used for ITC measurements and prepared with a Mini-extruder (Avanti Polar Lipids). Polycarbonate membranes with a pore sizes of 0.4  $\mu\text{m}$  and 0.1  $\mu\text{m}$  were used for extrusion. Lipids were mixed and dried in the same way as described above for SUVs. Then lipids were directly resuspended in 1 ml HP150 buffer and subjected to the Mini-extruder with a 0.4  $\mu\text{m}$  membrane for approximately 25 strokes. In a second step the membrane was exchanged with a 0.1  $\mu\text{m}$  pore size membrane and another 25 strokes were done. Hereby the lipids were pushed through the membrane and form liposomes of a defined size with approximately 100 nm diameter.

**Protein-lipid co-flotation assays** were investigated as previously described in [54, 55]. 5  $\mu\text{l}$  of 2  $\mu\text{M}$  protein was incubated with 45  $\mu\text{l}$  of liposomes for 10 min, RT

in 7 x 20 mm PC tubes (Beckman). Then the protein liposome sample was gently mixed with 50  $\mu$ l of 80 % Nycodenz (w/v in HP150 buffer) and overlaid with 50  $\mu$ l of 30 % Nycodenz. The gradient was covered with 30  $\mu$ l HP150 buffer. Samples were spun at 55000 rpm (275000 g) for 1.5 hours at 4 °C in a Sorvall Discovery M150 SE analytical ultracentrifuge (Thermo Scientific) using a S55-S swinging bucket rotor (Thermo Scientific). Six 30  $\mu$ l aliquots were taken afterwards and separated in 12 % SDS-PAGE and analyzed by Western blotting. ScHsv2 proteins were detected with an polyclonal rabbit antibody against ScHsv2 C-terminus. KIHsv2 and other His-tagged proteins were detected with a Penta His HRP conjugated antibody.

**Calculation of accessible PI3P and PI(3,5)P<sub>2</sub> in liposomes** for ITC analysis was through measurement of the total phosphate concentration of the liposomes with the phosphomolybdate method [56]. For this liposomes were diluted 1:10 with water. 20  $\mu$ l of 70 % HClO and 100  $\mu$ l of 7.2 M H<sub>2</sub>SO<sub>4</sub> were added and the sample heated at 300 °C for 2 hours. In this step, bound organic phosphates were released. Then the sample was cooled to RT and formed phosphate was dissolved in 1 ml H<sub>2</sub>O. Further, 100  $\mu$ l molybdate solution (3 % (w/v) ammonium molybdate, 0.12 % (w/v) Triton X-100) were added and the absorbance at 660 nm was measured exactly after 20 min after molybdate solution was added. A calibration curve from NaH<sub>2</sub>PO<sub>4</sub> (0.2 mM) was used to calculate phosphate concentrations.

Liposome size distribution was determined by field-flow fractionation coupled to multi-angle laser light scattering (FFF-MALLS) [57, 58]. In this experimental set up 50  $\mu$ l 1:50 diluted liposomes were first separated by their size (Eclips 2 system, Wyatt Technology) with a 0.1  $\mu$ m filtered buffer (20 mM Hepes pH 7.4, 150 mM KCl, 0.02 % (w/v) NaN<sub>3</sub>). Absolute size determination occurred in the next step using a conventional multi angle light scattering device (DAWN EOS) in combination with an Agilent 1100 series HPLC pump and autosampler. A channel flow of 1 ml/min was applied and sample was injected at 0.2 ml/min. The sample was concentrated by the system with a focus flow of 3 ml/min for 3 min. Right after concentration the liposomes were separated with a cross flow of 0.75 ml/min which was linearly decreased to zero in a time frame of 35 min. Detection and analysis was done with the manufacturers ASTRA software. Fitting of the data were performed with the coated-sphere model.

Knowing the size distribution of SUVs, the total phospholipid amount, weight ratio and molecular weight of the individual lipids as well as the number of phosphorus atoms in each phospholipid the concentration of phosphoinositide was determined. For this, an equal incorporation of all lipids was assumed. Further, the bilayer thickness was

considered to be 4 nm in SUVs with an average radius of 20 nm. The outer surface of the SUVs contain 60 % of total lipids.

### 2.2.6.7 Isothermal titration calorimetry

ITC measurements were done to determine binding affinities and stoichiometry of protein-protein or protein-liposome interactions. Further enthalpy and entropy of binding can be determined with this method.

The Microcal VP-ITC or ITC<sub>200</sub> were used for measurements. The two machines differ in their cell and syringe volume. The VP-ITC has a cell size of 1.4 ml and a syringe volume of 300  $\mu$ l, whereas the volumes for the ITC<sub>200</sub> are much smaller, the cell holds 200  $\mu$ l and the syringe 40  $\mu$ l. For measurements the concentration of the component in syringe was approximately 7 - 10 times higher than that of the interaction partner in the sample cell.

Buffer typically used for ITC was HP150 buffer (20 mM Hepes pH 7.4, 150 mM KCl). Otherwise the buffer composition is specified in the results section. Protein was dialyzed to HP150 buffer using Slide-A-Lyzer G2 Dialysis Cassette 3.5K MWCO (Pierce Protein Biology Products; Thermo Fischer Scientific). Liposomes were prepared in the same buffer as used for dialysis of the protein.

Settings of the machine for measurements are listed in table 2.17. For fitting of the data a single-site binding model was used and the MicroCal Origin 7.0 software was employed for analysis.

**Table 2.17:** Settings for isothermal calorimeters

	VP-ITC	ITC <sub>200</sub>
total injections	20	20
pre-injection volume	3 $\mu$ l	0.1 $\mu$ l
volume of injection	15 $\mu$ l	2 $\mu$ l
reference power	10 $\mu$ cal/sec	7 $\mu$ cal/sec
temperature	25 °C	20 °C
delay	120	120 sec
spacing	250/500 sec	90 sec
stirring speed	250 rpm	300 rpm
duration time	30 sec	4sec
filter period	3 sec	2 sec

### **2.2.6.8 Protein-lipid overlay assay (PIP strip, PIP array, membrane lipid strip)**

PIP strips, PIP arrays and membrane lipid strips were ordered directly from Echelon Biosciences Inc. or its distributor MoBiTec GmbH. These nitrocellulose membranes are spotted with pure lipids and used for determination of protein-lipid interaction. PIP strips are spotted with 100 pmol of all seven phosphoinositides and eight other biological important lipids. PIP arrays are spotted with a concentration gradient of phosphoinositol and seven phosphoinositides (per spot 100 pmol, 50 pmol, 25 pmol, 12.5 pmol, 6.25 pmol, 3.13 pmol and 1.56 pmol). Membrane lipid strips contain 15 biologically important lipids at a concentration of 100 pmol each.

In order to perform these protein-lipid overlay assays, membranes were incubated in blocking buffer for 30 min at RT, then protein was diluted in blocking buffer and added onto the membrane for 1 hour. Afterwards the membrane was washed 3 times with buffer. Bound protein was detected by primary and secondary antibody diluted in blocking buffer and incubated for 1 hour each. In between the nitrocellulose membrane was washed 3 times in buffer. Finally the HRP-conjugated antibody was detected using ECL solution in a Luminescence detector (also see Western blotting, section 2.2.6.1)

In order to test different conditions PBS or TBS were used as buffers and were supplemented with different concentrations of milk, BSA, Tween 20, MgCl<sub>2</sub> as specified in section 4.2.2.1. Also different protein concentrations were tested, here concentrations between 0.1 µg/ml and 1 µg/ml were used.

### **2.2.6.9 Cova PIP specificity plate**

Cova PIP specificity plates were purchased from Echelon Biosciences Inc. and used for quantification of protein-PIP binding. Each row of a 96-well plate is coated with phosphoinositol or one of the seven phosphoinositides at a concentration of 20 pmols per well.

In a first step, 100 µl of buffer with protein was incubated for one hour, while shaking at room temperature. Afterwards, wells were washed three times with buffer. The first antibody (anti-GST or anti-Hsv2) was incubated for one hour, shaking at room temperature. Before the secondary antibody was added in the same way, the wells were

washed again with buffer. The secondary antibody against GST was a goat anti-mouse antibody, anti-Hsv2 requires a goat anti-rabbit secondary antibody. Again the wells were washed with buffer.

Different buffers were tested to determine the best conditions. Here, PBS or TBS were tested with and without Tween 20 and either with or without  $\text{MgCl}_2$ . As blocking reagent milk and BSA were tested at different concentrations as specified in section 4.2.2.1.

Detection was performed by adding 100  $\mu\text{l}$ /well TMB (3,3',5,5' - tetramethylbenzidine) substrate solution, while incubating the solution onto the secondary HRP-conjugated antibody the solution turns blue. When a good visibility was reached (usually after 30 min) the reaction was stopped with 100  $\mu\text{l}$  of 0.16 M sulfuric acid. The color turns yellow. Absorbance was measured at 450 nm with the TECAN Genios Pro and its corresponding software.

#### 2.2.6.10 Analytical gel filtration

Analytical gel filtration was used to analyze protein-protein interaction with a Superdex 200 10/300 GL gel filtration column. The masses of protein complexes can be determined from a calibration curve using molecular weight standards provided in the Gel Filtration Molecular Weight Markers (12,400 - 200,000) kit from Sigma. This kit contains seven proteins of known molecular weight:

- Cytochrom c (from horse heart): 12.4 kDa
- Carbonic Anhydrase (from bovine erythrocytes): 29 kDa
- Albumin, Bovine Serum: 66 kDa
- Alcohol Dehydrogenase (from yeast): 150 kDa
- $\beta$ -Amylase (from sweet potato): 200 kDa
- Blue Dextran: 2,000 kDa

The size of unknown proteins is determined by comparing the ratios of  $V_e/V_o$ . Here  $V_e$  is the elution volume of the protein from the gel filtration column and  $V_o$  is the void volume of the column, representing the elution of high molecular weight compounds which are too big to interact with the matrix of the column and therefore are quickly eluted. The void volume was measured with Blue Dextran and all standards were run



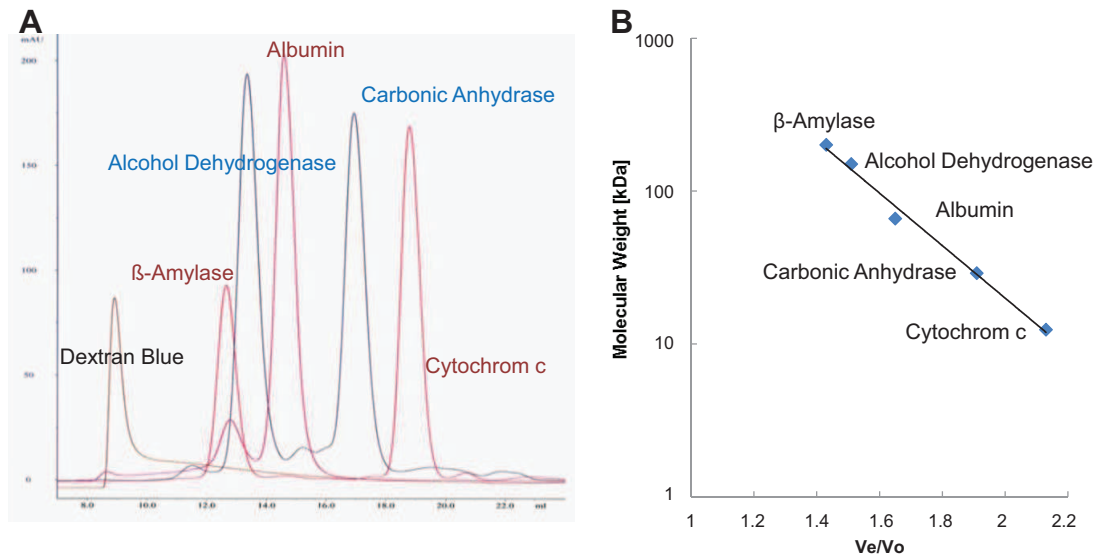


**Figure 2.1: Standard curve for analytical gel filtration**

(A) Gel filtration runs of molecular weight standards using the Superdex 200 10/300 GL detected with UV<sub>280</sub>. (B) Half logarithmic plot of the molecular weight of protein standards versus their respective  $V_e/V_o$ .

over the column. The logarithms of their molecular weight were plotted versus their  $V_e/V_o$ . Connection of these points resulted in a linear curve (see fig. 2.1).

In order to determine the void volume of the analytical gel filtration Blue Dextran was resuspended in the supplied buffer (50 mM Tris-HCl pH 7.5, 100 mM NaCl) supplemented with 5 % glycerol to a concentration of 2 mg/ml. 250  $\mu$ l of blue dextran was run over the column loaded with a 0.5 ml loop at 0.5 ml/min using 50 mM Tris-HCl pH 7.5, 100 mM NaCl as buffer. Fractions of 1 ml volume were collected, additionally UV<sub>280</sub> was detected during all runs. Next, cytochrom c (4 mg/ml) and  $\beta$ -amylase (8 mg/ml) were mixed and 250  $\mu$ l were applied onto the column. Also carbonic anhydrase (6 mg/ml) and alcohol dehydrogenase (10 mg/ml) were mixed and run together, then 250  $\mu$ l albumin (10 mg/ml) was loaded. Albumin elutes in two peaks (monomer and dimer) which can be both used for the standard curve.

Sample protein was dialyzed into the same buffer and 250  $\mu$ l were applied onto the column to calculate its  $V_e/V_o$  and using the standard curve the mass of the protein can be determined.

## 2.2.7 Crystallization and structure determination

### 2.2.7.1 Crystallization screen setup

First screening experiments for crystallization were set up in **96-well sitting drop** plates (MRC, Hampton Research), where two drops of different protein concentration were pipetted for each buffer condition. The Cartesian Microsys (Cartesian Dispensing Systems) robot was employed for setting drops. It dispensed 100 nl drops of protein per well and then added 100 nl screening buffer (reservoir solution).

Quickly after the robot finished the plate was covered with a transparent sealing tape to avoid drying in of the drops. Crystal plates were stored at 20 °C or at 4 °C in an automated Formulatrix crystallization imager. This took pictures of each single condition at programmed imaging times with the RockImager software (Formulatrix). Images were checked with the Rockmaker main Application software (Formulatrix).

Different companies supply crystallization screens including Hampton Research (SaltRx screen), Qiagen (AmSO<sub>4</sub>, Anions, Cations, ClassicLite, Classics I+II, Compas, JCSG+, PACT, PEGI+II, pHclearI+II, ProComplex screens) or Emerald Biosystems (Wiz1+2, Wiz3+4 screens).

When initial crystallization conditions were optimized **24-well Linbro hanging drop** plates (Jena Bioscience) were used. Here, screening buffers were self made and for each well 1 ml of reservoir solution were prepared. Then each well was greased with Bayer medium viscosity silicon grease (Jena Bioscience). 1  $\mu$ l protein and 1  $\mu$ l reservoir buffer were pipetted together on a siliconized cover slip (22 mm diameter), up to 4 drops were fitted on one slide. Afterwards the slide was flipped upside down onto the greased well to seal it air tight.

Another way of crystallization optimization was achieved by using the **Additive or Silver bullet screens**. For this the same reservoir solution was pipetted in all 96 wells. Crystal drops were pipetted as described before with the robot. As an additional step 20  $\mu$ l Additive or Silver bullet screen solution was added to 100 nl protein and 100 nl buffer drop.

A third way for optimization are 96-well plate **refinement grid screens**. These screens were prepared using the Tecan robot. The robot was used to pipette new optimized conditions from stock solutions into 1 ml 96-well master blocks. From these 96-well MRC plates for crystallization were pipetted.

**Streak seeding** of crystals was used for optimization of crystal growth, size, form and diffraction. For this, a crystal was crushed with an acupuncture needle. Then the

needle was streaked through a newly set up drop in similar buffer conditions. Crystal fragments left in the new drop serve as seeds for crystal growth.

**Molecularly imprinted polymers** (MIP) can be used as nucleation sites [59] and were added with a acupuncture needle to the freshly set up hanging drops. They were prepared by mixing 54 mg acrylamide with 6 mg N,N<sup>+</sup>-methylenebisacrylamide in a 15 ml Falcon tube and the powder was dissolved in 1 ml water. For each MIP 90  $\mu$ l acrylamide mix were added to 10  $\mu$ l of template protein (6 mg/ml) in a 1.5 ml test tube. Then 2  $\mu$ l of 10 % APS were added and the mixture degassed with nitrogen for 5 min. 2  $\mu$ l of 5 % (v/v) TEMED were added and the test tubes stored at RT for polymerization (approximately 18 hours). Afterwards the obtained gels were pressed through a 75- $\mu$ m sieve (diameter of 10 cm; Endecotts Limited). A 50 ml Falcon tube was placed under the sieve to collect the gel pieces. Sterile water was added onto the sieve to wash down left gel pieces. The falcon tube with gel pieces were spun at 2000 g for 3 min at RT in a Sigma centrifuge. Thereafter, 0.5 ml of 10 % (w/v) SDS dissolved in acetic acid were added to extract the protein from the gel pieces (SDS/acetic acid was put in the micro wave for dissolving). Finally, the samples were spun twice in a Sigma centrifuge (2000 g, RT, 3 min) and the supernatant discarded. The MIPs were stored at 4 °C.

#### 2.2.7.2 Flash cooling of crystals

Cryoprotectants were used for flash cooling of crystals to prevent ice formation around the crystal. For this cryoprotactants like ethylene glycol, xylitol, sucrose or PEG 400 were prepared with the same buffer as reservoir solution (mother liquor) in which crystals grew. When crystals were fished they were first put in fresh mother liquor, then transferred into a mixture of 1:1 mother liquor and cryoprotectant and finally in cryoprotectant. Crystals were fished out of the cryoprotectant and quickly flash frozen in liquid nitrogen.



# 3 Project I: Reconstitution of mammalian Atg12 and MAP1LC3 conjugation pathways

## 3.1 Introduction

### 3.1.1 Ubiquitin-like conjugation systems in autophagy

Two ubiquitin-like conjugation systems are involved in autophagy, namely Atg12 and MAP1LC3, the mammalian homolog of Atg8. These two systems are essential for autophagosomal membrane expansion [60, 61, 62]. Like in the canonical ubiquitin conjugation system, the ubiquitin-like (ubl) modifiers are conjugated to their targets by E1- and E2-like enzymes (see figure 3.1).

The Atg12 conjugation system requires Atg7, Atg10 and Atg5. Atg12 is activated at its C-terminal glycine by the E2-like enzyme Atg7 under consumption of ATP [63]. In a second step, Atg12 is transferred by the E2-like enzyme Atg10 to its final target Atg5. Conjugation of Atg12 to Atg5 takes place at Lys130 of Atg5 [23]. Furthermore Atg5 interacts with the N-terminus of Atg16 [64, 65], which oligomerizes and an Atg12-Atg5-Atg16 oligomer is formed. In contrast to yeast Atg16, the mammalian homolog contains a WD40 repeat domain at its C-terminus in addition to the N-terminal domain required for Atg5 binding and the coiled coil domain.

Both MAP1LC3 (LC3) and Atg12 conjugation systems share the E1-like enzyme Atg7. However, before LC3 is activated, its C-terminal amino acid needs to be cleaved by Atg4. Exposure of its C-terminal glycine after cleavage is essential for the conjugation to its target phosphatidylethanolamine, which is catalyzed by Atg7 and the E2-like enzyme Atg3 [66]. While Atg5-Atg12 conjugation is irreversible LC3 can be delipidated by

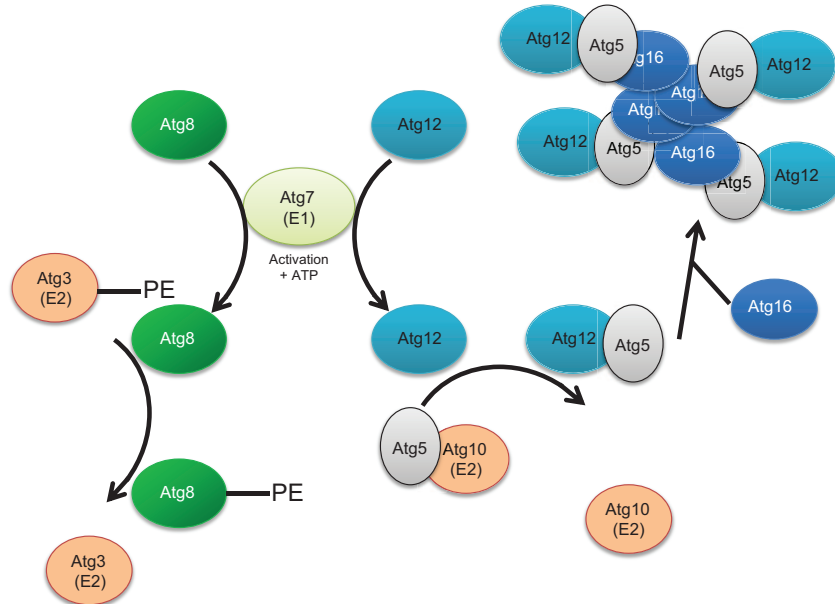


**Figure 3.1: Ubiquitin-like conjugation systems involved in autophagy.**

The complexes contain two ubiquitin-like proteins namely Atg12 and Atg8 (MAP1LC3), which are covalently linked to their targets Atg5 and PE, respectively. In both conjugation reactions E1- and E2-like enzymes are involved. Atg7 (E1-like) is activating the ubl proteins under consumption of ATP and then Atg3/Atg10 (E2-like) are linking the ubl protein to their targets. The Atg12-Atg5 conjugate binds to Atg16, which mediates oligomerization of the entire Atg12-Atg5-Atg16 complex.

cleavage of Atg4 [67]. Lipidation of LC3 renders its cytosolic localization to membrane bound.

The C-terminal exposed glycines of both Atg12 and MAP1LC3 form thioester bonds with the active site cysteins of the E1- and E2-like enzymes and amide bonds with its final conjugation targets [68].

Between both conjugation systems cross talk has been reported. Atg12-Atg5-Atg16 acts as an E3-like ligase for LC3 lipidation [69] and specifies the site of LC3 lipidation to PE [70]. Furthermore, Atg12 can also be conjugated to Atg3 and this conjugate is involved in mitophagy, mitochondrial-mediated cell death, and mitochondrial homeostasis [71].

### 3.1.2 Structure and function of Atg12

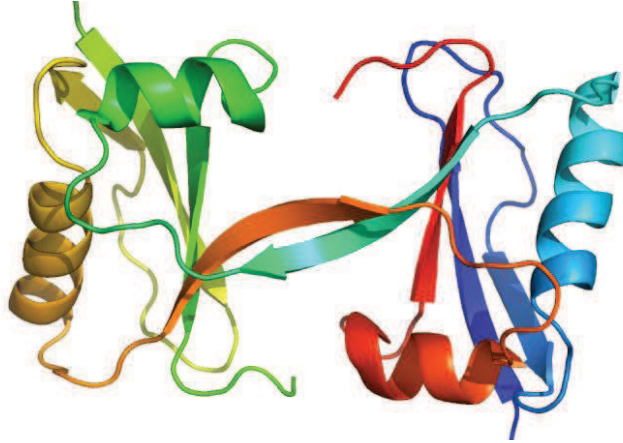


**Figure 3.2: Structure of Atg12 from *A. thaliana***

A ribbon diagram of Atg12 is shown colored from N-terminus in blue to C-terminus in red. Two molecules of Atg12 were found in the asymmetric unit of the crystal. Each molecule revealing a ubiquitin-fold. PDB code: 1WZ3.

Atg12 was the first ubiquitin-like modifier identified in autophagy [23]. The structure of Atg12 from *A. thaliana* was determined [31] and revealed a ubiquitin-fold region although it shares no significant sequence homology with ubiquitin (see figure 3.4). The asymmetric unit of the crystal contained two Atg12 molecules that forms an intertwiner dimer (see figure 3.2) but it is most likely that the monomeric form of Atg12 is biological relevant. The monomeric structure consists of four  $\beta$ -strands enclosed by two  $\alpha$ -helices. The C-terminus of the protein is exposed at the surface.

In complex with Atg16 Atg5-Atg12 is localized to the PAS (pre-autophagosomal structure) and there it mediates Atg8/LC3 lipidation in an E3 ligase like manner. Recently an additional function of this complex in membrane tethering was reported [72].

### 3.1.3 Atg8 and its human homologs

Atg8 is crucial for membrane elongation and hemifusion processes in yeast [73]. MAP1LC3B (referred to as LC3) is the most studied mammalian Atg8 homolog. Besides LC3B seven additional homologs are present in higher eukaryotes, namely LC3A which has two alternative splicing forms, LC3C, GABARAP, GABARAPL1, GABARAPL2 (GATE-16) and GABARAPL3. These homologs are classified in the LC3 and the



**Figure 3.3: Structure of LC3 from *R. norvegicus***

Ribbon diagram of rat MAP1LC3 colored from N-terminus in blue to C-terminus in red. Like AtAtg12 a ubiquitin-fold was determined for LC3. PDB code: 1UGM.

GABARAP/GATE-16 subfamily [74, 75]. LC3 is localized to autophagosomal membranes and recruits ubiquitinated cargo for degradation via the receptors p62 and NBR1 [76, 77]. GABARAP and GATE-16 were first described as intra-cellular trafficking factors [78, 79] and localize at autophagosomes which were induced by starvation [80].

Structures of rat LC3 (see figure 3.3) [27], GATE-16 [81], human GABARAPL1 (Structural Genomics Consortium) and yeast Atg8 [82, 83] are known. All contain the ubiquitin-fold comprising a core of two  $\alpha$ -helices and five  $\beta$ -strands and an additional N-terminal  $\alpha$ -helix (see figure 3.4).

### 3.1.4 Aims

The Atg12-Atg5-Atg16 and Atg8-PE (MAP1LC3II) conjugation systems are recruited to the phagophore and essential for autophagosome formation [60, 61]. The complexes contain the two ubiquitin-like proteins namely Atg12 and Atg8, which are covalently linked to their targets Atg5 and PE, respectively [23, 66]. In addition the covalently linked Atg12-Atg5 complex interacts via Atg5 with the N-terminus of Atg16



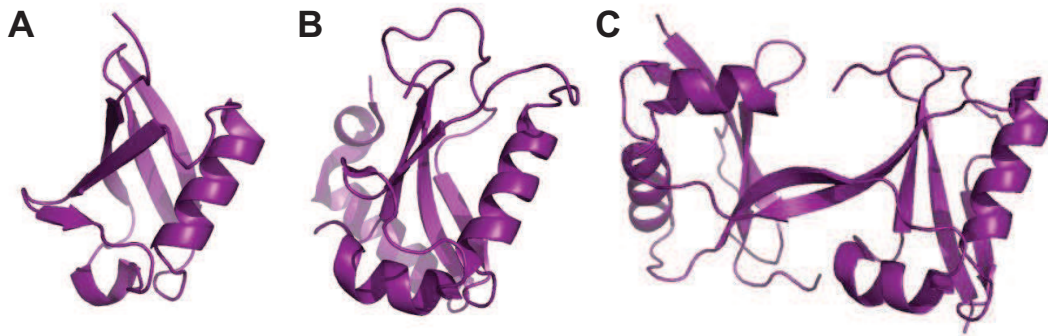


**Figure 3.4: Ubiquitin, LC3 and Atg12 share a ubiquitin fold**

In comparison (A) ubiquitin (B) murine MAP1LC3 (LC3) and (C) *A. thaliana* Atg12 are shown. LC3 and Atg12 show low sequence homology to ubiquitin, but the structures reveal a shared ubiquitin fold. The C-terminus necessary for conjugation is exposed at the surface.

[64, 65]. The structure of yeast Atg5 in complex with the N-terminus of Atg16 has been described already [84]. Up to now no structure of conjugated Atg5-Atg12 is published. However, the underlying molecular function of the ternary complex could not be elucidated from this structure.

The aim was the generation of mg amounts of lipidated LC3 and the Atg5-Atg12 conjugate either alone or in complex with Atg16 for structural studies. For this purpose the components of the two mammalian conjugation systems were co-expressed in insect cells and products were analyzed by mass spectrometry.

## 3.2 Results

### 3.2.1 Setting up the insect cell system for co-expression

Expression of large mammalian complexes are very challenging since the bacterial expression machinery is not constructed for huge proteins. So a different expression system needs to be chosen. On average, bacterial proteins (average of 317 aa) are much smaller than eukaryotic proteins (average of 510 aa in human) and hence the expression machinery is limiting [85]. Therefore, the insect cell expression system was chosen. Advantages of this system are the implementation of post-translational modifications and proper folding is more likely compared to bacteria [86]. An expression system for insect cells developed by I. Berger and colleagues [45] was employed. This system was optimized for expression of complexes using novel vectors, which can be combined by recombination and are expressed in insect cells together from a bacmid.

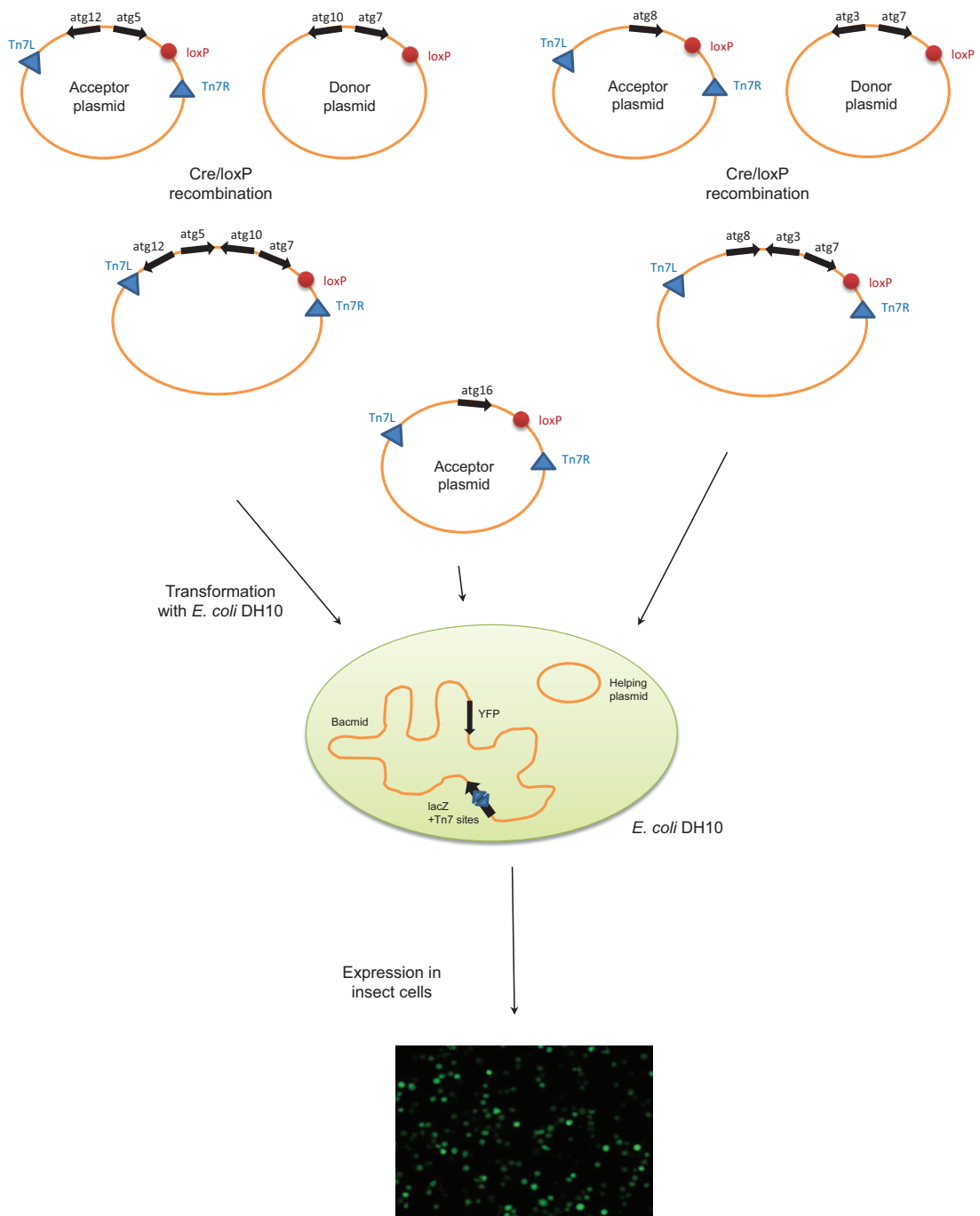


**Figure 3.5: Cloning strategy for expression of complexes in insect cells**

A set of acceptor and donor plasmids is generated for co-expression. With a Cre/loxP reaction those plasmids are fused. The expression cassettes are enclosed by Tn7 transposition sites which are used for integration of the cassette into the MultiBac baculovirus bacmid. Transfection and infection efficiencies of insect cells can be observed by co-expression of YFP from the bacmid.

The MultiBac baculovirus over-expression system used in this study consists of a set of acceptor and donor plasmids with each comprising two multiple cloning sites (see figure 3.5). Both plasmids share the loxP imperfect inverted repeat which was used for Cre recombination of acceptor with the donor plasmid. In addition the multiple cloning sites and the site for recombination of the acceptor plasmid are enclosed by the right and left termini of the Tn7 transposition sequences. Complementary Tn7 sequences are located within the *lacZ* gene encoded by the bacmid. Once the final acceptor plasmid was transformed with *E. coli* DH10 cells containing the MultiBac, the plasmid integrates via the Tn7 sites into the *lacZ* gene, which will be interrupted and can be used for subsequent blue-white screening of positive clones. The bacmid was extracted from *E. coli* cells (see section 2.2.2.2) and used for transfection of insect cells (see section 2.2.2.3). As a control of virus expression and therefore for the genes of interest, YFP is co-expressed from the bacmid and can be detected with a fluorescence microscope. In addition, YFP correlates with the expression levels of genes expressed under late-stage viral promoters as the genes of interest are (see section 2.2.2.5). The strong p10 and polyhedrin promoters are used for late-stage expression.

Before the genes of the human conjugation systems were cloned into the MultiBac vectors, the canonical hAtg7 isoform 1 and full length hAtg16 needed to be generated. Atg7 was in our lab only available as isoform 2 missing amino acids 626 to 652. In order to get isoform 1 the missing base pairs were added with PCR. In a first PCR step two fragments were amplified using primers RB13/RB5 and RB6/RB14 (see table 2.8), whereas primers RB5 and RB6 contain a overhang, adding the missing base pairs. *Atg7* isoform 2 was used as template. The second PCR was performed using both obtained fragments as template, which overlap each other for 23 base pairs, and primers RB13/RB14 (see table 2.8) were used. In a similar manner the missing 81 base pairs at the 5' site of *hatg16* were added. Two steps of PCR were done with first RB39/RB41 as primers and then RB40/RB41 as primer pair (see table 2.8). After this all necessary human genes for the expression of the complexes were available.

Genes required for both conjugation systems were cloned into either the pFL acceptor plasmid or pUCDM donor plasmid (see figure 3.6). Here, the E1- and E2-like enzymes were inserted in the pUCDM donor plasmid and the ubiquitin-like modifiers MAP1LC3 and Atg12 with its target Atg5 were cloned into the pFL acceptor plasmid. MAP1LC3 and Atg12 were prepared in a way that they were expressed as a recombinant protein carrying an N-terminal 10x His-tag and a TEV cleavage site, in addition it was important that MAP1LC3 presents the glycine needed for conjugation to PE at its C-terminus. Therefore the truncated form comprising residues 1-120 was used. Atg5

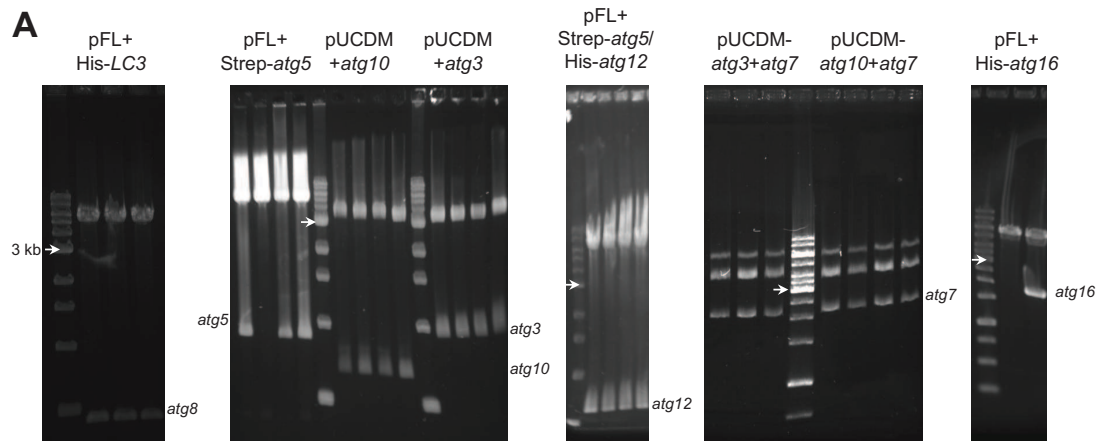


**Figure 3.6: Cloning strategy for expression of complexes in insect cells**

Restriction digestion check of successful cloning for co-expression of the proteins involved in the conjugation systems. Atg5-Atg12 and LC3 were cloned into the acceptor vector pFL, which consists of two multiple cloning sites (pFL-atg5-atg12 and pFL-LC3). The E1- and E2-like enzymes Atg7, Atg3 and Atg10, which catalyze the reactions, were cloned into the donor vector pUCDM (pUCDM-atg7-atg3 and pUCDM-atg7-atg10). The arrow is indicating the size of 3 kb.

was expressed with an N-terminal StrepII-tag and a TEV cleavage site. Atg3, Atg10 and Atg7 were not supposed to get purified and therefore kept untagged.

Besides, two viruses were generated expressing Atg16 either with an N-terminal 6x His-tag or a StrepII-tag both also containing a TEV cleavage site.

### 3.2.2 Expression and purification of modified human autophagy proteins

#### 3.2.2.1 The Atg12-Atg5 conjugate

Expression of the genes required for the Atg12-Atg5 conjugation system was done using the MultiBac expression system for insect cells. In order to express this protein complex the proteins of interest were cloned into the acceptor vector pFL, which consists of two multiple cloning sites (pFL-atg5/atg12). The E1- and E2-like enzymes Atg7 and Atg10, which catalyze the reaction, were cloned into the donor vector pUCDM (pUCDM-atg7-atg10). Multigene transfer vectors were created by *in vitro* fusion of the acceptor and the respective donor vector by using Cre recombinase (pFL-atg5/atg12/atg7/atg10). Next, the expression cassette, which is located in-between Tn7 transposition sequences, was integrated into the MultiBac baculovirus genome.

Extracted bacmid was then transfected into highly viable Sf21 or Sf9 insect cells, which were routinely checked for viability, cell density and diameter with a cell counter. 60 hours after transfection the cells were checked for YFP expression under a fluorescence microscope. Yellow fluorescent cells indicated transfected cells. If most cells fluoresce medium containing the virus ( $V_0$ ) was harvested. If necessary up to 72 hours after transfection were waited.

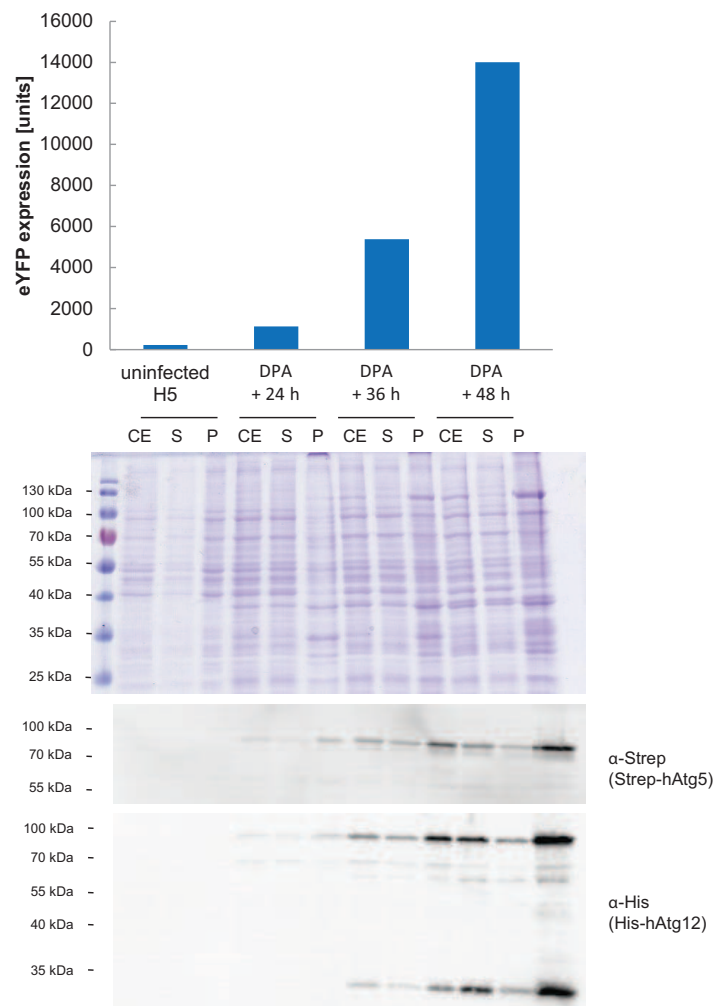


**Figure 3.7: Expression of Atg5 and Atg12 in insect cells**

Expression of YFP in High5 insect cells was monitored after day of proliferation arrest (DPA). YFP expression correlates with expression of Atg5-Atg12. Samples taken after the indicated time were analyzed by SDS-PAGE and Western blotting.

Higher virus titer and more volume of virus was produced by infection of Sf9/21 cells with ( $V_0$ ). From the obtained  $V_1$  generation High5 expression cells were infected and virus for later experiments was stored. High5 insect cells were used for expression and purification of the proteins since they are bigger in volume and therefore more protein can be expressed. While High5 cells were infected with virus the day of proliferation arrest (DPA) was determined by cell counting every 12 hours. When DPA was reached intracellular YFP levels were measured regularly every 12 hours (see figure 3.7). Along with this an expression profile of uninfected cells, DPA plus 24 hours, 36 hours and 48 hours was compiled. Here whole cell extract (CE), supernatant (S) and pellet (P) of all time points were checked by SDS-PAGE analysis. At the point of highest YFP expression High5 cells were harvested.

Figure 3.7 also shows detection of expressed StrepII-Atg5 and His-Atg12 after immunoblotting. Both proteins were detected around 100 kDa (expected size  $\approx$  60 kDa) indicating the conjugated complex. Only Atg12 was observed as unconjugated form below the 35 kDa marker band (expected size  $\approx$  20 kDa including the tag and TEV cleavage site).

Atg5-Atg12 was then purified from freshly harvested High5 insect cells using  $Ni^{2+}$ -sepharose beads. With the protocol described in caption 2.2.3.2 the Atg5-Atg12 conjugate was obtained in small amounts as indicated by the band between 70 and 100 kDa (see figure 3.8).

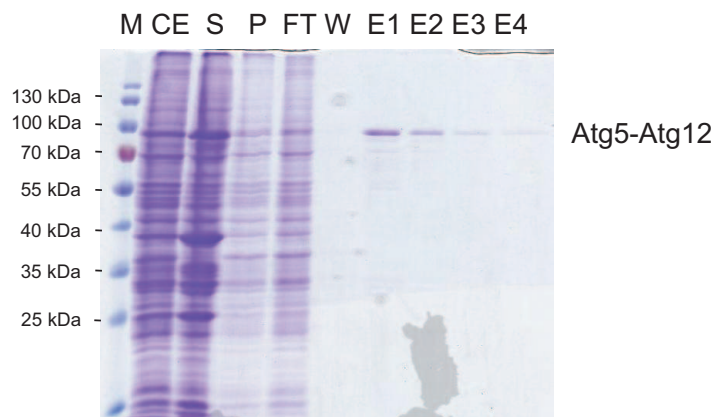


**Figure 3.8: Purification of Atg5-Atg12 from insect cells**

$Ni^{2+}$ -sepharose beads were used for purification of Atg5-Atg12 from High5 insect cells. Samples taken from different purification steps as cell extract (CE), supernatant (S), pellet (P), flow through (FT), washing (W) and elution (E1-E4) were analyzed on a Coomassie stained SDS gels.

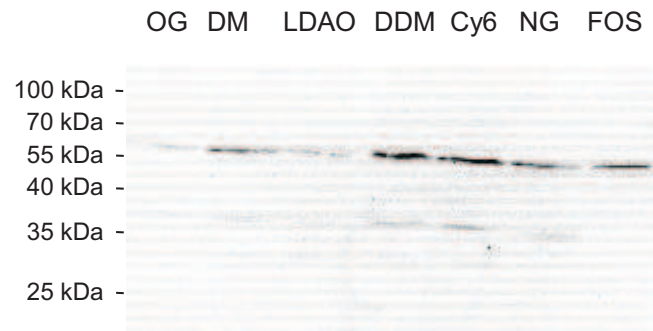


**Figure 3.9: Detergent test to increase Atg5-Atg12 solubility**

Insoluble membrane fractions of High5 cells expressing Atg5-Atg12 conjugate were treated with the Ni-NTA membrane protein kit containing seven different detergents namely octyl- $\beta$ -D-glucopyranoside (OG), n-dodecyl- $\beta$ -D-maltopyranoside (DM), N, N-Dimethyldodecylamine-N-oxide (lauryldimethylamine-N-oxide, LDAO), n-dodecyl- $\beta$ -D-maltoside (DDM), Cymal 6 (Cy6), n-Nonyl- $\beta$ -D-glucopyranoside (NG) and FOS-choline-16 (FOS). Soluble protein fraction received after this treatment were analyzed by immunoblotting with a penta-His antibody.

Atg5-Atg12 was reported to associate with the autophagosomal membrane [60]. Membrane bound or associated proteins usually display large hydrophobic patches which make them insoluble and therefore difficult to purify. Also here Atg5-Atg12 was detected mainly in the pellet fraction (see figure 3.8). Membrane proteins can be solubilized with detergents. Detergents are polar molecules which interact with the hydrophobic parts of the protein, thus solubilizing it. In addition to Triton X-100 which was already used for purification, different detergents can have variable effects on protein solubilization. Therefore a detergent screen was performed (see section 2.2.3.3).

Shown in figure 3.9 are soluble protein fractions after treatment with indicated detergents. A clear increase in soluble Atg5-Atg12 conjugate was detected when the membrane fraction was treated with DDM and Cy6 detergent. Also NG and FOS treated samples showed an increase although not as strong as DDM and Cy6.

For further optimization of the purification the results obtained from the detergent screen should be taken into consideration.

### 3.2.2.2 Atg16 expression and purification from insect cells

Atg5 the target of Atg12 conjugation also interacts with Atg16 [64]. In order to obtain the whole complex for crystallization, human Atg16 was expressed using the MultiBac baculovirus expression system for insect cells. After purification Atg5-Atg12

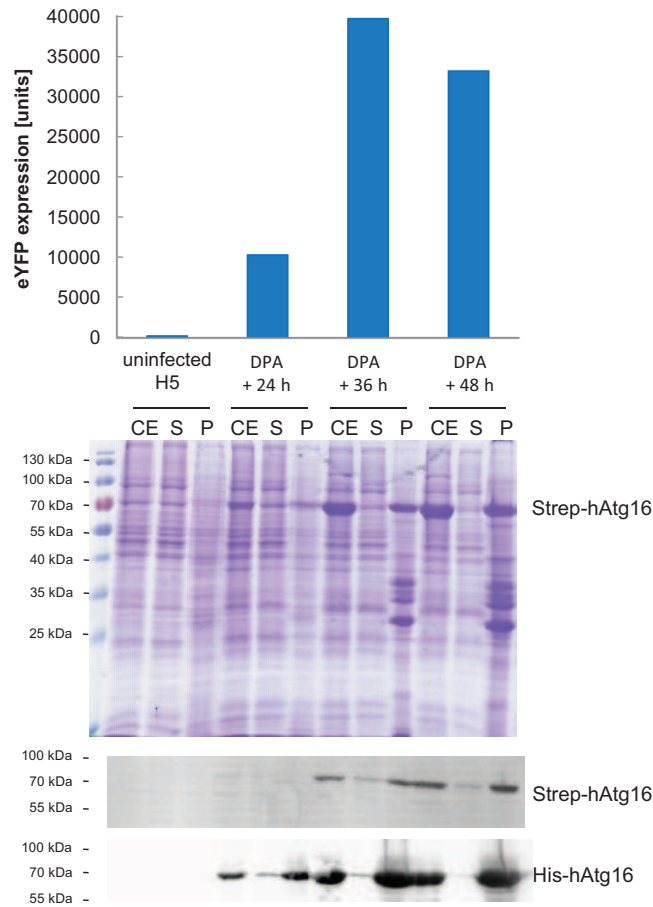


**Figure 3.10: Expression of Atg16 in insect cells**

Expression profile of human Atg16 in High5 insect cells. YFP expression was monitored over time and cell extract (CE), supernatant (S) and pellet (P) samples were analyzed by Coomassie stained SDS gels and Western blots.

and Atg16 will be pooled and further analyzed as well as subjected to crystallization screens. For this, Atg16 was cloned into the pFL-6x His and pFL-StrepII vector. Bacmid preparation and virus generation was done as described above. For final expression High5 insect cells were infected. The day of proliferation arrest was determined and then frequently YFP expression was monitored (see figure 3.10). Samples taken for YFP measurement were also analyzed with SDS-PAGE and subsequent Western blotting.

For Atg16 the strongest expression was detected after 36 hours. When High5 insect cells were incubated for additional 12 hours of expression their viability dropped and along with this expression of YFP decreased. Nevertheless, expression rates for Atg16 still increased as shown on a Coomassie stained SDS gel and with immunoblotting.



Comparisons of expression profiles with His-tagged or StrepII-tagged Atg16 revealed stronger expression of His-Atg16. Differences in virus titer and quality might be the reason. However, unfortunately Atg16 was detected exclusively in the insoluble protein and membrane fraction.

Several purification trials of Atg16 with either Ni<sup>2+</sup>-sepharose beads or Streptactin-sepharose beads failed. Addition of Triton X-100 did not alter solubility, also buffers at pH 7.5 or pH 8.0 were tested. Since it is known that proteins in complex formation might change their solubility, Atg16 cell extract was pooled with cell extract containing Atg5-Atg12. But still Atg16 could not be co-purified.

### 3.2.2.3 MAP1LC3II expression in insect cells

MAP1LC3 is the second ubiquitin-like modifier involved in autophagy [66]. Conjugation of LC3 to its target PE employs the E1- and E2-like enzymes Atg7 and Atg10, respectively. For expression of lipidated LC3 (LC3II) multigene transfer vectors were generated. LC3 was cloned into the acceptor vector pFL. In addition Atg7 and Atg10 were inserted into the two multiple cloning site of the donor vector pUCDM. Both vectors were combined in a Cre/loxP reaction followed by integration of the expression cassette into the MultiBac bacmid. Virus maintenance was done as described above.

Infected High5 insect cells were monitored regarding their viability, cell diameter and YFP expression levels (see figure 3.11). YFP expression correlates with the expression of the complex proteins and was detected at its highest level after DPA plus 36 h to 48 h. Furthermore expression of LC3 in insect cells was analyzed with SDS-PAGE and Western blot. The Coomassie stained SDS gel showed a band around 20 kDa coming up after DPA plus 36 hours. Also in immunoblotting this band was detected as well as a second band just below. The second band consists of lipidated LC3 (LC3II) as it was shown before that LC3II is shifted to lower molecular weight in SDS gel analysis compared to unlipidated LC3 [87]. LC3 seemed to be more soluble compared to LC3II as more LC3 was detected in the supernatant fraction.

Purification of LC3 and LC3II from High5 insect cells was done using Ni<sup>2+</sup>-sepharose beads. As solubility can be increased by treatment of the cells with 2 % Triton X-100 was reported before detergent was included in the purification protocol [87]. LC3 was obtained in high yields from insect cells as shown in figure 3.12. Elution fractions (E1 to E4) and protein still bound to the beads (B) were checked on Coomassie stained SDS

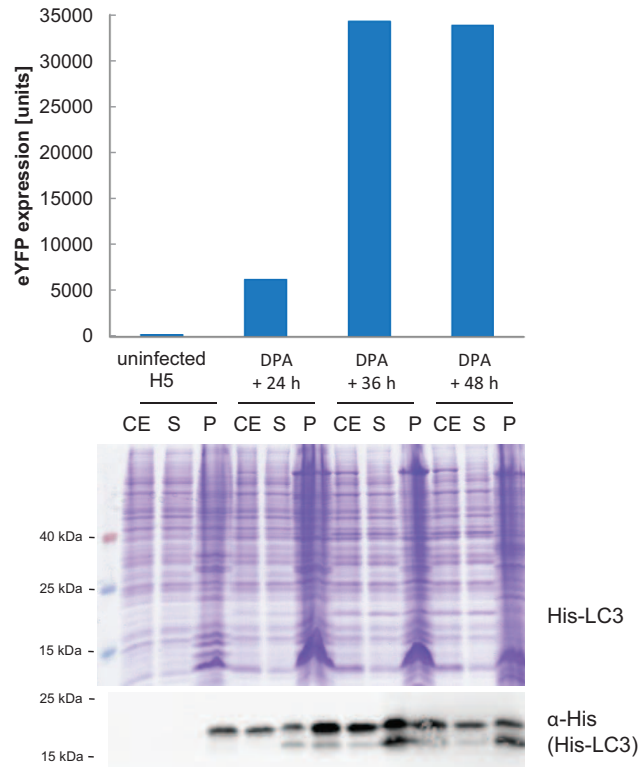


**Figure 3.11: Expression of MAP1LC3 in insect cells**

Monitoring of expression was done by measuring YFP levels over time. Cell extract (CE), supernatant (S) and pellet (P) of insect cells expressing LC3 were analyzed with Coomassie stained SDS gels and Western blotting.

gels and with Western blotting. Here some of the lipidated LC3 was found still bound to the beads.

Most of the LC3 expressed in insect cells was unlipidated. In order to purify sufficient amounts of lipidated LC3 the lipidation rate needs to be improved.

Unlipidated LC3 was also obtained in high yields expressed in bacteria. The purified protein obtained from *E. coli* was subjected to Thermofluor analysis for optimization of purification conditions (experiment was performed by our internship student S. Puranik under my supervision). Here a temperature shift was applied to the protein which was supplemented with Sypro Orange and 88 different solutions contained in the Addit screen. Dequenching of Sypro Orange fluorescence correlates with unfolding of the protein and was therefore monitored in a Real-Time PCR machine.

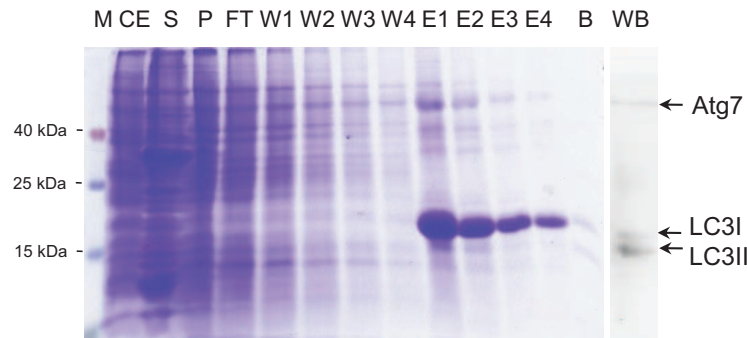


**Figure 3.12: Purification of MAP1LC3 from insect cells**

Purification of LC3 and lipidated LC3 was checked by testing different steps of purification on Coomassie stained SDS gels. Cell extract (CE), supernatant (S), pellet (P), flow through (FT), washing steps (W1-W4), elution fractions (E1-E4) and protein still bound to beads (B) were checked. Western blot analysis of bead bound fraction (WB) was done with a penta-His antibody.

Increase of Sypro Orange fluorescence was shifted towards higher temperatures in conditions with ammonium sulfate, potassium citrate, diaminopentane and polyvinylpyrrolidone (see figure 3.13). These substances increase the stability of LC3 and could be supplemented to the protein during purification to increase the yields of purified proteins.

### 3.2.3 Analyses of conjugated protein complexes

Western blot analysis with a penta-His and a StrepII specific antibody of the purified Atg5-Atg12 complex revealed two bands in the high molecular weight region. One band in the expected size for the conjugate of approximately 60 kDa and a second prominent band of almost 100 kDa. To assure the purification of the right complex and identification of all proteins represented by this band, the band was cut from an SDS gel, subjected to in gel tryptic digestion and then analyzed by mass spectrometry. This resulted that both bands contained the conjugated complex. In addition mass spectrometry analysis the exact conjugation site of Atg12 to Atg5 was identified. The C-terminal glycine of Atg12 is conjugated to Lys130 of Atg5. This showed clearly that the proteins expressed in insect cells are active and Atg12 conjugated to Atg5. Furthermore ubiquitin was also found to be conjugated to Atg5.

Also both bands of LC3 and LC3II were analyzed by mass spectrometry. Indeed both bands contained LC3, but also Atg3 was detected. Some Atg3 must have been co-purified with LC3 and stuck to the protein even during SDS gel separation.

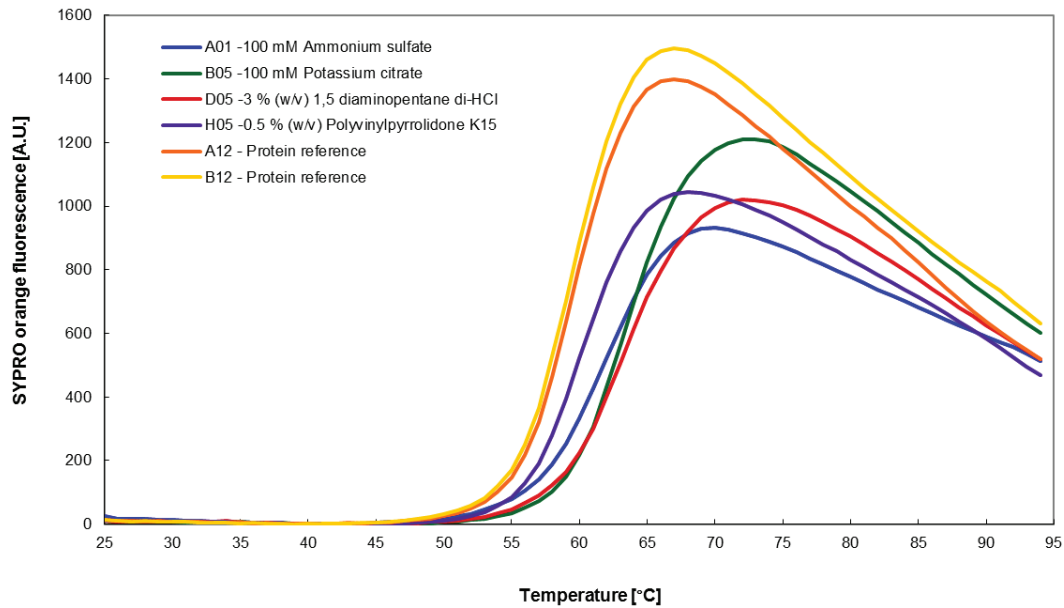


**Figure 3.13: Thermofluor analysis of MAP1LC3 purified from *E. coli* BL21 (DE) cells** Sypro Orange dequenching correlates with unfolding of LC3 in solution. 88 different additives were tested supplemented of LC3 in purification buffer. Indicated additives shifted unfolding of LC3 towards higher temperatures signifying stabilizing abilities of these substances. Experiment carried out by S. Puranik

Mass spectrometric analysis was done by M. Raabe and H.-H. Hsiao from the Bio-analytical Mass Spectrometry research group, MPI for Biophysical Chemistry.

### 3.2.4 Influence of Atg12-Atg5-Atg16 on MAP1LC3 lipidation

The yields of lipidated LC3 expressed from insect cells were quite low. Since LC3 and its E1- and E2-like enzymes are over-expressed, probably a lack of available amounts of PE might be the reason for low conjugation. In order to provide reasonable amounts of PE, we added PE to cell extract prepared from insect cells expressing the conjugation machinery.

We assumed from former purifications that 1 l insect cells express approximately 3 mg LC3 and added commercially available PE purified from brain in excess of an 1:2 ratio. PE was resuspended in buffer used for insect cell resuspension supplemented with 3 % OG. Furthermore along with PE 1 mM final concentration of ATP was added to the cell extract and incubated for 3 hours at RT. Atg12-Atg5-Atg16 complex was reported to function as an E3 ligase on LC3 conjugation [69]. Therefore, also cell extract from High5 insect cells expressing Atg5-Atg12 and Atg16 were pooled together with LC3

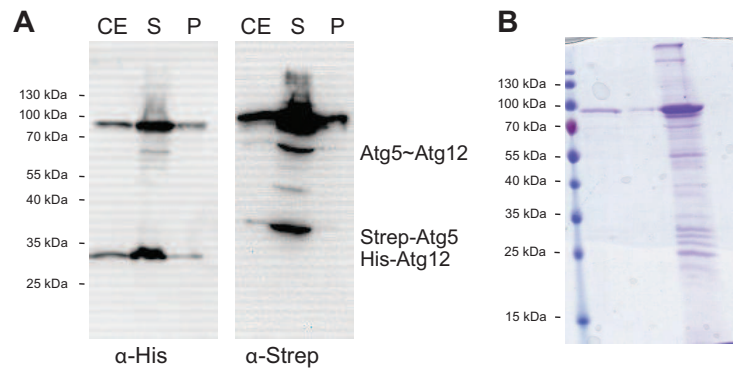


**Figure 3.14: Western blot analysis of the Atg5-Atg12 complex**

(A) In immunoblotting of cell extract (CE), supernatant (S) and pellet (P) from High5 insect cells expressing Atg5 and Atg12, both proteins alone in their expected size were detected with either His or StrepII antibody and the complex of 60 kDa. In addition another prominent band was detected around 100 kDa. (B) Coomassie stained SDS gel with purified Atg5-Atg12 complex. The band of 100 kDa molecular weight was cut from the gel and analyzed by mass spectrometry.

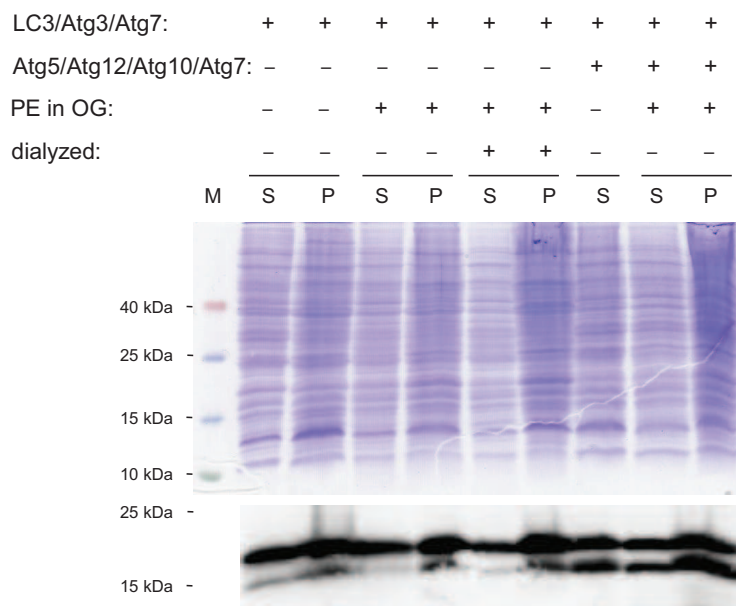
cell extract and PE and incubated. Afterwards, soluble and insoluble fractions were separated and both analyzed in SDS-PAGE and Western blotting.

Figure 3.15 shows that only addition of external PE is not sufficient to increase LC3II yields. Even dialysis against buffer, to decrease the OG amounts in the cell extract did not increase lipidation clearly. However addition of Atg5-Atg12 enhanced the lipidation rate independently upon supplementation of PE.

Taken these results together it was shown that the Atg12-Atg5 complex is required for efficient LC3 lipidation.

### 3.3 Discussion

Here, I show the *in vivo* reconstitution of full length human Atg12 and LC3 conjugation systems. Atg12-Atg5 conjugate was purified from insect cells after infection with the MultiBac baculovirus carrying the genes of human *atg5*, *atg10*, *atg7* and *atg12* for co-expression. Correct conjugation of the C-terminal glycine of Atg12 to the Lys130 of Atg5 was confirmed by mass spectrometric analysis. In addition LC3 was expressed and purified from insect cells and low yields of lipidated LC3 were obtained. The presence of the E1- and E2-like enzymes Atg7 and Atg3 were not sufficient for efficient lipidation. Addition of the Atg5-Atg12 conjugate was required to increase the lipidation rate



**Figure 3.15: *In vitro* lipidation of LC3**

Different conditions were tested to increase the yields of lipidated LC3. The first two lanes of the Coomassie stained SDS gel and Western blot show supernatant (S) and pellet (P) fraction of High5 cells expressing the proteins of the LC3 conjugation complex. In lane 3 and 4 external phosphatidylethanolamine PE was added. Next two lanes show S and P dialyzed against buffer to reduce OG detergent amounts. Lane 7 shows pooled fractions of LC3 and Atg12 complex expressing High5 cells. The last two lanes represent a mixture of both complexes together with addition of PE.

whereas addition of PE alone was not enough to increase lipidation of LC3. It has been reported, that the Atg5-Atg12 complex is sufficient as E3-like ligase [69].

*In vitro* reconstitution systems have already been described as from Fujioka *et al.* [22]. Here the conjugation system of Atg8 and Atg12 from *A. thaliana* were reconstituted using purified recombinant proteins from bacteria. By pooling these purified proteins low amounts of Atg5-Atg12 conjugate could be obtained, but the reaction was not as efficient as *in vivo* conjugation. In another *in vitro* reconstitution of mammalian Atg5-Atg12 expressed in bacteria addition of ribonucleic acid increased the conjugation yield [88]. Noda *et al.* [89] reported from co-expression of truncated forms of yeast Atg12 and Atg5 in bacteria together with Atg7 and Atg10. This truncated conjugation complex was then mixed with the N-terminus of Atg16 required for Atg5 interaction. They obtained crystals from this construct but no structure was published up to now.

In order to receive the conjugated proteins in the quantity required for crystallization and properly folded, an eukaryotic expression system was used here.

Only lipidated yeast Atg8 was obtained in decent yields using an *in vitro* reconstitution system [90]. Here Atg8-II was reconstituted on liposomes containing 70 % PE and 30 % PC. Reported *in vitro* reconstitution of LC3II showed low efficiency [91]. These results indicate the requirement of the E3 activity of Atg5-Atg12. This activity has been reported for yeast [61], mammals [92] and plant [69] indicating that this function is evolutionarily conserved. However, neither Atg12 nor Atg5 alone promote this reaction. Also excess amounts of Atg5-Atg12 inhibits LC3 lipidation [93].

Structural analysis of these complexes is required to gain further insight into the molecular function of these complexes. Despite their essential role in autophagosome formation, the mechanism of their activity is poorly understood. From structural analysis also further insights on their biochemical activity could be gained. Since these complexes are part of the core autophagy machinery and deletion of a single protein leads to breakdown of the whole autophagy machinery, some open questions are left to be answered on their molecular interplay.

### 3.4 Outlook

Purification of Atg12-Atg5 can be further optimized by implementation of the results from the detergent screen to increase soluble Atg5-Atg12 yields. Subsequently additional Thermofluor experiments should be performed to determine stabilizing conditions for this protein complex. By addition of identified stabilizing substances crystallization probability might be increased and crystal screens will be set up for the conjugate.

Furthermore Atg16 might be solubilized by using another detergent than Triton X-100, which needs to be determined using the detergent screen. Probably solubility of Atg16 could be increased by infection of one High5 insect cell culture with viruses for Atg16 and Atg5-Atg12 expression. Co-expression of all proteins in one culture might enhance Atg16 solubility. Another possibility of expressing Atg16 with the Atg5-Atg12 complex is cloning of Atg16 into an additional donor vector, which can be integrated via the loxP site into the acceptor vector. Then all five proteins belonging to the Atg12 conjugation system will be co-expressed from one bacmid. Even so, the aim is to purify full length proteins the N-terminal part of Atg16 needed for interaction with Atg5 could be purified and used co-crystallized instead.

When a complex of Atg12-Atg5-Atg16 will be purified the oligomerization state of this complex will be tested using analytical gel filtration or MALLS analysis. So far there seems to be a discrepancy between dimerization of this complex observed in the crystal

structure of Atg16 coiled coil domain reported by Fujioka *et al.* [33] and large molecular weight Atg12-Atg5-Atg16 complexes purified from both yeast and mouse, which would correspond to tetramers in yeast [94] or octamers in mouse [65], respectively.

Lipidation of LC3 *in vitro* by addition of the Atg5-Atg12 cell extract will be further optimized. Then the detergent screen will be employed to increase the solubility of LC3-PE. When LC3II is purified buffer optimization will be done with ThermoFluor experiments. Additionally, purified LC3II will be subjected to crystallization screens.

In case of purification of both complexes they can be pooled and biochemically analyzed. Also unlipidated LC3 is sufficient to investigate how the Atg12-Atg5-Atg16 complex interacts with LC3 and how this complex acts as an E3-like ubiquitin ligase on LC3 [69].



# 4 Project II: Insights into membrane binding of PROPPINs

## 4.1 Introduction

### 4.1.1 The autophagosomal membrane

For some decades it has been thought that autophagosomes are formed *de novo* unlike the formation of other vesicles in the cell, which are generated by budding off from existing membranes. The source of lipids for the growing isolation membrane (or phagophore) has been under debate. To our surprise, several membrane compartments were recently identified to provide membrane precursors. In higher eukaryotes most autophagosomes were reported to be generated close to the endoplasmatic reticulum (ER) and EM images showed direct connections between early isolation membrane and ER [95, 96, 97]. However, also mitochondria [98], the plasma membrane [99, 100] and Golgi [101, 102, 103, 104, 105] have been reported to give rise to autophagosomal membrane precursors.

Most autophagy protein complexes described are involved in early stages of autophagosome formation and membrane expansion, including the kinase-containing Atg1 complex (in mammals ULK1 complex) [106, 18, 107, 108, 109], the class III phosphatidylinositol 3-kinase complex Vps34 [19, 20], the Atg12 and Atg8 (LC3) conjugation systems [23, 33, 22, 92, 80], the transmembrane protein Atg9 [110, 111] and phosphoinositide binding proteins as Atg18 [112]. These complexes are well known but their molecular interplay has been less studied.

Recruitment of these complexes to the autophagosomal structure and therefore hubs of autophagosomes are less understood. Among a few others, one protein group is of special interest to build the connection between the autophagosomal membrane and

recruitment of other proteins to isolation membranes. This group of  $\beta$ -propeller proteins that bind polyphosphoinositides (PROPPINs) comprises three yeast homologs, namely Atg18, Atg21 and Hsv2 (in mammals: WIPI1-4). The PROPPIN family members bind PI3P.

Production of the phosphoinositide PI3P is essential for autophagosome formation and induced upon starvation. PI3P is generated by the Vps34 kinase complex [113, 114, 115]. Yeast isolation membranes are enriched with PI3P [116]. Recently it was also shown that dephosphorylation of PI3P is necessary for final fusion of the autophagosome with the vacuole since Atg proteins stay associated to the membrane [117].

#### 4.1.2 Phosphoinositide effectors

The seven natural phosphoinositides are enriched in specific membrane compartments. PI(4,5)P<sub>2</sub> is localized to the plasma membrane, PI3P and PI(3,5)P<sub>2</sub> are present on early and late endosomes, respectively and PI4P is mainly found at the Golgi complex [118]. A distinctive property of the PIPs is their fast rate of appearance and disappearance in the membrane. The PI-metabolizing enzymes rapidly synthesize them upon induction where and when they are required, and they are also rapidly consumed. This fact makes them ideal determinants for dynamic processes, such as membrane trafficking and recruitment.

A range of PI effector domains are known and their structures were described (see figure 4.1). First, the pleckstrin homology (PH) domain was reported to recognize phosphoinositides [119, 120, 121]. Since then number of domains were found including the ANTH (AP180 N-terminal homology) [122, 123, 124], C2 (conserved region-2 of protein kinase C) [125], ENTH (epsin N-terminal homology) [126], FERM (4.1, ezrin, radixin, moiesin) [127], FYVE (Fab1, YOTB, Vac1 and EEA1) [128, 129], GOLPH3 (Golgi phosphoprotein 3) [130, 131], PDZ (postsynaptic density 95, disk large, zonula occludens) [132], PROPPINs ( $\beta$ -propellers that bind PIs) [133], PTB (phosphotyrosine binding) [121], PX (Phox homology) [134, 135, 136] and Tubby modules [137, 138]. Recently the first PROPPIN structures were solved [24, 25, 26]. These effectors show high specificity to one or two phosphoinositides, in contrast two domains PX and PH were shown to bind several phosphoinositides.

Many of these phosphoinositide binding motifs have a low affinity and make use of different mechanisms to increase affinities. One mechanism used is domain oligomerization as reported for the FYVE and PH domain. Some proteins comprise two of

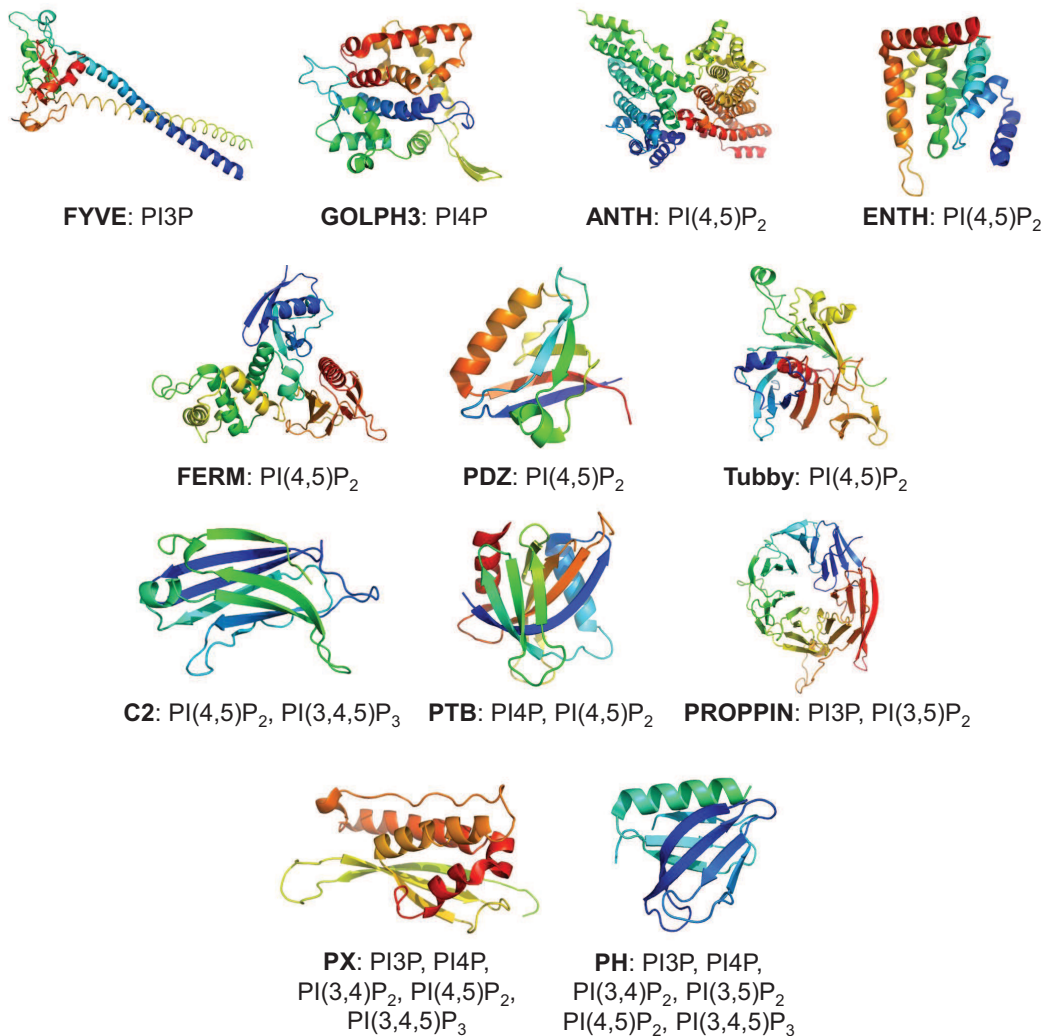


**Figure 4.1: Overview of phosphoinositide binding motifs and their structure**

Shown here are the known domains binding phosphoinositides. Different domains bind different phosphoinositides as indicated. Some show specificity to only one kind of phosphoinositides, some to two phosphoinositides or like the PX and PH domain to a range of different phosphoinositides. Domains are colored from the N-terminus in blue to C-terminus in red.

these phosphoinositide effector domains. The C2, PH and PX domains were also found to bind other lipids as phosphatidylserin or phosphatidic acid in addition to phosphoinositides. In addition, proteins carrying a phosphoinositide binding domain might also interact with a membrane protein to get into proximity of the membrane. Furthermore, partial membrane insertion of the domain is quite common as e.g. described for the FYVE, PX and ENTH domain. [139].

### 4.1.3 Phosphoinositide effectors involved in autophagy

PI3P signaling is crucial for autophagy initiation and is generated by two complexes in yeast, the Vps34 PI3-kinase complex I comprising Vps34, Vps15, Vps30 (in yeast also: Atg6, in mammals: Beclin 1) and Atg14 (in mammals: Barkor) and complex II in which Atg14 is replaced by Vps38 [19]. Complex I functions in autophagy and the Cvt (cytoplasm-to-vacuole-targeting) pathway, whereas complex II is involved in vacuolar sorting of carboxypeptidase Y. Followed by the generation of PI3P at the PAS a string of PI effectors are recruited to the autophagosomal membrane.

Atg14 binds to PI3P and PI(4,5)P<sub>2</sub> and recruits the class III phosphatidylinositol 3-kinase I to the early autophagosomal structure [140]. The PX domain harboring proteins Atg20 and Atg24 bind PI3P and function in the Cvt pathway [141, 142].

The PROPPIN family comprises the three yeast homologs Atg18, Atg21 and Hsv2. Atg18 is recruited to the PAS and forms a complex with Atg2 and mediates cycling of Atg9 between a peripheral compartment and the PAS [142]. Furthermore, Atg18 regulates the Fab1/PI(3,5)P<sub>2</sub> synthesizing complex [143]. Atg18 is also involved in vesicular transport from the vacuoles to the Golgi [133]. Atg21 is needed for proper localization of Atg8-PE to the autophagosomal membrane and is involved in the Cvt pathway [144]. Also Hsv2 binds both phosphoinositides and is required for efficient piecemeal microneurophagy [112]. The pexophagy (degradation of peroxisomes) specific protein Atg26 binds specifically to PI4P through its GRAM domain [145, 146, 147]. The PI3P effector protein Atg27 (Etf1) is also involved in the Cvt pathway [148].

Further PI effectors were shown to be involved in autophagy, including ALFY (autophagy linked FYVE protein) [149], FYCO1 (a novel FYVE and coiled-coil domain-containing protein) [150] and mammalian DFCP1 (double FYVE-containing protein 1) [95].

### 4.1.4 PROPPINs and their role in autophagy

$\beta$ -propellers that bind polyphosphoinositides (PROPPINs) comprise a WD-40 repeat containing domain that forms a seven bladed  $\beta$ -propeller [133, 24, 25, 26]. Within this domain the highly conserved FRRG motif is located, which has been shown to be essential for phosphoinositide binding [144, 133, 151]. The three yeast PROPPINs Atg18, Atg21 and Hsv2 are highly conserved. The mammalian PROPPIN homologs are denoted as WIPI (WD40 repeat containing proteins that interacts with PtdIns) pro-

teins [152]. Four WIPI homologs have been identified. WIPI1 and WIPI2 are orthologs of Atg18 [153].

Atg18 is part of the core autophagy machinery and involved in macroautophagy, Cvt-pathway and piecemeal microautophagy of the nucleus (PMN) [154, 155, 151]. PI3P is necessary for recruitment of Atg18 in early stages of the autophagosomal membrane formation [142]. In complex with Atg2 it mediates cycling of Atg9 to and from the PAS [21]. Beside PI3P Atg18 binds to PI(3,5)P<sub>2</sub> and localizes to the vacuole where it is a regulator of the PI3P 5-kinase Fab1 complex [143].

The function of Atg21 is restricted to the Cvt pathway and PMN [156, 144, 112]. Atg21 was reported to act upstream of the Atg8 conjugation system and is involved in its proper localization to the growing membrane [156, 155].

Hsv2 is the least studied PROPPIN and its function is still unclear, so far it was only described to be involved in PMN [112].

#### 4.1.5 WD40 repeat containing proteins in autophagy

Among the ten most abundant domains across eukaryotes is the WD40 repeat containing domain which is also present in prokaryotes [157, 158]. A single WD40 repeat has a length of 44 to 60 residues. Characteristic features of a WD repeat are a conserved GH dipeptide 11 to 24 residues after the beginning of the motif and a second conserved WD dipeptide at its C-terminus. Caused by the low sequence conservation of only two dipeptides it is difficult to predict WD40 repeat containing proteins in the genome [157, 159, 160, 161, 162]. WD40 repeat containing proteins fold as  $\beta$ -propellers. They consist of four to eight blades. However, most so far described structures of WD40 containing proteins fold into a seven bladed  $\beta$ -propeller.

Providing a platform for protein-protein and also protein-nucleic acid interactions, WD40 proteins were reported to play a role in central biological processes as hubs in cellular networks. WD40 proteins function in signal transduction, cell division, cytoskeleton assembly, chemotaxis and RNA processing. Up to date no WD40 containing protein has been identified with catalytic activity [157, 159, 163, 164].

The  $\beta$ -propeller structure represents a scaffold for interactions and for this reason WD40 proteins form hubs for huge molecular machineries. Three different interaction sites are provided on the propeller, the top and bottom region of the propeller and its circumference, in addition some interactions include the entry site of the central channel

of the  $\beta$ -propeller [157]. Besides interaction with other proteins, WD40 domains can interact with each other and therefore provide a platform for complex formation.

A whole range of WD40 repeat containing proteins are known to be involved in the ubiquitin-proteasome pathway, in which they mediate substrate specificity and recruit cargo to the ubiquitination machinery. Besides recruiting proteins for ubiquitination WD40 proteins were also shown to provide a binding site for ubiquitin itself [165, 166].

Autophagy involves several WD40 repeat containing proteins like the proteins containing to the PROPPIN subfamily, Atg16, ALFY, EPG-6 and Ambra-1. Atg16 is part of the Atg12 conjugation system and only Atg16L homologs of higher eukaryotes contain the C-terminal WD40 domain. So far Atg16 was reported to be involved in oligomerization of the Atg12-Atg5-Atg16L complex, but this interaction is not dependent on the WD40 domain and no other interaction partner was identified for this domain, yet [65]. In selective autophagy the multidomain protein ALFY links p62 labeled cargo by interaction with its C-terminal BEACH domain to the autophagic machinery. It is interacting with Atg5 via its WD40 domain and with PI3P containing membranes using its FYVE domain [167, 149]. EPG-6 an autophagy protein found in *C. elegans* contains a WD40 domain and was shown to directly interact with Atg2 and is a homolog of WIPI4 [168]. Ambra-1 a highly conserved vertebrate WD40 repeat containing protein is involved in Beclin1/Vps34 activation of autophagy [169, 170].

#### 4.1.6 Structure of Hsv2

During the time course of this thesis the structure of *K. lactis* Hsv2 [24, 25] and *K. marxianus* Hsv2 [26] were published by us and others. Crystals of KlHsv2 grown diffracted up 3.0 Å [24]. The structure was solved by SAD (single-wavelength anomalous diffraction phasing) using selenomethionine labeled protein.

The structure of KlHsv2 revealed a seven bladed  $\beta$ -propeller (see figure 4.2). Each blade comprises four antiparallel  $\beta$ -strands. Unlike most other  $\beta$ -propeller structures, KlHsv2 shows a non-velcro like closure. Here the last blade is formed completely by the C-terminus. In other structures containing a velcro-like closure the final blade is partially formed by the N-terminus [171, 159].

Loop regions connect each  $\beta$ -strand within the  $\beta$ -propeller. These loops are quite unconserved among PROPPINs and differ in their lengths. KlHsv2 possesses quite short loops compared to *S. cerevisiae* Hsv2. Besides one long loop connecting strand C and D of blade 6. In most crystals some residues of this loop did not give good

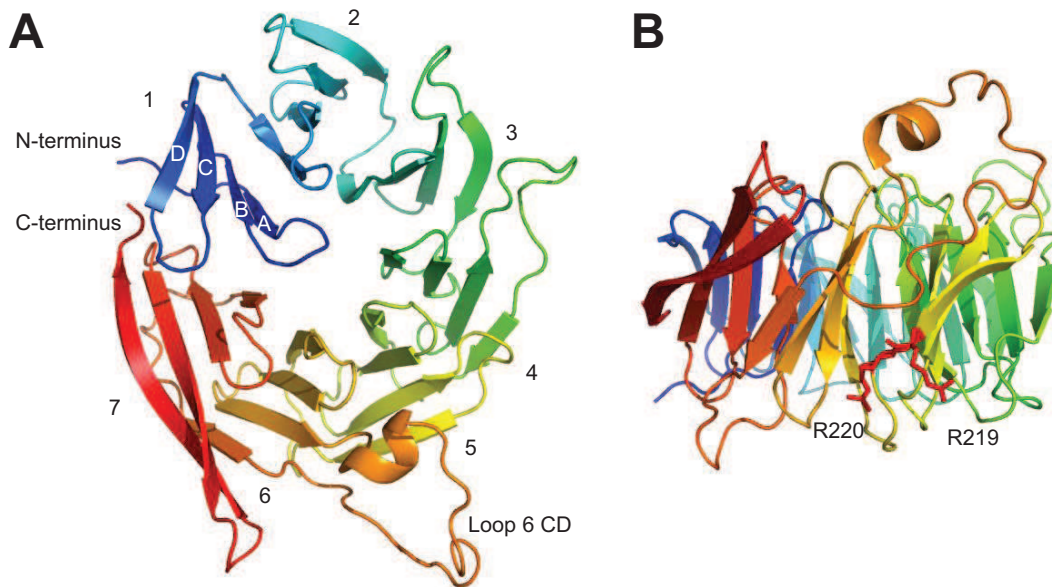


**Figure 4.2: Structure of the PROPPIN KIHsv2**

(A) KIHsv2 forms a seven bladed  $\beta$ -propeller (indicated by numbers Atg16L homologs), each propeller comprises four  $\beta$ -strands (indicated by letters). The loop connecting strand C and D of blade 6 is especially long and disordered. (B) Shows a  $90^\circ$  rotation of the structure to demonstrate the orientation of the two arginines pointing into opposite directions. PDB code: 4AV8 (See also [24])

electron densities caused by its high flexibility. Due to its flexibility part of the loop was disordered in the  $3.0 \text{ \AA}$  crystal structure. However, we also determined a  $3.3 \text{ \AA}$  crystal structure where the complete loop could be built [24].

Interestingly the two arginines of the FRRG motif (Arg119 and Arg120), located in blade 5 strand D and reported to be essential in phosphoinositide binding, did not form a single phosphoinositide binding pocket as expected. Rather they point into opposite directions indicating two potential binding sites. To exclude crystal packing constraints causing the arginines sticking to their observed positions, molecular dynamics simulations were carried out resulting in the confirmation of the position of both arginines towards opposite directions. Furthermore each of the indicated potential phosphoinositide binding pockets were occupied by sulfate ions originating from crystallization conditions. Before it was already reported that sulfate and phosphate ions indicate potential phosphoinositide binding pockets [172, 173, 174].

Therefore we speculate that PROPPINs contain two possible phosphoinositide binding sites.

### 4.1.7 Aims

Atg18, Atg21 and Hsv2 are PROPPINs involved in autophagy. They are highly conserved among each other but adopt different functions in autophagy.

How they act in concert with other proteins and how they interact with membranes is still not well understood. Their structures were of great interest, since WD40 repeat containing proteins are often a scaffold for protein-protein interactions [157, 159] making PROPPINs to candidates for the recruitment of other proteins to autophagosomal membranes. How do PROPPINs consisting of a single domain combine binding of other proteins and additional binding to membranes?

The aim of this project was to express, purify and crystallize the autophagic yeast PROPPINs Atg18, Atg21 and Hsv2. In addition, their membrane binding should be further characterized using biochemical and biophysical approaches based on our Hsv2 structure (see figure 4.3).

## 4.2 Results

### 4.2.1 Expression and purification of yeast PROPPINs

#### 4.2.1.1 Expression and purification of yeast PROPPINs in insect cells

Earlier expression studies revealed that expression of *S. cerevisiae* Atg18 and Atg21 (hereafter ScAtg18 and ScAtg21) in *E. coli* gives very small yields of purified protein or the protein is localized in inclusion bodies and therefore found in the insoluble fraction during purification. For this reason, I used the insect cell expression system to obtain soluble ScAtg18 and ScAtg21 [45]. An advantage of this system is, that it is an eukaryotic expression system and if the protein needs post translational modifications i.e. glycosylation, those modifications will be made in the insect cells.

For insect cell expression ScAtg18 and ScAtg21 were amplified for Gateway pENTR/D-TOPO cloning. During this step a Kozak sequence, 10x His-tag and a TEV cleavage site were added to the N-terminus of the genes. Furthermore, in an LR recombinase reaction the genes were transferred from the pENTR vector to the pDEST8 vector, which is suitable for the integration of the genes into the bacmid. Then, competent *E. coli* DH10 MultiBac cells were transformed with pDEST8 vector carrying either ScAtg18 or ScAtg21 genes. The genes integrate into the bacmid via Tn7 sites, which are located in



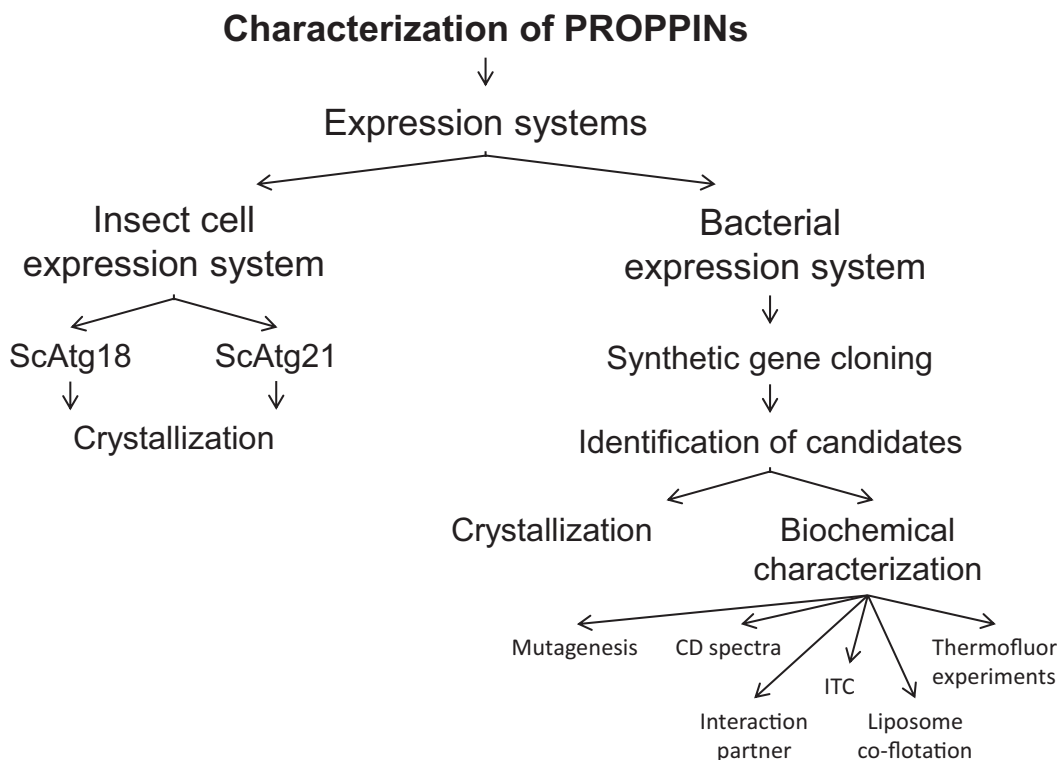


**Figure 4.3: Approach for the characterization of PROPPINs.**

Flow chart to illustrate the approach for project II. Starting out with two different expression systems the main goal is the characterization of PROPPINs through X-ray crystallographic structure determination and biochemical methods.

the *lacZ* gene and this was used for blue-white screening. Thereafter, for transfection of Sf21 insect cells the bacmids were extracted from *E. coli* DH10 cells (see section 2.2.2.2).

Purified bacmid was transfected into Sf21 insect cells for virus generation. It is very important to ensure high viability of insect cells. If this is the case a high transfection efficiency can be reached. Therefore, Sf21 cells were checked under the microscope after Trypan blue addition to stain dead cells. In addition, cell number and viability was measured using a cell counter. Viability of these cells should be at least 92 % for efficient transfection (see section 2.2.2.3). The transfection rate can be monitored under a fluorescence microscope within 48 hours to 60 hours due to expression of YFP from the bacmid. As a result, virus ( $v_0$ ) should be released to the media in 60 hours to 72 hours and was harvested in this time frame.

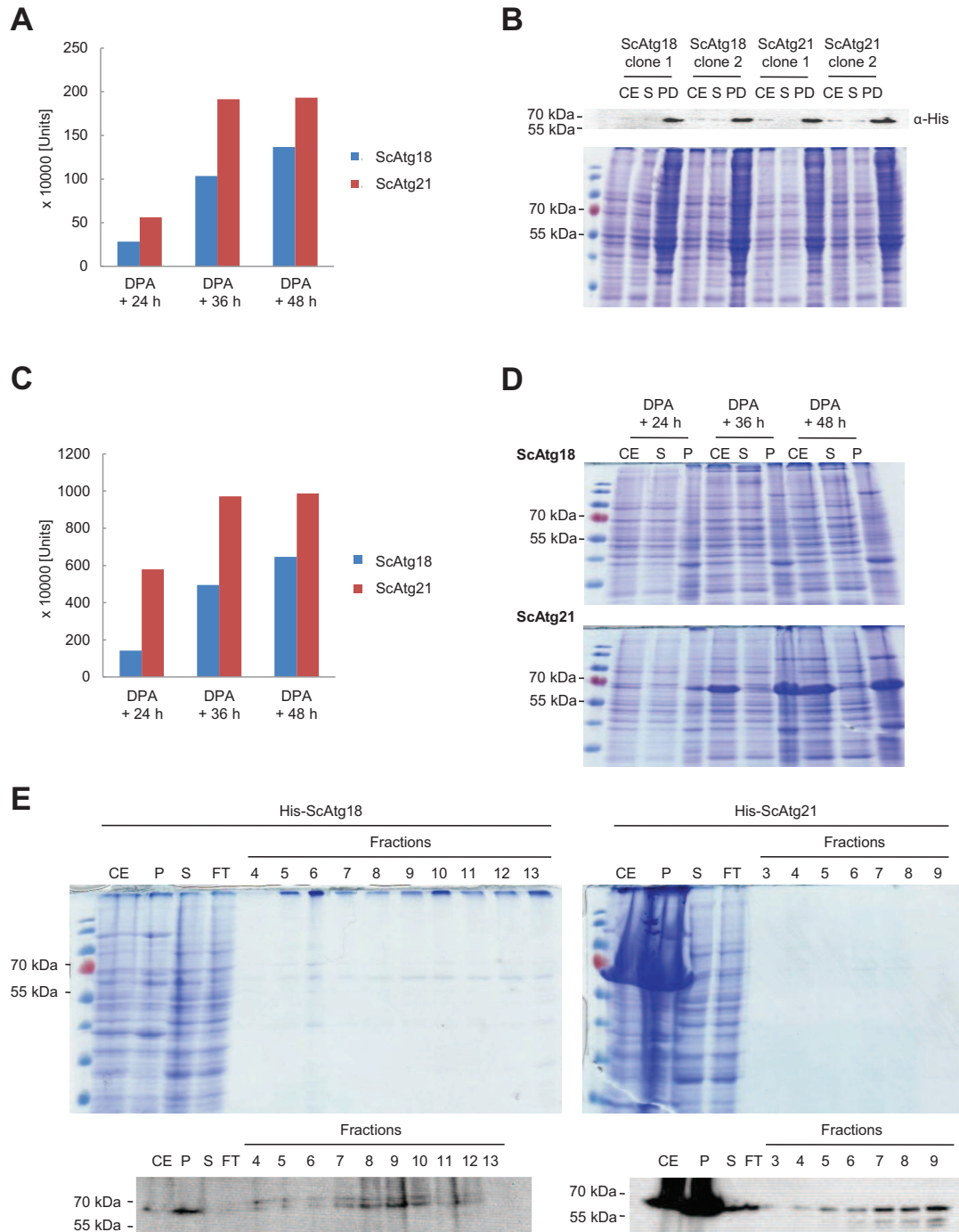


**Figure 4.4: Expression of ScAtg18 and ScAtg21 from insect cells.**

(A) Measurements of YFP expression in Sf21 insect cells. Samples taken 24 h, 36 h and 48 h after day of proliferation arrest (DPA). Comparison of YFP expression in ScAtg18 and ScAtg21 co-expressing cells. (B) Pull down experiment of ScAtg18 and ScAtg21 expressing insect cells. Loaded on 12 % SDS-PAGE gels are whole cell extract (CE), supernatant (S) and fraction after pull down (PD) from two different clones of both ScAtg18 and ScAtg21. Expression of the PROPPINs was confirmed in Western blotting analysis using an antibody against His-tag. (C) YFP determination from infected High5 insect cells. Samples taken 24 h, 36 h and 48 h after DPA. (D) Following expression of ScAtg18 (upper gel) and ScAtg21 (lower gel) over the time. Shown are whole cell extract (CE), supernatant (S) and pellet (P) after DPA + 24 h, + 36 h and + 48 hours. (E) Purification of ScAtg18 and ScAtg21 using an 1 ml His-Trap FF column. 12 % SDS-PAGE and Western blotting analysis with anti-His antibody show whole cell extract (CE), pellet (P), supernatant (S), flow through (FT) and elution fractions (fraction No.).

Large scale production of virus in Sf21 cells was necessary to reach a higher virus titer and to store virus for several expression experiments. For this purpose, 3 ml of virus was added to 25 ml Sf21 cell suspension. Infection of Sf21 cells with the virus was determined by measuring cell density. Stagnation of cell division indicates the day of proliferation arrest (DPA). In addition, to follow expression of genes encoded by the bacmid, YFP expression was measured (see section 2.2.2.5) every 12 hours starting after the DPA (see figure 4.4 A). YFP expression over time increases as expected and is a direct indicator for late expressed virus genes, since it is regulated by a late stage viral promoter like ScAtg18 and ScAtg21 genes. In a next step, a test purification of ScAtg18 and ScAtg21 using Ni<sup>2+</sup>-sepharose beads (see section 2.2.2.4) was carried out with the same samples taken for YFP measurement (see figure 4.4 B). In fractions containing proteins enriched with Ni<sup>2+</sup>-sepharose beads (PD) a prominent band close to 70 kDa is visible. This band was confirmed to contain a His-tag in Western blot analysis and consequently represents expressed ScAtg18 and ScAtg21, respectively. Between 60 to 72 hours virus (v<sub>1</sub>) was harvested again by centrifugation of the cell suspension at 1,000 rpm for 20 min, 4 °C.

High5 insect cells were used for large scale expression of the PROPPINs. These cells are bigger in diameter and therefore more suitable to express higher protein amounts. After infection of two times 400 ml with v<sub>1</sub> virus cell density, viability and diameter was monitored as well as expressed YFP amounts (see figure 4.4 C). YFP expression increase stronger in High5 cells than in Sf21 cells. Also the cell diameter increased more drastic in High5 cells (from 19 μm up to 24.5 μm) than in Sf21 cells (from 17.5 μm up to 20 μm). When the day of proliferation arrest was determined by measuring cell density High5 cells were harvested at DPA plus 48 hours, since this time point was determined by YFP measurement as point of highest protein expression. In figure 4.4 D whole cell extract, supernatant and pellet of DPA plus 24 h, 36 h and 48 h are shown. ScAtg18 is expressed in very low amounts and hardly visible as a band around 70 kDa. In contrast, ScAtg21 is expressed in high amounts but most of the protein is present in the pellet fraction.

During different purification trials the purification protocol for these proteins (see section 2.2.4.2) were optimized. One of the obstacles to overcome was the problem that insect cells have much higher chromosomal DNA amounts than i.e. bacteria. Since adding DNaseI to the cell extract is not sufficient, chromosomal DNA was precipitated with streptomycin sulfate and pelleted during centrifugation. Another problem was the high insolubility of ScAtg21, for this reason cell extract was treated with Triton X-100 to disrupt membranes and inclusion bodies. Also an additional purification step was

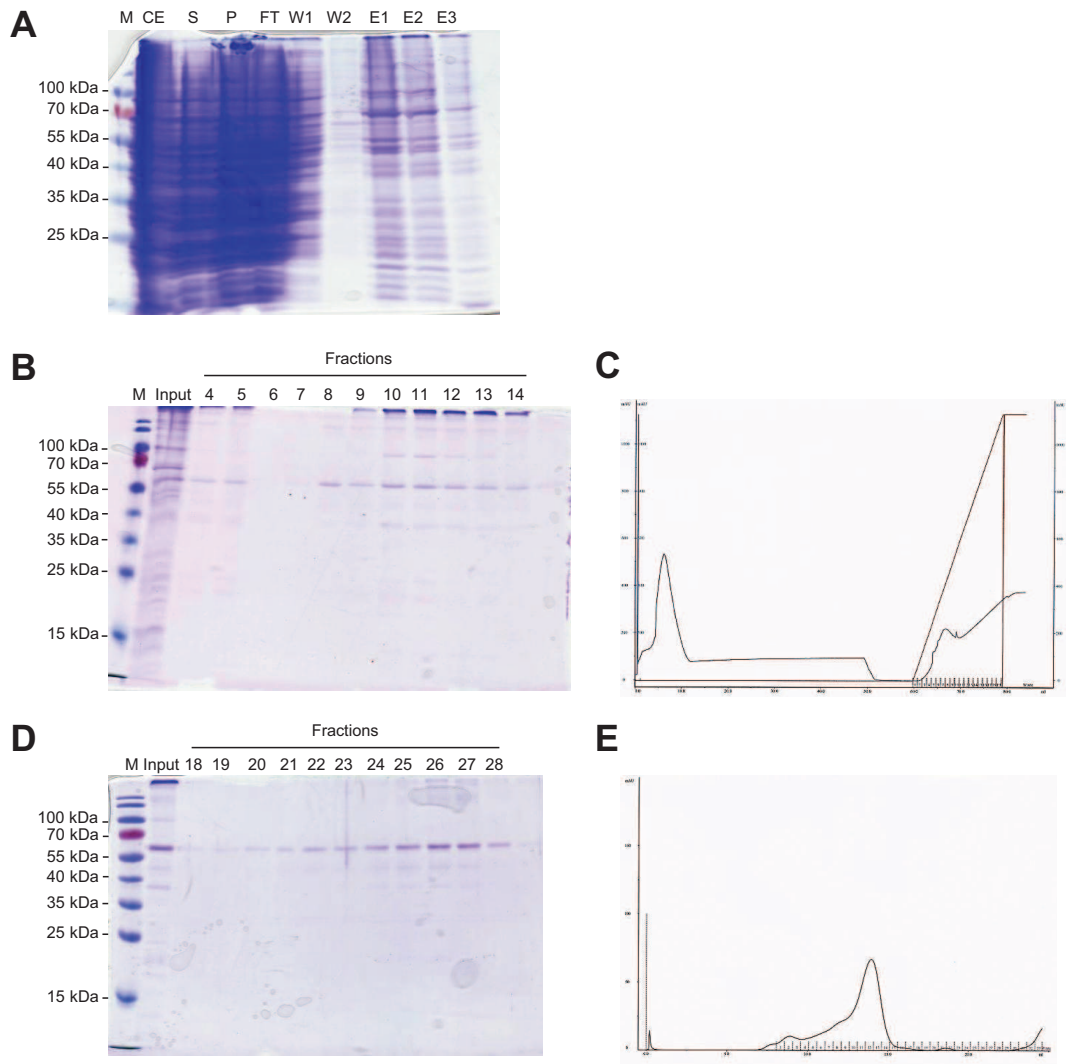


**Figure 4.5: Purification of ScAtg18 from High5 insect cells with optimized protocol**  
 (A) Purification of ScAtg18 with Ni<sup>2+</sup>-sepharose beads. The Coomassie stained SDS gel shows fractions to follow the purification steps and efficiency. (B+C) Purification of ScAtg18 with 1 ml His-Trap FF column. Fractions taken during purification were checked in SDS-PAGE and by UV<sub>280</sub> detection. (D+E) Final purification of ScAtg18 using size exclusion chromatography with a gel filtration S200 HR 10/30 column.

included. As a first purification step Ni<sup>2+</sup>-sepharose beads were used for affinity purification. Second step was a complementary 1 ml His-Trap FF column purification with an Äkta to increase purity of the elution fractions. Gel filtration chromatography was employed as final step to reach protein purity applicable for crystallization. Following this optimized protocol small amounts of ScAtg18 were purified (see figure 4.5).

#### 4.2.1.2 Bacterial expression and purification of yeast PROPPINs

Expression of ScAtg18 and ScAtg21 from insect cells yielded low amounts of purified proteins or protein remained insoluble. For this reason, I tried to find homologs for Atg18, Atg21 and Hsv2 from other yeast species. Criteria for selection were for example the length of loops which connect the blades of the propeller. Since the loops are unstructured and highly flexible, proteins with shorter loops are more suitable for crystallization and solubility of the proteins might be increased. Another indication for crystallization suitability gave the online tool TarO (Target Optimisation Utility; <http://www.compbio.dundee.ac.uk/taro>). This tool combines a broad range of bioinformatic techniques to calculate different protein properties. Besides, it gives an overview of protein characteristics. Another factor for our decision was the prediction of the crystallization propensity of the proteins (see table 4.1). Based on these facts I decided to order synthetic genes optimized for bacterial expression of the following homologs:

- *Schizosaccharomyces pombe*: Atg18, Atg21 and Hsv2
- *Pichia angusta*: Atg18 and Atg21
- *Kluyveromyces lactis*: Atg21
- *Caenorhabditis elegans*: Atg18
- *Drosophila melanogaster*: Atg18

*S. pombe* homologs and *D. melanogaster* Atg18 are especially short proteins. Here, unstructured loop regions that might inhibit crystallization are very short and the overall prediction of disordered regions are quite low (compare table 4.1). *P. angusta*, *C. elegans* and *K. lactis* Atg18 and Atg21 have a higher potential to crystallize (high score or amenable) in agreement with TarO.

**Table 4.1:** PROPPIN homologs analyzed by TarO

PROPPIN	Species	Crystallization propensity prediction	Sequence length [aa]	Molecular weight [Da]	Disorder prediction	Glycosylation sites	Phosphorylation sites
Atg18	<i>S. cerevisiae</i>	recalcitrant	500	55,102	0.17	1	34
	<i>S. pombe</i>	recalcitrant	373	41,109	0.11		16
	<i>P. angusta</i>	high score	525	57,936	0.25		36
	<i>C. elegans</i>	high score	412	45,274	0.17		25
	<i>D. melanogaster</i>	recalcitrant	377	41,739	0.03	1	20
Atg21	<i>S. cerevisiae</i>	recalcitrant	496	55,198	0.25	1	27
	<i>S. pombe</i>	recalcitrant	335	37,108	0.05		20
	<i>P. angusta</i>	amenable	388	42,854	0.10		20
	<i>K. lactis</i>	amenable	500	43,555	0.05		21
Hsv2	<i>S. cerevisiae</i>	recalcitrant	448	51,237	0.16	2	20
	<i>K. lactis</i>	amenable	339	39,167	0.00		10
	<i>S. pombe</i>	amenable	364	41,011	0.09		16

Atg18 is part of the core autophagy machinery and highly conserved throughout eukaryotes. In order to determine the structure of Atg18, I ordered synthetic genes of its homologs from *S. pombe*, *P. angusta*, *C. elegans* and *D. melanogaster*. Homologs of Atg21 were ordered from *S. pombe*, *P. angusta* and *K. lactis*. For crystallization of Hsv2 I used the *S. pombe* homolog. These genes were optimized for bacterial expression, by the algorithms of the company Mr. Gene GmbH. KlHsv2 was also ordered and the sequence optimized for bacterial expression, I used this protein for biochemical analysis together with ScHsv2.

The ordered genes were cloned into the pET28a expression vector and first expression trials were done in *E. coli* BL21(DE3) cells.

Expression of SpAtg18 and SpAtg21 was tested in different medias, including LB media, TB + salt media and autoinducible media. In addition, *E. coli* Rosetta(DE3) cells were tested as an expression strain for these homologs. Detection of expression could not be confirmed neither on Coomassie stained SDS-PAGE gels nor in Western blot analysis. Another approach was it, to co-express these genes with each other or with SpHsv2 from the pET-Duet1 vector. However, this did not lead to expression of SpAtg18 or SpAtg21. Sequencing verified the correct insertion of these genes in the expression vectors. Therefore, work with SpAtg18 and SpAtg21 was stopped at this point.

The expression of PaAtg18, CeAtg18, DmAtg18, PaAtg21 and KlAtg21 was optimized using *E. coli* BL21(DE3) cells cultured in different media. First, LB media was tested as media and expression was induced by IPTG addition. None of the proteins

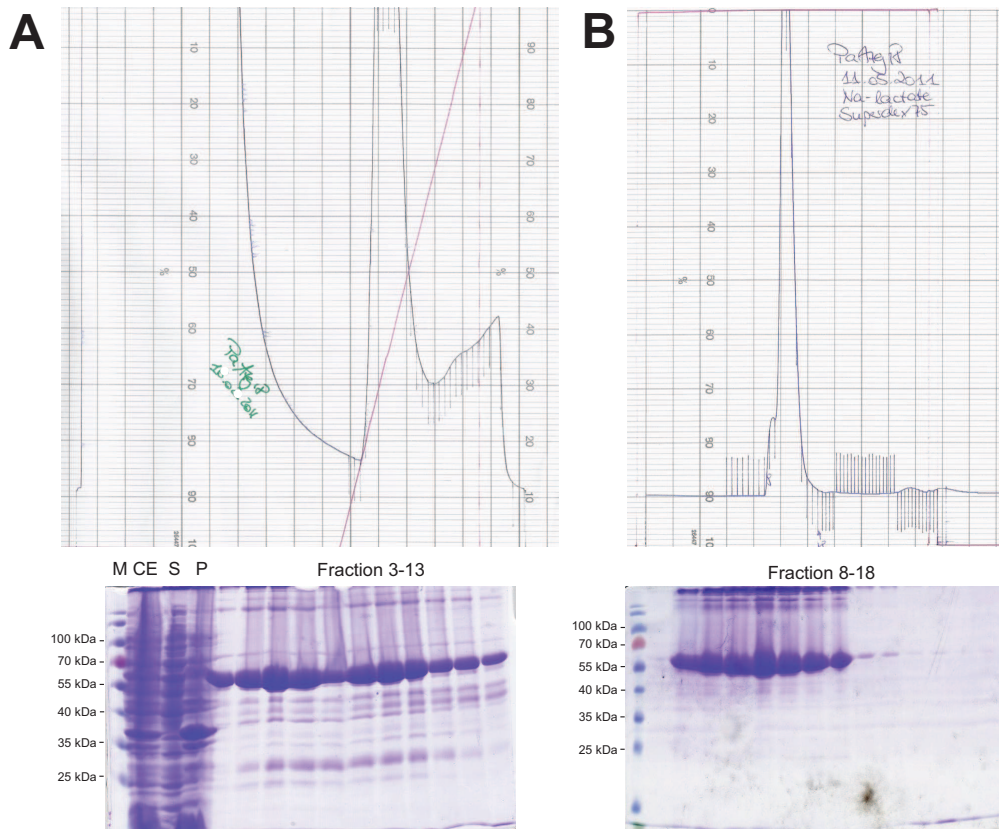


**Figure 4.6: Purification of PaAtg18 from *E. coli* BL21(DE3) cells**

Chromatograms and SDS-PAGE gels of PaAtg18 purified by (A) affinity chromatography using a His-Trap FF column followed by (B) gel filtration with HiLoad 16/60 Superdex S75 column.

showed a distinct over expression band (see suppl. figure 5.1 A). Therefore, autoinducible media was tested. In order to check the over expression of the protein homologs, batch purification using  $\text{Ni}^{2+}$ -sepharose beads was done and analyzed on SDS gels together with cell extract and supernatant (see suppl. figure 5.1 B). Over expression of PaAtg18 and KlAtg21 was observed. Therefore, autoinducible media was chosen for large scale purification of these proteins.

All five homologs were expressed in 9 l autoinducible media from *E. coli* BL21(DE3). Expression was done for three hours at 37 °C and then shifted for over night incubation to 22 °C. After 24 hours of culturing the cells were harvested and after lysis, proteins were purified by affinity chromatography using a His-Trap FF column followed by size exclusion chromatography. Protein purity and obtained protein yields were tested by loading cell extract (CE), supernatant (S), pellet (P) and elution fractions on an SDS gel, which was thereafter stained with Coomassie.

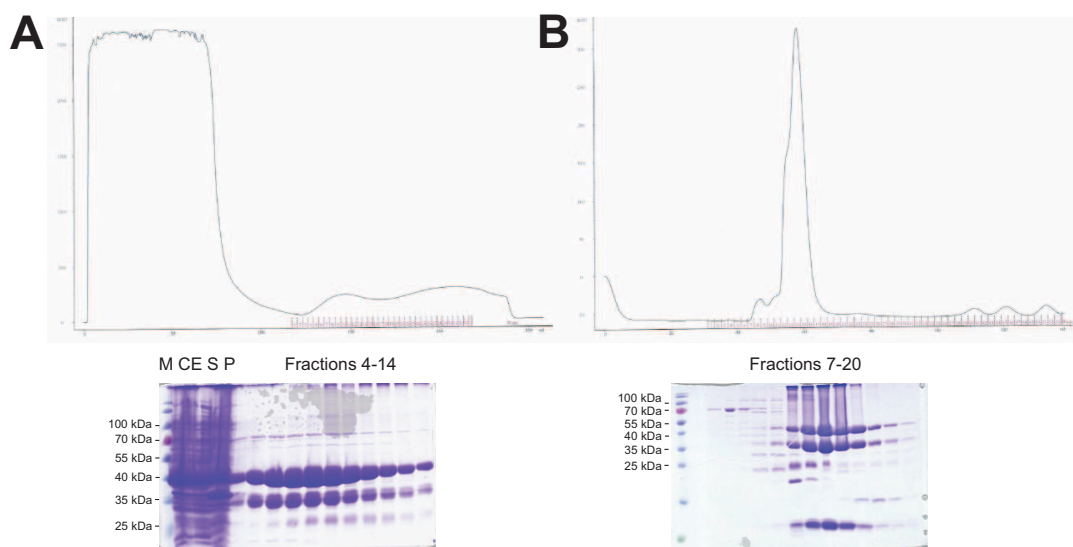


**Figure 4.7: Purification of KlAtg21 from *E. coli* BL21(DE3) cells**  
 Chromatograms and SDS-PAGE gels of KlAtg21 purified by (A) affinity chromatography using a His-Trap FF column followed by (B) gel filtration with HiLoad 16/60 Superdex S75 column.

*P. angusta* Atg18 was purified in high yields and purity after gel filtration purification was of good quality (see figure 4.6). PaAtg18 was also purified from minimal media with selenomethionine as supplement. The same purification protocol was followed. The protein was stored for crystallization trials in conditions were native protein crystallized. In contrast, Atg18 from *C. elegans* was obtained in small yields from His-Trap purification, but after gel filtration CeAtg18 could not be enriched or purity improved, instead the protein seems to be very instable and precipitated or got degraded (see suppl. figure 5.2). DmAtg18 was not expressed in high levels and with affinity purification the protein could not be enriched. Gel filtration purification yielded two bands of purified protein, like CeAtg18 this protein could not be purified sufficiently for crystallization trials (see figure 4.6).

Next, KlAtg21 was expressed at high levels. Its purification check on SDS gel showed a double band and the lower band did not disappear after size exclusion chromatography. Most likely, the second band represents a smaller, stable fragment of the protein (see figure 4.7). In addition, selenomethionine labeled KlAtg21 was purified for crystallization. In small yields PaAtg21 was purified, the protein was of good purity (see suppl. figure 5.4).

Optimal expression conditions were tested for SpHsv2. For this purpose, LB media was used and expression was followed for different temperatures. The inoculated culture



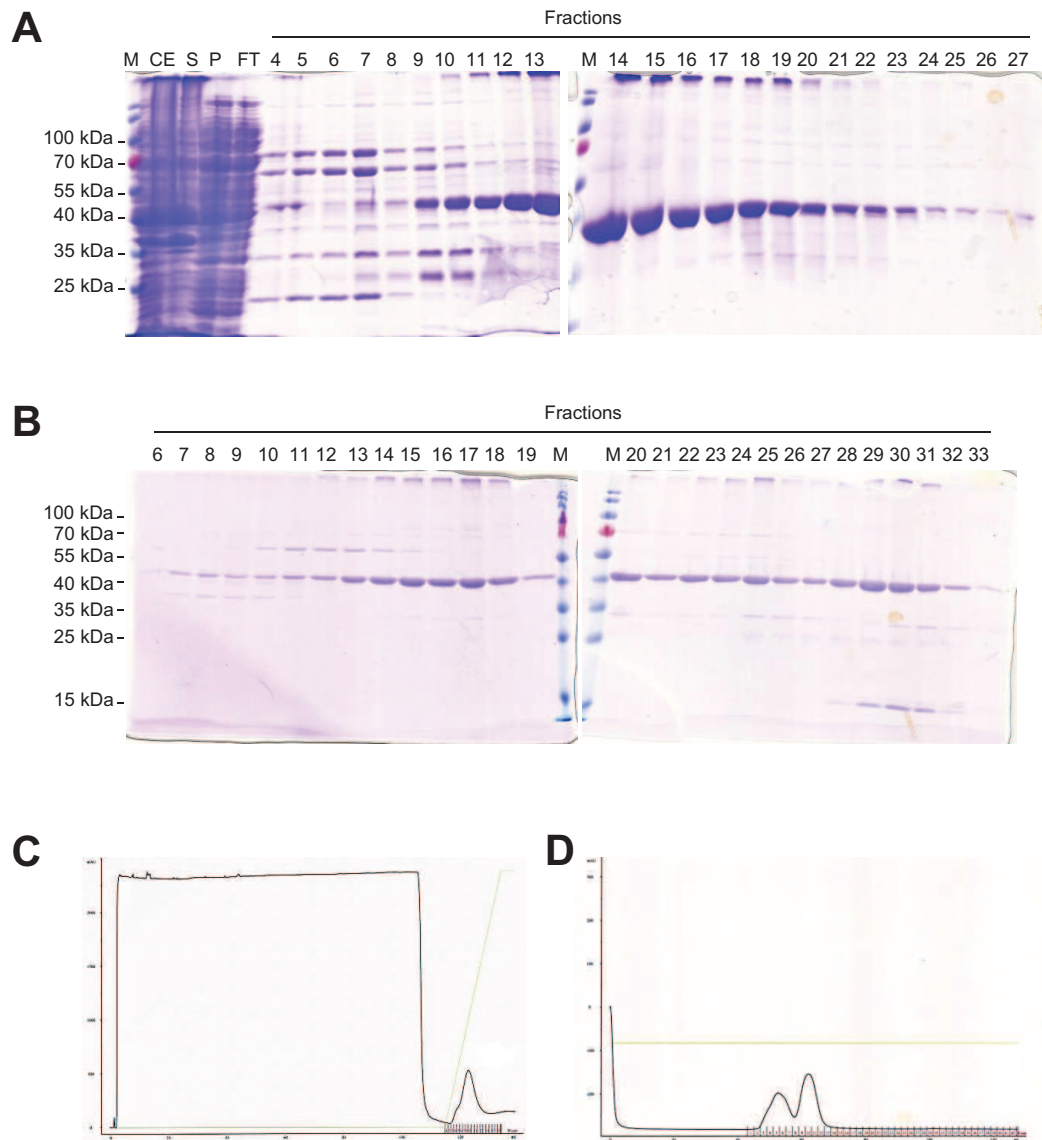


**Figure 4.8: Purification of SpHsv2 from *E. coli* BL21(DE3) cells**

(A) Purification of SpHsv2 with 1 ml His-Trap column and analysis of fraction with SDS-PAGE. (B) Followed by size exclusion chromatography. (C)+(D) Chromatograms of SpHsv2 purification with 1 ml His-Trap FF column (C) and analytical gel filtration with a Superdex 200 10/300 GL column (D) using an Äkta purifier.

was first incubated at 37°C until an OD of 0.6. At this time point the expression was induced by addition of IPTG and then samples were taken from the culture after every hour. Furthermore, a second culture was shifted to 25°C after IPTG was added. Here, the last sample was taken after over night incubation. Samples of the supernatant were checked on Coomassie stained SDS gels. Over-expression of SpHsv2 was observed for the over night incubated culture (see suppl. figure 5.5). This condition was used for large scale expression of SpHsv2. Already after His-Trap purification the protein was almost pure and high yields could be obtained (see figure 4.8 A and C). However, size exclusion purification of SpHsv2 displayed two peaks, which were both analyzed with SDS-PAGE (see figure 4.8 B and D). Only one protein band was detected on SDS gels, suggesting that SpHsv2 might form a dimer.

For biochemical analysis of Hsv2, I purified ScHsv2, which can be obtained in high yields from bacterial expression. In addition, biochemical studies on PROPPINs membrane binding were done with KlHsv2. The structure of KlHsv2 was solved by Dr. K. Kühnel in our lab and based on the structure mutagenesis studies were planned.

ScHsv2 was expressed from pGEX-4T3 vector with an N-terminal GST-tag. *E. coli* BL21(DE3) cells were used for expression of this construct in autoinducible media. After over night incubation at 22°C the cells were harvested and ScHsv2 purified with a GSTrap FF column. On SDS gels co-purification of high yields of free GST was ob-

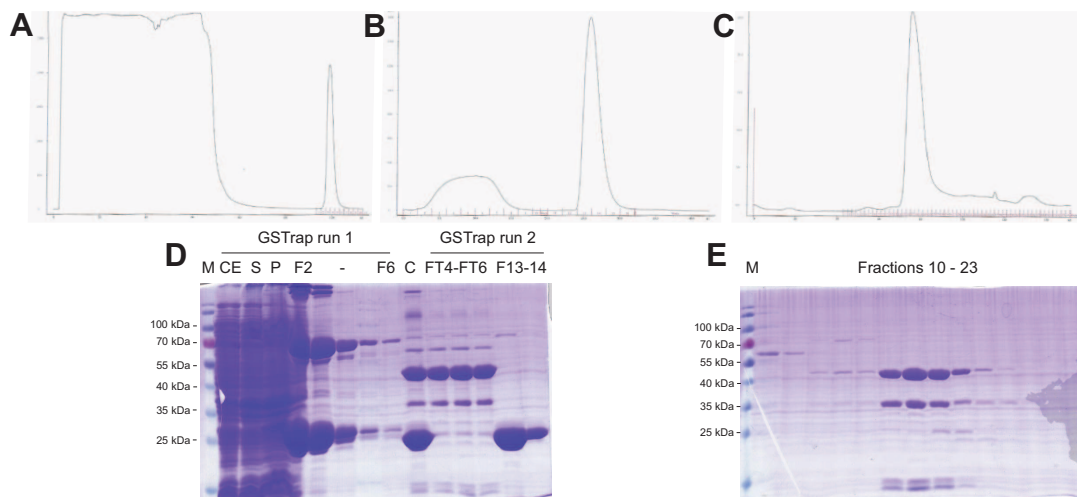


**Figure 4.9: Purification of ScHsv2 from *E. coli* BL21(DE3) cells**

(A) GSTrap purification, (B) second GSTrap run after thrombin cleavage followed by (C) gel filtration with a HiLoad 16/60 Superdex S75 column. Analysis of (D) GSTrap run one and two (E) and gel filtration on SDS-PAGE. Cell extract (CE), supernatant (S), pellet (P), elution fractions (F), thrombin cleaved fraction (C) and flow through fractions (FT) were checked.

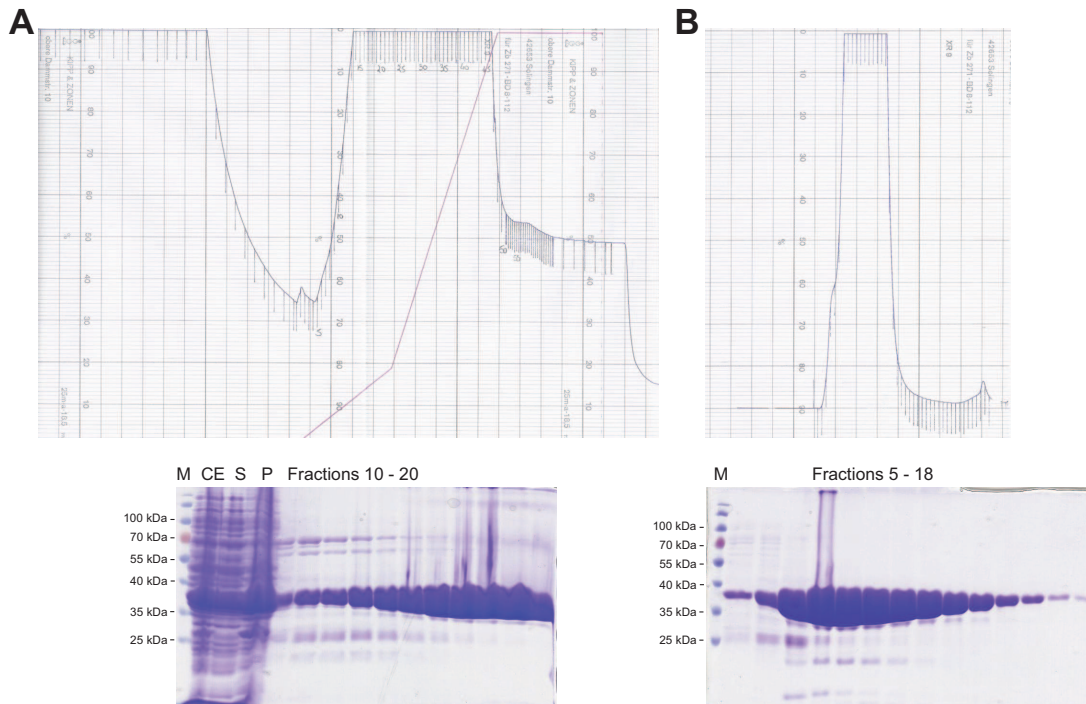


**Figure 4.10: Purification of KIHsv2 from *E. coli* BL21(DE3) cells**

Chromatograms and SDS-PAGE gels of KIHsv2 purified by (A) affinity chromatography using a His-Trap FF column followed by (B) gel filtration with HiLoad 16/60 Superdex S200 column.

served (see figure 4.9 A and D). Since the GST-tag is known to dimerize and might influence with biochemical analysis, the tag was cleaved by thrombin treatment of the purified protein. After this a second GSTrap run was performed. Here, the flow through was collected, which contained the cleaved protein. Free GST and uncleaved protein remained bound to the column (see figure 4.9 B and D). In size exclusion chromatography the protein purity was further improved (see figure 4.9 C and E). High amounts of KIHsv2 were obtained after expression from *E. coli* BL21(DE3) cells in autoinducible media. His-Trap purification of this cell extract yielded almost pure protein in high amounts. An additional gel filtration run was performed (see figure 4.10). Mutants of ScHsv2 and KIHsv2 for biochemical experiments were purified in the same way as wild type proteins.

Wild type KIHsv2, used for crystallization, KIHsv2<sup>GSlinker</sup>, KIHsv2<sup>Q274E</sup>, KIHsv2<sup>Q274D</sup> and KIHsv2<sup>Y272A/F273A</sup> were cloned and purified by Dr. K. Kühnel.

#### 4.2.1.3 Characterization of purified PROPPINs

During protein purification thermal shift assays were performed for the PROPPIN homologs PaAtg18, CeAtg18, DmAtg18, KlAtg21, PaAtg21 and SpHsv2. In this Thermofluor experiments 88 different buffer compositions (pHat screen) or additives (Addit screen) were tested. Purified proteins mixed either with different buffers or additives were supplemented with Sypro Orange. This fluorescent dye is quenched in aqueous conditions. However, during the thermal shift from 25 °C to 95 °C the proteins unfold. During this unfolding hydrophobic patches of the protein are exposed and Sypro Orange can bind and Sypro Orange gets dequenched. An increase in fluorescence indicates unfolding of the protein. Therefore, fluorescence changes correlate to unfolding of the protein. With this method the melting temperature of a protein can be determined. Different buffer conditions and additives can influence protein stability. A more stable protein will unfold at higher temperature. As a control the protein in its purification buffer was used. The crystallization probability of a protein increases, when the protein is more stable. For this reason Thermofluor experiments were performed and purification protocols were optimized based on these results.

The pHat screen was generally done after affinity purification of a new protein. A buffer condition, which increases the melting temperature of this protein the most was used for gel filtration purification of the protein and was therefore dialyzed into this buffer overnight. After gel filtration the protein was subjected to the Additive screen. Initial purifications of these PROPPINs were done in sodium phosphate buffer (50 mM  $\text{NaH}_2\text{PO}_4$  pH 7.5, 300 mM NaCl). Protein in this buffer was used as a reference in the assay.

A clear shift of the melting temperature towards higher temperatures was observed for PaAtg18 in sodium lactate buffer at pH 4.0 (see figure 4.11 A). In addition, different other acidic buffers such as MES pH 5.0 and pH 5.4, sodium acetate pH 4.6 and sodium lactate pH 4.4 increased the melting temperature. The Addit screen revealed some salts (ammonium sulfate, potassium citrate, sodium malonate), spermine, PIPES and imidazole as stabilizing additives (see figure 4.11 B). CeAtg18 was the only protein preferring only basic buffers of all PROPPINs. Its stability was slightly increased in buffers from pH 7.4 up to pH 8.8 (see suppl. figure 5.6 A). For further purification I dialyzed the protein in CHES pH 8.0. Both CeAtg18 and DmAtg18 had an overall low melting temperatures and the buffer conditions tested with the pHat screen did not shift the stability much. However, further purification of DmAtg18 was done in MES

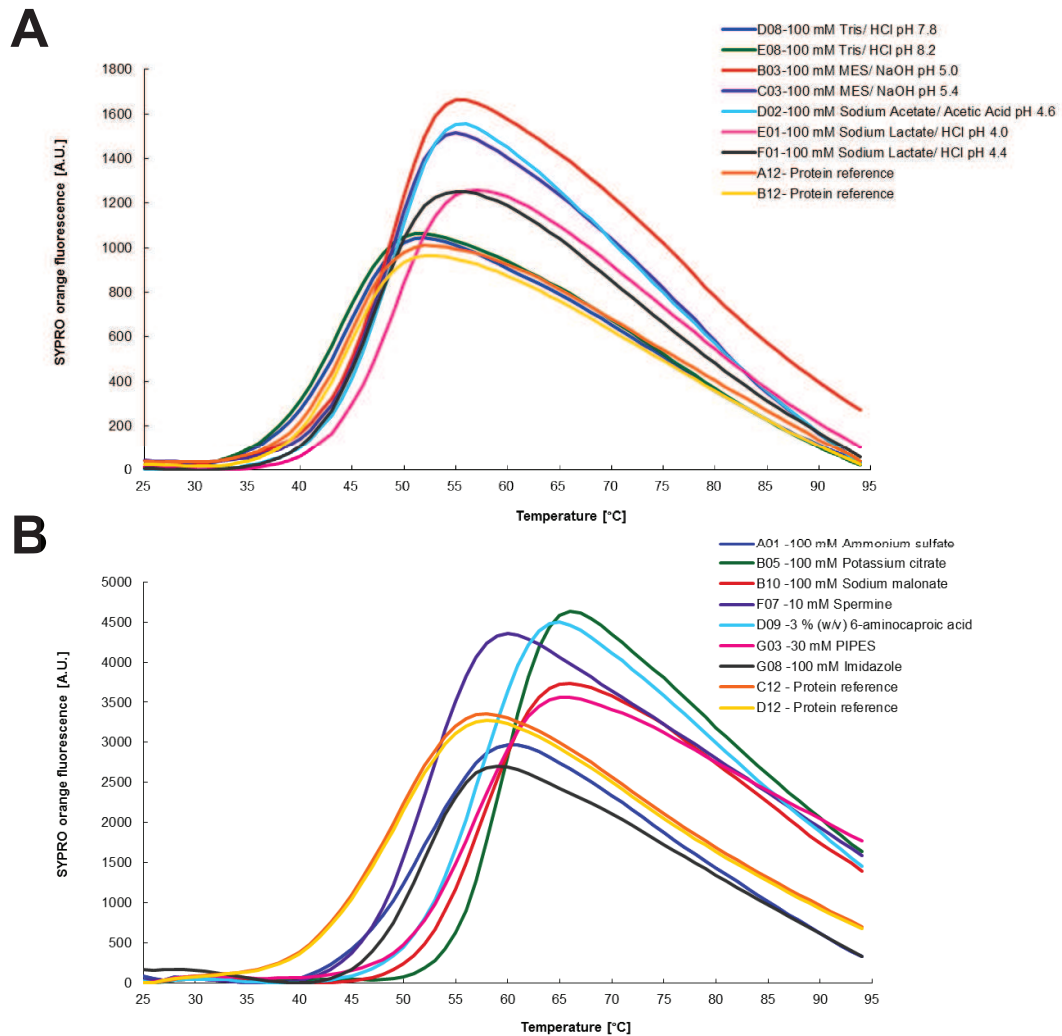


**Figure 4.11: Thermofluor analysis of PaAtg18**

Thermofluor experiments for PaAtg18 using the (A) pHat and the (B) Addit screen. Sypro Orange fluorescence was monitored and dequenching indicates unfolding of the proteins. Temperature was shifted from 25 °C to 95 °C. Shown conditions increased protein stability in comparison to protein reference.

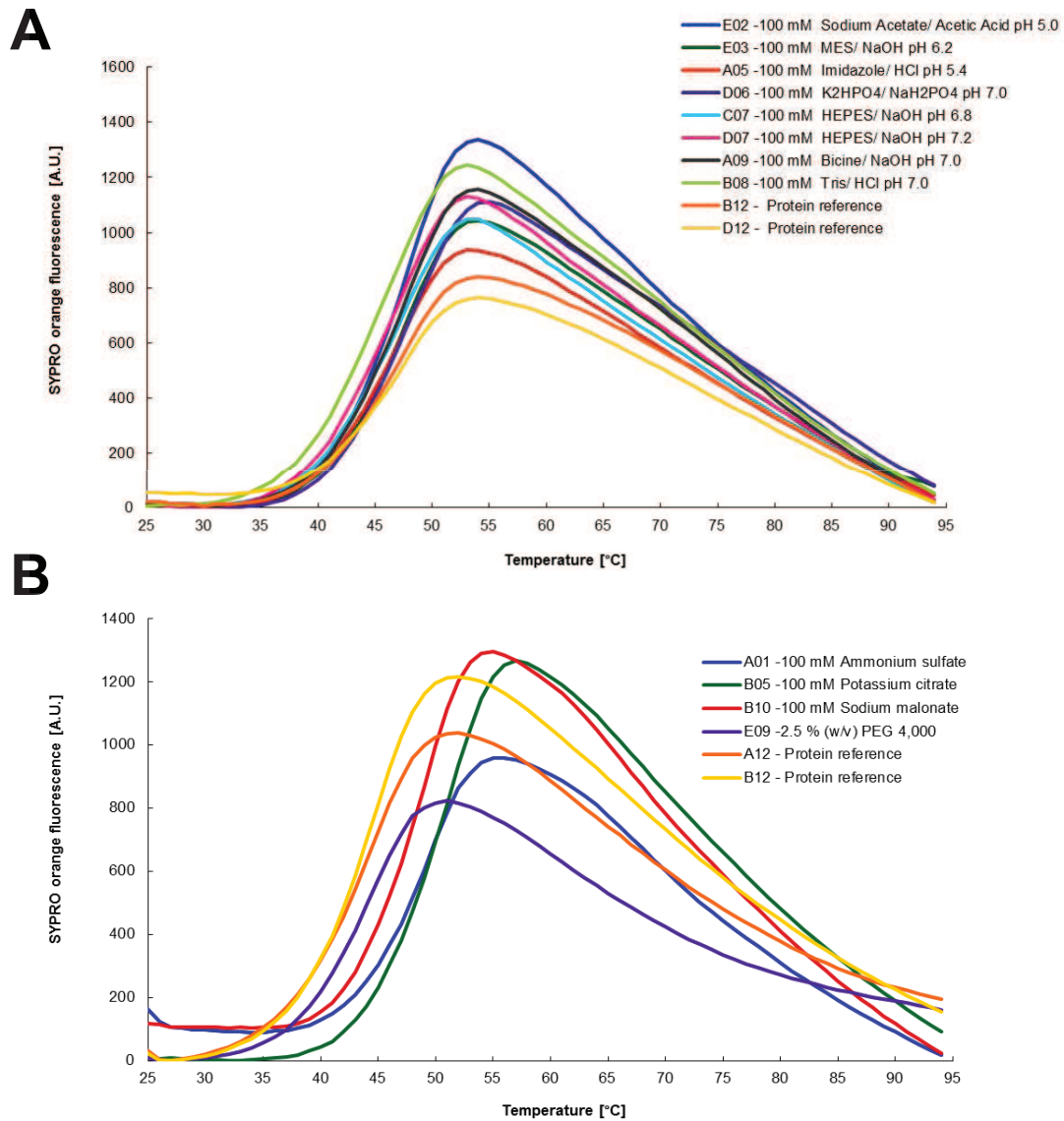


**Figure 4.12: Thermofluor analysis of K1Atg21**

Thermofluor experiments using the (A) pHat and the (B) Addit screen. Dequenching of Sypro Orange correlates with unfolding of the protein. Temperature was shifted from 25 °C to 95 °C. Shown conditions increased protein stability in comparison to protein reference.

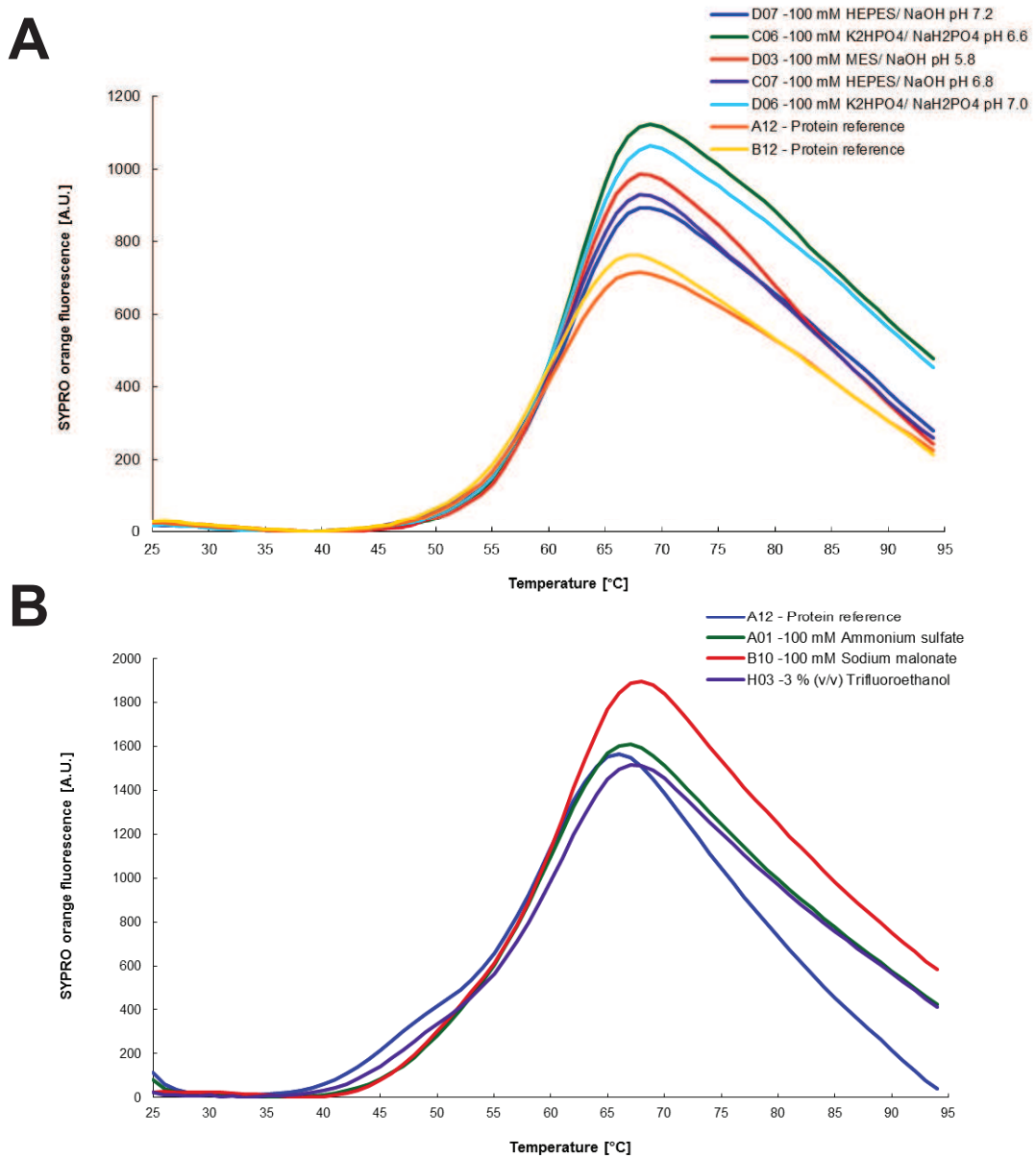


**Figure 4.13: Thermofluor analysis of PaAtg21**

Thermofluor experiments using the (A) pHat and the (B) Addit screen. Dequenching of Sypro Orange correlates with unfolding of the protein. Temperature was shifted from 25 °C to 95 °C. Shown conditions increased protein stability in comparison to protein reference.

pH 5.2 (see suppl. figure 5.6 B). Different buffers in a pH range between 5.0 and 7.0 were identified for KlAtg21 to show the same curve as the reference curve or shifted the fluorescence slightly towards higher temperatures (see figure 4.12 A). Therefore, MES buffer pH 5.8 was chosen for further purification. Stronger effects on stability were observed for some additives including the salts ammonium sulfate, potassium citrate and sodium malonate as well as the polymer PEG 4,000 (see figure 4.12 B). In contrast to the other PROPPINs PaAtg21 showed higher stability, since an increase in the Sypro Orange fluorescence was detected at higher temperatures. From buffers tested in figure 4.13 A, MES pH 5.8 was selected for further PaAtg21 purification. The additives tested with the Addit screen did not further increase the stability of PaAtg21. Ammonium sulfate, sodium malonate and trifluoroethanol had small increasing effects on PaAtg21 stability (see figure 4.13 B). Also the purification protocol for SpHsv2 was optimized using Thermofluor experiments. Here, citric acid buffer pH 5.5 supplemented with 500 mM NaCl were found to stabilize the protein.

After successful purification of PaAtg18, KlAtg21, PaAtg21 and SpHsv2, their CD spectra in far UV were monitored in order to analyze their secondary structures. These measurements were carried out in NaF buffer. These proteins are predicted to fold as  $\beta$ -propellers therefore the typical spectrum of a protein consisting of  $\beta$ -strands was expected. CD spectra from 190 nm to 260 nm were measured for PaAtg18 and PaAtg21 (see suppl. figure 5.7 A) as well as KlAtg21 and SpHsv2 (see suppl. figure 5.7 B). All spectra showed a minimum around 216 nm. This minimum indicates the secondary structure of these proteins consists of mainly  $\beta$ -strands. In addition, stability of these proteins was investigated with far UV. Stability of proteins is important for their crystallization, since it can take weeks or even months before a protein crystallizes. Therefore, I recorded the thermal unfolding curves of these PROPPINs between 20 °C and 90 °C at 216 nm (see suppl. figure 5.7 C and D). All proteins were stable and their unfolding occurred in a single transition. SpHsv2 and PaAtg21 had their transition midpoints around 65 °C, PaAtg18 and KlAtg21 had their midpoint around 52 °C.

In order to determine stable fragments of PaAtg18, KlAtg21 and PaAtg21 suitable for crystallization, proteolytic digestions of these proteins were performed with twelve different proteases each. Smaller fragments are usually more compact and less disordered and therefore crystallization probability increases. Limited proteolysis was done for different time frames either 5 min, 10 min, 15 min or 30 min and for comparison undigested protein was also loaded onto the gel. For PaAtg18 no stable fragment comprising the core  $\beta$ -propeller domain was found, instead subtilisin and proteinase K digested this



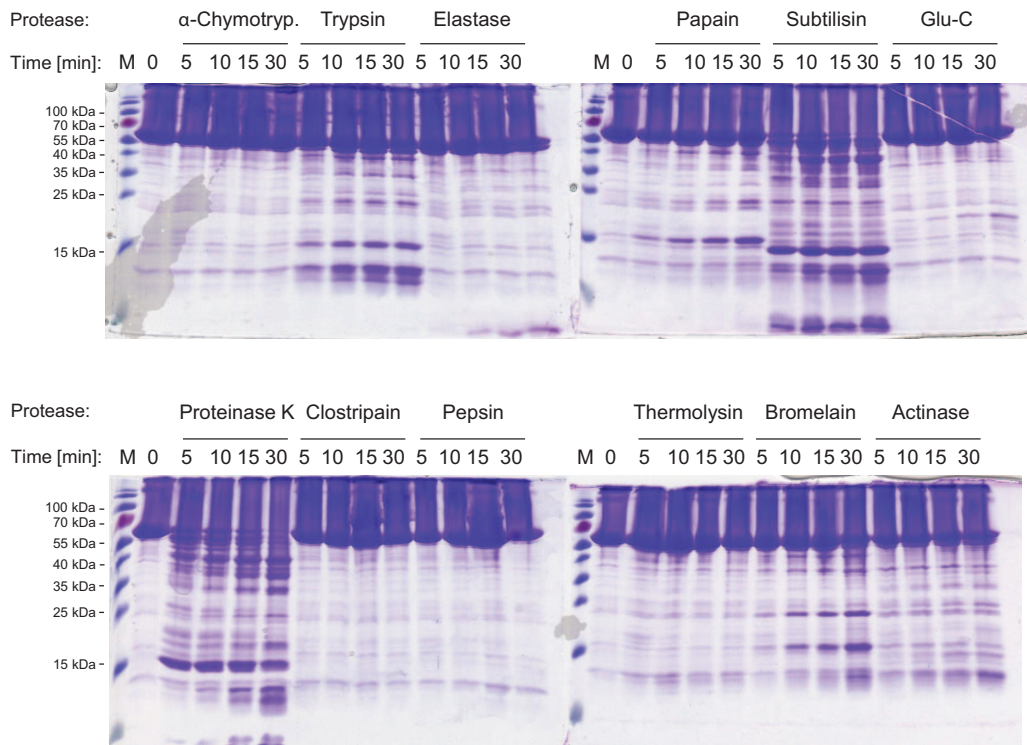


**Figure 4.14: Limited proteolysis of PaAtg18**

Purified protein was cleaved with the indicated proteases for a time course up to 30 min at RT. Samples were analyzed with Coomassie stained SDS gels.

protein very quickly. Treatment of all other proteases resulted the uncleaved protein band (see figure 4.14).

KlAtg21 showed already after purification a double band and with proteolytic digestion I wanted to check in addition, whether the second smaller band corresponds to a stable fragment. Indeed, treatment of purified KlAtg21 thermolysin and actinase resulted in digestion of the larger molecular weight band whereas the smaller band stayed unchanged (see figure 4.15). Furthermore subtilisin and proteinase K again completely digested the protein. Only the before observed band of 35 kDa could be identified as stable fragment of KlAtg21. This band was isolated and analyzed by N-terminal protein sequencing. The N-terminal His-tag was detected with this method, consequently the C-terminus was cleaved. In limited proteolysis of PaAtg21 only very small fragments of less than 15 kDa were observed after treatment with trypsin, clostripain and bromelain (see suppl. figure 5.8).

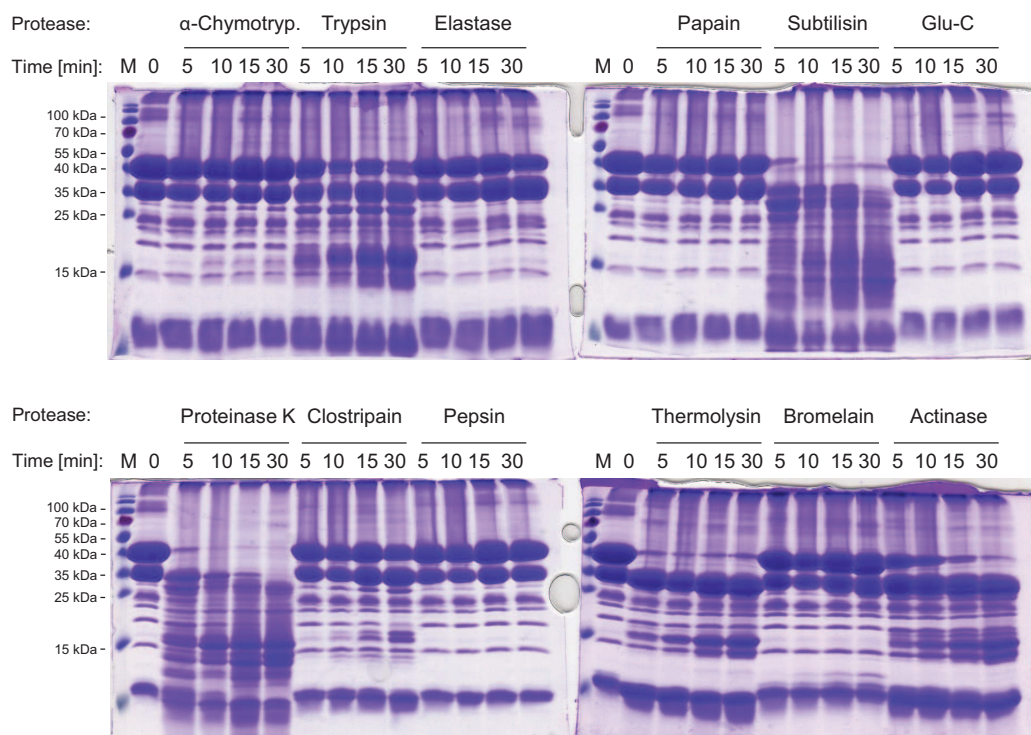


**Figure 4.15: Limited proteolysis of KlAtg21**

Purified protein was cleaved with the indicated proteases for a time course up to 30 min at RT. Samples were analyzed with Coomassie stained SDS gels.

During purification of SpHsv2 over the gel filtration column the protein was eluted in two peaks (see figure 4.16 A). In order to investigate whether SpHsv2 forms an oligomer I performed an analytical gel filtration experiment to determine the molecular weight of the protein in both peaks. Standards of molecular weight markers were run on the column and a standard curve was determined by plotting the ratio between elution volume and void volume ( $V_e/V_o$ ) versus their molecular weights (see figure 4.16 B).

SpHsv2 peak I eluted after 14 ml and the molecular weight of this complex is 82 kDa. The second peak was observed after 16 ml and corresponds to 41 kDa. These results indicate, that SpHsv2 peak I contain a SpHsv2 dimer and peak II to a monomer. However, dimerization of PROPPINs has not been described so far and complex formation can also be induced by oxidation of cysteine residues. SpHsv2 contains cysteines and therefore I tested in a next step, whether a reducing agent can prevent dimerization of SpHsv2. Indeed, addition of TCEP to the protein led to one prominent peak

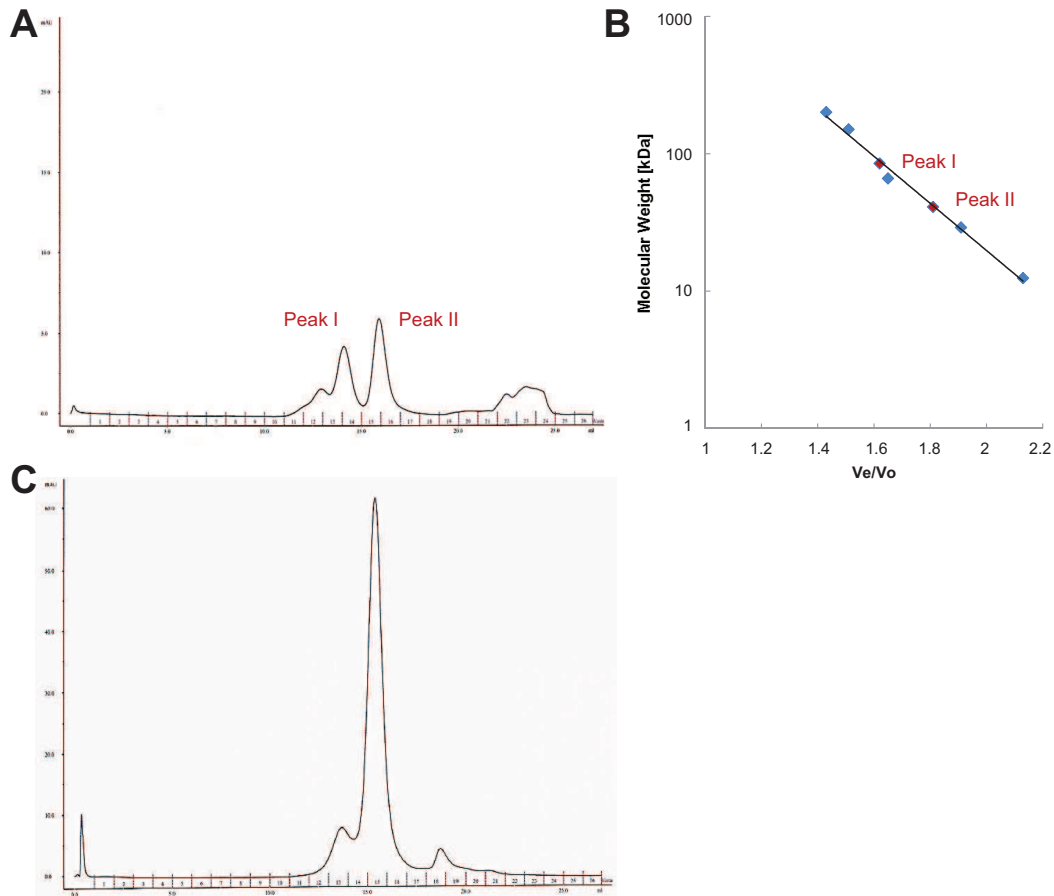


**Figure 4.16: Analytical gel filtration analysis of SpHsv2**

(A) In analytical gel filtration peak I eluted after 14 ml and peak II after 16 ml. (B) Comparison of the  $V_e/V_o$  to protein standards revealed that peak I represents a dimerized of 82 kDa and peak II corresponds to a monomer of 41 kDa. (C) Addition of the reducing agent TCEP reduced dimerization.

in analytical gel filtration (see figure 4.16 C). This peak contained the monomeric form of SpHsv2. In addition, other reagents like DTT and  $\beta$ -mercaptoethanol reduced the dimer formation of SpHsv2.

#### 4.2.1.4 Crystallization of PROPPINs

One major aim of this project was to crystallize Atg18, Atg21 or alternatively Hsv2. Therefore, I purified several proteins from different species of either Atg18, Atg21 or Hsv2. The buffer conditions were optimized in a way, that the proteins were most stable and their secondary structures were checked. In a next step, ScAtg18, PaAtg18, KlAtg21

and SpHsv2 were subjected to crystallization screens in order to get first crystallization hits, then improving these conditions and finally obtaining well diffracting crystals were the goal.

ScAtg18 was purified from High5 insect cells in a buffer containing 50 mM  $\text{NaH}_2\text{PO}_4$  at pH 8.5 and 500 mM NaCl. This protein was obtained in very small yields and could be concentrated up to 5 mg/ml. This was used to set up a crystal screen with one drop per condition and incubate at 20 °C. The RockImager took frequently images of each single condition, so that possible crystal growth was monitored. From this crystallization screen two conditions yielded spherulites (see figure 4.17 A and table 4.2). In order to check these pre-crystalline structures for their protein content, a dye was added to the crystallization condition. After some time, the dye was taken up by the spherulites, indicating that these consists of protein and not salt. Due to low protein yields, working with ScAtg18 was stopped and no further optimization was done.

Furthermore, SpHsv2 was subjected to crystallization screens. Purified in 30 mM citric acid pH 5.5 and 500 mM NaCl, crystal plates for SpHsv2 were set up separately with protein from dimer (peak I) and monomer fraction (peak II) as well as with protein treated with DTT. Different protein concentrations of 30 mg/ml, 20 mg/ml, 15 mg/ml and 10 mg/ml were tested. From these screens I found a few conditions in which pre-crystalline structures were formed (see figure 4.17 B and table 4.2). Protein involvement in these structures were confirmed by staining with a dye. In further optimization screens 1  $\mu\text{l}$  protein drops were mixed with 1  $\mu\text{l}$  mother liquor of crystallization buffer. Here, also different protein concentrations of 30 mg/ml, 20 mg/ml and 10 mg/ml were tested. However, none of the optimization screens yielded crystals.

Moreover, KlAtg21 was purified and dialyzed into different buffers before it was subjected to crystallization screens. For membrane proteins it was reported, that their binding specificity can be improved by addition of  $\text{MgCl}_2$  [133]. Probably due to effects on changed protein packing. Therefore, one buffer used for crystallization trials of KlAtg21 contained 30 mM MES pH 5.8, 300 mM NaCl, 5 mM  $\text{MgCl}_2$  and 1 mM DTT. If  $\text{MgCl}_2$  has an influence on a tighter packing of the protein, the crystallization probability would be increased. Crystallization trials set up with KlAtg21 in a concentration range from 10 mg/ml to 30 mg/ml also yielded in spherulites (see figure 4.17 C and table 4.2). Protein content was again confirmed by staining. Subsequently, optimization screens were set up in 24 well format with 1:1  $\mu\text{l}$  drops and in the 96 well format. Here, also the stability improving additives found with the Addit screen in Thermofluor analysis were implemented. Crystallization conditions containing PEG 4,000 and sodium malonate were prepared. Some conditions of the optimization screens were found with improved

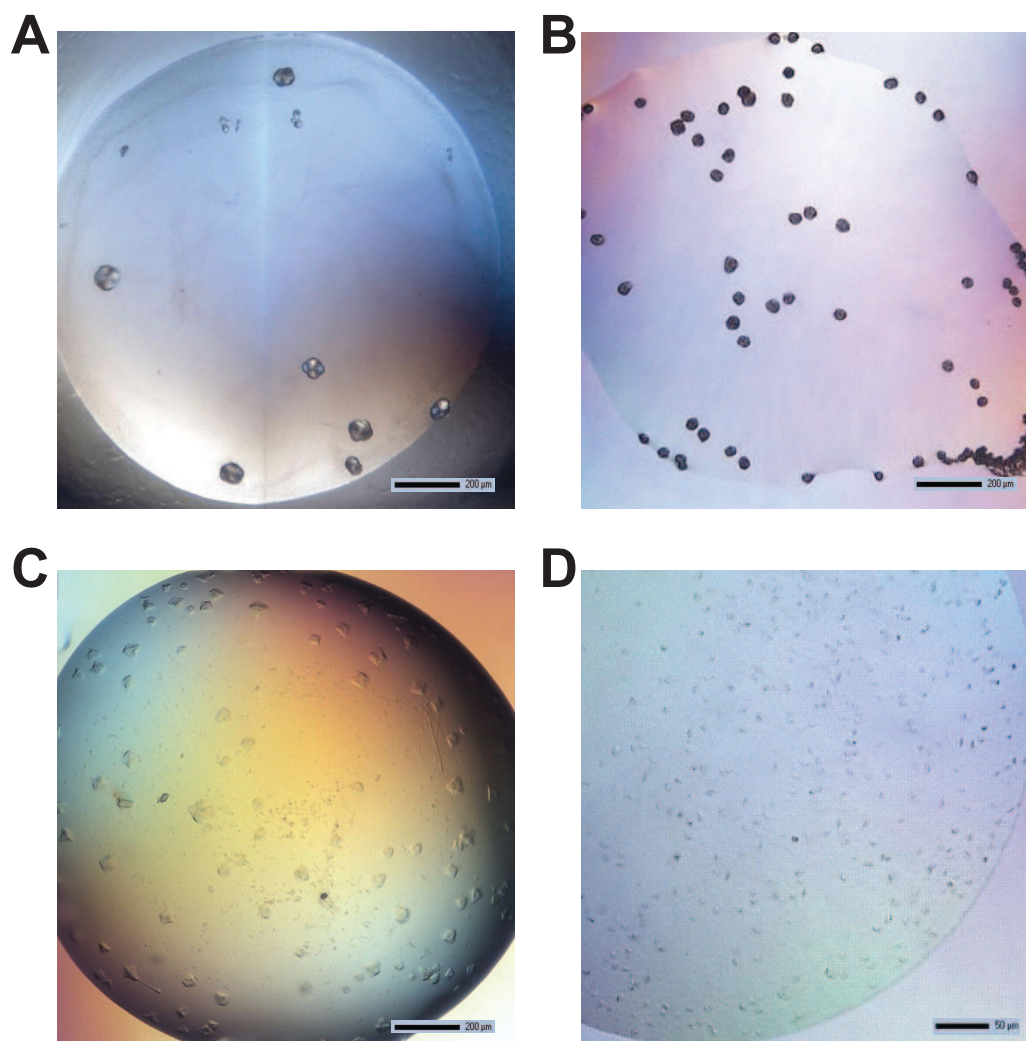


**Figure 4.17: Spherulites resulting from PROPPIN crystallization**

Spherulites obtained from crystallization trials of (A) ScAtg18 (No. 2) (B) SpHsv2 (No. 9) (C) KlAtg21 (No. 5) and (D) PaAtg18 (No. 3). The number correspond to the crystallisation conditions in table 4.2.

crystal packing. These crystals were sent to the synchrotron for X-ray data collection. Unfortunately, all crystals showed the typical diffraction pattern of salt crystals. In addition, buffer consisting of 10 mM MES pH 5.8, 300 mM NaCl and 1 mM DTT was used. The buffer concentration was reduced and MgCl<sub>2</sub> was taken out to minimize salt crystal formation. Protein in the concentration of 38 mg/ml and 18.8 mg/ml was used for new screens. So far, no additional potential crystallization conditions were identified.

**Table 4.2:** Initial crystallization conditions for PROPPINs

No.	PROPPIN	Concentration	Condition	Drop set up	Temp.
1	ScAtg18	5 mg/ml	0.1 M Tris pH 8.5 1 M Lithium sulfate monohydrate 0.01 M Nickel-II-chloride hexahydrate	100:100 nl	20 °C
2	ScAtg18	5 mg/ml	0.1 M Hepes pH 7.5 1.5 M Lithium sulfate monohydrate	100:100 nl	20 °C
3	PaAtg18	6.5 mg/ml	0.1 M Tris pH 8.5 20 % (w/v) PEG MME 2,000 200 mM Trimethylamine-N-oxide	100:100 nl	20 °C
4	KlAtg21	20 mg/ml	0.1 M MES monohydrate pH 6.5 0.6 M Sodium fluoride	100:100 nl	20 °C
5	KlAtg21	30 mg/ml	0.1 M MES monohydrate pH 6.0 0.9 M Sodium fluoride	100:100 nl	20 °C
6	KlAtg21	15 mg/ml	0.1 M MES monohydrate pH 6.0 15 % (v/v) PEG 400 0.1 M Calcium acetate hydrate	100:100 nl	20 °C
7	KlAtg21	30 mg/ml	0.1 M tri-Sodium citrate dihydrate pH 5.6 1 M Ammonium phosphate monobasic	100:100 nl	20 °C
8	KlAtg21	20 mg/ml	0.1 M Hepes pH 7.5 2.4 M Sodium malonate	100:100 nl	20 °C
9	SpHsv2	30+15 mg/ml	0.1 M Tris pH 7.5 20 % (v/v) Ethanol	100:100 nl	20 °C
10	SpHsv2	30+15 mg/ml	0.1 M Sodium cacodylate trihydrate pH 6.5 18 % (w/v) PEG 8,000 0.2 M Calcium acetate hysdrate	100:100 nl	20 °C
11	SpHsv2	10 mg/ml (dimer)	Citric acid anhydrous pH 4.0 3 M Sodium chloride	100:100 nl	20 °C

Crystallization screens were also set up for PaAtg18. For first screens I used protein purified in 30 mM sodium lactate pH 4.0, 300 mM NaCl and 1 mM DTT buffer. The protein was used at a concentration of 30 mg/ml, 15 mg/ml, 12 mg/ml and 6 mg/ml. In addition, protein at a concentration of 13 mg/ml, 6.5 mg/ml, 3 mg/ml and 1 mg/ml purified in 10 mM sodium lactate pH 4.0, 300 mM NaCl and 1 mM DTT was used. Since for long time no initial crystal hits were observed, crystallization screens were set

up at 20°C and 4°C. Recently microcrystals were observed and optimization screens were carried out, but further optimization is needed (see figure 4.17 D and table 4.2).

A recent paper reported from crystallization initiation and crystal diffraction improvement using molecularly imprinted polymers (MIP) [59]. These polymers were added to crystallization screens and can function as nucleation sites. I prepared these MIPs for KlAtg21, PaAtg18 and KlHsv2. Crystallization conditions were in the meanwhile optimized, therefore I used KlHsv2 as a control to see, whether crystallization is influenced. These MIPs were added to the hanging drops of 24 well plates. So far, no further initial crystallization conditions could be identified for neither KlAtg21 nor PaAtg18. However, crystals were obtained for KlHsv2 and sent to the synchrotron. The taken diffraction data sets showed, that the crystals diffracted up to 3 Å. Crystal diffraction in this case was not improved to the previously determined KlHsv2 structure, but MIPs also did not disturb crystal growth. Molecular printed polymers can be implemented again, when initial crystal hits are identified.

## 4.2.2 Functional analysis of PROPPINs

### 4.2.2.1 Optimization of methods to analyze protein-lipid interaction

In order to study protein-lipid interaction of PROPPINs I first needed to establish conditions where no non-specific membrane lipid interactions occurred [175]. So far, PROPPIN membrane binding was mainly investigated using protein-lipid overlay assays [144, 133, 151]. For this reason, I wanted to use this method first to probe lipid binding, of the ScHsv2 mutants with PIP strips to study the involvement of these residues in PIP binding. Therefore, I started first to optimize the buffer and blocking solutions for PIP strips to find optimal conditions for comparison of all mutants. BSA and milk powder are commonly used blocking reagents, in addition PBS, TBS or 50 mM Tris-HCl pH 7.5 were tested (see figure 4.18 A). The buffer was additionally substituted with 0.5 mM MgCl<sub>2</sub>, which was reported to increase the specificity of PROPPIN phosphoinositide binding [133]. Here, PBS-T, 0.5 mM MgCl<sub>2</sub> and 2 % BSA were found to give best results with a low background. The protein concentration used was 1 µg/ml. After the buffer conditions were optimized, ScHsv2 mutants with GST-tag and also free GST as a control were analyzed with PIP strips. However, in some repetitions free GST bound to PI3P. Also, testing the mutants with these PIP strips did not give conclusive results. Thereafter, for quantitative analysis of ScHsv2 mutants, I analyzed the mutants with Cova PIP specificity plates. Here, TMB (3,3',5,5' - tetramethylbenzidine) is provided

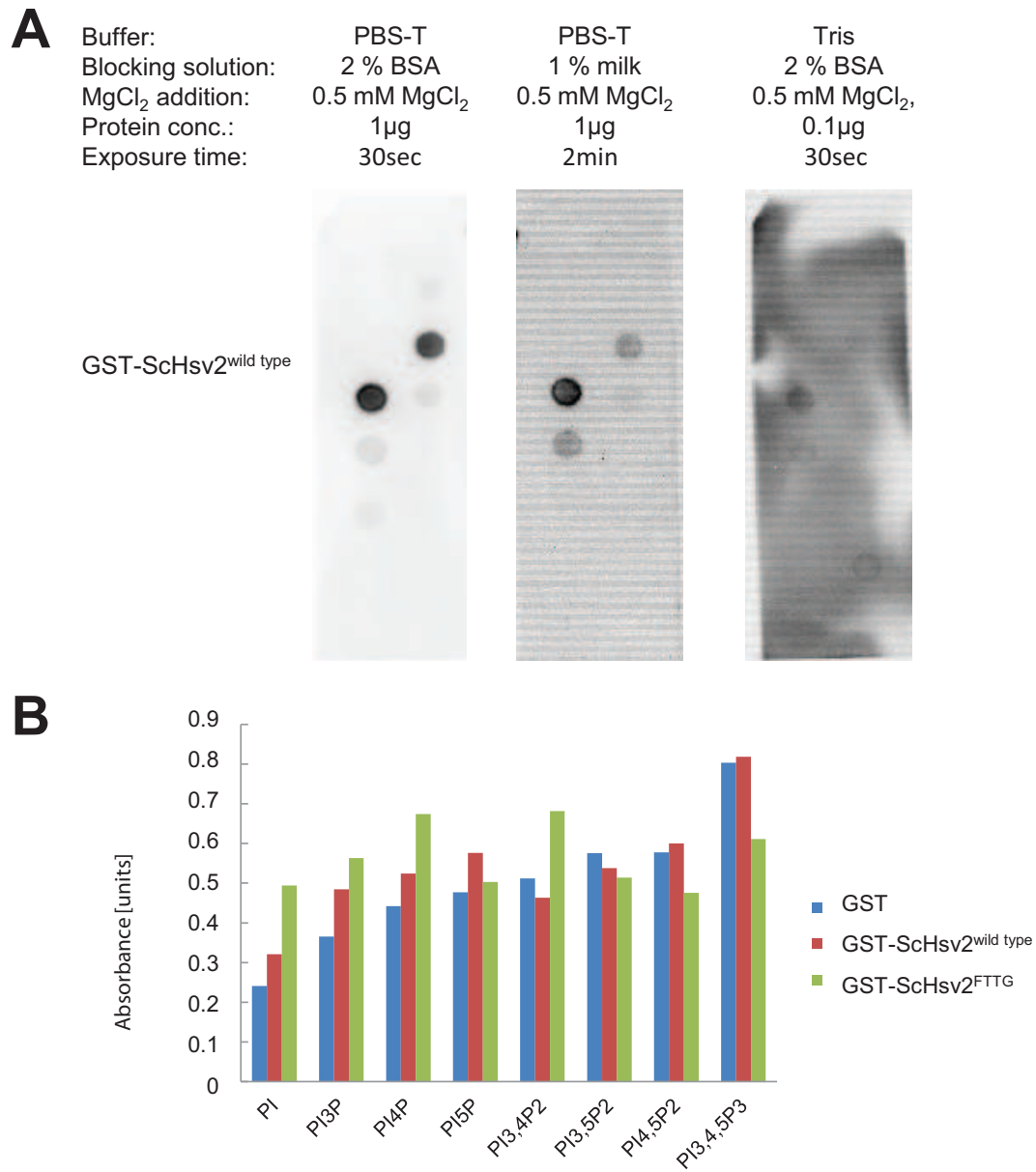


**Figure 4.18: Optimization of PIP strips and Cova PIP plate**

(A) Buffer optimization for PIP strip analysis using either BSA or milk as blocking reagent dissolved in PBS, TBS or 50 mM Tris-HCl pH 7.5. 0.5 mM MgCl<sub>2</sub> was added to the buffer. Protein was tested at different concentrations of 1 μg/ml and 0.1 μg/ml. (B) Cova PIP specificity plate used for quantitative analysis of PIP specificity of ScHsv2.



as a substrate for HRP (horse radish peroxidase) which can then be monitored by absorbance measurements. I also tried different buffer conditions for the Cova PIP specificity plate, but wild type ScHsv2 did not show any binding specificity for a certain PIP. For free GST, wild type ScHsv2 and ScHsv2<sup>FTTG</sup> similar absorbances were detected (see figure 4.18 B).

Since GST alone bound to PIP strips and dimerization of GST-tagged protein might also affect binding, I then cleaved the GST-tag from all proteins with thrombin and used untagged ScHsv2 protein for further analysis. Thrombin cleavage was more efficient in Hepes buffer pH 7.0 compared to citric acid pH 5.5 buffer, which was previously used to purify ScHsv2 (see suppl. figure 5.9 A). For removal of free GST and uncleaved GST-tagged ScHsv2 a second GSTrap run followed by a final gel filtration step was performed. In order to detect free ScHsv2 two rabbit serums with antibodies raised against the C-terminus of ScHsv2 were tested (provided by Prof. M. Thumm). For this purpose, purified protein was spotted onto a nitrocellulose membrane. Wild type ScHsv2, GST and ScHsv2<sup>FTTG</sup> mutant were tested in different concentrations and also the antibodies were used in two concentrations (1:1000 and 1:2000). The antibodies specifically detected ScHsv2 wild type and FTTG mutant, but not GST (see suppl. figure 5.9 B). In a next step, purified ScHsv2 protein without GST-tag was checked for its stability. Here, the protein was subjected to an analytical gel filtration run to exclude aggregation of the protein. ScHsv2 eluted in a single peak from the column, an additional peak was observed in the molecular weight range of thrombin (see suppl. figure 5.10). SDS gel check of the eluted peak showed pure ScHsv2 with small amounts of thrombin contamination. Thrombin cleaved ScHsv2 mutant proteins were again used to probe PIP strips and the Cova PIP specificity plates using different buffer conditions and with or without addition of MgCl<sub>2</sub>. Data were not reproducible similar to the situation with GST-tagged protein. Freezing and thawing might also influence phosphoinositide binding of Hsv2. In order to avoid this problem the mutant proteins were purified using GST SpinTrap columns, which allowed the “fresh” purification of several mutants at the same time (see suppl. figure 5.11). Wild type and mutant proteins were again cleaved with thrombin and a second GST SpinTrap purification step was performed. The fresh purified protein was then directly used for PIP strip analysis. However, also PIP strip experiments performed with non-thawed proteins did not give conclusive results (see suppl. figure 5.12).

Taken these results together, PIP strip experiments and quantification using the PIP specificity plate were not reproducible and did not give conclusive results for mutagenesis studies of ScHsv2.

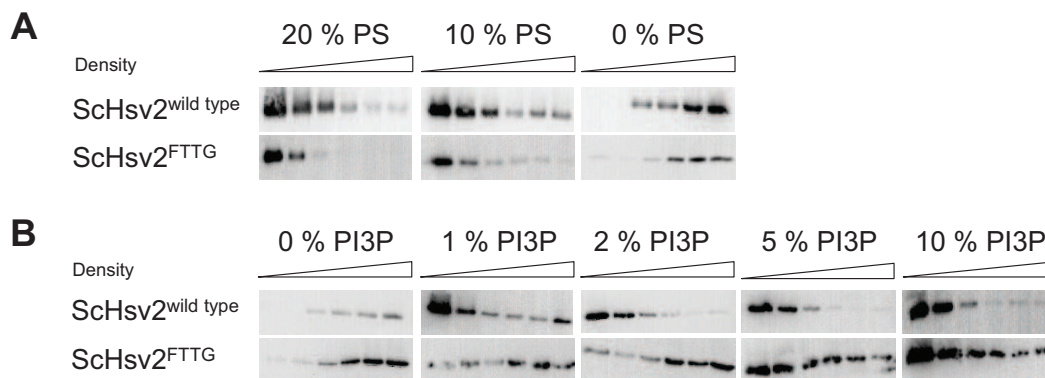


**Figure 4.19: Optimization of lipid composition for flotation assay**

(A) ScHsv2<sup>wildtype</sup> and ScHsv2<sup>FTTG</sup> were found to bind non specifically to liposomes containing 20 % or 10 % PS. Neutral liposomes consisting of 75 % PC, 23 % PE and 2 % Texas Red-PE were not bound by both ScHsv2 proteins. (B) Upon addition of different amounts of PI3P restored liposome binding was investigated. 1 % and 2 % PI3P in neutral liposomes were found to be bound by wild type ScHsv2. In 5 % and 10 % containing liposomes unspecific binding of ScHsv2<sup>FTTG</sup> was observed. (Busse *et al.*, submitted)

Another approach to probe protein-lipid interactions are liposome co-flotation assays. Here, the protein is incubated with liposomes before the mixture is put at the bottom of a non-continuous Nycodenz gradient. If the protein interacts with the liposomes, it floats with the liposomes to the top of the gradient during centrifugation. After centrifugation aliquots are taken and checked in Western blot analysis. First, I identified conditions where no unspecific protein-lipid binding was observed. To start with I prepared commonly used small unilamellar vesicles (SUVs) containing PC, PS, PE, PI3P and Texas Red-PE for visualization. This experiment was performed with wild type ScHsv2 and the FTTG mutant as a negative control. Strong binding of both wild type and ScHsv2<sup>FTTG</sup> was observed in the presence of either 10 % PS or 20 % PS. Therefore, I continued to optimize the liposome lipid composition in a way, that binding of the FTTG mutant was diminished. Since negatively charged lipids are often involved in unspecific binding, PS was left out. Only liposomes without any PS showed no interaction with the tested proteins (see figure 4.19 A). In a next step, different PI3P concentrations were added to the liposomes in order to observe liposome binding of wild type ScHsv2 but no binding of ScHsv2<sup>FTTG</sup> upon PI3P. Here, 2 % PI3P was found to be sufficient for interaction of wild type ScHsv2, but the FTTG mutant did not bind (see figure 4.19 B). ScHsv2<sup>wildtype</sup> protein also bound to 1 % PI3P containing liposomes. When 5 % or 10 % PI3P was added, also ScHsv2<sup>FTTG</sup> bound to the

liposomes. Binding of ScHsv2<sup>FTTG</sup> was likely due to non-specific ionic interactions at higher PI3P concentrations.

Presence of the liposomes in the low density region of the gradient after centrifugation was confirmed by fluorescence measurements of an SDS gel. Fluorescence of Texas Red was scanned with 532 nm excitation and 670 nm emission wavelength. The liposomes were detected in the upper two fractions, corresponding to the low density part of the gradient (see suppl. figure 5.13).

2 % PI3P, 73 % PC, 23 % PE and 2 % Texas Red-PE containing liposomes are optimal for studying ScHsv2 mutant interaction with liposome flotation assays.

In addition to the identification of residues involved in binding to phosphoinositides, I also wanted to determine the binding affinities and directly measure the stoichiometry for PIP binding of PROPPINs. The method of choice for this purpose is isothermal titration calorimetry (ITC). However, studying protein-lipid interaction by ITC is challenging. I started to use the water soluble head group of PI3P (PI3P-diC4) for first titration experiments with purified ScHsv2. For this purpose, PI3P-diC4 was dissolved at a final concentration of 50  $\mu\text{M}$  in HP150 buffer (20 mM Hepes pH 7.4, 150 mM KCl). The ligand was stepwise added to 2  $\mu\text{M}$  ScHsv2 in a total of 20 injections, each 15  $\mu\text{l}$  and a spacing time of 250 sec in between. Measurements were done at 25 °C in the VP-ITC MicroCalorimeter. However, no significant heat changes were observed (see figure 4.20 A). Also changes in concentrations and titrating ScHsv2 into the ligand instead did not give any indication for binding.

In another experiment I used PaAtg18 for titration analysis, this protein can be purified also in high yields and showed strong binding to PI(3,5)P<sub>2</sub> in PIP strip analysis. The soluble analogue of PI(3,5)P<sub>2</sub> (PI(3,5)P<sub>2</sub>-diC6) was dissolved in 20 mM Hepes and 300 mM NaCl buffer. Different concentrations of 100  $\mu\text{M}$  and 50  $\mu\text{M}$  for the ligand were tested and titrated in 1 mM PaAtg18. These experiments were done in an ITC<sub>200</sub> MicroCalorimeter, since here the needed volumes are much smaller. Even upon addition of 0.5 mM MgCl<sub>2</sub> no heat changes were detected. Furthermore, bubble formation interfered with measurements.

Since no binding of the soluble head groups to either ScHsv2 or PaAtg18 was observed, I next tested PI3P incorporated into liposomes for binding ScHsv2. I prepared large unilamellar vesicles (LUVs) in HP150 buffer with the extrusion method. The mean diameter of LUVs was determined by DLS and was 140 nm. LUVs were placed into the sample cell, of the VP-ITC machine, and ScHsv2 was titrated into the liposomes. The liposomes consisted of either 2 % or 5 % PI3P, 73 % or 70 % PC, respectively, 23 % PE and 2 % Texas Red-PE. Different concentrations of ligand in the liposomes (2 % and

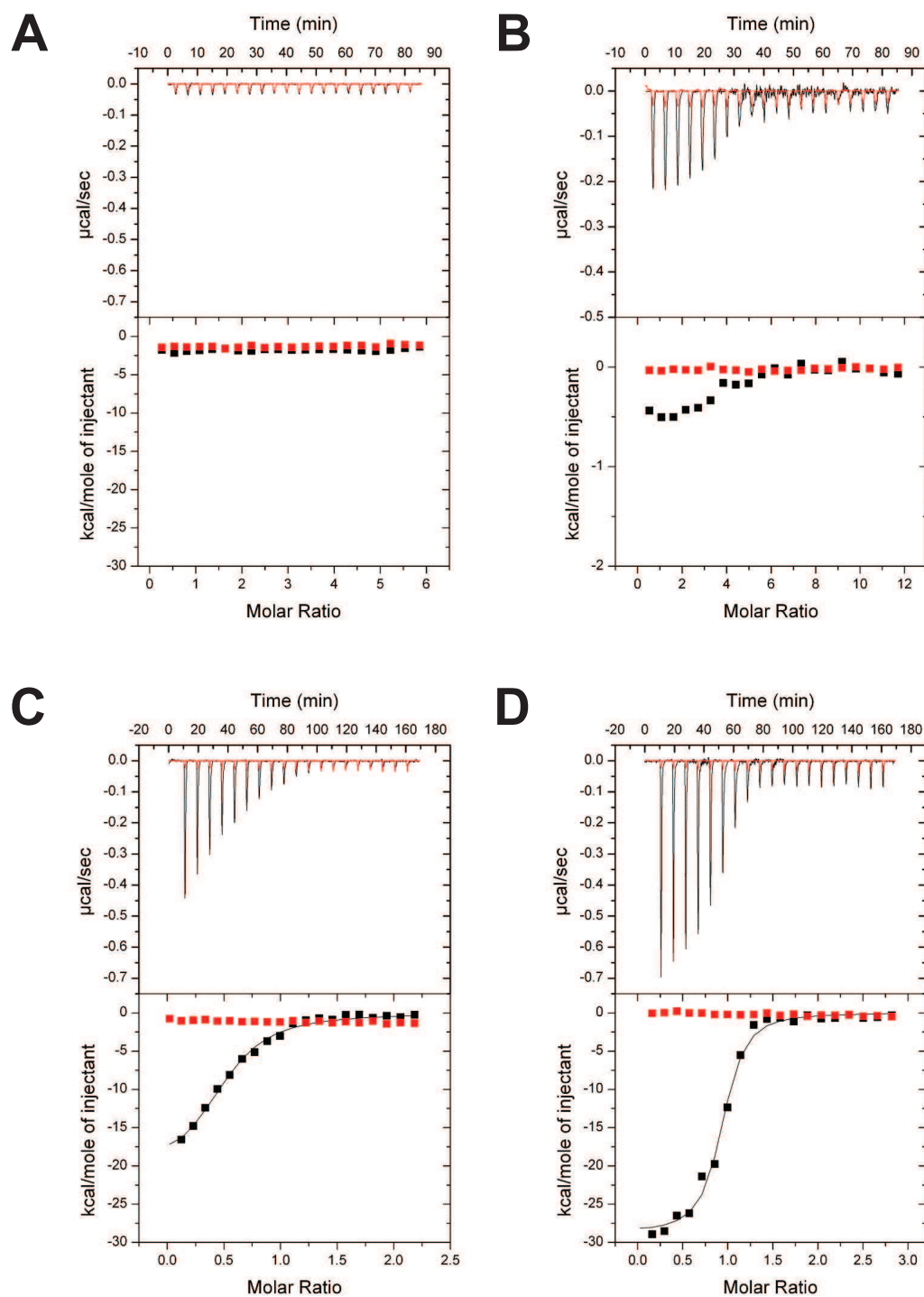


**Figure 4.20: Optimization of ITC measurements**

(A) Titration of dibutyl-PI3P into ScHsv2 (black line) in comparison to buffer titration (red line). (B) Titration of ScHsv2 into large unilamellar vesicles containing 2 % PI3P (black line) and the control buffer titration (red line). (C) Titration of ScHsv2 into small unilamellar vesicles with 2 % PI3P (black line). Red trace shows the buffer titration. (D) Titration of ScHsv2 into small unilamellar vesicles with 2 % PI(3,5)P<sub>2</sub> (black line). Red trace shows the buffer titration.

5 % PI3P), liposomes (1 mg/ml - 4 mg/ml total lipid) and ScHsv2 (20  $\mu$ M - 190  $\mu$ M) were tested. However, for some measurements a heat change was observed for the first injections, but all titrations resulted in precipitation of protein with liposomes. That the liposomes precipitated was visible due to incorporation of Texas Red (see figure 4.20 B). Stirring of the LUVs during the measurements might lead to precipitation, even when the slowest stirring speed was chosen. In addition, the extrusion method does not prevent micelle formation of some lipids, which might induce aggregation and precipitation.

Therefore, I prepared small unilamellar vesicles, which were also used for flotation assays. Liposome formation is done with a Sephadex G50 column, this avoids that micelles elute together with vesicles like on a size exclusion chromatography. Furthermore, SUVs are smaller in size. Using FFF-MALLS analysis of either 2 % PI3P or PI(3,5)P<sub>2</sub>, 73 % PC, 23 % PE and 2 % Texas Red-PE containing liposomes revealed a mean size distribution of the radii of 18 nm for 2 % PI3P containing liposomes and 21 nm for PI(3,5)P<sub>2</sub> containing liposomes (these measurements were done by Dr. J. M. Hernandez). Total phosphate concentration was determined by the phosphomolybdate method and then the PI3P concentration calculated. ITC measurements were done with an accessible PI3P concentration in the liposomes of 5  $\mu$ M to 10  $\mu$ M and a ScHsv2 concentration ranging from 50  $\mu$ M to 100  $\mu$ M. ScHsv2 was titrated into the liposomes using a VP-ITC machine with a total of 20 injections. The first injection was done with a volume of 3  $\mu$ l and the following ones with 15  $\mu$ l each. The spacing time was increased to 500 sec to allow recovering of the heat change to the baseline. Measurements were done at 25 °C. During measurements large enthalpy changes were observed in the beginning, which decreased until saturation was reached (see figure 4.20 C). These measurements were used to determine the binding affinity and stoichiometry of phosphoinositide binding. Furthermore, liposomes were also prepared with PI(3,5)P<sub>2</sub> and similar concentrations for the titration were used. Here, also a titration curve was observed, that was suitable for characterization of the binding reaction (see figure 4.20 D).

#### 4.2.2.2 PROPPINs binding specificity to phosphoinositides

*S. cerevisiae* homologs of Atg18 and Atg21 purified from *E. coli* could only be obtained in small yields or with tags like GST (glutathione-S-transferase) [133, 151] or MBP (maltose binding protein) [144]. However, the GST-tag leads to dimerization of

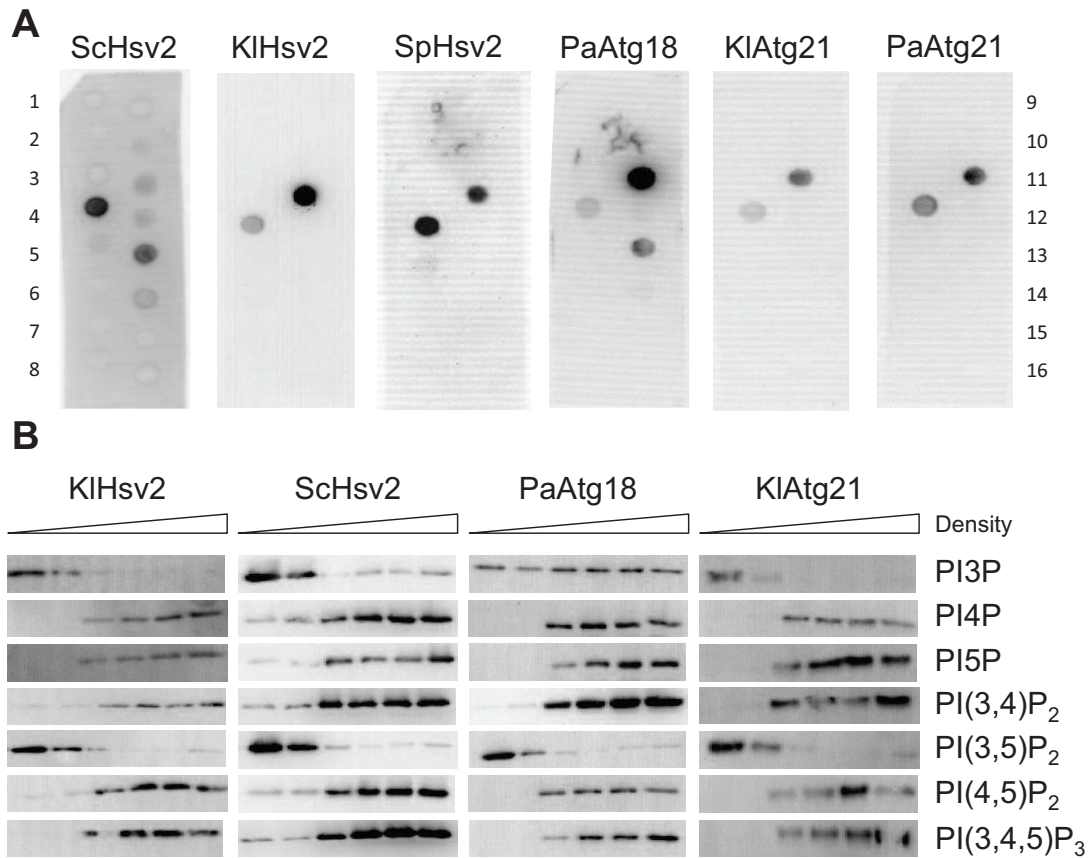


**Figure 4.21: Selective binding of PROPPINs to phosphoinositides**

(A) Protein-lipid overlay assay analysis of ScHsv2, KlHsv2, SpHsv2, PaAtg18, KlAtg21 and PaAtg21. The following lipids were spotted on the membrane - 1: Lysophosphatidic Acid (LPA), 2: Lysophosphocholine (LPC), 3: PI, 4: PI(3)P, 5: PI(4)P, 6: PI(5)P, 7: PE, 8: PC, 9: Sphingosine-1-phosphate (S1P), 10: PI(3,4)P<sub>2</sub>, 11: PI(3,5)P<sub>2</sub>, 12: PI(4,5)P<sub>2</sub>, 13: PI(3,4,5)P<sub>3</sub>, 14: Phosphatidic Acid, 15: PS, 16: Blank. (B) Flotation assay of ScHsv2, KlHsv2, PaAtg18 and KlAtg21 with liposomes containing 1 % of the indicated phosphoinositide, 74 % PC, 23 % PE and 2 % TR-PE. All conditions were tested with at least three replicates.

the proteins and Dove *et al.* [133] reported a 2.5 fold difference in binding affinity of ScAtg18 in comparison to GST-ScAtg18.

During this study, I purified homologs of Atg18, Atg21 and Hsv2 from other yeast species, which can be obtained in high amounts, carrying a small 6x His-tag or are stable without any tag. In a first step, I used PIPstrips to analyze the phosphoinositide binding specificities of these proteins (see figure 4.21 A). ScHsv2 was detected using the Hsv2-antibody and showed binding to PI3P and to a small amount to PI(3,4,5)P<sub>3</sub>. KlHsv2 and SpHsv2, both with His-tag, show binding to PI3P and PI(3,5)P<sub>2</sub> and binding was detected with a penta-His antibody. KlHsv2 seems to have a higher affinity to PI(3,5)P<sub>2</sub>

than SpHsv2, which binds stronger to PI3P. PaAtg18 binds strongly to PI(3,5)P<sub>2</sub> and to a lower extent to PI3P and PI(3,4,5)P<sub>3</sub>. Weak binding to PI3P and PI(3,5)P<sub>2</sub> was detected for both KlAtg21 and PaAtg21.

These PIPstrips were mainly used in literature to investigate phosphoinositide binding specificity. Here, flotation assays were employed as a second method to characterize phosphoinositide specificities. Furthermore this method is more reliable since liposomes are used instead of a plain membrane spotted with concentrated phosphoinositides. Liposomes containing 74 % PC, 23 % PE, 2 % TR-PE and 1 % of indicated phosphoinositide were used (see figure 4.21 B). Liposomes were incubated with purified ScHsv2, KlHsv2, PaAtg18 and KlAtg21, subjected to ultracentrifugation with a nycodenz gradient and fractions were analyzed by immunoblotting. All PROPPINs bound to both PI3P and PI(3,5)P<sub>2</sub>, because the proteins were present in the top fractions. When no binding occurs protein is found in the lower fractions, which corresponds to a high Nycodenz concentration. Compared to the other PROPPINs PaAtg18 shows weaker binding to PI3P because the protein was detected to the same extent in all 6 lanes.

Taken together, these data show that PROPPINs bind with high specificity to PI3P and PI(3,5)P<sub>2</sub>.

#### 4.2.2.3 Characterization of Hsv2 membrane binding sites

The FRRG motif of PROPPINs was reported to be essential for phosphoinositide binding [151]. Mutagenesis of this motif to FTTG resulted in loss of binding. Our structure of KlHsv2 revealed that the two arginines of this motif point into opposite directions. Each indicating a separate potential binding pocket. In the KlHsv2 crystal structure both potential pockets were occupied by sulfates. A third sulfate was found on the other side of the  $\beta$ -propeller.

In order to investigate the involvement of amino acids from both potential pockets in phosphoinositide binding they were mutated to alanines in ScHsv2. For controls, the FTTG and FAAG mutants were generated as well as the ScHsv2<sup>R123A</sup> mutant. This residue was chosen because of its location close to the third sulfate in KlHsv2. Binding site I includes the Arg264, the first Arg from the FRRG motif. In addition His223, Ser243, Thr247, Arg250 and Glu262 were mutated to alanines. From the second pocket the conserved residues Arg265, Lys290, Thr292, His294 and Lys269 were mutated to alanines.

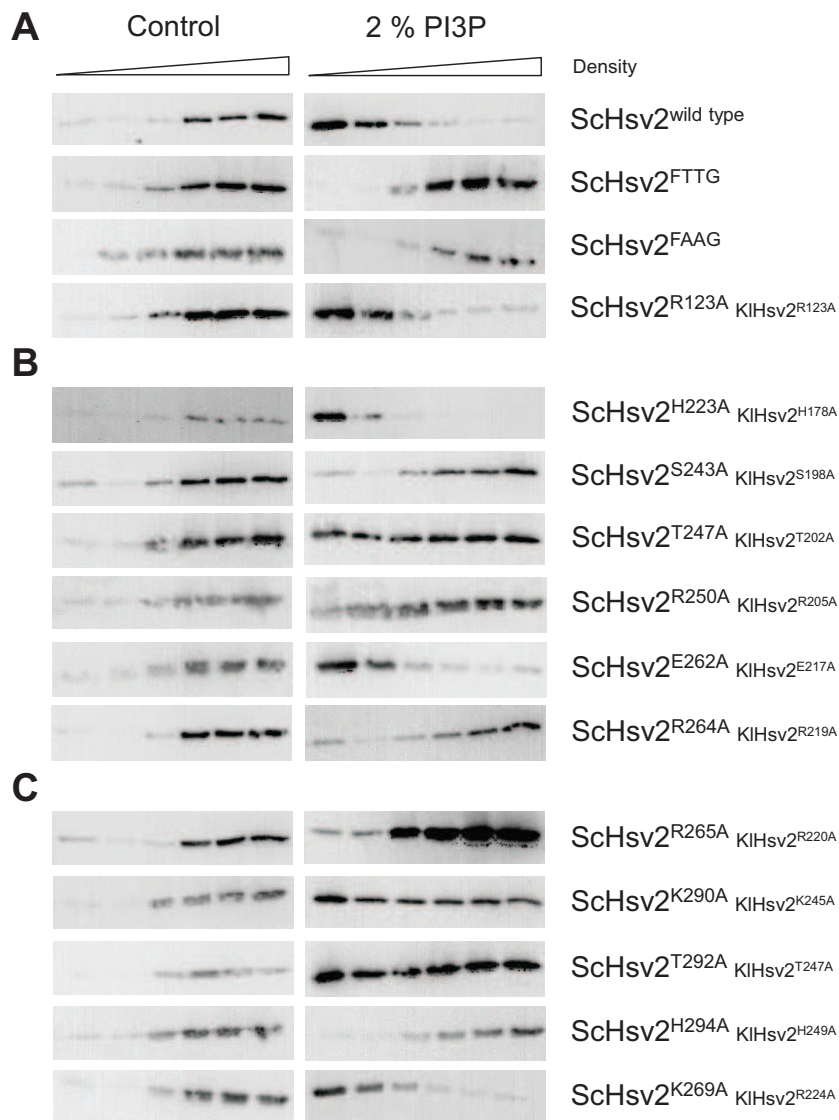


**Figure 4.22: Characterization of ScHsv2 membrane binding site I and II**

Analysis of amino acids involved in phosphoinositide binding by mutagenesis of conserved residues in ScHsv2. Flotation assays were performed with both control liposomes consisting of 23 % PE, 2 % TR-PE and 75 % PC and liposomes composed of 2 % PI3P, 23 % PE, 2 % TR-PE and 73 % PC. **(A)** Wildtype ScHsv2, FTTG and FAAG mutants were tested as well as ScHsv2<sup>H123A</sup> as controls. **(B)** Amino acids conserved in the potential binding site I were analyzed. **(C)** Mutated residues of binding pocket II are shown. In small letters the corresponding amino acids in KIHsv2 are given. At least three replicates were done for each condition.

Flotation assays with liposomes consisting of 2 % PI3P, 23 % PE, 2 % TR-PE and 73 % PC were done with each alanine mutant. As control liposomes containing 23 % PE,



2 % TR-PE and 75 % PC were used to show that binding is PI3P specific. Figure 4.22 A shows wild type ScHsv2 and ScHsv2<sup>R123A</sup> binding to 2 % PI3P containing liposomes but not to control liposomes lacking PI3P. This shows that the region surrounding the third sulfate is not involved in membrane binding. ScHsv2<sup>FTTG</sup> and ScHsv2<sup>FAAG</sup> do not bind to liposomes.

In the potential binding site I (see figure 4.22 B) Ser243 and Arg264 mutation resulted in loss of PI3P binding. These residues are essential for PI3P binding. Mutants ScHsv2<sup>T247A</sup> and ScHsv2<sup>R250A</sup> showed reduced ability to bind to liposomes with PI3P, suggesting an involvement in binding, but these residues are not essential. ScHsv2<sup>H223A</sup> and ScHsv2<sup>E262A</sup> are not effected in binding to PI3P containing liposomes.

In the second potential phosphoinositide binding site Arg265 and His294 are essential residues, in addition Lys290 and Thr292 are involved in binding (see figure 4.22 C). In contrast, mutation of Lys269 showed no effect and behaved like wild type ScHsv2.

The analysis of ScHsv2 mutants with flotation assays identified a set of conserved amino acids essential or involved in PI3P binding. These results strongly support the presence of two phosphoinositide binding sites in PROPPINs.

#### 4.2.2.4 Determination of binding affinity and stoichiometry

In order to directly determine the stoichiometry and affinities for PI binding PROPPINs ITC measurements were performed.

ITC measurements were done by titrating purified proteins into liposomes containing 23 % PE, 2 % TR-PE, 73 % PC and either 2 % PI3P or 2 % PI(3,5)P<sub>2</sub> in HP150 buffer at pH 7.4. When KlHsv2 was titrated into liposomes with 2 % PI3P a  $K_D$  of 480 nM was determined (see figure 4.23 A, data summarized in table 4.3) and a three fold higher binding affinity for PI(3,5)P<sub>2</sub> was measured. ScHsv2 (figure 4.23 B) and PaAtg18 (figure 4.23 C) show similar affinities for PI3P as KlHsv2. Also ScHsv2 is comparable in PI(3,5)P<sub>2</sub> binding to KlHsv2. Interestingly, PaAtg18 has a very high affinity for PI(3,5)P<sub>2</sub> ( $K_D = 70$  nM). KlAtg21 has lower affinities to the two tested phosphoinositides (figure 4.23 D).

ScHsv2 has a binding stoichiometry of 0.5 to PI3P, meaning a 1:2 protein to ligand ratio. The other tested PROPPINs show a lower stoichiometry between 0.35 and 0.37. These titrations into PI3P containing liposomes need to be further optimized to obtain a better curve start and resulting from this a more distinct binding stoichiometry.

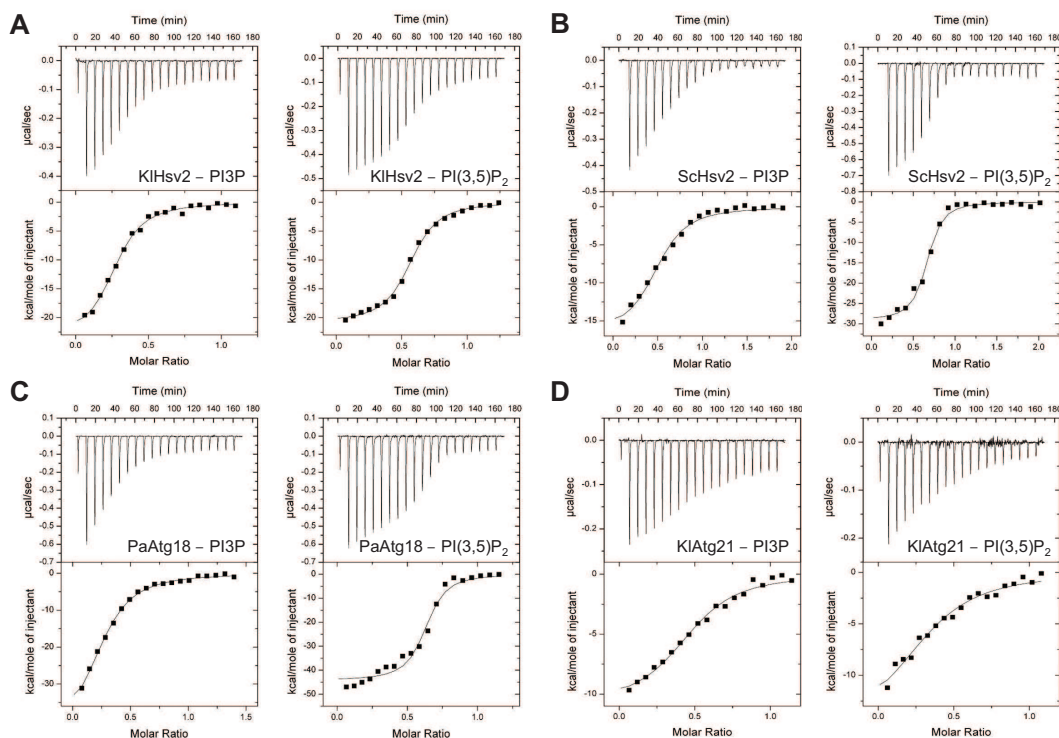


**Figure 4.23: ITC measurements of PROPPINs with liposomes containing PI3P or PI(3,5)P<sub>2</sub>**

Isothermal titration calorimetry curves are shown from titrations of (A) KIHsv2 (B) ScHsv2 (C) PaAtg18 (D) KIAtg21 into liposomes consisting of 23 % PE, 2 % TR-PE, 73 % PC and either 2 % PI3P or 2 % PI(3,5)P<sub>2</sub>. Data was fitted with a One Set of Sites fitting model.

For PI(3,5)P<sub>2</sub> the stoichiometry was in general less than the 1:2 ratio observed for PI3P ( $N \approx 0.6$ ). Which might indicate that not all proteins bind a second ligand, which might depend on the pH.

I also used flotation assays to study binding affinities. With this method phosphoinositide concentrations in liposomes needed for sufficient PROPPIN binding were determined. A set of liposomes were prepared containing PI3P in a range of 0 % to 10 % (0 %, 0.025 %, 0.05 %, 0.1 %, 0.2 %, 0.3 %, 0.4 %, 0.5 %, 1 %, 2 %, 5 % and 10 %) and the same liposomes were also prepared with PI(3,5)P<sub>2</sub>, PC amounts in the liposomes were adjusted accordingly. ScHsv2 and KIHsv2 were added to these liposomes and binding was analyzed by immunoblotting followed by quantification of the Western blots using the AIDA software.

Here, the upper (low density) two fractions from flotation assays were considered to be liposome bound protein, the lower 4 fractions contain unbound protein. After quantification the sum of the upper fractions was divided by sum of all 6 fractions and

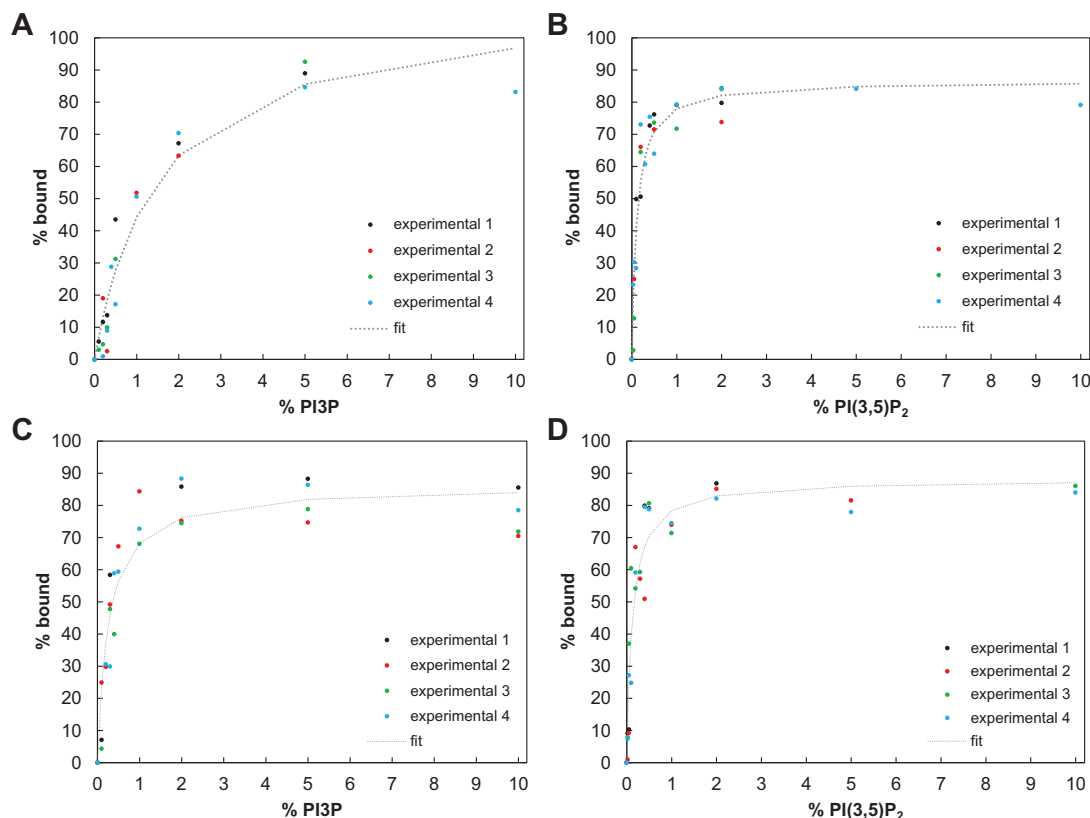


**Figure 4.24: Local membrane concentration of phosphoinositides needed for Hsv2 binding**  
 Quantification of flotation assays and plotting of bound protein fractions versus % phosphoinositide concentration for (A) KIhsv2 with PI3P containing liposomes, (B) KIhsv2 on PI(3,5)P<sub>2</sub>, (C) ScHsv2 with PI3P liposomes and (D) ScHsv2 with liposomes of PI(3,5)P<sub>2</sub>. Data analysis together with A. Scacioc.

multiplied with 100 % to get the percentage of bound protein. The bound protein fraction was plotted versus the phosphoinositide concentration in liposomes. All conditions were measured in four replicates and all data were plotted together for subsequent data fitting (see figure 4.24). Fitting was performed in order to get  $K_D$ , minimal  $K_D$  and maximal  $K_D$ . Data are summarized in table 4.4.

Resulting from this a  $K_D$  of 1.52 % was determined for binding of KIhsv2 to PI3P (figure 4.24 A) and 0.11 % for PI(3,5)P<sub>2</sub> containing liposomes (figure 4.24 B). This means that a local concentration of 1.5 % of PI3P is needed for 50 % of KIhsv2 to bind. In contrast, ten times less PI(3,5)P<sub>2</sub> is needed. ScHsv2 has a  $K_D$  of 0.26 % for PI3P and 0.12 % for PI(3,5)P<sub>2</sub>. These data were analyzed together with A. Scacioc.

These results are in agreement with the ITC data showing that the affinity of PROP-PINs is higher to PI(3,5)P<sub>2</sub> than to PI3P.

**Table 4.3:** Binding affinities and stoichiometries of PROPPINs to phosphoinositides

PROPPIN	Phosphoinositide	Binding affinity $K_D$ [ $\mu$ M]	Stoichiometry N	Number of measurements
KlHsv2	PI3P	$0.48 \pm 0.04$	0.35	3
	PI(3,5)P <sub>2</sub>	$0.18 \pm 0.01$	0.58	3
ScHsv2	PI3P	$0.67 \pm 0.02$	0.50	7
	PI(3,5)P <sub>2</sub>	$0.22 \pm 0.07$	0.66	4
PaAtg18	PI3P	$0.53 \pm 0.09$	0.37	3
	PI(3,5)P <sub>2</sub>	$0.07 \pm 0.012$	0.62	3
KlAtg21	PI3P	$0.89 \pm 0.08$	0.37	3
	PI(3,5)P <sub>2</sub>	$1.38 \pm 0.23$	0.39	3

(average  $\pm$  SEM\*)

\* Average and SEM was determined from at least three measurements.

**Table 4.4:** Determination of binding affinity  $K_D$  based on %-bound protein versus % phosphoinositide in liposomes

PROPPIN	Phosphoinositide	$K_D$ [%]	$K_{Dmin}$ [%]	$K_{Dmax}$ [%]
KlHsv2	PI3P	1.52	1.02	2.32
	PI(3,5)P <sub>2</sub>	0.11	0.07	0.14
ScHsv2	PI3P	0.26	0.17	0.31
	PI(3,5)P <sub>2</sub>	0.12	0.10	0.17

#### 4.2.2.5 pH dependency of phosphoinositide binding for Hsv2

Docking of PI3P and PI(3,5)P<sub>2</sub> into KlHsv2 binding sites I and II were performed by A. Scacioc [24]. Interestingly docking of PI(3,5)P<sub>2</sub> could only be performed when KlHsv2 His178 of binding site I and His294 of binding pocket II were protonated. ScHsv2 contains an additional histidine in binding site II. Considering the stoichiometry of PROPPINs to PI(3,5)P<sub>2</sub> of  $\approx 0.6$  we speculated that protonation of these histidines might influence the stoichiometry of PI(3,5)P<sub>2</sub> binding. Furthermore it is well known that acidification of e.g. endosomes and lysosomes/vacuole is needed for subsequent

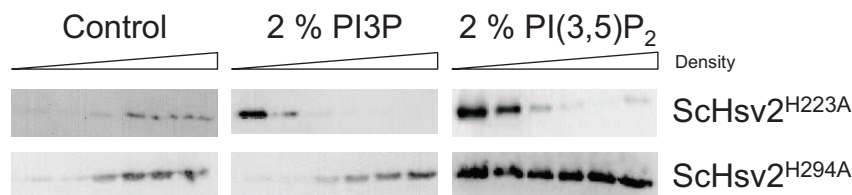


**Figure 4.25: Involvement of ScHsv2 histidines from binding sites 1 and 2 on phosphoinositide binding**

Flotation assays with ScHsv2<sup>H223A</sup> and ScHsv2<sup>H294A</sup> mutants on control liposomes of 75 % PC; 23 % PE and 2 % TR-PE. In addition liposomes with either 2 % PI3P or 2 % PI(3,5)P<sub>2</sub>, 23 % PE, 2 % TR-PE and 73 % PC were used.

cellular functions [176, 177]. Whereas the overall intracellular cytoplasmic pH in yeast is 7.0 to 7.2, but i.e upon glucose starvation the pH decreases [178].

Hence, the effect of mutated ScHsv2 His223 (KIHsv2 His178) and His294 (KIHsv2 His249) was tested on PI(3,5)P<sub>2</sub> in addition to the measurements with PI3P shown in figure 4.22. Flotation assays with liposomes consisting of 2 % PI(3,5)P<sub>2</sub>, 23 % PE, 2 % TR-PE and 73 % PC were done with the ScHsv2<sup>H223A</sup> and ScHsv2<sup>H294A</sup> mutants in HP150 buffer at pH 7.4. Figure 4.25 shows that His223 in pocket I has no effect on phosphoinositide binding. In contrast His294 mutation abolished binding to PI3P containing liposomes and reduced binding to PI(3,5)P<sub>2</sub>.

In order to address a potential underlying pH dependence of binding, isothermal titration calorimetry measurements were performed at different pHs with KIHsv2 and ScHsv2 using liposomes containing either 2 % PI3P or 2 % PI(3,5)P<sub>2</sub>, 23 % PE, 2 % TR-PE and 73 % PC. As buffers 20 mM BisTris pH 6.5, 20 mM Hepes pH 7.4 or 20 mM Tris pH 8.0, all containing 150 mM KCl, were used for titrations. Figure 4.26 shows the titration of ScHsv2 and KIHsv2 into 2 % PI(3,5)P<sub>2</sub> containing liposomes, data obtained for PI3P and PI(3,5)P<sub>2</sub> are summarized in table 4.5.

KIHsv2 shows no pH effect on binding affinity or stoichiometry when titrated into PI3P containing liposomes. Also no effect was observed for the stoichiometry when titrated into liposomes with PI(3,5)P<sub>2</sub> (see figure 4.26 A and table 4.5). Compared to pH 7.4 the  $K_D$  at pH 6.5 and 8.0 increased 2.5 to 3 fold in PI(3,5)P<sub>2</sub> containing liposomes. ScHsv2 shows higher affinities to both phosphoinositide liposomes at pH 6.5 (see figure 4.26 B and table 4.5). Interestingly, when ScHsv2 is titrated into PI(3,5)P<sub>2</sub> the  $K_D$  and stoichiometry increases dependent on the pH. In pH 8.0 stoichiometry reaches nearly a 1:1 ratio, suggesting that only one of the two binding sites seems to bind PI(3,5)P<sub>2</sub>.

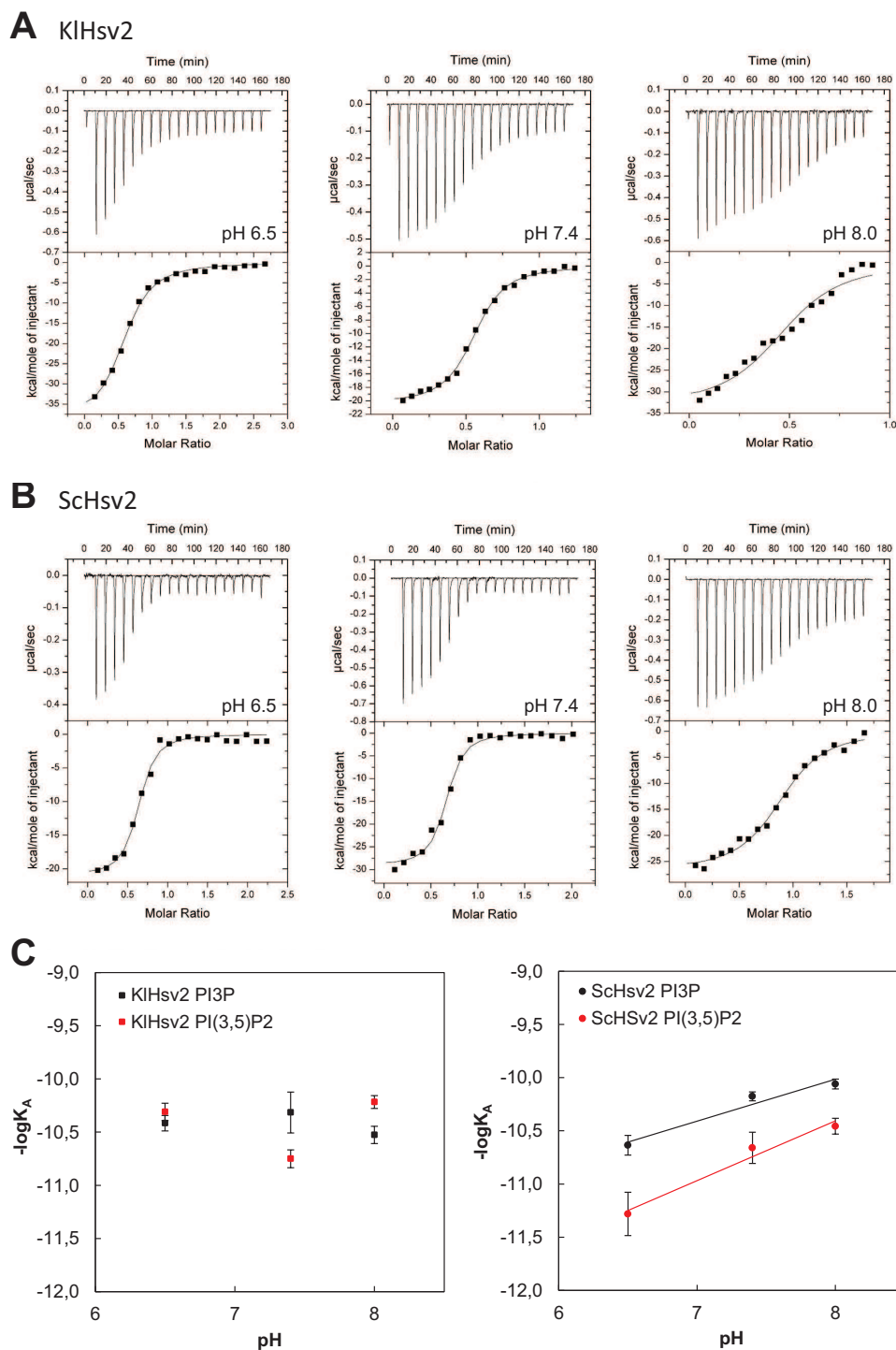


**Figure 4.26: ITC measurements of KIHsv2 and ScHsv2 with PI(3,5)P<sub>2</sub> liposomes in different pHs**

(A) KIHsv2 and (B) ScHsv2 were titrated into either 2 % PI3P or 2 % PI(3,5)P<sub>2</sub>, 23 % PE, 2 % TR-PE and 73 % PC containing liposomes at different pHs. BisTris buffer at pH 6.5, Hepes pH 7.4 and Tris pH 8.0 were tested, all containing 150 mM KCl. (C) Diagrams showing the negative logarithm of  $K_A$ s plotted versus pH for KIHsv2 (right panel) and ScHsv2 (left panel).

Visualization of affinity changes depending on pH were done by plotting the negative logarithm of  $K_A$  versus pH (see figure 4.26 C). KlHsv2 data points lie on a horizontal line. Linear regression analysis of the data points for ScHsv2 showed an increase in PI3P and PI(3,5)P<sub>2</sub> affinity depending on the pH. Supporting the fact of an underlying pH switch.

Taken these results together a pH switch was observed for ScHsv2 when titrated into PI(3,5)P<sub>2</sub> and to a smaller extent for PI3P containing liposomes. For KlHsv2 no clear effect was observed.

**Table 4.5:** Binding affinities and stoichiometries of Hsv2 in different pHs

PROPPIN	Phosphoinositide	pH	Binding affinity $K_D$ [ $\mu$ M]	Stoichiometry N
KlHsv2	PI3P	6.5	$0.38 \pm 0.02$	0.30
		7.4	$0.48 \pm 0.04$	0.35
		8.0	$0.30 \pm 0.02$	0.38
	PI(3,5)P <sub>2</sub>	6.5	$0.49 \pm 0.08$	0.64
		7.4	$0.18 \pm 0.01$	0.58
		8.0	$0.61 \pm 0.01$	0.50**
ScHsv2	PI3P	6.5	$0.23 \pm 0.03$	0.39
		7.4	$0.67 \pm 0.02$	0.50
		8.0	$0.87 \pm 0.12$	0.27
	PI(3,5)P <sub>2</sub>	6.5	$0.05 \pm 0.02$	0.57
		7.4	$0.22 \pm 0.07$	0.66
		8.0	$0.35 \pm 0.02$	0.93
(average $\pm$ SEM*)				

\* Average and SEM was determined from at least three (\*\*two) measurements.

Whether the proteins are stable in the used pHs was investigated by Thermofluor experiments. Here, proteins were subjected to a temperature gradient from 25 °C to 95 °C and Sypro Orange fluorescence was measured. An increase in fluorescence correlates with protein unfolding. KlHsv2 shows almost the same stability in all buffers with a small increase in stability for BisTris buffer at pH 6.5, indicated by the shift of the curve towards higher temperatures (see figure 4.27 A). ScHsv2 is more stable in Hepes buffer at pH 7.4 and BisTris buffer pH 6.5. In comparison ScHsv2 starts to unfold at

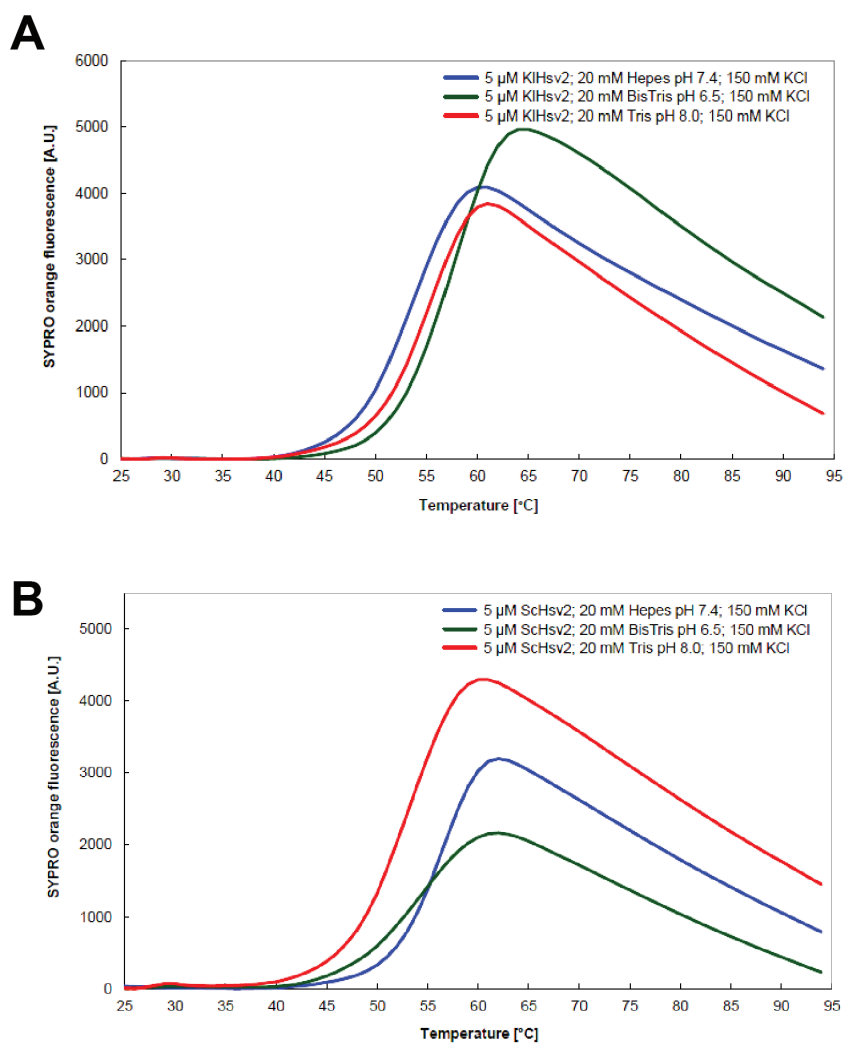


**Figure 4.27: Stability of KIHsv2 and ScHsv2 in different pHs**

Thermofluor analysis of (A) KIHsv2 and (B) ScHsv2 in BisTris pH 6.5, Hepes pH 7.4 and Tris pH 8.0 buffer all supplemented with 150 mM KCl.

lower temperatures in Tris pH 8.0 (see figure 4.27 B). Both proteins are stable and folded in all buffers and at the temperature used for ITC measurements.

#### 4.2.2.6 Role of loop 6CD for membrane binding

The structure of KIHsv2 adopts a seven bladed  $\beta$ -propeller, whose blades and  $\beta$ -strands are connected by loops. Interestingly, blade 6 contains a long loop sticking out



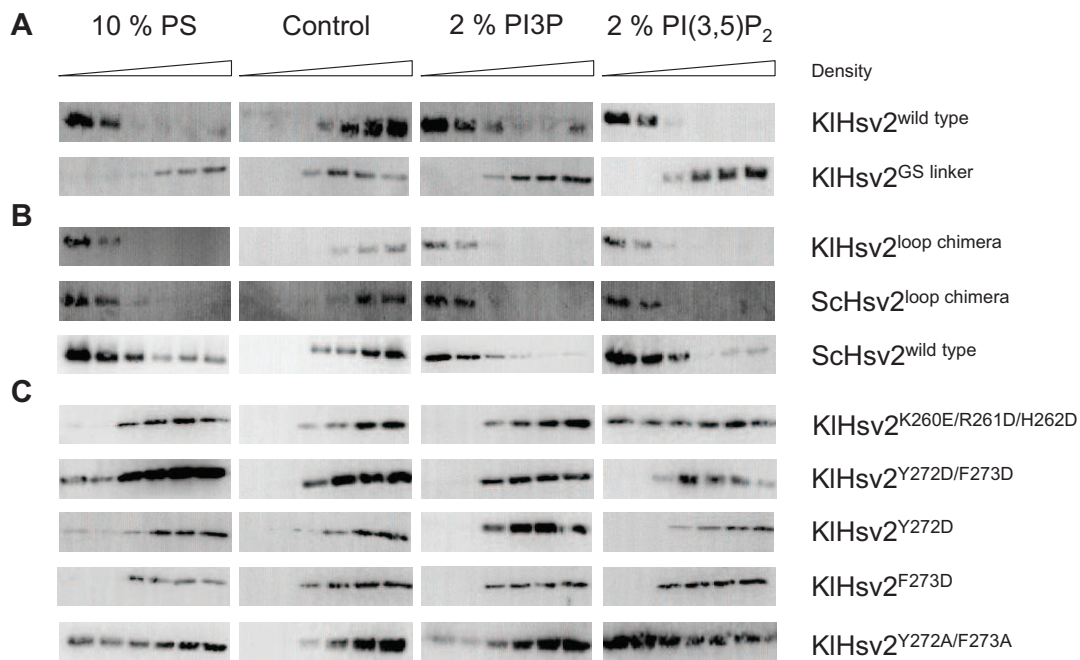


**Figure 4.28: The impact of loop 6CD on membrane binding**

Flotation assays using 10 % PS, 2 % PI3P and 2 % PI(3,5)P<sub>2</sub> containing liposomes and control liposomes consisting of 75 % PC, 23 % PE and 2 % Texas Red-PE only. **(A)** Showing KIHsv2<sup>wildtype</sup> and KIHsv2<sup>GSlinker</sup> subjected on the liposomes. **(B)** KIHsv2<sup>loopchimera</sup>, ScHsv2<sup>loopchimera</sup> and wild type ScHsv2 after flotation analysis. **(C)** Shows KIHsv2 loop mutants KIHsv2<sup>K260E/R261D/H262D</sup>, KIHsv2<sup>Y272D/F273D</sup>, KIHsv2<sup>Y272D</sup>, KIHsv2<sup>F273D</sup> and KIHsv2<sup>Y272A/F273A</sup>

of the  $\beta$ -propeller structure. This loop connects strand C and D of blade 6 and is in close proximity to the FRRG motif in blade 5, which is essential for PIP binding. This close proximity led us raise the question, if this loop is involved in membrane binding.

To address this question flotation assays were performed using wild type KIHsv2 and a GS linker construct in which the loop 6CD (amino acids 258 to 274) was replaced by a (GS)<sub>4</sub>G motif. Liposomes containing 10 % PS, 65 % PC, 23 % PE and 2 % TR-PE were used. These negatively charged liposomes were used to test unspecific membrane binding. Control liposomes, which are known that wild type KIHsv2 does not bind, and liposomes consisting either 2 % PI3P or 2 % PI(3,5)P<sub>2</sub>, 23 % PE, 2 % TR-PE and 73 % PC were used. Figure 4.28 A shows binding of wildtype KIHsv2 to liposomes with 10 % PS, but not to liposomes without PS or phosphoinositide (control). Binding occurs to liposomes containing either 2 % PI3P or 2 % PI(3,5)P<sub>2</sub>. When the loop 6CD was replaced by the GS linker motif no binding was detected to any of the liposomes.

These data show that besides the two PIP binding sites also the loop 6CD is required for membrane binding.

In a next step, I tested whether the loop 6CD region from KIHsv2 and ScHsv2 can replace each other and therefore recover membrane binding. This loop region is disordered and less conserved throughout PROPPINs, e.g. the loop in ScHsv2 is longer compared to KIHsv2 (suppl. figure 5.15). I used synthetic loop chimera constructs to analyze this binding with flotation assays. Here, KIHsv2<sup>loopchimera</sup> showed wild type-like liposome binding, suggesting that the binding ability is completely recovered. Also ScHsv2<sup>loopchimera</sup> and wild type ScHsv2 bind the same liposomes. These results show that the loop regions can substitute for each other.

How loop 6CD insertion into the membrane occurs was next investigated. First we analyzed loop 6CD by alignment of this region in different PROPPINs. The human Hsv2 homologs WIPI3 and WIPI4, Hsv2 from *A. thaliana*, *Y. lipolytica*, *A. gossypii* and *C. glabrata* as well as ScHsv2 and KIHsv2 were aligned (suppl. figure 5.16). The alignment was manually modified by A. Scacioc according to properties like hydrophobicity and charges. This loop is not conserved, but in the middle region of the loop is a small patch of positively charged amino acids (amino acids with red background) and at the end of the loop aromatic amino acids (Tyr, Phe) are located. KIHsv2 was used for mutagenesis studies of the positively charged patch. Here, Lys260, Arg261 and His262 were mutated into negatively charged amino acids K260E/R261D/H262D. Furthermore, the aromatic residues Tyr272 and Phe273 were exchanged, here the double mutants Y272D/F273D and Y272A/F273A were generated as well as single Asp mutants of both residues.

In flotation assay analysis the KIHsv2<sup>K260E/R261D/H262D</sup> triple mutant showed neither binding to 10 % PS containing liposomes nor to 2 % PI3P. Its binding was reduced on 2 % PI(3,5)P<sub>2</sub> liposomes (see figure 4.28). The two double mutants KIHsv2<sup>Y272D/F273D</sup> and KIHsv2<sup>Y272A/F273A</sup> were diminished in binding to 10 % PS and 2 % PI(3,5)P<sub>2</sub> containing liposomes. PI3P binding was completely abolished. Binding to all liposomes was lost in KIHsv2<sup>Y272D</sup> and KIHsv2<sup>F273D</sup> mutants. In conclusion these results show that membrane binding of loop 6CD occurs through both hydrophobic and ionic interaction with the membrane lipids.

PIP binding of KIHsv2 and ScHsv2 loop mutants were also tested on PIPstrips (suppl. figure 5.17). Wild type KIHsv2 and the loop chimera construct were detected on spots containing PI3P and PI(3,5)P<sub>2</sub>. ScHsv2 bound PI3P and PI(3,4,5)P<sub>3</sub>, the loop chimera of ScHsv2 showed unspecific binding to all 7 phosphoinositides. The GS linker construct of KIHsv2 showed strongly reduced binding to PI3P and PI(3,5)P<sub>2</sub>. In addition, KIHsv2<sup>Q274E</sup> and KIHsv2<sup>Q274D</sup> mutants were tested. In these mutants the last

amino acid of the loop 6CD was mutated. In line with the flotation assays of KIHsv2 loop mutants also these mutants were strongly reduced in binding to PI3P or PI(3,5)P<sub>2</sub>.

Taken together loop 6CD is important for membrane binding while the two PIP binding sites coordinate membrane specific binding to the phosphoinositides PI3P and PI(3,5)P<sub>2</sub>.

#### 4.2.2.7 Analysis of stability of Hsv2 mutants

Mutants with either single or double mutations in loop 6CD were checked for protein folding. For this CD spectra were taken and Thermofluor experiments were carried out.

First, CD spectra for wild type ScHsv2 and KIHsv2 were taken from 190 nm to 260 nm (see figure 4.29 A and B). Typical spectra for  $\beta$ -strand containing proteins were observed with a minimum around 216 nm. Next, ScHsv2<sup>FTTG</sup>, ScHsv2<sup>loopchimera</sup> and KIHsv2<sup>loopchimera</sup> were analyzed and compared to wild type ScHsv2 (see figure 4.29 B). Both mutants showed also the minimum around 216 nm. In addition, CD spectra for KIHsv2<sup>GSlinker</sup>, KIHsv2<sup>K260E/R261D/H262D</sup>, KIHsv2<sup>Y272D/F273D</sup>, KIHsv2<sup>Y272D</sup> and KIHsv2<sup>F273D</sup> were monitored (see figure 4.29 C). All mutants showed a similar CD spectrum to wild type KIHsv2. This analysis showed, that folding of the  $\beta$ -sheets were not influenced by the mutations.

Protein stability was examined by following the behavior of the protein at 216 nm during a thermal shift from 20 °C to 90 °C. Here, the protein mutants were compared to wild type protein (see suppl. figure 5.18). Mutant proteins showed only slight shifts

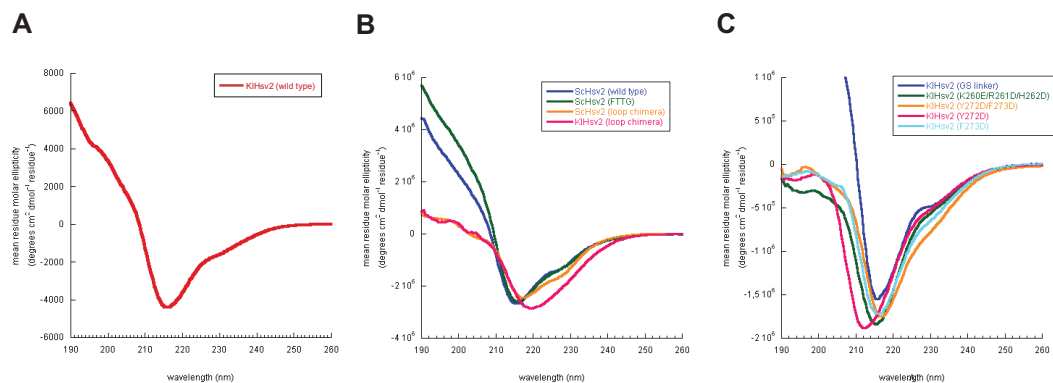


**Figure 4.29: CD spectra of KIHsv2 and ScHsv2 mutants**

CD spectra taken from 260 nm to 190 nm for (A) KIHsv2 (B) ScHsv2<sup>wildtype</sup>, ScHsv2<sup>FTTG</sup>, ScHsv2<sup>loopchimera</sup> and KIHsv2<sup>loopchimera</sup> (C) KIHsv2<sup>GSlinker</sup>, KIHsv2<sup>K260E/R261D/H262D</sup>, KIHsv2<sup>Y272D/F273D</sup>, KIHsv2<sup>Y272D</sup> and KIHsv2<sup>F273D</sup>.

of the curves compared to wild type protein, but no unfolding curve changed dramatically towards lower temperatures. Unfolding of all proteins (besides KIHsv2<sup>loopchimera</sup>) occurred in one transition.

A second method to monitor protein stability was employed by using ThermoFluor experiments. Unfolding was recorded by following fluorescence changes of Sypro Orange, which is dequenched, when protein unfolds and represents hydrophobic patches for binding of Sypro Orange. Wild type Schsv2 and KIHsv2 and their corresponding loop chimera constructs showed almost the same stability, the transition midpoint was in the range between 55 °C and 58 °C (see suppl. figure 5.19 A). On the other hand, the transition midpoint of KIHsv2<sup>G<sub>Slinker</sub></sup> shifted to 62 °C. Indicating, that deletion of the loop increases protein stability significantly. The mutants KIHsv2<sup>Y272A/F273A</sup>, KIHsv2<sup>Q274D</sup> and KIHsv2<sup>Q274E</sup> were only slightly shifted compared to wild type KIHsv2 (see suppl. figure 5.19 B). Furthermore, a comparison of KIHsv2<sup>wildtype</sup>, KIHsv2<sup>K260E/R261D/H262D</sup>, KIHsv2<sup>Y272D/F273D</sup>, KIHsv2<sup>Y272D</sup> and KIHsv2<sup>F273D</sup> in ThermoFluor experiments revealed that mutant KIHsv2<sup>F273D</sup> had an improved protein stability (see suppl. figure 5.19 C). None of the mutant proteins were strongly affected in their stability.

### 4.2.3 Co-expression and interaction studies of PROPPIN homologs with Atg8

#### 4.2.3.1 Cloning, expression and purification using the ACEMBL system

In order to test for Atg21 and Hsv2 binding to Atg8, I ordered synthetic genes of KlAtg8 and PaAtg8 with a C-terminal One-StrEP-tag, optimized for bacterial expression and cloned them together with either KlAtg21, PaAtg21 or KIHsv2 into the ACEMBL system for bacterial complex expression [46].

The multi protein expression system for *E. coli* employs a set of acceptor and donor vectors similar to the MultiBac baculovirus system for insect cell expression. Both acceptor and donor vectors contain the loxP imperfect inverted repeat for Cre recombination and different antibiotic resistances for plasmid screening. An important difference between acceptor and donor vectors is their origin of replication. Acceptor vectors contain the ColE1 origin of replication whereas the donor vectors possess the conditional origin of replication derived from R6K $\gamma$ . This origin is dependent on a host strain expressing the *pir* gene like in *E. coli* BW23474 cells.

The Atg8 homologs were cloned with a C-terminal One-StrEP-tag into both the pACE acceptor and the pDK donor vector for single and complex expression. The genes

coding for KlAtg21, PaAtg21 and KlHsv2 were cloned into the pACE-His acceptor vector. Multi gene expression cassettes were generated by the Cre/loxP reaction. Verified expression vectors were then transformed with *E. coli* BL21(DE3) cells for expression. The three complexes of KlAtg21/KlAtg8, KlHsv2/KlAtg8 and PaAtg21/PaAtg8 were expressed in autoinducible media for three hours at 37°C and then shifted to 22°C for overnight incubation. The cultures were harvested, cell extracts were prepared and the soluble protein fraction subjected to affinity purification with an 1 ml His-Trap FF column for co-purification of the complexes in 30 mM Hepes pH 7.0 and 300 mM NaCl buffer. However, the His-tagged PROPPINs were purified, but no Atg8 co-eluted from the column. Therefore, cultures were grown again and this time subjected to a Strep-Trap column. Here, the Atg8 homologs were purified, but the co-expressed proteins again did not co-elute. In a next approach, the proteins were expressed separately and their interaction was analyzed.

#### 4.2.3.2 Purification of *K. lactis* and *P. angusta* Atg8

KlAtg8 and PaAtg8 were expressed from *E. coli* BL21(DE3) in autoinducible media. The proteins were purified in 30 mM Hepes pH 7.0 supplemented with 300 mM NaCl buffer. Soluble protein fraction derived from cell extract was subjected to a 5 ml Strep-Trap column. Both proteins were obtained in high yields after elution with 2.5 mM desthiobiotin (see figure 4.30 A and C). The peak fractions were checked with SDS-PAGE. Afterwards, the protein fractions were pooled and loaded onto a Superdex S75 column (see figure 4.30 B and D). The peak fractions were loaded on an SDS gel again, the protein concentrated and snap frozen in liquid nitrogen. Storage of the protein was done at -80°C.

The purified proteins were analyzed for their secondary structure and stability using CD spectroscopy. NaF buffer was used for measurements. CD spectra of both KlAtg8 and PaAtg8 were taken from 190 nm to 260 nm at 20°C. Here, both Atg8 homologs showed the typical minimum of an  $\alpha$ -helix containing protein at 208 nm (see figure 4.31 A). The second minimum of  $\alpha$ -helix containing proteins is reduced due to the proteins additional  $\beta$ -strands. This confirms the expected secondary structure of Atg8. The X-ray crystallographic structures of *S. cerevisiae* Atg8 and its mammalian homolog MAP1LC3 revealed a ubiquitin-like fold consisting of two  $\alpha$ -helices enclosing four  $\beta$ -strands in its core.

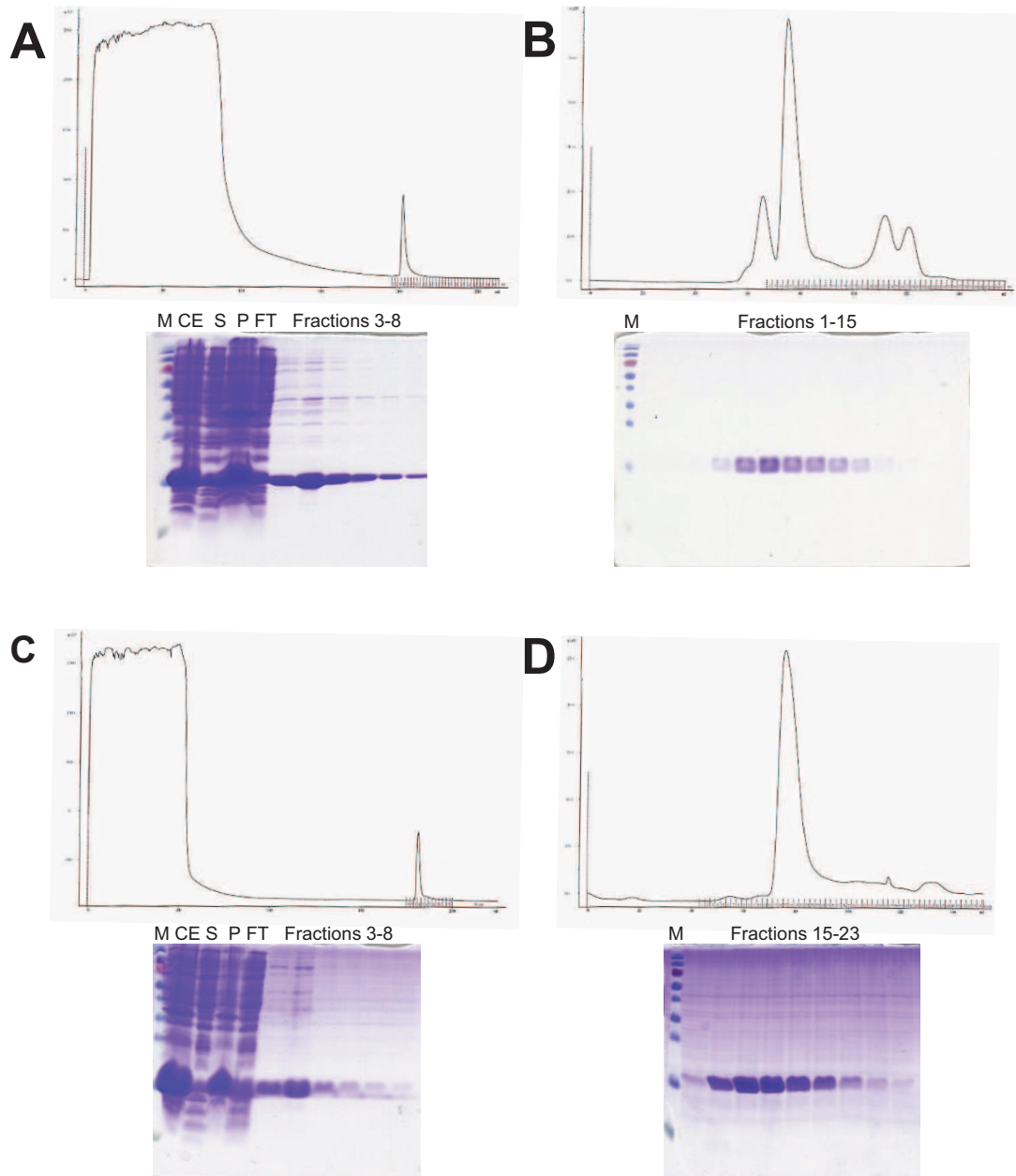


**Figure 4.30: Purification of KlAtg8 and PaAtg8 from *E. coli* BL21(DE3) cells**  
 (A) Affinity purification of KlAtg8 using a 5 ml Strep-Trap column followed by (B) gel filtration with a HiLoad 16/60 Superdex 75 column. (C) Affinity purification of PaAtg8 with a 5 ml Strep-Trap column and by (D) gel filtration with a Superdex 75 column. All purification steps were analyzed with SDS-PAGE.

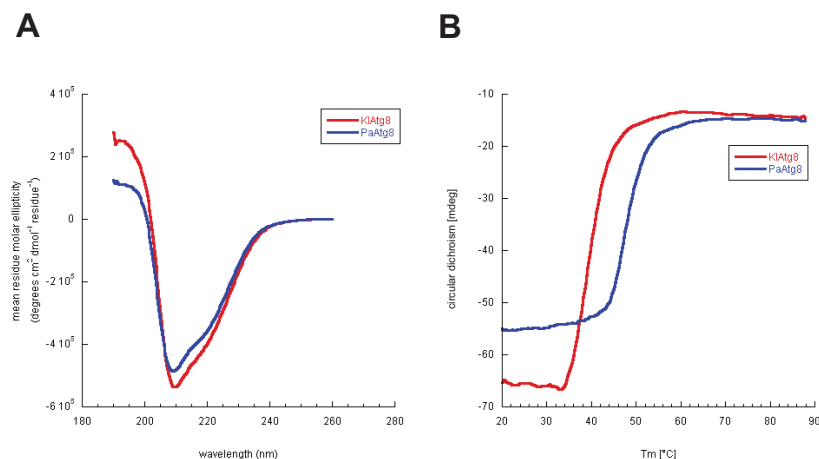


**Figure 4.31: CD spectra and melting curve of KlAtg8 and PaAtg8**

(A) CD spectra of KlAtg8 and PaAtg8 were measured from 160 nm to 190 nm. (B) Melting curves of KlAtg8 and PaAtg8 were taken at 208 nm from 20 °C to 90 °C

In addition, stability of purified KlAtg8 and PaAtg8 was investigated by recording the minimum at 208 nm along a thermal gradient from 20 °C to 90 °C. Both proteins unfolded in a single transition curve, thereby PaAtg8 started to unfold at higher temperatures compared to KlAtg8 (see figure 4.31 B). The transition midpoint of PaAtg8 was at 48 °C and for KlAtg8 at 40 °C. These results showed that both proteins are stable and folded.

#### 4.2.3.3 Biochemical analysis of interactions

Investigation of the interaction of Atg21 and Hsv2 with Atg8 was done using different approaches. First, the separately purified proteins were subjected to analytical gel filtration and their elution profile was monitored. Then KlAtg21 and KlAtg8 were mixed and loaded together onto the column. Here, the recording of UV<sub>280</sub> showed that the protein eluted in two peaks (see figure 4.32 A). Both peaks correspond to the peaks monitored for each protein alone. In addition, the peak fractions of KlAtg21-KlAtg8 were analyzed on an SDS gel. This showed that both proteins were present in different elution fractions. The interaction of KlAtg21 with KlAtg8 could not be confirmed with analytical gel filtration analysis.

The same result was observed for PaAtg21 and PaAtg8. In addition, KlHsv2 and KlAtg8 were combined and run over the analytical gel filtration column. Interestingly, the peak of the potential complex eluted in between the peaks of the single proteins (see

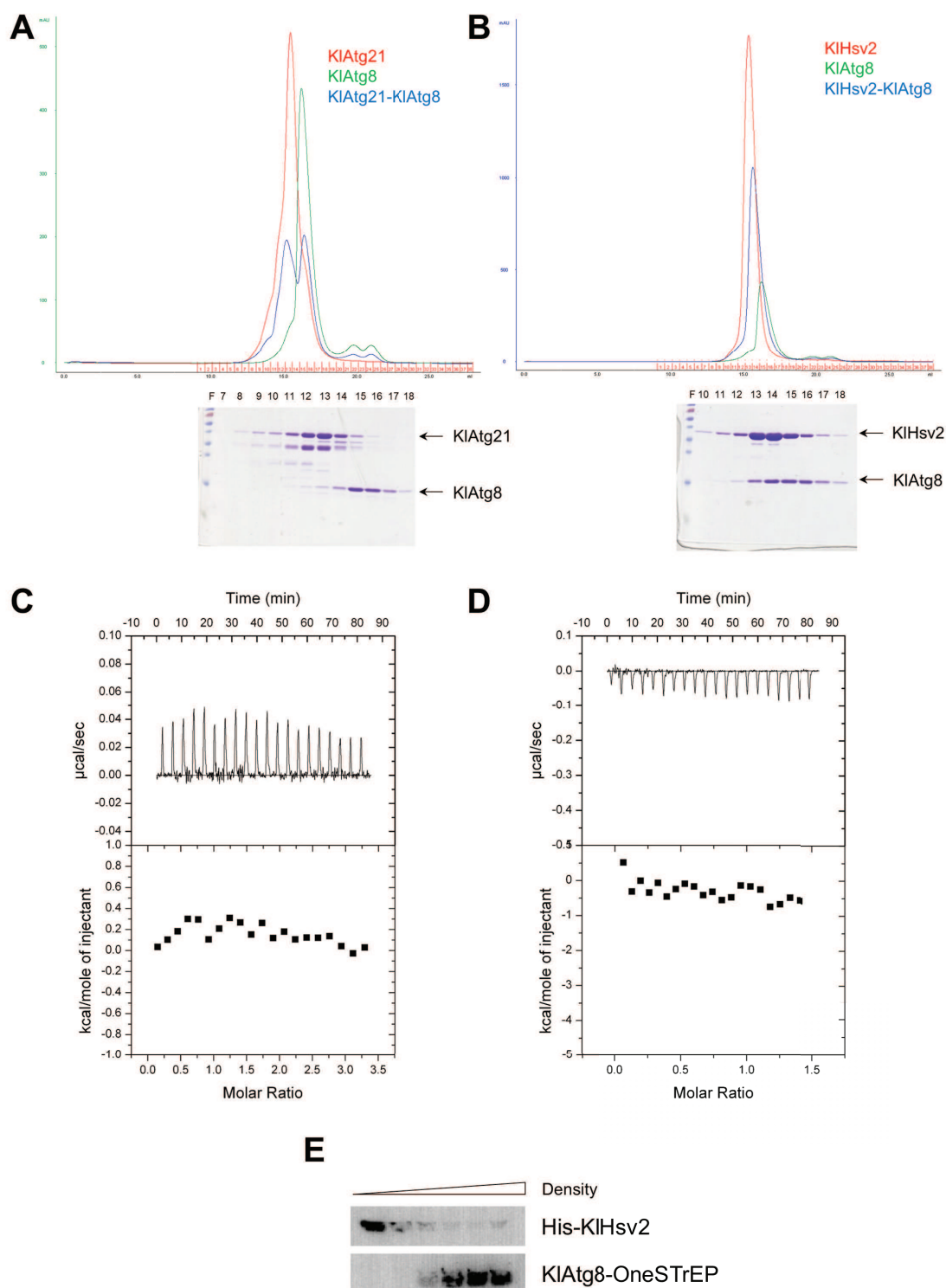


**Figure 4.32: Interaction studies on KIHsv2 and KlAtg8**

(A) Analytical gel filtration of KlAtg21, KlAtg8 and KlAtg21-KlAtg8 in complex. (B) Analytical gel filtration of KIHsv2, KlAtg8 and KIHsv2-KlAtg8 in complex. (C) Titration of 250  $\mu\text{M}$  ScHsv2 in 20  $\mu\text{M}$  KlAtg8. (D) Titration of 150  $\mu\text{M}$  KlAtg8 into 25  $\mu\text{M}$  KIHsv2. (E) Co-floitation analysis of KIHsv2 and KlAtg8 with liposomes containing 2 % PI3P, 73 % PC, 23 % PE and 2 % Texas Red-PE.



figure 4.32 B). Therefore, the peak fractions were analyzed with Coomassie stained SDS gels. Here, both proteins were observed in the same fractions, indicating that KlHsv2 and KlAtg8 might form a complex.

Further analysis of the KlHsv2 and KlAtg8 interaction was done with ITC measurements. This method is highly sensible and allows detection of weak interactions. ITC measurements were performed in Hepes buffer (30 mM Hepes pH 7.0, 300 mM NaCl). First, 250  $\mu$ M KlHsv2 was titrated into 20  $\mu$ M KlAtg8. The titration was done with 20 injections of each 15  $\mu$ l at 25 °C. For this measurement no significant heat change was observed (see figure 4.32 C). Therefore, the titration was also done the other way around and 150  $\mu$ M KlAtg8 was titrated into 25  $\mu$ M KlHsv2. However, no heat change was detected (see figure 4.32 D). Taken the ITC results together, no interaction was observed for KlHsv2 and KlAtg8.

KlHsv2 binds to phosphoinositides. This binding might cause structural changes in the protein and affect its affinity to interaction partners. Therefore, flotation assays were performed to test for protein-protein interaction. Liposomes containing 2 % PI3P, 73 % PC, 23 % PE and 2 % Texas Red-PE were prepared and mixed with KlHsv2 and KlAtg8. This mixture was overlaid with a Nycodenz gradient and centrifuged at high speed. Fractions taken after centrifugation were analyzed by immunoblotting using a penta-His antibody to detect KlHsv2 and a Strep-tag II antibody for KlAtg8-OneSTrEP. KlHsv2 was found in the low density fractions indicating its co-flotation with the liposomes, whereas KlAtg8 was present in the high density fractions indicating no binding to KlHsv2.

Different approaches for probing the Atg21-Atg8 and Hsv2-Atg8 interactions were tried, but no binding was detected with these methods. High ionic strength buffer (300 mM NaCl) might prevent binding in the analytical gel filtration and ITC experiments.

#### 4.2.3.4 Co-expression of ScAtg21 and ScAtg8 in insect cells

Interaction of PROPPINs with Atg8 was identified in *S. cerevisiae*. In order to investigate binding of ScAtg21 and ScAtg8, I co-expressed both proteins in insect cells using the MultiBac baculovirus expression system. Therefore, I cloned ScAtg8-StrepII into the second multiple cloning site of the pFL vector carrying the gene for His-ScAtg21 expression. This expression vector was transformed with *E. coli* DH10 cells carrying the MultiBac bacmid. The expression cassette integrates into the bacmid via Tn7 transposition sites. The bacmid was extracted from *E. coli* cells and transfected into Sf9 insect

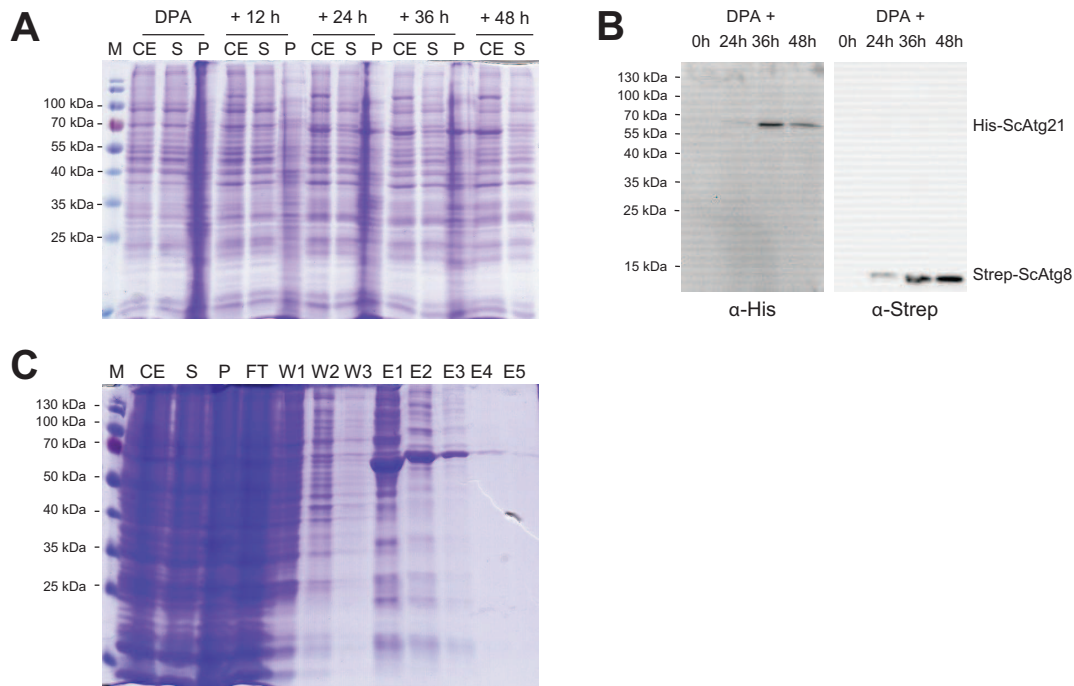


**Figure 4.33: Coexpression of ScAtg21 and ScAtg8 in insect cells**

(A) Expression profile of ScAtg21 and ScAtg8 in High5 insect cells. Samples taken at indicated time points were checked on SDS gels. (B) Western blot analysis of cell extract from ScAtg21 and ScAtg8 co-expressing insect cells. ScAtg21 was detected with a penta-His antibody and ScAtg8 with a Strep-MAB-Classic HRP conjugated antibody. (C) Show the coomassie stained SDS-PAGE of ScAtg21 and ScAtg8 co-purification from insect cells.

cells. The virus was generated and harvested after approximately 60 hours. An additional virus generation was produced by infection of Sf9 cells. Here, generally the virus titer increased and larger High5 insect cell cultures could be infected at once. During infection of High5 insect cells the day of proliferation arrest (DPA) was monitored by counting the cells per ml culture. When the DPA was reached samples were taken every 12 hours until DPA + 48 hours. From the samples cell extract, supernatant and pellet fraction were prepared and analyzed on SDS gels. Here, a band appeared after DPA + 24 hours in the size of 70 kDa (see figure 4.33 A). The expected size of ScAtg21 corresponds to 70 kDa. An additional band for ScAtg8 was not observed. Therefore, the expression was also tested with Western blotting. The cell extract of High5 insect cells was checked with a penta-His antibody for detection of ScAtg21 and a Strep-tag II antibody for ScAtg8. Western blot analysis showed that both proteins were expressed in insect cells. The band of 70 kDa was recognized by the His antibody, for ScAtg8 a band around 15 kDa was detected (see figure 4.33 B).

Next, I tried to co-purify ScAtg21 and ScAtg8 from the insect cells. For this purpose, High5 insect cells were harvested after DPA + 48 hours and cell extract was prepared using Hepes buffer (30 mM Hepes pH 7.0, 300 mM NaCl, 30 mM imidazole). The soluble protein fraction was loaded onto 2 ml Ni<sup>2+</sup>-sepharose beads. The beads were incubated for three hours with the supernatant, then washed and bound protein was eluted with Hepes buffer and 500 mM imidazole. Samples taken during the purification were analyzed with SDS-PAGE. Coomassie staining showed that ScAtg21 was purified using the Ni<sup>2+</sup>-sepharose beads (see figure 4.33 C). No band corresponding to ScAtg8 was observed on the SDS gel. In contrast, when ScAtg21 was expressed alone in insect cells it was not soluble.

Taken together these results did not confirm the interaction of ScAtg21 and ScAtg8. The fact that co-expression of both proteins led to increased solubility of ScAtg21 however suggests that both proteins have an effect on each other.

#### 4.2.3.5 Crystal soaking for KlHsv2 with Atg8 peptide

Analytical gel filtration analysis of the KlHsv2 and KlAtg8 suggested a potential interaction of both proteins. Although in ITC measurements binding could not be confirmed. In our lab KlHsv2 was crystallized and its structure determined (work from Dr. K. Kühnel). These crystals can be used for soaking experiments with an Atg8 peptide. In addition, co-crystallization of KlHsv2 and KlAtg8 can be tried.

In a first step, I wanted to co-crystallize full length KlAtg8 with KlHsv2. Therefore, I mixed both separately purified proteins in a 1:1 molar ratio and subjected them to a Superdex S75 gel filtration column. Here, both proteins co-eluted in a single peak

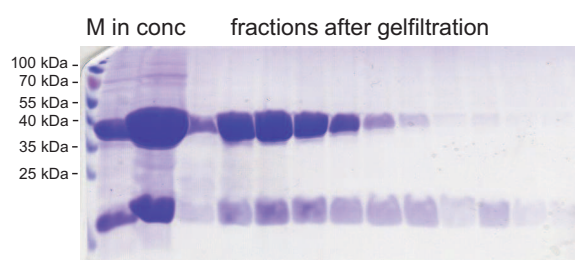


**Figure 4.34: Gel filtration purification of KlHsv2 and KlAtg8**

Both proteins were mixed in a 1:1 molar ratio (in), concentrated (conc) and purified with size exclusion chromatography.

and analysis of the peak fractions confirmed the presence of both proteins in the same elution fractions (see figure 4.34).

In order to optimize the buffer conditions for the protein complex, Thermofluor experiments were performed using the pHat and the Addit screen. Sodium lactate pH 5.2 and MES buffers in the range of pH 6.2 to 7.0 shifted the fluorescence curve towards higher temperatures and increased stability of the complex. Therefore, KIHsv2 and KlAtg8 were dialyzed in MES buffer pH 6.5 and 300 mM NaCl. Next, the Addit screen was performed. Caesium chloride, samarium bromid and DMSO increase stability (see figure 4.35).

Crystal screens were set up with KIHsv2-KlAtg8 in Hepes buffer with low ionic strength (30 mM Hepes pH 7.0, 150 mM NaCl) and in MES buffer (30 mM MES pH 6.5, 300 mM NaCl, 5 % DMSO). The protein concentration ranged from 5 mg/ml to 20 mg/ml. Some interesting crystallization conditions were observed, but so far no crystals or spherulites were grown.

Additionally, to get an insight how the proteins interact, I reproduced KIHsv2 crystals under conditions used for solving its structure and performed soaking experiments. In those experiments a peptide comprising the N-terminal eight amino acids of ScAtg8 was added to the conditions containing KIHsv2 crystals (see figure 4.36). Also KIHsv2 crystals were seeded into fresh crystallization conditions containing KIHsv2 and the Atg8

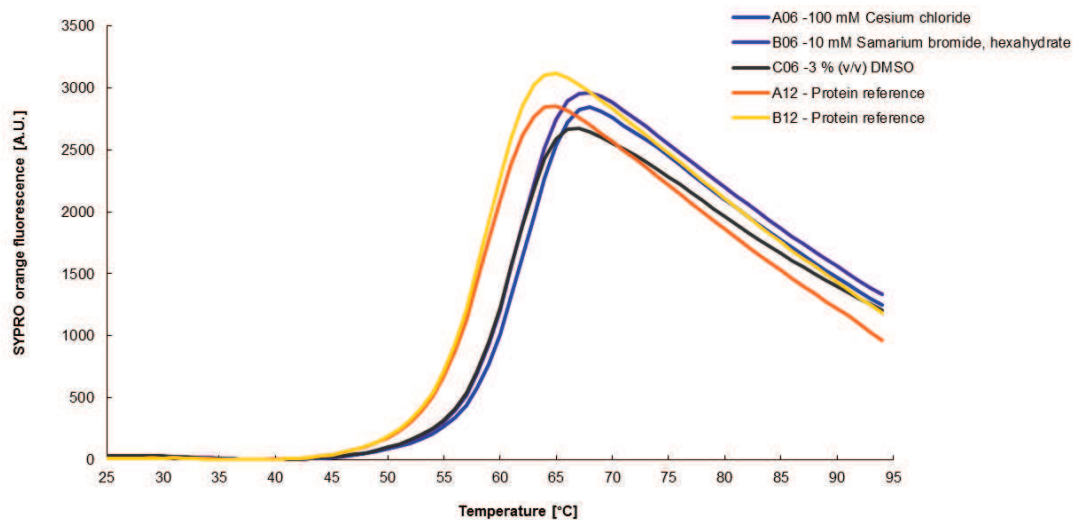


**Figure 4.35: Thermofluor analysis of KIHsv2 in complex with KlAtg8**

Thermofluor experiments using the Addit screen of the KIHsv2-KlAtg8 complex. Sypro Orange fluorescence was monitored, since dequenching correlates with protein unfolding. Out of 88 different tested conditions indicated additives increased protein stability.

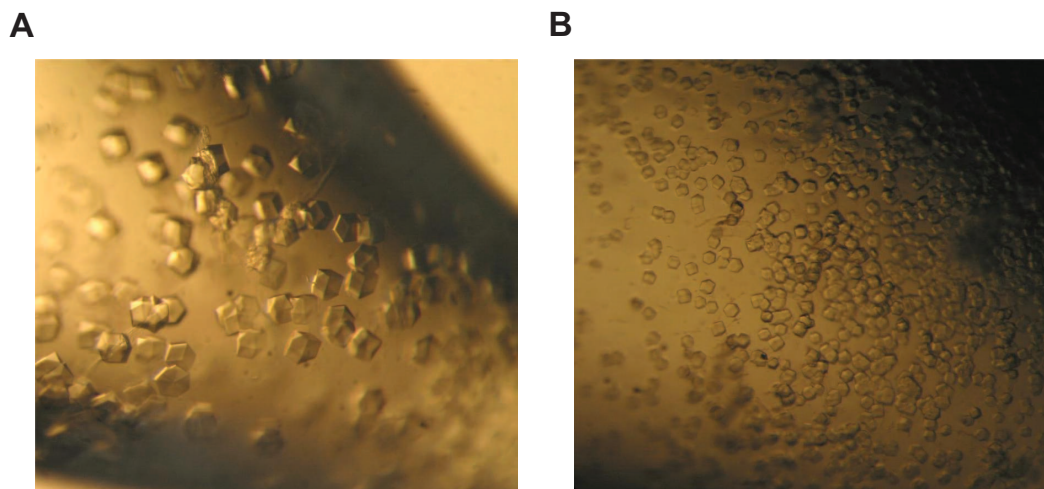


**Figure 4.36: KIHsv2 crystals for Atg8 peptide soaking**

Purified KIHsv2 (35 mg/ml protein in 0.2 M NaCl, 30 mM citrate pH 5.5) was subjected to crystallization. (A) In condition with 0.1 M HEPES pH 7.0, 1.5 M MgSO<sub>4</sub> and (B) 0.1 M HEPES pH 6.5, 1.5 M MgSO<sub>4</sub> crystals of KIHsv2 were reproduced.

peptide. These crystals were sent to the synchrotron and data sets were collected. The structure was solved using molecular replacement with the KIHsv2 structure. However, none of the crystals contained the Atg8 peptide. Incorporation of the peptide into the crystal might be inhibited due to different reasons, e.g. the sequence was not optimized for *K. lactis* Atg8, the ionic strength in the crystallization conditions was too high (1.2 - 2 M MgSO<sub>4</sub>) or the first eight amino acids are not sufficient for binding. Therefore, in a parallel experiment co-crystallization conditions for KIHsv2 with the peptide were screened, but yielded no crystals.

### 4.3 Discussion

Different yeast PROPPIN homologs were purified during this study. Their stabilities were characterized with Thermofluor experiments and measurements of their melting curves with CD spectroscopy. Stable fragments were identified by limited proteolysis, which can be useful for crystallization. Proteolytic digestion of KlAtg21 yielded in a stable fragment of 35 kDa, which was also observed during purification. Analysis of this fragment revealed cleavage of a 5 kDa fragment at the C-terminus of KlAtg21. Secondary structure analysis of this protein with different bioinformatical prediction

algorithms and IUPRED for disorder prediction showed that KlAtg21 contains an additional small  $\alpha$ -helix at its C-terminus. Homology modeling of the Atg18 and Atg21 homologs from *A. Scacioc* revealed that both Atg18 and Atg21 possess this additional C-terminal  $\alpha$ -helix in contrast to Hsv2.

So far, no crystals were obtained from a variety of crystal screens which were set up with ScAtg18, PaAtg18, KlAtg21 and SpHsv2. However, crystallization conditions yielding in pre-crystalline structures like spherulites were observed. Microcrystals of PaAtg18 were obtained in one screen but could not be reproduced.

Previous studies mainly characterized PROPPINs phosphoinositide specificity with protein-lipid overlay assays using PIP strips. Controversial results for PIP specificities were reported. GST-tagged ScAtg18 was shown to have a high specificity for PI3P and PI(3,5)P<sub>2</sub> in dot blot assays, but specifically interacted with PI(3,5)P<sub>2</sub> containing membranes in surface plasmon resonance studies [133]. In a different study, high specificity for PI3P and a weak affinity to PI(3,5)P<sub>2</sub> was shown for GST-ScAtg18 with PIP strips. GST-ScAtg21 in contrast showed strong binding to PI3P and PI(3,5)P<sub>2</sub> and weak interactions with PI4P and PI5P [151].

PIP strip analysis with MBP-tagged proteins revealed strong binding of ScAtg18, ScAtg21 and ScHsv2 to PI3P but no binding to PI(3,5)P<sub>2</sub> [144]. In a previous study we showed binding of GST-ScHsv2 to PI3P and PI(3,5)P<sub>2</sub> and weak interaction with PI4P, PI5P and PI(3,4)P<sub>2</sub> [24].

Flotation assays are a suitable alternative method. However, caution has to be taken with the lipid composition of liposomes used for flotation assays to avoid binding due to non-specific electrostatic interactions. Unspecific binding of the protein has to be tested with control liposomes without the ligand being incorporated. I here used neutral liposomes as a control, containing only PC, PE and Texas Red-PE. In addition, the ligand concentration had to be optimized, since concentrations above 5 % (w/w) PI3P resulted in unspecific binding of the binding incapable FTTG mutant.

In order to answer the question of phosphoinositide binding specificity of the yeast PROPPINs, I optimized the lipid composition of liposomes for PROPPINs to perform flotation assays. Using this method I showed a distinct phosphoinositide binding specificity of Atg18, Atg21 and Hsv2 to PI3P and PI(3,5)P<sub>2</sub>. The tested liposomes contained 1 % (w/w) phosphoinositide, 74 % (w/w) PC, 23 % (w/w) PE and 2 % (w/w) Texas Red-PE. An advantage of using liposomes to study membrane binding is the incorporation of phosphoinositides into membranes at different concentrations whereas pure phosphoinositides are spotted on a flat membrane on PIP strips. PIP strips can be used to test whether phosphoinositide binding can be detected at all, but the results

have to be verified with a second method [175]. Especially for quantification PIP strips are not reliable, as shown in this study.

In a recent study liposome sedimentation assays were used to study phosphoinositide specificity of PROPPINs. Here, multilamellar liposomes containing 15 % phosphoinositides and 30 % PS were used. Co-sedimentation of the protein with the liposomes indicates liposome binding. KlHsv2, ScHsv2 and the human WIPI1, WIPI3 and WIPI4 were tested and showed binding to PI3P, PI5P and PI(3,5)P<sub>2</sub> [25].

The structure of KlHsv2 showed that the two arginines of the FRRG motif, which is essential for phosphoinositide binding, point into opposite directions, indicating two potential binding pockets for phosphoinositides. Using flotation assays with 2 % PI3P containing liposomes I identified a set of conserved residues comprising both pockets. Thus supporting the hypothesis, that PROPPINs possess two binding pockets for PI3P. Amino acids Ser243, Thr247, Arg250 and Arg264 from ScHsv2 are part of binding pocket one, the second pocket comprises ScHsv2 Arg265, Lys290, Thr292 and His294. *In vivo* localization studies were performed by Dr. R. Krick in the group of Prof. M. Thumm with these ScHsv2 mutants and also with the corresponding ScAtg18 mutants. The *in vivo* data of Dr. R. Krick are consistent with my *in vitro* studies. The mutants shown to be unable to bind to liposomes also showed cytosolic localization compared to the punctate localization indicating membrane association of wild type ScAtg18 and ScHsv2 [24]. Furthermore, docking studies of PI3P and PI(3,5)P<sub>2</sub> into the KlHsv2 structure were done. These studies are in agreement with the *in vitro* and *in vivo* studies because residues involved in binding in the studies were also shown to be important for binding in our experiments. Only Thr247 did not show an interaction to PI3P or PI(3,5)P<sub>2</sub> [24].

A similar study was published at the same time from Baskaran *et al.* [25]. The structure of KlHsv2 was determined as well, leading to the observation of two potential binding pockets in Hsv2. In contrast to the here used liposome flotation assays, liposome sedimentation assays were performed to identify residues of KlHsv2 involved in PI3P binding. All tested mutants of binding site I did not show an effect on PI(3,5)P<sub>2</sub>. Like us Arg250 (Kl:205) and Arg264 (Kl:Arg219) were found to interact with PI3P in binding site I. Arg265 (Kl: Arg220), Lys290 (Kl:Lys245) and His294 (Kl: His249) were identified in binding site II.

With flotation assays, *in vivo* localization experiments and computational docking studies the residues involved in phosphoinositides binding were identified. In order to further characterize the binding of PROPPINs with PI3P and PI(3,5)P<sub>2</sub>, binding stoichiometries and affinities were determined using isothermal titration calorimetry. ITC measurements with the water soluble PI3P-diC4 and PI(3,5)P<sub>2</sub>-diC6 as well as with

large unilamellar vesicles (LUVs) did not give any heat changes or resulted in precipitation. Whereas LUVs are quite big and therefore prone to aggregation due to stirring while the measurements are done, soluble PI3P or PI(3,5)P<sub>2</sub> analogs were not sufficient for binding. Incorporation of the phosphoinositides into small unilamellar vesicles (SUVs) were suitable for these measurements. Furthermore, the method for preparation of vesicles can be important. SUVs were prepared by size exclusion chromatography using a Sephadex G50 column. In contrast, LUVs were formed using the extrusion method. Here, micelle formation can not be avoided, which could drive precipitation of protein and LUVs during the measurement. For analysis of the ITC data, the precise concentrations of protein and ligand are needed. Therefore, analysis of liposomes is necessary as described here to calculate the accessible PIP concentration. The phosphate concentration was measured with the phosphomolybdate method and the size distribution of SUVs was determined by FFF-MALLS. From the total phosphate concentration, the phosphoinositide concentration was calculated. Then accessible PIP amounts were derived by considering a double-layered membrane with a surface area ( $A = 4\pi r^2$ ).

KIHsv2, ScHsv2, PaAtg18 and KlAtg21 were used for ITC measurements. The two Hsv2 homologs and PaAtg18 showed a similar  $K_D$  to PI3P containing liposomes in the range of 0.5  $\mu\text{M}$ . KlAtg21 in comparison binds with a weaker affinity to PI3P of 0.9  $\mu\text{M}$ . However, its binding affinity to PI(3,5)P<sub>2</sub> containing liposomes is even less ( $K_D = 1.4 \mu\text{M}$ ). In contrast, Hsv2 ( $K_D = 0.2 \mu\text{M}$ ) and Atg18 ( $K_D = 0.07 \mu\text{M}$ ) have a stronger affinity to PI(3,5)P<sub>2</sub> compared to PI3P. These differences in binding affinities might be important for the different functions of the various PROPPIN homologs in autophagy. Determination of the binding stoichiometry showed that two PI3P molecules bind to one ScHsv2 protein. KIHsv2, PaAtg18 and KlAtg21 had an average molar ratio of 0.37. Binding of PI(3,5)P<sub>2</sub> revealed a molar ratio of 0.6 for Hsv2 and Atg18.

Binding affinities of PROPPINs were also determined with reflectometric interference spectroscopy (RIfS). Here, a lipid bilayer was formed on wafers and interference fringes were detected. Incubation of the membrane with GST-ScHsv2 resulted in a  $K_D$  of 1.3  $\mu\text{M}$  [24]. Differences between binding affinities from ITC and RIfS measurements might be due to using untagged versus GST fusion proteins and differences in membrane composition. 3 % PI3P were used in RIfS measurements. From FRET measurements of KIHsv2 affinities in the submicromolar range were estimated, but no precise numbers were given from Baskaran *et al.* [25]. Dove *et al.* [133] obtained a  $K_D$  of 0.18  $\mu\text{M}$  by surface plasmon resonance measurements with GST-ScAtg18 to PI(3,5)P<sub>2</sub>.

Quantification of flotation assays showed that 0.1 % PI(3,5)P<sub>2</sub> are required in liposomes for recruitment of 50 % of the present KIHsv2 and ScHsv2. In contrast, ScHsv2



needs 0.26 % PI3P whereas KlHsv2 requires 1.52 % PI3P in liposomes. These data are in agreement with the binding affinities derived from ITC measurements, that due to higher affinity for PI(3,5)P<sub>2</sub> less of this phosphoinositide is needed in the liposomes for recruitment of Hsv2.

*In silico* docking studies of KlHsv2 with PI(3,5)P<sub>2</sub> were only successful, when the histidines in the binding pockets were protonated. Besides, determination of molar ratios for the binding of PI(3,5)P<sub>2</sub> suggested one or two ligands bound to PROPPINs. ITC measurements at different pHs showed that ScHsv2 binding to phosphoinositides is dependent on the pH. Here, the molar ratio in acidic buffers was 0.57, whereas basic buffers completely disabled one phosphoinositide binding site ( $N = 0.93$ ). The binding affinity was increased in acidic buffers. This pH dependency was shown for ScHsv2 binding to either PI3P or PI(3,5)P<sub>2</sub>. This effect was stronger for PI(3,5)P<sub>2</sub>. However, KlHsv2 did not show a difference neither in stoichiometry nor in binding affinity. This difference between KlHsv2 and ScHsv2 might be caused by the additional histidine in ScHsv2 binding site II. This histidine is not conserved and KlHsv2 possesses a lysine at this position instead. The stronger effect of the pH dependency for ScHsv2 binding to PI(3,5)P<sub>2</sub> and PI3P can be explained by the stronger negative charge of PI(3,5)P<sub>2</sub> compared to PI3P.

A similar effect was described for FYVE domain containing proteins. Increase of the pH disrupted binding of the FYVE domain to PI3P, a decrease caused an enhanced affinity. This pH dependency was due to a pair of conserved histidine residues [129, 179].

I also showed that the loop 6CD is essential for membrane binding. Substitution of the loop by a GS linker abolished the binding to liposomes. Loop insertion into the membrane is due to hydrophobic and ionic interactions with membrane lipids. The involvement of loop 6CD was also described by Baskaran *et al.* [25]. Here, basic patches of the protein at the rim of the  $\beta$ -propeller were mutated and loop 6CD substituted with a GS linker. In sedimentation assays they showed that only deletion of the loop had an effect on membrane binding. Thus, suggesting an edge on binding of Hsv2 and probably other PROPPINs towards the membrane. Furthermore, they showed that PROPPIN homologs with more hydrophobic residues in the loop have a higher binding affinity to the membrane.

The insertion of a loop to increase membrane affinity was also described for FYVE domain containing protein like EEA1 and the PX domain of Vam7. The PI3P specific binding domains alone have a too low affinity to PI3P to allow membrane recruitment [128]. Dimerization of the FYVE domain and additional loop insertion is required for FYVE domains to bind sufficiently to membranes. Some residues of the PX domain

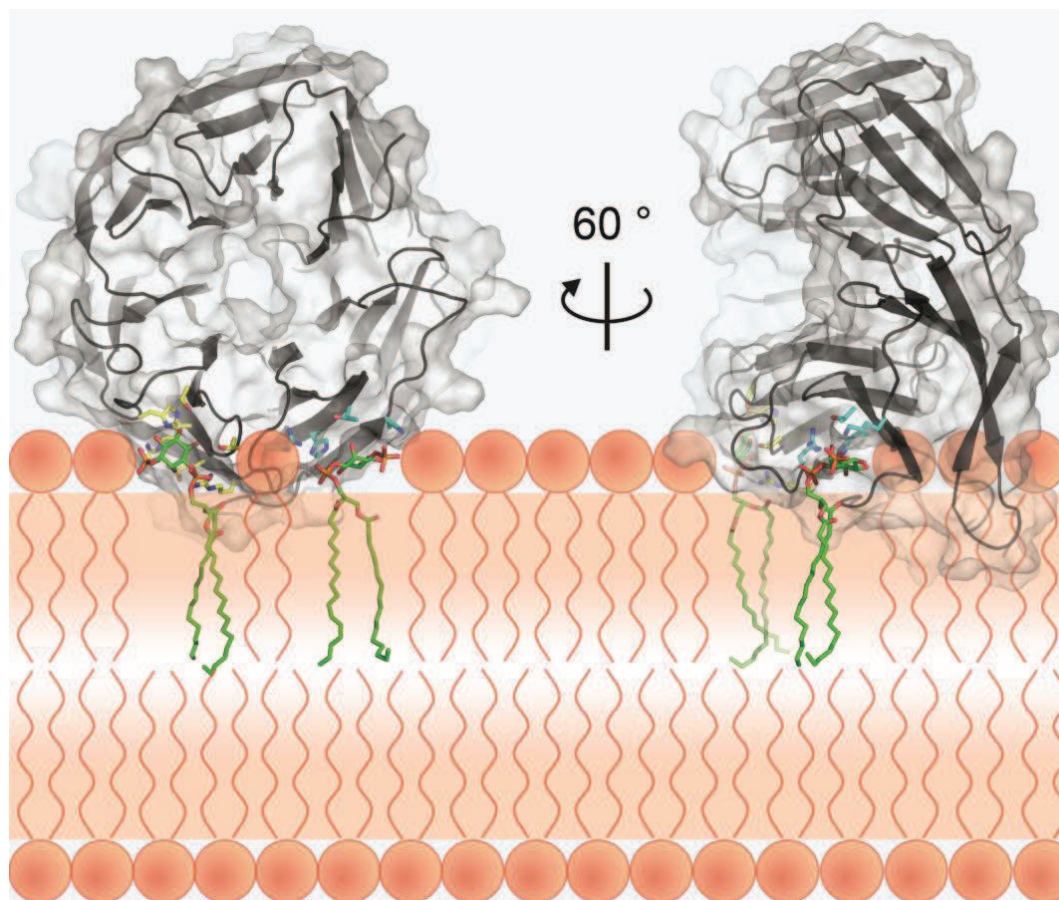


**Figure 4.37: Proposed model of Hsv2 membrane binding**

Our studies suggest a perpendicular binding of PROPPINs to the membrane. Two PI3P or PI(3,5)P<sub>2</sub> molecules are bound one in each of the two binding sites. In addition a long flexible loop inserts into the membrane to stabilize binding. Figure derived from [24]

have been shown to penetrate into the membrane, deletion of these residues diminished membrane binding [180].

Taking our *in vivo* and *in vitro* data and the computational studies together, we postulated a binding model for KIHsv2 to the membrane containing PI3P or PI(3,5)P<sub>2</sub> (see figure 4.37 [24]). Hsv2 binds with two phosphoinositide binding pockets towards the membrane in an edge on geometry. This allows penetration of loop 6CD into the membrane. A similar model was described by Baskaran *et al.*, [25].

Phosphoinositide binding domains often use multidomain cooperativity to increase their membrane binding affinities. This is achieved either by dimerization of the PIP binding domain, addition of a loop that inserts into the membrane or interaction with

additional membrane binding proteins (reviewed in [139]). Here, we showed that PROPPINs employ two phosphoinositide binding sites in the  $\beta$ -propeller domain. In addition, I showed the requirement of loop 6CD in membrane binding.

$\beta$ -propeller proteins generally form a platform for protein-protein interactions. As PROPPINs bind in an edge on manner to the membrane the  $\beta$ -propeller sticks out of the membrane and is accessible for potential interaction partners. Atg18 at the PAS was shown to bind to Atg2 and mediates cycling of the membrane protein Atg9 [142]. Atg18 in complex with Atg2 is recruited from the cytosol to the membrane [21]. Interaction studies of Atg18 with Atg2 showed that Atg2 binds with blade 2 of Atg18 [26]. Furthermore, Atg18 is part of the PI3P 5-kinase complex including Fab1 at the vacuolar membrane [181, 143].

Atg21 was shown to be involved in recruitment of Atg8-PE to the PAS [144, 156]. In order to characterize binding of Atg21 to Atg8, I performed different experiments to confirm a direct interaction between the PROPPINs Atg21 and Hsv2 to Atg8. However, ITC measurements of Hsv2 with Atg8 did not give any detectable heat change and analytical gel filtration of Atg21 with Atg8 resulted in elution of two separate peaks from the column. Soaking experiments of an Atg8 peptide into crystals containing Hsv2 did not show additional electron density for the Atg8 peptide. In addition, co-expression experiments did not yield any crystals, yet. Earlier affinity isolation and yeast two hybrid screens with Atg21 were performed and no interaction was achieved [144]. Probably the interaction between Atg21 and Atg8 requires additional factors or posttranslational modifications which are absent when working with recombinant proteins.

## 4.4 Outlook

The purification protocols for the investigated PROPPINs are set up and first crystallization screens were done for *K. lactis* Atg21 and *P. angusta* Atg18. These screens yielded in some pre-crystalline structures, which need further optimization. These proteins might be suitable for crystallization, since the disorder prediction of IUPRED displayed only small stretches of disorder in the N-terminal and C-terminal region. Homology modeling and secondary structure predictions showed an additional C-terminal  $\alpha$ -helix for Atg18 and Atg21 proteins, which is not present in Hsv2. The importance of this region can be analyzed by deletion of this region followed by *in vivo* localization studies in comparison to wild type protein. Probably this region is involved in protein-

protein interactions and potential interaction partners can be identified using a yeast two hybrid screen or co-purification of interaction partners with the tandem affinity purification (TAP) method.

In addition, to the biochemical analysis of PROPPINs membrane binding, bioinformatic studies are carried out by A. Scacioc to study the role of loop 6CD for membrane binding of PROPPINs. Starting from the existing coarse-grained model of Hsv2 binding to the membrane [24] (see figure 4.37), an atomistical model will be derived. This model allows a more detailed analysis of membrane binding regarding the loop insertion and identification of which residues go into the membrane. By insertion of the protein into a membrane and pulling it out of the membrane virtually, binding affinities can be achieved and compared to the *in vitro* results.

Furthermore, ITC measurements for KIHsv2, PaAtg18 and KlAtg21 to PI3P containing liposomes and KlAtg21 to PI(3,5)P<sub>2</sub> containing liposomes need to be optimized to achieve a conclusive binding stoichiometry for all tested PROPPINs. Here, adjusting of the protein concentration might lead to a longer starting phase of the curve, which is required for optimal fitting and therefore for calculation of the stoichiometry.

Since so far no crystal structure of Atg18 and Atg21 is available, their structures will be determined on an atomistical scale using homology modeling with the Hsv2 structure by A. Scacioc. Analysis of their binding sites and modeling of PI3P and PI(3,5)P<sub>2</sub> will be performed to support and validate my *in vitro* data.

In order to show the importance of loop 6CD, *in vivo* localization studies are planned in collaboration with Prof. M. Thumm. The loop mutants of KIHsv2 characterized in this study will be cloned into a yeast expression plasmid. The recombinant protein will be tagged with an N-terminal GFP for fluorescence microscopy in *S. cerevisiae*. Membrane binding of the loop mutants in comparison to wild type KIHsv2 protein will be investigated.

Interaction of Atg21 and Hsv2 with Atg8 could not be confirmed with the here used methods. Further investigations should be done to determine, whether an additional factor is needed for interaction. Most likely the interaction between PROPPINs and Atg8 is on an indirect level. Therefore, interaction partners of Atg21 can be identified using a yeast two hybrid screen.

# 5 Appendix

## 5.1 Structures of autophagy-related proteins in the PDB

The following table is ordered by the release date of the structures in PDB.

**Table 5.1:** Structures of autophagy proteins in PDB (2)

Protein	PDB entry	Structure type	Reference
<i>R. norvegicus</i> LC3 (Atg8)	1UGM	X-ray, 2.05 Å	Sugawara <i>et al.</i> , <i>Genes Cell</i> (2004) [27]
plant Atg12	1WZ3	X-ray, 1.80 Å	Suzuki <i>et al.</i> , <i>Autophagy</i> (2005) [31]
human Atg4B	2CY7	X-ray, 1.90 Å	Sugawara <i>et al.</i> , <i>JBC</i> (2005) [28]
human Atg4B	2D1I	X-ray, 2.00 Å	Kumanomidou <i>et al.</i> , <i>J Mol Biol</i> (2006) [182]
<i>S. cerevisiae</i> Atg5-Atg16(1-46)	2DYM	X-ray, 2.20 Å	Matsushita <i>et al.</i> , <i>JBC</i> (2007) [84]
<i>S. cerevisiae</i> Atg5-Atg16(1-57)	2DYO	X-ray, 1.97 Å	Matsushita <i>et al.</i> , <i>JBC</i> (2007) [84]
<i>S. cerevisiae</i> Atg3	2DYT	X-ray, 2.5 Å	Yamada <i>et al.</i> , <i>JBC</i> (2007) [29]
Bcl-xL/Beclin 1 complex	2P1L	X-ray, 2.50 Å	Oberstein <i>et al.</i> , <i>JBC</i> (2007) [183]
	2PON	solution NMR	Feng <i>et al.</i> , <i>J Mol Biol</i> (2007) [184]
human Atg4A	2P82	X-ray, 2.10 Å	Walker <i>et al.</i> , Structural Genomics Consortium (2007)
Atg4B-LC3(1-120)	2Z0D, 2Z0E	X-ray, 2.10 Å	Satoo <i>et al.</i> , <i>EMBO J</i> (2009) [185]
human GABARAP1	2R2Q	X-ray, 1.65 Å	Tempel <i>et al.</i> , Structural Genomics Consortium (2007)
M11/mouse Beclin 1 (106-124)	3BL2	X-ray, 2.30 Å	Ku <i>et al.</i> , <i>Plos Pathog</i> (2008) [186]
M11/mouse Beclin 1 BH3 domain	3DVU	X-ray, 2.50 Å	Sinha, <i>Autophagy</i> (2008) [187]
LC3/p62	2ZJD	X-ray, 1.56 Å	Ichimura <i>et al.</i> , <i>JBC</i> (2008) [188]
LC3/p62	2K6Q	solution NMR	Noda <i>et al.</i> , <i>Genes Cell</i> (2008) [189]
MAP1ALC3	3ECI	X-ray, 2.65 Å	Walker <i>et al.</i> , Structural Genomics Consortium (2008)
<i>S. cerevisiae</i> Atg8-Atg19(412-415)	2ZPN	X-ray, 2.70 Å	Noda <i>et al.</i> , <i>Genes Cell</i> (2008) [189]
human Atg4B(C74S)/LC3(1-124)	2ZZP	X-ray, 2.05 Å	Satoo <i>et al.</i> , <i>EMBO J</i> (2009) [185]
p62 PB1 domain	2KKC	solution NMR	Yokochi & Inagaki, <i>J Biomol NMR</i> (2009) [190]
<i>Trypanosoma brucei</i> Atg8	3H9D	X-ray, 2.30 Å	Koopmann <i>et al.</i> , <i>Autophagy</i> (2009) [191]
<i>S. cerevisiae</i> Atg16 coiled coil domain	3A7O	X-ray, 2.50 Å	Fujioka <i>et al.</i> , <i>JBC</i> (2009) [33]
<i>S. cerevisiae</i> Atg16	3A7P	X-ray, 2.80 Å	Fujioka <i>et al.</i> , <i>JBC</i> (2009) [33]

Protein	PDB entry	Structure type	Reference
Keap1 with Sequestosome-1/p62	3ADE	X-ray, 2.80 Å	Kurokawa & Yamamoto, <i>Nat Cell Biol</i> (2010) [192]
p62 PB1 dimer	2KTR	solution NMR	Saio <i>et al.</i> , <i>J Biomol NMR</i> (2010) [193]
<i>D. melanogaster</i> Vps34/2-methyladenine	2X6F	X-ray, 3.30 Å	Miller <i>et al.</i> , <i>Science</i> (2010) [36]
<i>D. melanogaster</i> Vps34	2X6H	X-ray, 2.90 Å	Miller <i>et al.</i> , <i>Science</i> (2010) [36]
<i>D. melanogaster</i> Vps34/PIK-90	2X6J	X-ray, 3.50 Å	Miller <i>et al.</i> , <i>Science</i> (2010) [36]
<i>D. melanogaster</i> Vps34/PI-103	2X6K	X-ray, 3.50 Å	Miller <i>et al.</i> , <i>Science</i> (2010) [36]
Atg8	2KQ7	solution NMR	Schwarten <i>et al.</i> , <i>Biochem Biophys Res Commun</i> (2010) [82]
Atg8	2KWC	solution NMR	Kumeta <i>et al.</i> , <i>J Biomol NMR</i> (2010) [83]
Atg19 $\alpha$ -mannosidase binding motif	2KZB	solution NMR	Watanabe <i>et al.</i> , <i>JBC</i> (2010) [194]
Atg34 $\alpha$ -mannosidase binding motif	2KZK	solution NMR	Watanabe <i>et al.</i> , <i>JBC</i> (2010) [194]
<i>Bombyx mori</i> Atg8	3M95	X-ray, 2.40 Å	Hu <i>et al.</i> , <i>Acta Crystallogr Sect F</i> (2010) [195]
GABARAPL-1/NBR1-LIR	2L8J	solution NMR	Rogov <i>et al.</i> , <i>J Mol Biol</i> (2011) [196]
p62 UBA domain/ubiquitin	2RRU	solution NMR	Isogai <i>et al.</i> , <i>JBC</i> (2011) [197]
p62 UBA domain/ubiquitin	3B0F	X-ray, 1.40 Å	Isogai <i>et al.</i> , <i>JBC</i> (2011) [197]
<i>S. cerevisiae</i> Atg7 (1-595)	3VH1	X-ray, 3.00 Å	Noda <i>et al.</i> , <i>Mol Cell</i> (2011) [30]
<i>S. cerevisiae</i> Atg7 (1-613)	3VH2	X-ray, 3.30 Å	Noda <i>et al.</i> , <i>Mol Cell</i> (2011) [30]
<i>S. cerevisiae</i> Atg7 CTD/Atg8	3VH3	X-ray, 2.00 Å	Noda <i>et al.</i> , <i>Mol Cell</i> (2011) [30]
<i>S. cerevisiae</i> Atg7 CTD/Atg8	3VH4	X-ray, 2.65 Å	Noda <i>et al.</i> , <i>Mol Cell</i> (2011) [30]
MgATP			
Atg8/Atg7C30	2LI5	solution NMR	Noda <i>et al.</i> , <i>Mol Cell</i> (2011) [30]
Atg7C/Atg8	3RUI	X-ray, 1.91 Å	Hong <i>et al.</i> , <i>Nat Struct Mol Biol</i> (2011) [198]
yeast Atg7 N-terminus	3RUJ	X-ray, 2.10 Å	Hong <i>et al.</i> , <i>Nat Struct Mol Biol</i> (2011) [198]
<i>S. cerevisiae</i> Atg7 (289-630)	3T7E	X-ray, 2.25 Å	Taherbhoy <i>et al.</i> , <i>Mol Cell</i> (2011) [199]
<i>S. cerevisiae</i> Atg7 (1-289)	3T7F	X-ray, 1.89 Å	Taherbhoy <i>et al.</i> , <i>Mol Cell</i> (2011) [199]
<i>S. cerevisiae</i> Atg7 (1-289)/Atg3 (128-144)	3T7G	X-ray, 2.08 Å	Taherbhoy <i>et al.</i> , <i>Mol Cell</i> (2011) [199]
<i>S. cerevisiae</i> Atg7 (1-289)	3T7H	X-ray, 1.60 Å	Taherbhoy <i>et al.</i> , <i>Mol Cell</i> (2011) [199]
Beclin 1 coiled coil domain	3Q8T	X-ray, 1.90 Å	Li <i>et al.</i> , <i>Nat Commun</i> (2012) [34]
Beclin 1 ECD domain	4DDP	X-ray, 1.55 Å	Huang <i>et al.</i> , <i>Cell Res</i> (2012) [35]
Vps30/Atg6 BARA domain	3VP7	X-ray, 1.55 Å	Noda <i>et al.</i> , <i>JBC</i> (2012) [200]
<i>Kluyveromyces lactis</i> Hsv2 complete loop 6CD	4AV8	X-ray, 3.35 Å	Krick <i>et al.</i> , <i>PNAS</i> (2012) [24]
<i>Kluyveromyces lactis</i> Hsv2	4AV9	X-ray, 3.00 Å	Krick <i>et al.</i> , <i>PNAS</i> (2012) [24]
<i>Kluyveromyces marxianus</i> Hsv2	3VU4	X-ray, 2.60 Å	Watanabe <i>et al.</i> , <i>JBC</i> (2012) [26]
<i>Kluyveromyces lactis</i> Hsv2	4EXV	X-ray, 3.00 Å	Baskaran <i>et al.</i> , <i>Mol Cell</i> (2012) [25]
<i>Kluyveromyces marxianus</i> Atg10	2LPU	solution NMR	Yamaguchi <i>et al.</i> , <i>Structure</i> (2012) [32]
<i>Kluyveromyces marxianus</i> Atg5	3VQI	X-ray, 2.50 Å	Yamaguchi <i>et al.</i> , <i>Structure</i> (2012) [32]
<i>S. cerevisiae</i> Atg8/Atg32 peptide	3VXW	X-ray, 3.00 Å	Kondo-Okamoto <i>et al.</i> , <i>JBC</i> (2012) [201]

Protein	PDB entry	Structure type	Reference
Atg10	4EBR	X-ray, 2.70 Å	Hong <i>et al.</i> , <i>Acta Crystallogr D Biol Crystallogr</i> (2012) [202]

## 5.2 Supplementary figures

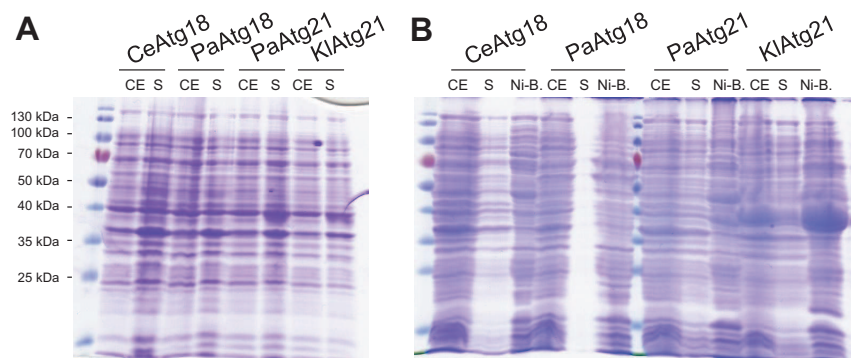


**Figure 5.1: Testexpression of CeAtg18, PaAtg18, PaAtg21 and KIAtg21 in *E. coli* BL21(DE3) cells**

Cultures were grown (A) in LB media and (B) in autoinducible media. LB culture was induced with IPTG at OD 0.6. In autoinducible media grown cells were incubated for 3 hours before the temperature was shifted to 22 °C. Also the LB culture was shifted after induction. After another 20 hours samples were taken of all cultures and subjected to SDS-PAGE analysis. Here cell extract (CE), supernatant (S) and Ni<sup>2+</sup>-sepharose beads bound (Ni-B) fractions were checked.

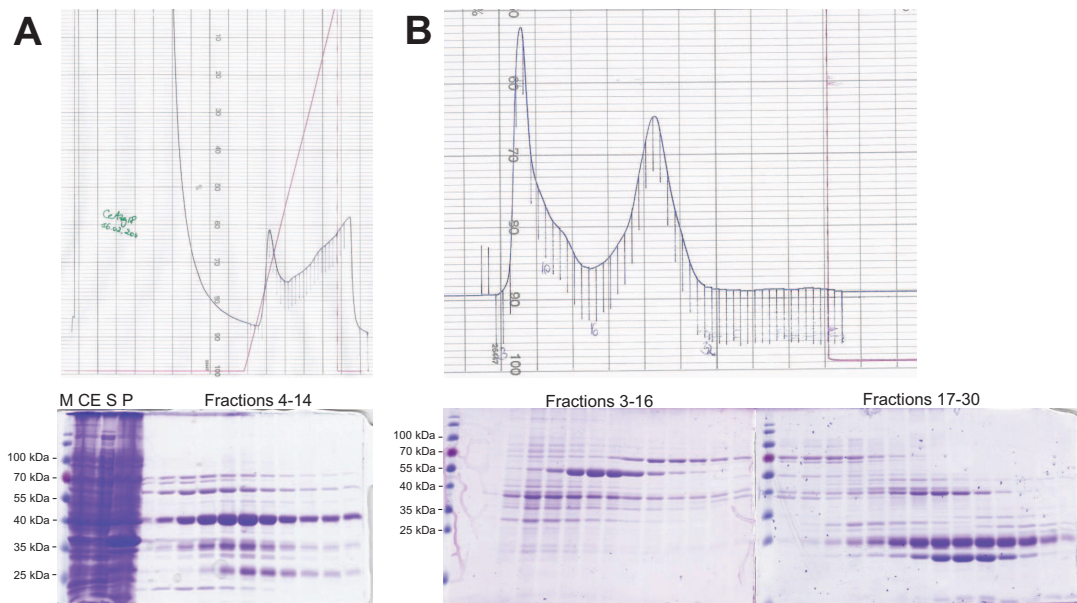


**Figure 5.2: Purification of CeAtg18 from *E. coli* BL21(DE3) cells**

Chromatograms and SDS-PAGE gels of CeAtg18 purified by (A) affinity chromatography using a His-Trap FF column followed by (B) gel filtration with HiLoad 16/60 Superdex S75 column.



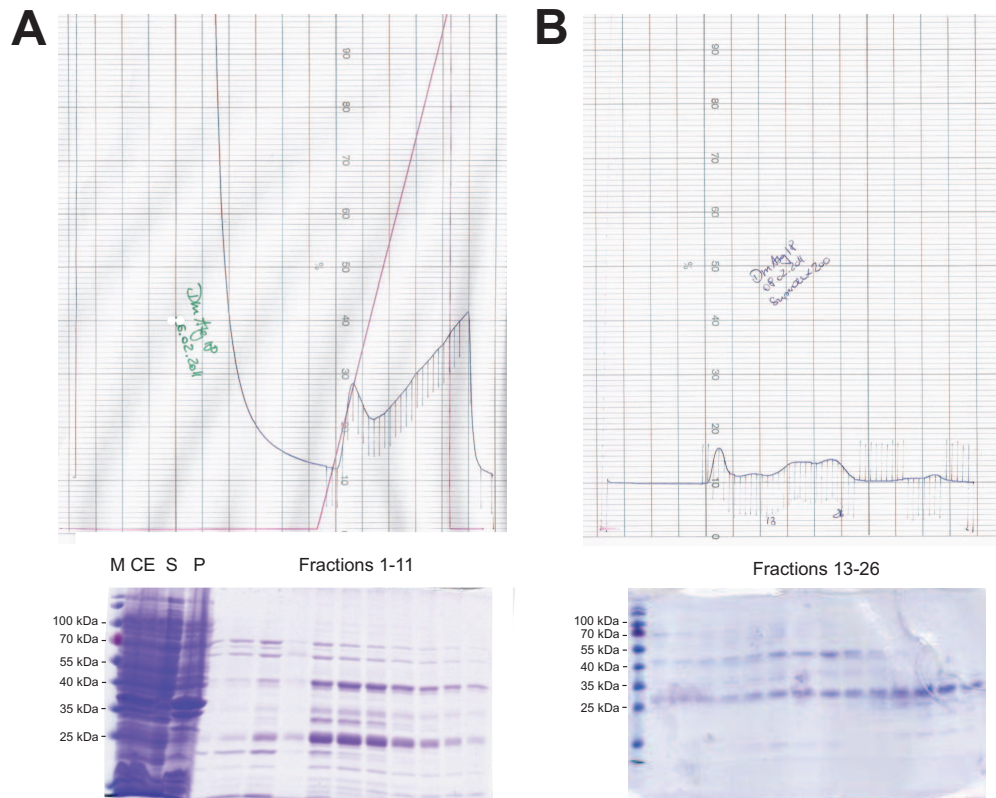


**Figure 5.3: Purification of DmAtg18 from *E. coli* BL21 (DE3) cells**

Chromatograms and SDS-PAGE gels of DmAtg18 purified by **(A)** affinity chromatography using a His-Trap FF column followed by **(B)** gel filtration with HiLoad 16/60 Superdex S200 column.

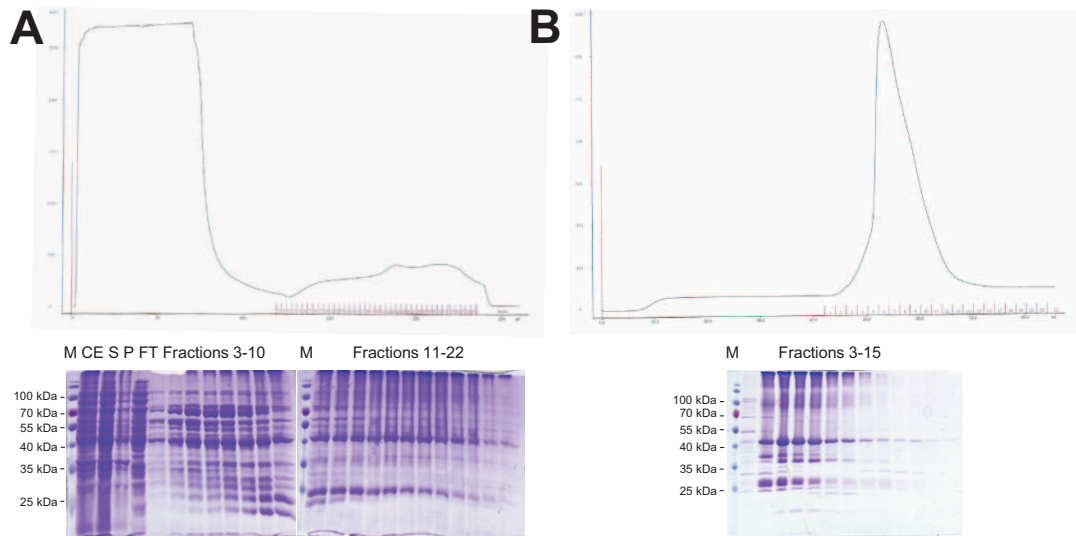


**Figure 5.4: Purification of PaAtg21 from *E. coli* BL21(DE3) cells**

Chromatograms and SDS-PAGE gels of PaAtg21 purified by (A) affinity chromatography using a His-Trap FF column followed by (B) gel filtration with HiLoad 16/60 Superdex S75 column.

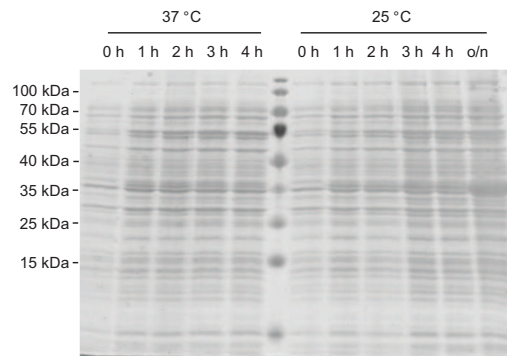


**Figure 5.5: Testexpression of SpHsv2 in *E. coli* BL21(DE3) cells**

Two *E. coli* cultures with the plasmid for SpHsv2 expression were incubated at 37 °C until OD of 0.6 and induced with IPTG (0 h). Then one culture was shifted to 25 °C. Samples were taken after each hour and over night (o/n) and analyzed with SDS-PAGE.

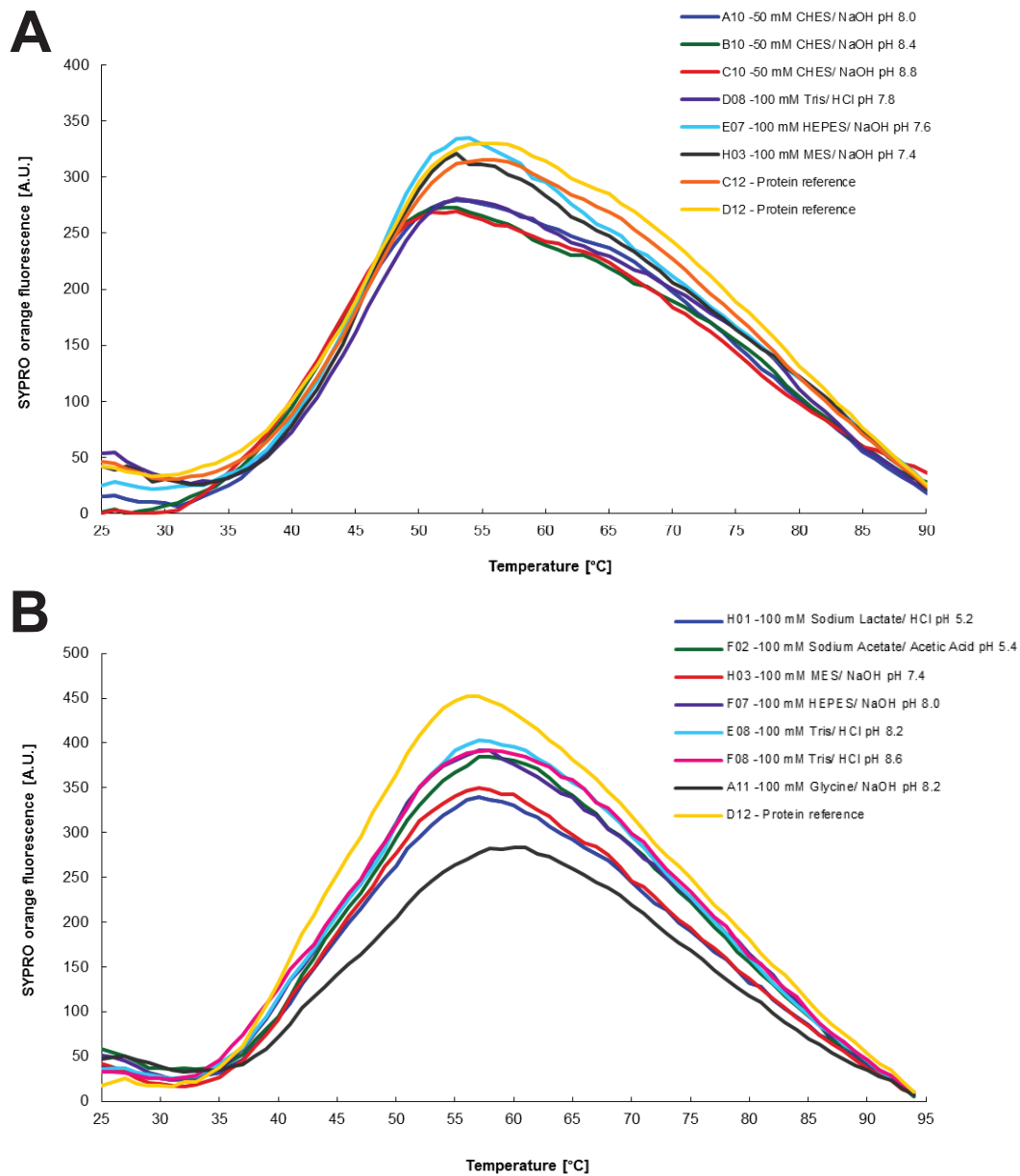


**Figure 5.6: Thermofluor analysis of CeAtg18 and DmAtg18**

Thermofluor experiments using the pHat screen of (A) CeAtg18 and (B) DmAtg18. Sypro Orange fluorescence was monitored and dequenching indicates unfolding of the proteins. Temperature was shifted from 25 °C to 90/95 °C. Shown conditions increased protein stability in comparison to protein reference.

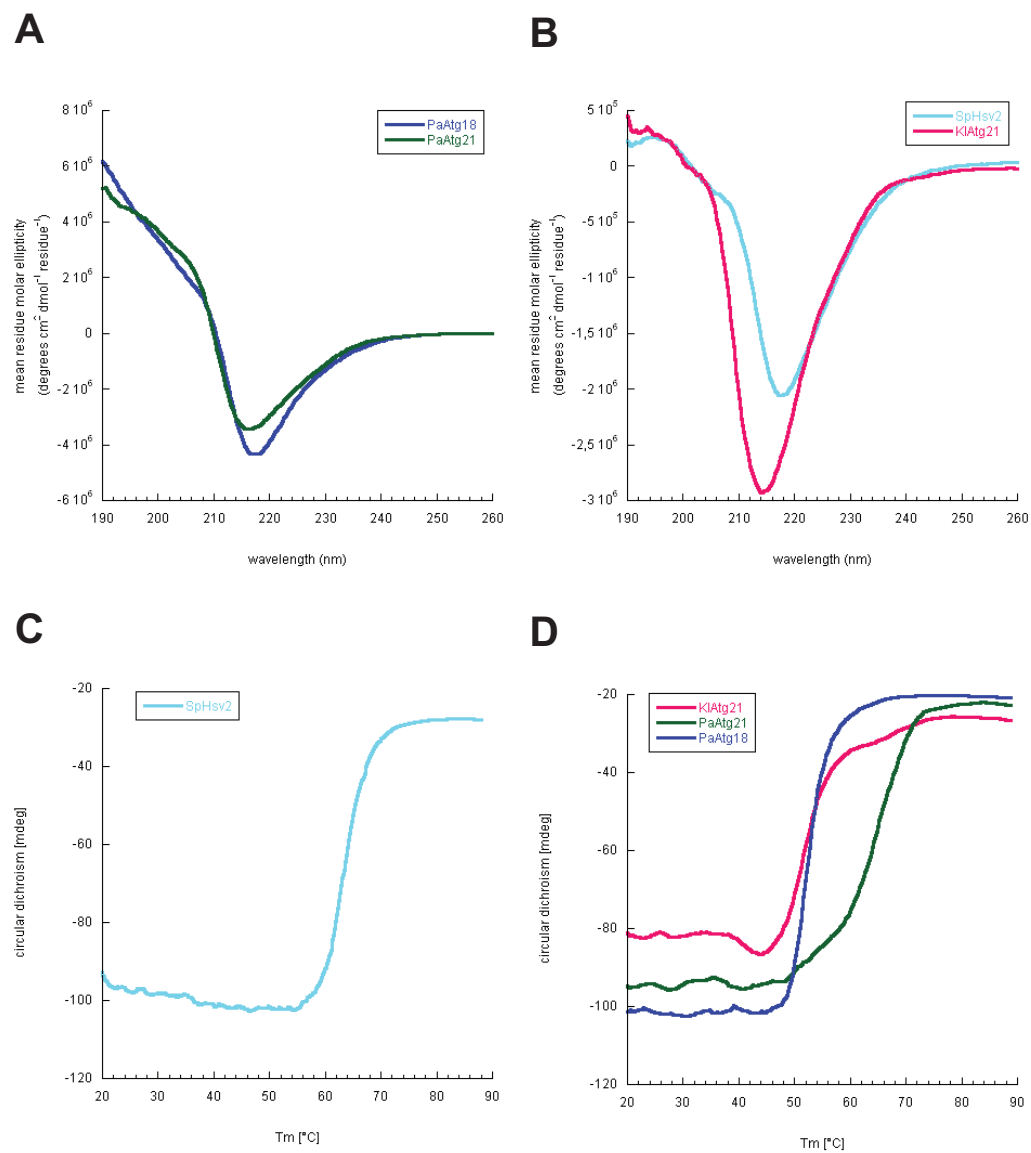


**Figure 5.7: CD spectra and melting curves of yeast PROPPINs**

CD spectra taken from 260 nm to 190 nm for (A) PaAtg18, PaAtg21, (B) SpHsv2 and KlAtg21. Melting curves of (C) SpHsv2, (D) KlAtg21, PaAtg21 and PaAtg18 were monitored at 216 nm over a temperature shift from 20 °C to 90 °C.

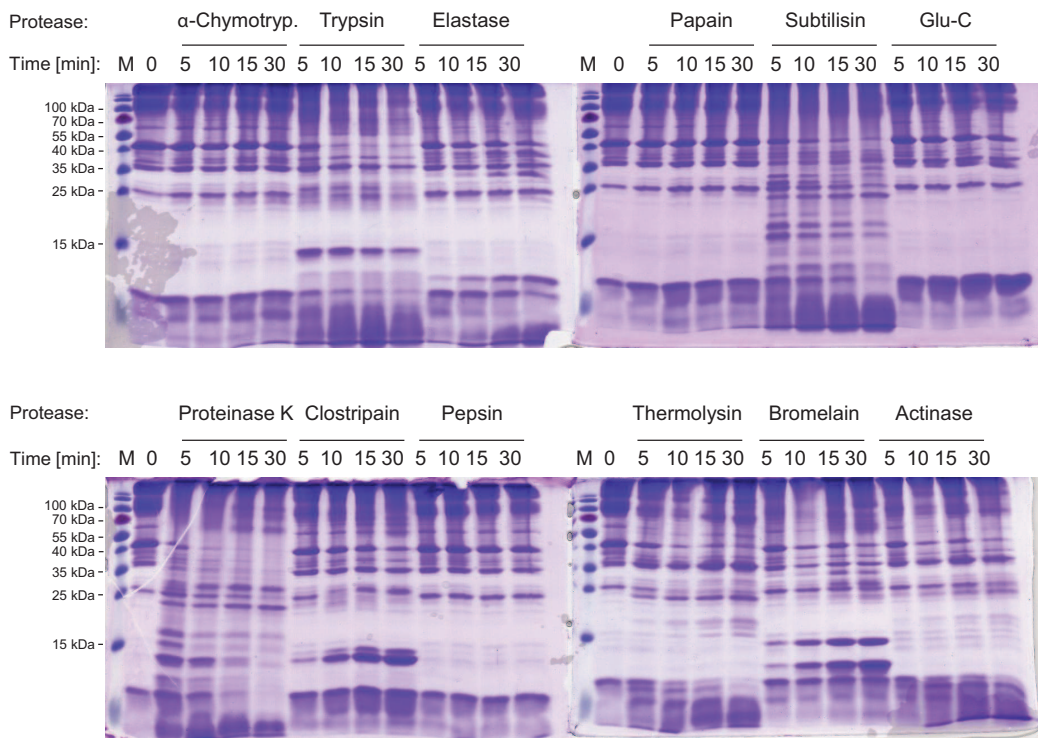


**Figure 5.8: Limited proteolysis of PaAtg21**

Purified protein was cleaved with the indicated proteases for a time course up to 30 min at RT. Samples were analyzed with Coomassie stained SDS gels.

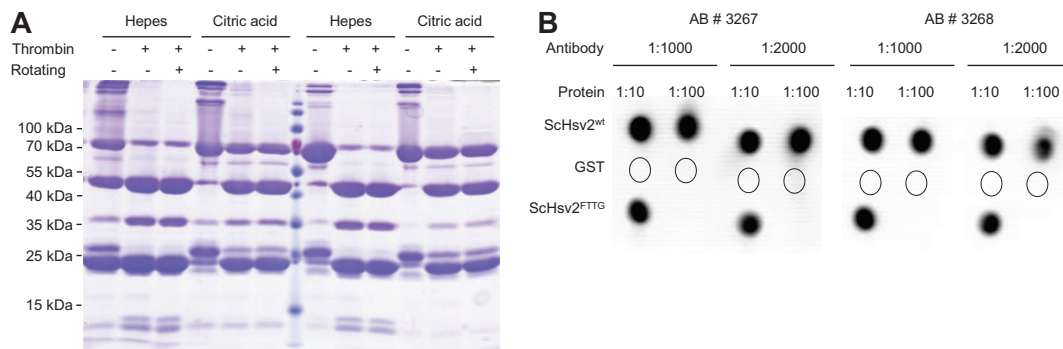


**Figure 5.9: Buffer optimization for thrombin cleavage of ScHsv2 and Hsv2 antibody test**

(A) Buffer optimization for thrombin cleavage of wild type ScHsv2 (left) and ScHsv2 FTTG mutant (right) using Hepes pH 7.0 and citric acid pH 5.5 buffer. (B) ScHsv2 antibodies were tested in 1:1000 and 1:2000 dilutions on wild type and FTTG mutant of ScHsv2 as well as on purified GST. Proteins (5 mg/ml) were spotted in 1:10 and 1:100 dilutions onto a nitrocellulose membrane.

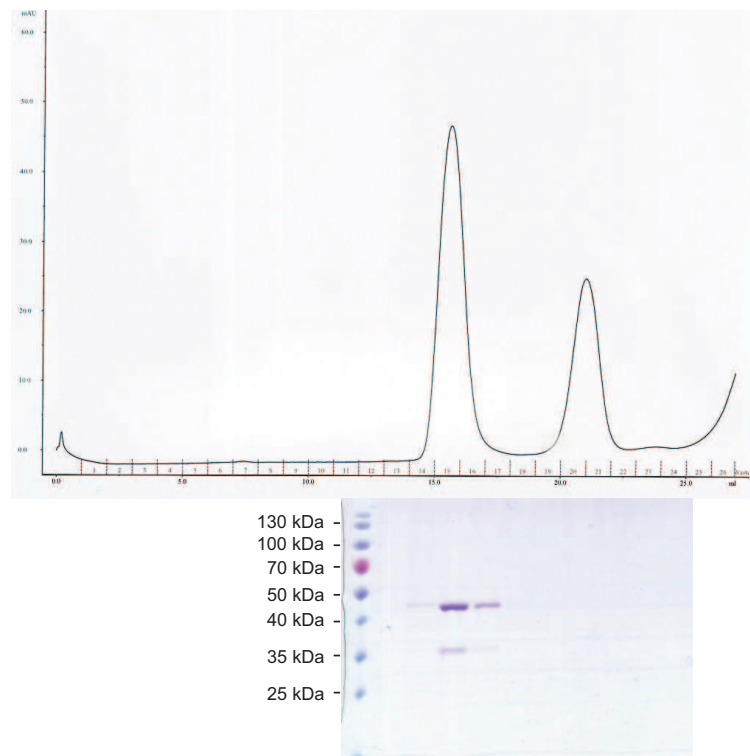


**Figure 5.10: Analysis of ScHsv2 after thrombin treatment for stability using an analytical gel filtration**

Purified GST-ScHsv2 was treated over night with thrombin and then GSTrap purified. ScHsv2 without tag was analyzed with an analytical gel filtration and fractions under the elution peak were tested on SDS gel.

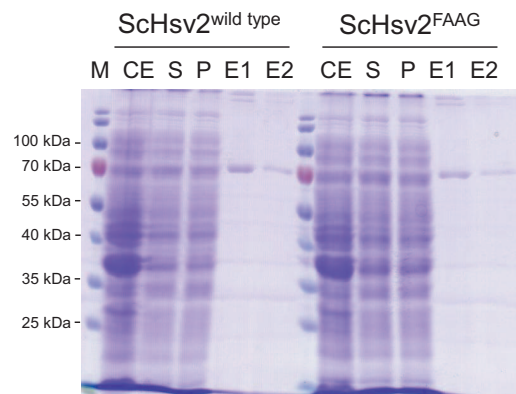


**Figure 5.11: GST SpinTrap purification of ScHsv2 homologs**

Samples taken during the purification of wild type ScHsv2 and ScHsv2<sup>FAAG</sup> with GST SpinTrap columns were tested on Coomassie stained SDS gels.

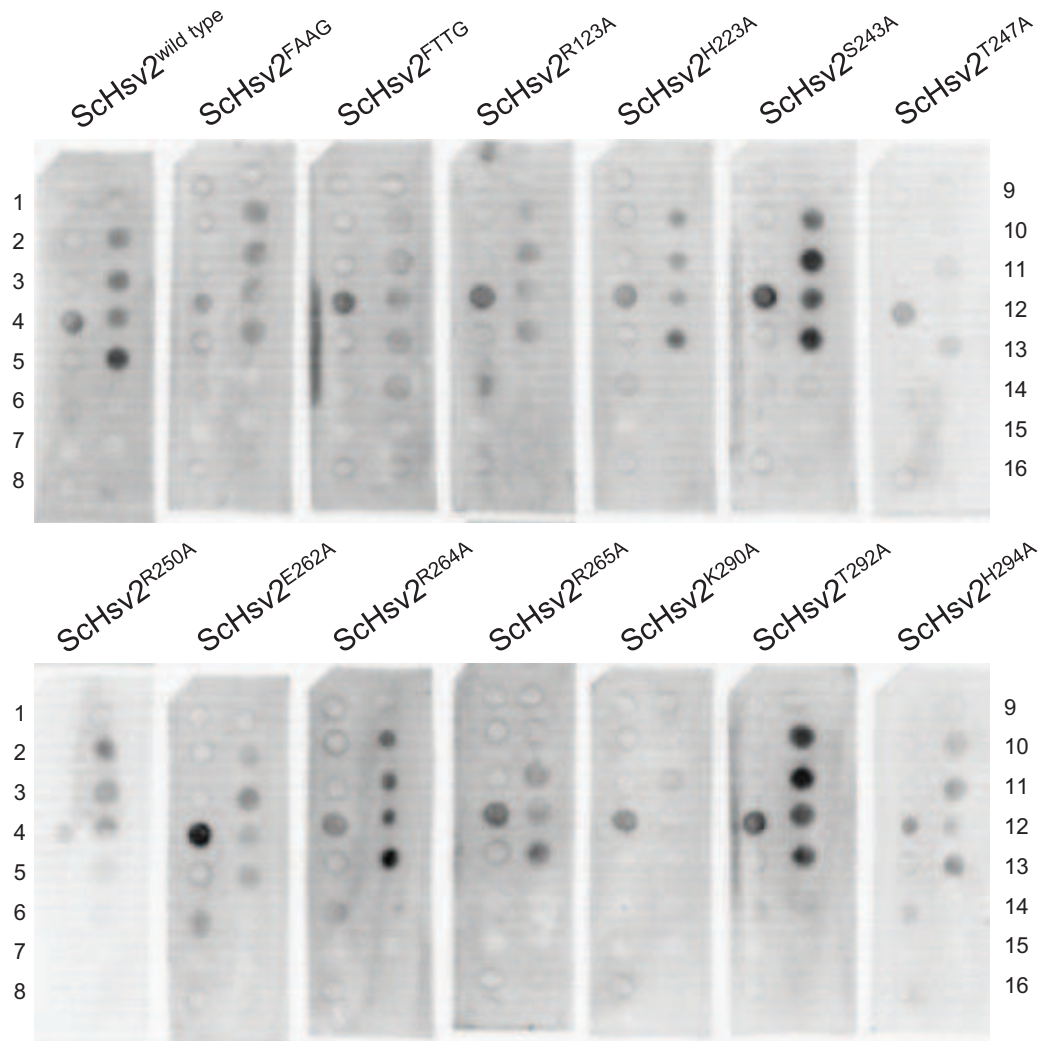


**Figure 5.12: PIPstrip analysis of ScHsv2 binding site mutants**

PIP strip analysis using 1  $\mu\text{g}/\text{ml}$  GST SpinTrap purified protein without GST-tag. 2 % BSA in PBS-T was used as buffer. The protein was detected using a ScHsv2 antibody and a secondary anti-rabbit antibody with HRP conjugation at 30 sec exposure time. The following lipids were spotted on the membrane - 1: Lysophosphatidic Acid (LPA), 2: Lysophosphocholine (LPC), 3: PI, 4: PI(3)P, 5: PI(4)P, 6: PI(5)P, 7: PE, 8: PC, 9: Sphingosine-1-phosphate (S1P), 10: PI(3,4)P<sub>2</sub>, 11: PI(3,5)P<sub>2</sub>, 12: PI(4,5)P<sub>2</sub>, 13: PI(3,4,5)P<sub>3</sub>, 14: Phosphatidic Acid, 15: PS, 16: Blank.

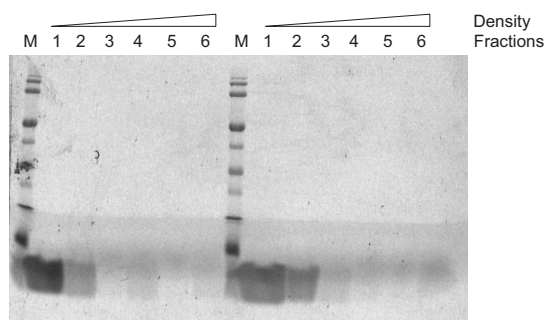


**Figure 5.13: Liposome floating analysis with SDS-PAGE**

Floating of the liposomes towards the low density region of a non-continuous Nycodenz gradient during centrifugation was shown by fluorescence scanning of Texas Red at 532 nm excitation and 670 nm emission wavelength. Fractions of the gradient were taken from top (1) to bottom (6). 2% Texas Red-PE, 73 % PC, 23 % PE and 2 % PI3P containing liposomes were used.

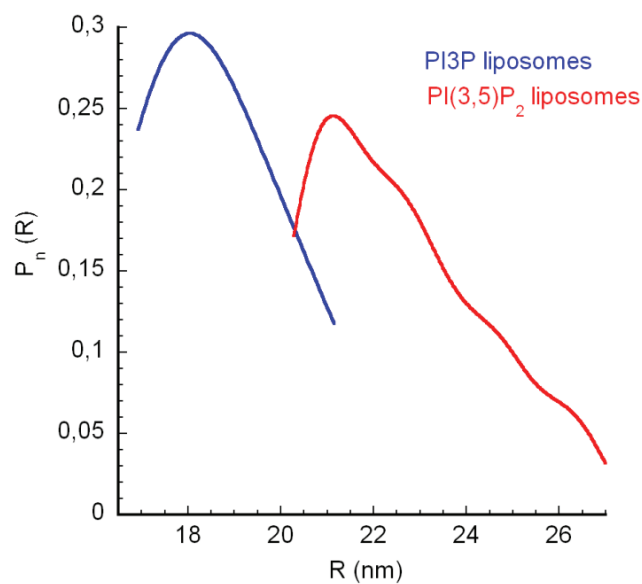


**Figure 5.14: Determination of liposome size distribution by FFF-MALLS**

The number of liposomes of a certain size ( $P_n$ ) was plotted against their geometric radii ( $R$ ). 2 % PI3P and 2 % PI(3,5)P<sub>2</sub> containing liposomes were subjected to FFF-MALLS analysis and their size homogeneity was confirmed. 2 % PI3P liposomes showed an average radius of 18 nm, whereas 2 % PI(3,5)P<sub>2</sub> liposomes were slightly bigger with a mean of 21 nm in radius.



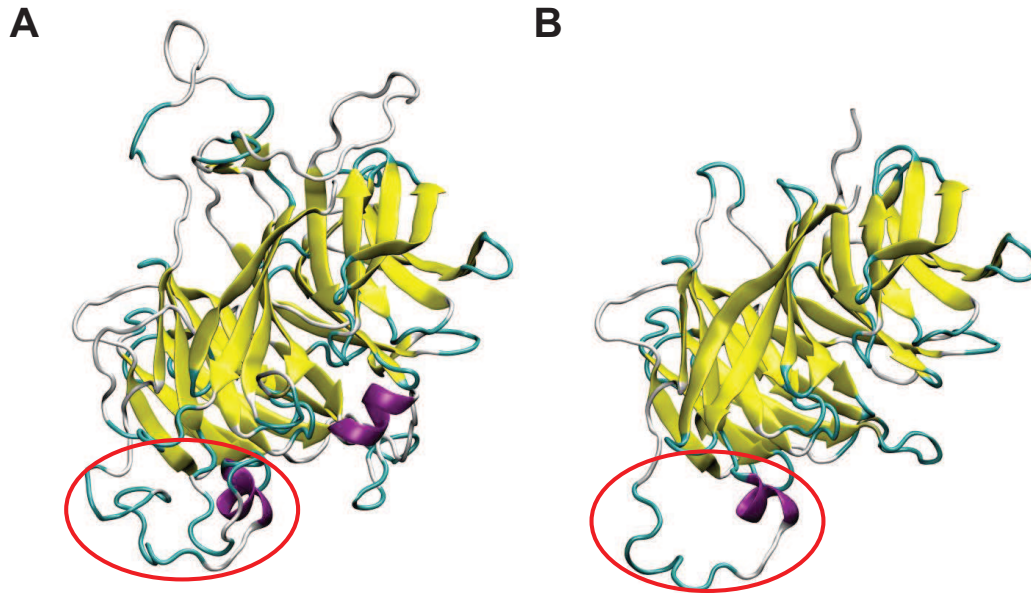


**Figure 5.15: Structure of KIHsv2 and homology model of ScHsv2**

(A) Homology model of ScHsv2 was derived by using (B) the structure of KIHsv2 as template. Marked with a red circle is the loop 6CD. Modified figure derived from A. Scacioc.

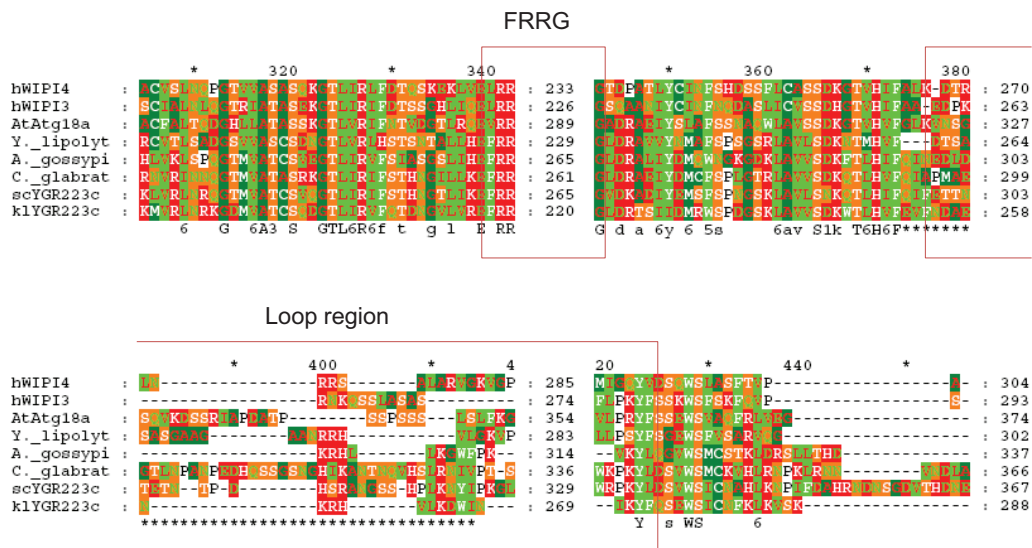


**Figure 5.16: Alignment of the loop 6CD region of different Hsv2 homologs**  
 Shown is the alignment of the human Hsv2 homologs WIPI3 and WIPI4, Hsv2 from *A. thaliana*, *Y. lipolytica*, *A. gossypii* and *C. glabrata* as well as ScHsv2 and KIHsv2. Marked is the conserved region containing the FRRG motif and the unconserved loop region. Modified figure derived from A. Scacioc.

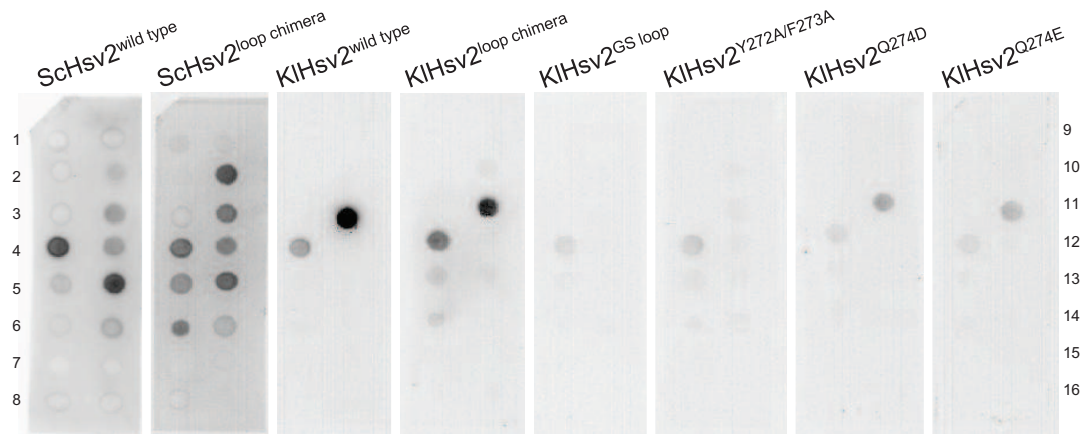


**Figure 5.17: PIPstrip analysis of loop 6CD mutants**

Purified proteins were subjected to PIPstrips spotted with the following lipids - 1: Lysophosphatidic Acid (LPA), 2: Lysophosphocholine (LPC), 3: PI, 4: PI(3)P, 5: PI(4)P, 6: PI(5)P, 7: PE, 8: PC, 9: Sphingosine-1-phosphate (S1P), 10: PI(3,4)P<sub>2</sub>, 11: PI(3,5)P<sub>2</sub>, 12: PI(4,5)P<sub>2</sub>, 13: PI(3,4,5)P<sub>3</sub>, 14: Phosphatidic Acid, 15: PS, 16: Blank

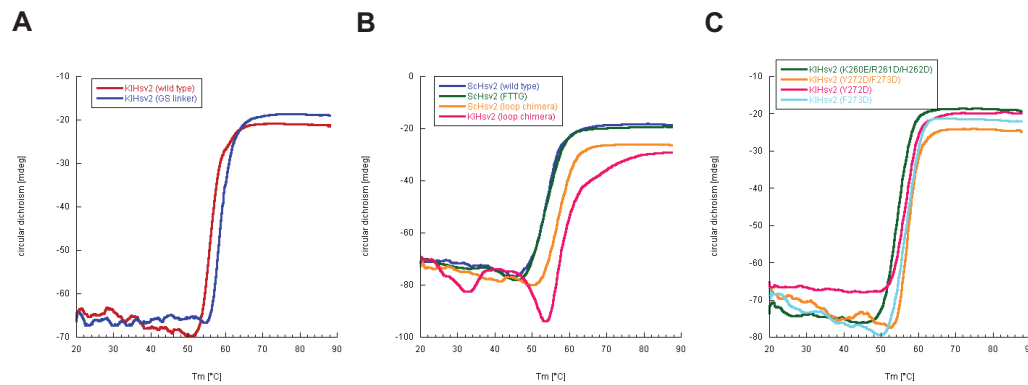


**Figure 5.18: Melting curves of KIHsv2 and ScHsv2 mutants**

Melting curves taken at 216 nm 20 °C to 90 °C for (A) KIHsv2 (B) ScHsv2<sup>wildtype</sup>, ScHsv2<sup>FTTG</sup>, ScHsv2<sup>loopchimera</sup> and KIHsv2<sup>loopchimera</sup> (C) KIHsv2<sup>GSlinker</sup>, KIHsv2<sup>K260E/R261D/H262D</sup>, KIHsv2<sup>Y272D/F273D</sup>, KIHsv2<sup>Y272D</sup> and KIHsv2<sup>F273D</sup>.

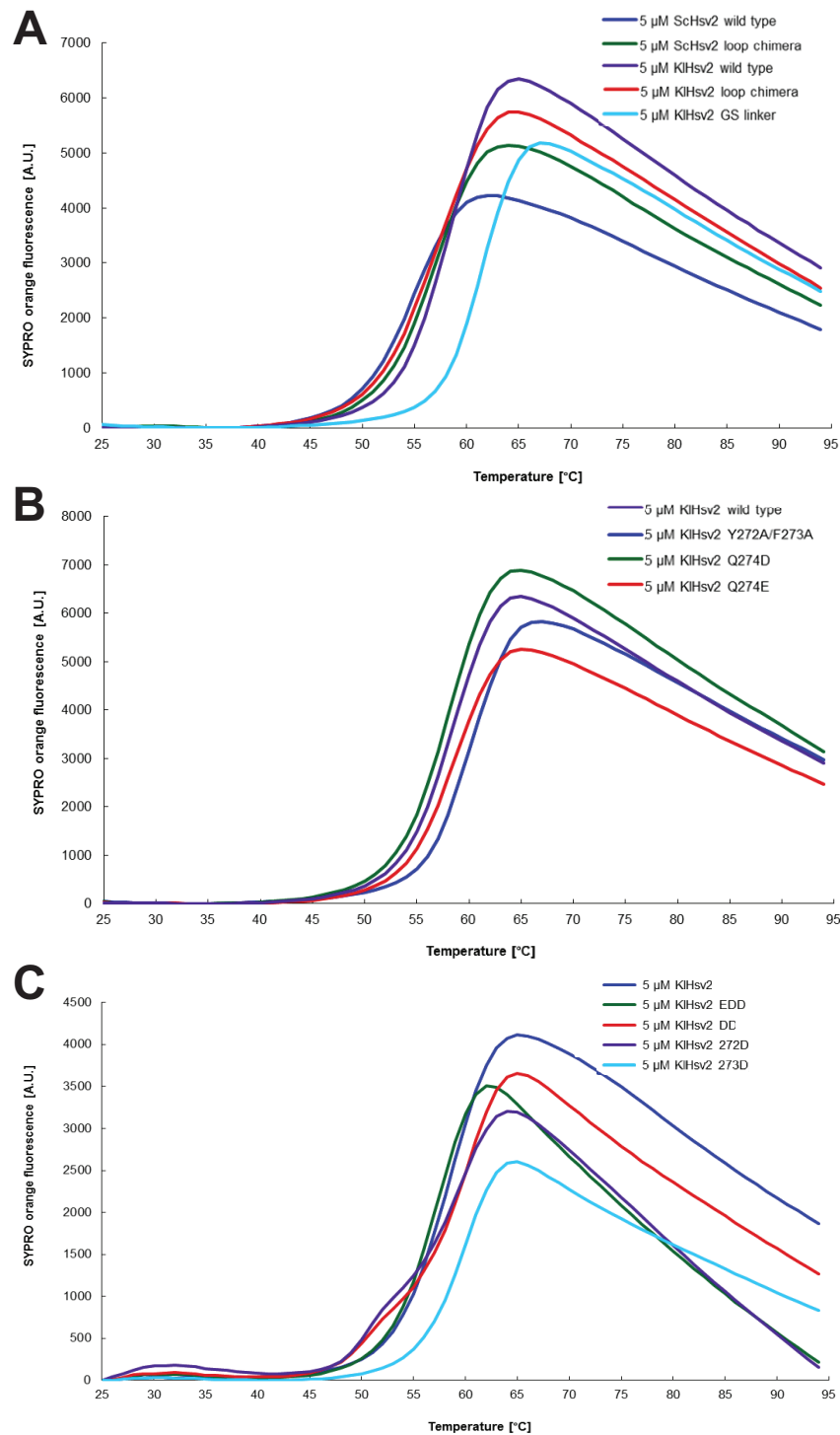


**Figure 5.19: Stability analysis of KIHsv2 and ScHsv2 mutants using Thermofluor**

Increase of Sypro Orange fluorescence during a thermal shift assay correlates with protein unfolding. (A) Shows ScHsv2<sup>wildtype</sup>, ScHsv2<sup>loopchimera</sup>, KIHsv2<sup>wildtype</sup>, KIHsv2<sup>loopchimera</sup> and KIHsv2<sup>GSlinker</sup>. In (B) KIHsv2<sup>wildtype</sup>, KIHsv2<sup>Y272A/F273A</sup>, KIHsv2<sup>Q274D</sup> and KIHsv2<sup>Q274E</sup> were compared. (C) Shows KIHsv2<sup>wildtype</sup>, KIHsv2<sup>K260E/R261D/H262D</sup>, KIHsv2<sup>Y272D/F273D</sup>, KIHsv2<sup>Y272D</sup> and KIHsv2<sup>F273D</sup>. The temperature was shifted from 25 °C to 95 °C.

### 5.3 Sequence of synthetic genes

**Table 5.2:** Sequence of synthetic genes used in this study

Name	Sequence
<b>SpHsv2</b>	
5' UTR	CAT ATGAGCACGATCAACACAGTTTCCCTGAATCAAGATGCCAGCTGT ATGAGTGTAGCACTGGATACCGGCTATAAAATCTTCCAGATTAAC CCGCTGAAACTGCGTGCACAACGCCAATTCAACGATGGTGGTCTG TCTATTGTAAAAATGCTGTTCCGCTCCAATGTCCTGCTGCTGGTA GGAGGTGGTGGAAATCCGAAATATGCCCCGAACAACTGATTGTG TGGGATGACGTGAAAGAACGCCCTGTAAAAGAAGTGGAACTGAAC TTCGAGATCAAAGGGATCTGCTTCGATGGAAAAGTCTGGCCATT GCCACAGCTTCTAAACTGTTTCTGTATCAGTTCGGCAACAACCTG AAAGTGCAGCGTTGTCTGGATACTCAGAACCCGAAAGGTCTGTGT GCCATGGTTACCACAGTCGAGAAAACCGCTATCGTATTCCCGAGC CGTAAAGTTGGTCAACTGCAAATCCTGTTTCTGTTCAAAGATCAC ATGAACACCTCAATCGTTCCGGCCCATGATTCTGAAATCAGCTGC CTGGGTATCAGTAAAACCGGCTCCAAAATTGCCTCTAGCAGTACC AATGGTACGCTGATCCGTATTTGGAATAGCGAAACGGGCGAAAAA ATCTGTGAATTCCGCCGTGGCTATCAGCACACTGCCGTTTGTGAG CTGGCCTTTTCTCCGGATGAGCTGCTGCTGGCCTGTGCTAGCAAA AAAGAGACTCTGCACATCTTTAGCCTGCATGGATCGCCTAATACT ATCCGTCAACTGACCAGCGAAGAACCGTATGAAGAAGCCTCCGAG TTCAAAAGCTCTACCACCGAACCTCGTCAGACTCACTGGAAACGT AAAGTCTGAAACTGATCGATTCCGGTAAACGTGCCATTGGCGT ATCCAAGTGTATCAAAGCAATCCGGTTCTGCTGCATTGGCTGGAC GAAATGACCATCCTGATCTGCTATAAAGACGCCGCCTATCAAAAA CTGAAACTGACCATTGAGGAAAGCAGCAAAAAGCGTTGAACATGCC AACCAGCATGTGTGCTTCCACTATGACTATAACCCTGGAGGCCGAC GGAAGTCTGTGT
3' UTR	TAACCTCGAG

Name	Sequence
<b>SpAtg18</b>	optimized for bacterial expression:
5' UTR	<p>CAT</p> <p>ATGCATTTCTTCGTCCGTAAATATCGTGGTAAAGCCGCTCTGCTG  TCCATTGGCACATTCGATGGCTATAAAATCTATAACTGTGACCCG  TTCGGCAAATGTTTCCACAAAATTCAGGGCGCCACCTCTATCGTT  GAGATGCTGTTCTCTACAAGCCTGGTTGCTCTGGTTGAAAAAGAT  GACGGCAATAACCGTAAACTGAAACTGATTAACACCAAAAAAAGC  ACAACAATCTGTGAGCTGACCTTTCCTACTCCACTGCTGGCTGTA  AAACTGAACCGTAAACGCCTGCTGGCTGTTCTGGAGGAACAAATC  TATGTGTATGACATTAGTAACATGCTGCTGCTGCACACAATTGAA  ACCACCAGTAACGTGTTTGCTGTCTGTGCTCTGTCTCCGAAT  AGCGAAAATTGCTATCTGGCCTATCCTGATTCTCGTGACCATGAA  CCTCGTACCGAAGGTGAAAGCTCTTCTCCTAACGTGTCCAATAGC  GCCGTGTCTGGCCAAGTGATCCTGTGGGATGTGATCAACTGTAAA  CAAATCACCAAAATCGAGGCCATAAAGATTCACTGGCATGCCTG  GCCTTTAATAGTGATGGCACCATGCTGGCAACTGCTAGCGATAAT  GGCCGTATCATTTCGTGTCTTTGCTATCCCGTCCGGACAACGTCTG  TATCAATTCGCCGTGGTTCTCTGCCTGCTCAGATCTATAGCATT  GCTTTCCACCCGGATTCTTCCCTGCTGACCGTGACAAGTTCTACT  CAGACCGTCCACATCTTCCGTCTGAAAGAAGTGTATTCCAACCTG  GAACGTCAAGGACTGCTGCCTTCTAGTCCACCTCCGAAAGAGTCG  CTGCTGCGTCGTTCTTCTCGTAGCCTGATTGGCACCGTTGGCGGA  TATCTGCCACAAAGCGTGTCTGGTATGCTGGACCCGGAGCGTGAC  TTCGCCATATGCTCATATTCCTGGCGACAAAGTGACCTCAATCGCC  GCCTTTGGTCCTGATAACACGATCGTGAACGTGGCAACCTATGAT  GGTAACCTGTATTTCATTCGGTGTAACCTGCGCACTGGCGGGGAG  TGTGCTATGGTGAACCATTTCTGTGTTGGACTGACCGCTGCA</p>
3' UTR	TAACTCGAG

Name	Sequence
<b>SpAtg21</b>	optimized for bacterial expression:
5' UTR	CAT ATGCCGTCGATCATCCTGTATTGCTCGTGGAATCAAGACCG TGGCTTTCTGAGTATTGGTAGCGAGAATGGCTATCAGGTGTATCG TTCTAACCCGTTTACCCTGTGCTTTTCTAAAAAAGCGAACGGTGC CAGCATTGTGAGATGCTGTATGAGAGCAGTCTGCTGGCCTTTGT TAACATTAGCCCGGAATCCACACGCCTGCTGAAACTGGTCGACAT CAAACGTGATATCGTGCTGTGCCGTATCTTTTATCCGTCACCGGT TCTGTGAGTCCGTTTCACCTGGAATCGTCTGGTTGTGCTGATTA AAGGGTCCATCTATGTCTATAATCTGAAAAACATGGAGCTGATCAA CACCCTGAATACGAGTAAAGGAAATGTGATTGCCTTCGCCGTACA CGAAAACCTATGTGGCCTATAACAGTCCTACTAACCCCTGGGGACAT CTATCTGGCTAGCCTGGATACTGCCATCCCGGTAACACTGATCCA TTGCCATAGCAGTGCTGTTCAAGTGGTGGACTTTCATCCTCGTGG TCATCTGATTGCTACTGCCTCTGCCAAAGGAACCGTTATCCGTGT GATTACCACCTCTGATGGTGAGCTGGTTACTGAACTGCGTCGTGG GTATATTCCCTGCTTCCATCGTGAGTATCAGCTTTCACCCGGTTGA ACCATTTCTGGCATGTGCCTCCGAAAATGGGACCATTACAGTGTT TAAATCTCAAACAGCCGTCTGACCCGAATAGTAGTCCGACCTC TAGCGTTACAGTGAGTTCTTCATGGTCAAATATCTGACGTCCAA CGTCGCCAAAGTTTGGGATACCCGTAAAGAGTTTGCCACCGCCAA AATCCCTGAAGCGAGCTTTTATGGGAAAATCATCTTTTCTTCGAG CGTCCCTCATATCCAAGTTGCTTCGTATAGCGGCCACTATTATCG TTTTGCCGTGAACCTGAAAAACGGCGGCAATTGTGCTCTGCTGGA GCGTTATATCTTCGATGAC 3' UTR TAACCTCGAG

Name	Sequence
<b>ScAtg18</b>	<p>optimized for insect cell expression:</p> <p>ATGTCTGATTCATCACCTACTATCAACTTTATTAATTTCAATCAA  ACCGGAACGTGTATTTCCCTTGGAAACGTCGGCTGGTTTCAAATA  TTCAATTGTGAGCCCTTCGGAGCTTTTTATTTCAGAGGACAGTGGG  GGCTATGCTATCGTCGAGATGTTGTTCTCCACCTCGTFACTAGCC  CTCGTTGGGATAGGCGATCAACCTGCGCTTTCACCAAGGAGATTG  CGTATAATCAACACAGCTGCTCATTCTATTATCTGTGAGGTGACT  TTCCCTACTTCTATTCTGAGTGTGAAAATGAATAAGTCTCGATTG  GTGGTACTTTTAGCTGCTGCTATTTATATTTATGATATCAACACC  ATGAGACTATTGCATACTATAGAAACAAACCCTAACCCACGTGGC  CTTATGGCTATGTCTCCTTCGGTAGCCAACAGCTATTTAGTGTAT  CCATCACCACCAAAGTTATTA ACTCCGAAATTAAGCTCATGCC  ACCACAAACAATATCACATTGTCAGTTGGTGGCAACACAGAGACC  AGTTTCAAGAGAGATGCTGCTGATGCTGGCCATAGTGACATTAGC  GACTTGGATCAGTATTTCGAGCTTTACTAAGAGGGATGATGCGGAT  CCAACAAGCAGTAACGGCGGTAACAGCAGTATAATAAAGAATGGT  GATGTGATCGTATTCAACTTGGAAACATTACAGCCAACCATGGTC  ATCGAAGCTCATAAGGGCGAGATTGCTGCAATGGCAATTAGTTTT  GATGGGACACTAATGGCTACCGCCTCTGATAAAGGTACTATCATC  AGGGTCTTTGACATTGAAACGGGTGATAAGATCTACCAATTCAGG  AGAGGGACGTACGCGACAAGAATTTACTCCATATCATTTCAGTGAA  GATAGCCAGTACTTGGCGGTTACCGGCTCTTCCAAAACCGTG CAT  ATCTTCAAATTTGGGGCATTCAATGAGCAACAATAAACTAGACAGC  GATGATAGCAACATGGCTGCTGCTGCAGCCGATGATTCATCGCTC  GATACCACCAGTATCGATGCGCTGAGTGACGCTGCTAACCCGACA  AGACTCGCAAGAGAACCATATGTGGATGCATCAAGAAAGACAATG  GGTAGGATGATACGTTACTCTTCTGCTGCTCTATCCCGAAGAGCT  GCCAGAACATTGGGTCAGATTTTCCCATCAAAGTTACATCGTTG  TTGGCTTCCTCGCGCCATTTTGCGTCTTTGAAACTTCCCGTTGAA  ACCAATTCCCATGTAATGACCATATCAAGTATAGGCTCTCCAATA  GATATAGACACATCCGCAGCTCCGGA ACTCTTCGAAACTGGCAAT  TCCGCAAGTACAGcGTCCTACCATGAGCCTGTTATGAAGATGGTC  CCCATCAGGGTCGTTTCTCGGATGGATACCTATACTTTGTT  ATGGACCCGGAGAGAGGGCGGCGATTGCTTAATATTGTCACAGTAT  TCCATCTTGATGGATTGA</p>

Name	Sequence
<b>ScAtg21</b>	<p>optimized for insect cell expression:</p> <p>ATGAAAGTATTACAATTCAATCAAGATGCAACGTGCTGTGTGGTG  GCCGCGTCATCGCATCAGATTTTCGATTTTTAACTGCGACCCCTTT  GGTAAATGTTTTGAAATTGACACTAAGAATTCCAAGAAGAAGACT  TCAAACAATAACGGTTCAGCTTCAAACCTCAGAATCACGGAATAAT  GAGGAGAGCATATTAATAACTAATGGCTCCCGCGATCGTACTGAT  GCAGAAGAAGAGGAAGATAATGAAGATAATGCCCTCGTTACAGGA  AATATACTGAAAGAAGGGGAGTTTGTTCATTGAAATGTTGTTTTCA  ACTAGTCTTATTGCTATTGCAGATAGAGGACAAGGTCTAAACAAA  GGAAAAAAGCTGAAGATTGTCAATACAAAGAGAAAATGTACTATT  TGTGAAATAGTTTTCCACATGAAATTGTTGATGTGGTCATGAAT  AGAAAAAGAATGTGCGTACTTCTTGAAAGTGACCAGATATTCATT  TATGATATATCTTGTATGAAACCCTTAGAACTATCGATCTTTGG  GAAGATCATTATAAGAGGTCCCAAGCCAATTCGTTCTCAAATGCG  TCAAATACTGGTACTTTGGAGGGAGATTCTGCAAATTTGAACAGG  GTGGCTACCAATTTACTAGCAAATGCCACTCAAAAAAGTGTGAAT  GGATCTAATCCTAGTGTAAGAACCAGAAGAACTCTCTAAGAAGT  AAAATAAGGCCAAGAATGGTTTTAAGTAACGATGATAGAAGTATA  CTGTGTTTTACTGCGTATAGCTCGCCAAGAAGAATAAGCCCAAT  TCAGAAGCACTATATGATGTAGTGATTTATGACACATTAAATGTG  ACGCCAGTTAATTACTTGAATTCGTTTCATAAGGGGAATGTTGCA  TGTTTAGCAGTAAGTCACGATGGTAAACTGCTTGCTACTGCCTCA  GATAAGGGGACCATAATAAGGGTGTTCATACGGGGGTAGATTTCG  GACTATATGTCTTCAAGGTCACTGTTTAAAGAATTTAGACGGGGT  ACCAGATTGTGCAATTTGTATCAGCTAGCTTTTCGATAAGAGTATG  ACTATGATTGGATGTGTAGGTGATACGGGACACTATTCATCTTTTC  AACTTGATGACGCCTCTAATAGCCTCCCTGGAGATAATTCTAGC  AATGGCCACTGGAATGAAGAGGAATATATACTAGCATCAAATTCA  AATCCCAGTATGGGAACTCCAAAGGAAATACCTCTCTCGAAACCA  AGAATTGCGAATTACTTCTCGAAAAAATAAAATCTTCAATACCA  AACCAGAACCTGAGCCGTAACCTTTGCTTATATAACAGTTAATGAA  TCGAACAGGAGTTGCTTAGGGTTTCCAGACGAATTTCCCAACCAA  GTCTATATTGCCTCTGATGATGGAACCTTCAGTATATATAGTATT  CCGTCAAAACCTGGTGAATGTGTGCTGACTAAAAATAATAAATTT  ACATAA</p>



Name	Sequence
<b>CeAtg18</b>	optimized for bacterial expression:
5' UTR	<p>CAT</p> <p>ATGAGTGCCACCACCAGTGAAGAAAACCCGGATAGCATCAA  CTATATCGGCTTTAACCAAGACAGCAAAGTCATCTGTGTGGGTCA  CAAAGACGGGTATATGTTCTATAAAAACGGCCGACATCCTGGAAAA  CAATACGCTGACCTATGAAGGCGAAAATCTGACACACCTGGGCCT  GAACAATTGCCTGATCATCGAACGCCTGTTTAGCAGTGCTCTGAT  GGTCGTTATTAGCCAGAAAGATCCTCGTGTCTGCATGTCTATCA  CTTTACCAGCCGTAACATCATCTGTGATCACCGCTTCAACAAAAG  CGTGCTGACTGTTTCGTCTGAATCGTGACCGTATCGTTGTCTGTCT  GGAGGATTGTATCTATATCTATAACCTGAAAGACATGAAAATGAT  GCACAACATCATGGATACCCCGACCAATAAACTGGGTGTACTGGA  CCTGACCTCTAACCCTGGAAATGCCCTGATTGCTTATCCTGGAAG  CACCGACACCGGTTCCGTTACCTGTTTGACGCCATTAATCTGTC  GAGCGTTAGCACATTCAATGCTCATGAGGGGACTATCGCTTGCCT  GAAATTCAACCAAGAGGGTAATATGATTGCCACAGCCTCTACCAA  AGGCACCGTGATTTCGTGTGTATAGCGTGCCGAATGGTCATCGTCT  GTTTCGAGTTTCGTTCGTGGTGTACACGTTGTGTGAACATCTATTC  CCTGTGCTTTTCTAGCGACTCCAAATATCTGACCTCTAGCAGCAA  CACTGAAACCGTCCACGTGTTCAAACCTGGAAAAAACCGAAGGCCT  GGATAACAAACCGGAAGCATCCACAGAAGGTGGAGGTTGGTTTCGA  CGCCATCAACAAAACCTTTAGCGCCTATATGCCTAGCCAAGTTCT  GCAAGTTGGTGAGCTGATGACAACCGAACGTTCTTTTGCCACAGC  AAAACCTGCCTGGTGCCGCTCGTTCTAATCAAGTGTCCCTGGTGTC  CCATAAAAATCAGCAGTATGTCATGGCAGCCACCAGTGATGGATT  CGTTTATGCCTATCGCCTGGACCCTGAGGGTGGAGAGCTGGACCT  GATTAACAACACAATATCGGCCCGAAATCTGATACTAGCCGTGC  TAGTCCGACTTCTACAGGTTCTGGAGGTGCCGCCAAATCAGCGGA  AGCCTCTAATCAAAGCGTGCCCTAACATGGACGATCCGGATGATTT  CCCTCCGATGTCTCATACTAGTGGT</p>
3' UTR	TAACTCGAG

Name	Sequence
<b>PaAtg18</b>	optimized for bacterial expression:
5' UTR	<p>CAT</p> <p>ATGGCAAGCCCGAATCCTCTGGCGTTTGAAGCAGCAACAGC  GGCACATGAAGTGGCAGCGTCCTATGTTACAGAACACAAACCTCG  TAAAAACGACAATATCAACTTCGCCAATTTCAACCAGGACTTCTC  CTGTGTGTCAGTGGGTATAGCAATGGGTATAAAATCTATAATTG  TGAGCCGTTTCGGCCAGTGTTATTTCGAAAAGCGACGGCAGCATCGG  AATTGTGGAATGCTGTTTCTGCTCATCTCTGCTGGCTATCGTTGG  TATGGGGGAGCAACATTTCTGTCACCTCGTCTGAAAATCAT  CAACACGAAACGTCAAACCACCATCTGTGAACTGACCTTCCAGG  TGCCATTCTGGCGGTTAAACTGAATCGTGAGCGTCTGGTAGTACT  GCTGGAGGAAACCATCTATATCTATGACATTAACAACATGCGTCT  GCTGCATACGATTGAAACCCCGAGCAATCCGAATGGTCTGATTGC  CCTGTCTCCGTCTAGTGAGAACAACCTATCTGGCGTATCCGTCACC  TCAAAAACCTGGCGCCTAATCCACAGACTGAGGTTACCCTGCACTC  AAATCCACAGACAGTCCGTAATGGTGATGTGATCATCTTTGATGC  CAAACTCTGCAGCCAACCTCCGTTATCGAAGCACATCGTACCAG  CCTGGCGGCAATTGCCCTGTCTAAAGACGGTCTGCTGCTGGCAAC  AGCAAGCGATAAAGGCACCATCATCCGTGTGTTTAGCGTTGCTAC  CGGCATTAAACTGTATCAATTTTCGCCGTGGGACATATCCGACAAA  AATCTATTCCCTGGCGTTTAGTCCGGACAACCGTTTTGTAATCGC  CTCTTCCGCTACTGAAACTGTTTACATCTTTTCGCCTGGGTGAAGA  AGAAGCGGCTAACACGATCAAAGCGCCAACAAAAAGCACGTCT  GACCAAAGCACAAAGTGCCAAATCCTCTGGAGACTAGCCCTGACAT  TTATCCACACAACCAGCATAACAAGCAGCGACGAAGATGAAGAACT  GAACGAGGATGAGGAGGATCTGGACGGCGACGAAGATGAGGATCT  GGAAGATGACGCCCATGTTCCGGTTAGTCTGCAACGTGGTCTGTTT  TAGTAGTAGTACCGGCAGCTTTCATTCTAGCGAGAGCATGACCGA  TAAACTGAAAGAACCGCTGGTTCGACAACAGTCGTAAAAGTGTGGC  CCGTATGCTGCGTTCGTACAAGTCAATCTCTGGGCCGTAAAGCGGC  TGAGAAAATGGGAACCTATCTGCCTCCAAAATTTTCGTCCATCCT  GGAGCCTAATCGTCATTTTGCCTCCCTGAAAGTTCCTGCTAGCAA  AGAAACCAAACCGTGGTGGGTGTTGGTAGTAAAATCTGGGACGA  CCTGATTCCTAGCGTGTATCTGAAAGACGATGCCAATAGCATCAC  CGAAACCAGCGAAGATCTGGTGAACAAAAAACTGGTCCACATTAT  GGTGATTACCAGTGAGGGATTCTTCTATAAATTCGGCCTGGACCC  TGAACGTGGCGGTGACTGTGTCTGCTGCACCAGCAATCTCTGTT  TGGT</p>
3' UTR	TAACTCGAG

Name	Sequence
<b>KIAtg21</b>	optimized for bacterial expression:
5' UTR	CAT ATGGCCCTGAAACTGCTGGGTTTTAACCAGGATGCCACGTG CTTTAGCGTGATTTTCGAGCAACAAAGGTGTCACCATCTATAACTG TGATCCGTTTCGGCAAATGTTTTGAGCTGGAAAAATCCACCTCCAA CGATGAAGAACTGGACTTTCTGGTTCGAGATGCTGTTTAGTACCAG CCTGATCGCCGTGGTTGATAAACGATTGGTGCCAGCAAACGTAA AAAACTGAAAATTGTGAACACGAAACGTAAAGCCACCATCTGTGA GCTGACATTCCCTCATGAGATCATGGACGTGATTATGAACCGTAA AATCATCTGTGTGGTGTGAAAAGTGACCAAATCTTCGTCTATGA CATCAGCTGTATGAAACTGCTGCGTACCATCGATGTTTCGTGGCGA GAAACTGAAATCGACGAGCAAATTCGTAACAGTGAAGCGGTGGG GGATATCGGGGTCCGTGTGTCTCTGTCTACCGACAACAACCTCTAT TCTGTGCTATTCCCTCCTATTCCAAAAGCGACAAAGAGAATGCTCC GCTGAACGACATTGTGGTGTGTTGATGCCCTGAAATGTATCCAGAT TAACGTGCTGCCTGCTGTCCACCAGTCTAATATCGTCTGTATCGC CTGTTCTCCGGACGGTATGCTGATGGCAACAGCCAGCGAAAAAGG CACGATTATCCGTGTGTTCAAACCATCGACACCGAGAACGATGA GCCTATTCTGGTGAACGAATTTTCGTTCGTGGTAGTCCTAGCCG TATCAGTGAATGAAATTC AACCATGACAACACCCTGCTGGCTTG TGTTGGTCAAAGCGACACCATCCACATTTTTGCCCTGCCGGTTAC AACAACTGAAGCAGACGCCAATGAAGATGACACTCTGCAGCAATC TTCTCATAGCCTGAGCAGCTCCATTAATGGTCTGCAGTATATCTC CAAAGGTCTGGCGAACCGTTTTGGGAAAATCATTGTGAGCAAAT CCCGACCCAGTCTCAACAACGTCATGTGGCCTATATCAAATCCC TGAGAACGCCAAATATCGTATCGGTTTCCCGAAAGACACGACCAA TACCATTACATCTGTGGCGAGGATGGCAATTATCTGGTGTATTCC CATCCCTCGTAACGAAGTTGGACCGTGTACACTGGTCAAATCCAA CACCTTCGAC
3' UTR	TAACTCGAG

Name	Sequence
<b>PaAtg21</b>	optimized for bacterial expression:
5' UTR	<p>CAT</p> <p>ATGGCACTGCGCTCAATCTCGTTTAACCAGGACTATACGTG  TCTGGCGGCAGGTTTTGATGCTGCTTATAAAGTCTATAACTGTGA  CCCGTTTGGTGAATGCTTTCAGAAAGCCGATGATGGTGGTGCTAA  TCTGGTGGAAATGCTGTTTTCTACGAGCCTGATTGCCGTAGTGGG  TATTGGAGACAAACCGGCCGAATACAATGCGTAAACTGAAAATCAT  CAACACGAAACGTAAAGCGGTGATCTGTGAACTGACCTTCCCAAC  TGCTATCCTGTATGTGAAAATGAACCGTAAACGCCTGGTGGTTGT  TCTGGTTGATCAGATCTTTGTGTATGACGTGAGCTGTATGAACT  GCTGCACTCCATTGAAGCAAGTGTGGGCTGGACGATCGTATCAT  CTGTGACCTGTGTGCCGACGATGAATCTGTGCTGGTGTTCACA  ATCTGGGTCTAGCGACGAACTGGCTGCTAACGCTGGTACTGTTGT  CGTCTTTGACGCTCTGCAAATTCAGCCTATTAACGTTATCGAGTG  TCACCGTTCACCTCTGCAGCGTATTGCTGTGTGAAAGATGGACG  TCTGCTGGCAACGGCTAGTGTAAGGCACTATCGTCCGTGTTTT  CCGTGTAGCCGATGGTCGTAAAGTTCATGAGTTCGCGCGTGGCTC  TTATACTGCCCAAATCTCTTGCCCTGTCTTTAATGTGGATGCCAC  CGTACTGTGCTGTTCCCTCTAACACTGGCACGGTCCACTTTTTTCG  TCTGGACGACGTTGATCGCCGTCGTTCTACAGGTTCCATCGACGC  CAATATTGATGGCAGCGAAACACTGCCTCGTGAATCATCCATTAC  CGAGGAAGAAAGTTCCGAAATCAATCGCCTGATTAACAGTCAGCT  GGGTGGCCATAATGGGTTTGCCAAAAAAAATCGGCCGAGAGCCT  GAAAAACTTCATCTGGAGCAAAGCAAACGTATCTGCCGAGCCA  GATTAATAGCATCCTGGAGCCGAAACGTGACTATGCCTTCATCAA  ACTGACGACCGAAGTTGAATCAGTTGTGGGTCTGGTCGACAACAA  TTGCTATGTTGCCACCCGTGCTGGAGATTTCTTCGTGTATAGCGT  TCAGCCTGGTCAATGTGTTCTGCTGAAACATTATAAAATCGAG</p>
3' UTR	<p>TAACCTCGAG</p>

Name	Sequence
<b>KlAtg8</b>	optimized for bacterial expression:
5' UTR	CAT ATGAAAAGCGCCTTCAAAAGCGAGTTTCCGTTTCGAAAAACGTAA AGCCGAGAGTGAGCGTATTGTCCAAAAATTCCACAACCGTAT CCCGGTGATCTGTGAGCGTGGTGGTAAAAGCGATATCCCTGACAT CGATAAACGTAAATATCTGGTGCCGGGTGACCTGACAGTTGGTCA GTTTCGTGTATGTGATCCGTAAACGTATCAAACCTGCCGGCCGAAAA AGCAATCTTCATCTTCGTGAACGACACACTGCCTCCAACAGCAGC ACTGATGAGTAGCATCTATCAACAACACAAAGACAAAGACGGGTT CCTGTATGTCTCTTATAGCAGCGAGAACACCTTTGGTGATGACGC CCTGTTTTCTGAGGAGCC
3' UTR	OneSTrEP-tag ATGGCTGGTCCCTCGTGGGTCTAGCGCCTGGTCCCATCCACAA TTCGAGAAAGGCGGTGGTTCAGGTGGAGGTTCTGGCGG GGGAAGCTGGTCCCATCCACAATTTGAGAAA TGACTCGAG
<b>PaAtg8</b>	optimized for bacterial expression:
5' UTR	CAT ATGCGTAGCCAGTTCAAAGATGAGCACCCGTTTCGAGCGTCGTAA AGCAGAAGCAAGTCGTATTCGTGGGAAATTCCTGGACCGTAT CCCGGTGATTTGTGAAAAAGTGGAGGAGTCCGATATTCCGGAGAT CGATAAACGTAAATATCTGGTGCCGAGCGATCTGACTGTTGGTCA GTTTGTCTATGTGATCCGTAAACGTATTCAGCTGCCGTCCGAAAA AGCCATTTTCATTTTCGTGAACGACATTCTGCCTCCAACCTGCTTC ACTGATGTCCACGATCTATGAGCAGTATAAAGACGAGGATGGGTT CCTGTATATTCTGTATAGCGGCGAGAACACCTTTGGGCAACTGGA AGGCGTTGAAGAAACACTGCC
3' UTR	OneSTrEP-tag ATGGCTGGTTCCACGTGGTTCCTAGTGCTTGGTCCACACCCTCAA TTCGAGAAAGGCGGCGGTTCTGGGGGTGGTTCCTGGCGGAGG ATCTTGGTCCACCCACAATTTGAGAAA TGACTCGAG

Name	Sequence
<b>KIHsv2</b>	optimized for bacterial expression:
5' UTR	<p>CAT</p> <p>ATGCTGACCCGTAACCCGATTGTGCCTGAAAACCATGTGTCTAA  CCCTATTGTGGACTATGAGTTCAACCAGGATCAGAGCTGCCT  GATTGTTTCTACCCCGAAAAGCTTCGACATCTATAACGTTTCATCC  GCTGAAACGTATCATGAGCCAGGAAATGCCAGACGCTGGAACCAT  TCGTATGCTGCATCGTACCAACTATATCGCCTTCGTGAGCACCAA  AAAAGAGCTGCTGCACATCTGGGACGACGTGAAAAAACAGGACAT  TACCCGTGTGAAACTGGATGCCGCCGTGAAAGACCTGTTCCCTGTC  ACGTGAGTTTATCGTGGTTAGTCAGGGTGATGTGATTAGCATCTT  CAAATTCGGCAATCCGTGGAATAAAATCACCGAGGATATCAAATT  TGGGGGTGTGTGTGAATTCGCCAACGGTCTGCTGGTGTATAGCAA  CGAGTTTAACCTGGGGCAGATTCATGTCACTCGCCTGCAAACCTGA  TGCTGAACAAGTGGTGGGTAAAGGTGTTCTGGTCAAAGCCCACGC  CAACCCAGTAAAAATGGTCCGCCTGAACCGTAAAGGAGACATGGT  AGCGACTTGCTCTCAAGACGGTACACTGATTCGTGTTTTCCAGAC  AGACAACGGAGTACTGGTCCGTGAATTTTCGTTCGTGGACTGGACCG  TACAAGCATTATCGATATGCGCTGGTCACCTGATGGTAGTAACT  GGCCGTGGTGAGCGACAAATGGACACTGCACGTGTTCGAAGTGTT  CAATGACGCCGAGAATAAACGCCATGTGCTGAAAGATTGGATCAA  CATCAAATATTTCAAAGTGAATGGAGCATCTGTAACCTTCAAAC  GAAAGTGAGCAAAGGCTCCAATGACTGTAAAATCGCCTGGATTAG  CGACACCGGACTGGTCATCGTGTGGCCAAACCGCCGCCTGGCCGA  CACTTTTAAACTGAACTATAACGACGACGAGCATGTTTGGTGGCT-  GCAGCTGAATCAGCGTAACGAAATCCCTCTG</p>
3' UTR	TGACTCGAG

Name	Sequence
<b>KIHsv2</b>	
<b>loop</b>	
<b>chimera</b>	
5' UTR	<p>CAT</p> <p>ATGTTGACTAGAAACCCTATTGTCCCCGAAAATCATGTTTCTAA  TCCGATTGTGGATTATGAATTCAACCAAGATCAATCATGCCTCA  TAGTATCGACACCAAAAAGCTTCGATATATACAACGTACATCCG  TTGAAACGTATCATGAGTCAAGAGATGCCCGATGCTGGTACCAT  CAGAATGTTGCATCGCACAAACTACATTGCATTTGTTAGTACAA  AGAAAGAGTTACTTCATATTTGGGATGACGTTAAGAAACAAGAT  ATCACAAGAGTTAAGCTCGATGCTGCTGTTAAGGACTTGTCTTCT  TTCAAGGGAGTTTATAGTAGTATCACAGGGCGATGTGATATCCA  TTTTCAAGTTTGGTAACCCCTGGAATAAGATTACTGAAGACATT  AAGTTCGGAGGAGTGTGCGAGTTTGCCAATGGATTGTTGGTGTGA  CTCCAATGAGTTCAATCTGGGTCAGATCCACGTAAGTAGATTGC  AGACCGATGCAGAGCAGGTTGTTGGAAAAGGTGTCCTAGTGAAG  GCCCATGCCAATCCAGTGAAAATGGTAAGATTAAATAGGAAAGG  AGACATGGTTGCCACTTGTTCGCAGGATGGAACGCTAATTAGAG  TTTTCCAAACGGACAATGGAGTCTTGGTTTCGAGAGTTTAGAAGA  GGACTGGACAGAAGTAGTATTATAGATATGCGTTGGTCACCAGA  TGGATCAAATTAGCTGTTGTCAGTGACAAATGGACGTTACACG  TTTTTGAAGTGTTTCGAAACAACCAATACAGAAACGAATACACCA  GACCACTCTCGTGCCAATGGTTCGAGCCATCCCTTGAAAAATTA  TATACCGAAGGGCCTATGGAGGCCCAAGTATTTGGACTCTGTGT  GGAGCATTGCAATTTTAAATTGAAGGTCAGTAAAGGATCCAAT  GACTGCAAAATCGCATGGATATCAGATACAGGTCTCGTTATAGT  ATGGCCCAATAGAAGGTTGGCAGATACTTTTAAATTGAACTACA  ACGATGACGAGCATGTATGGTGGCTCCAATAAACCAGAAAC  GAAATACCCTTA</p>
3' UTR	TGACTCGAG

Name	Sequence
<b>ScHsv2</b>	
<b>loop</b>	
<b>chimera</b>	
5' UTR	<p>CAT</p> <p>ATGGATGTTTCGTCGACCTATAAGGGAGGCAGTCAACAACAGGAG  GAAACCAAATTTTTGAGCGTTTCGTTTAACCAAGATGATTCGT  GTTTCAGCGTGGCGTTAGAGAATGGATTTTCGTATTTTCAATACA  GATCCATTGACTAGTAAGCTATCGAAAACATTTAAAGAGTCTGC  GACCAACCAATCCAGGGGCACTGGGATTGGCTATACCAGGATGC  TTTATCGTACGAATTACATCGCACTAGTCGGAGGTGGTAAACGA  CCAAGGCATGCTCTAAATAAACTGATCATCTGGGATGATCTTTT  GCAAAGGAAACGATTACTTTGAAGTTTATGTCTTCCATTAAG  ACGTGTTTTTATCTAGGATTCATATTGTGGTAGTCCTGGAGAAC  ACAATAGAGATCTTCCAATTTCAAACCAATCCTCAAAGAATTTG  TCCTATTTTGGATATCCCTCCCAATGGATCAGTGGACTATGTCG  TTTGTAGCAGCAAACATCTCCAGTCGCAAGCATCGCAGTCACAG  TCTAAAATCTTAGAAATCATTGCATTCCTCATCGAATAAATGCGT  AGGCCAAATTCAAGTAGCCGACCTATCACAAATAAAATATAATT  CACAAAACCCGAAGGAATCAGCGCTTTTGCCCACTTCCATCATT  AAAGCACATAAAAATCCCATCAAACCTGGTTAGACTGAACCGTCA  AGGCACCATGGTAGCAACATGTTCCGTCCAGGGTACACTTATAA  GAATCTTCAGTACGCATAACGGTACTTTAATCAAAGAATTTAGA  AGAGGGGTGGACAAGGCGGATATTTACGAGATGAGTTTCAGCCC  CAATGGTAGTAAGTTGGCCGTATTGTCAAATAAGCAAACATTGC  ATATTTTCAAATTTTAAATGACGCCGAGAACAAGAGACACGTA  CTTAAGGATTGGATCAATATAAAGTACTTCAAAGCGAGTGGTC  GATATGCAATGCTCACTTAAAGAACCCAATCTTTGACGCTCACA  GAAATGACAACAGTGGTGTGTAACCTCACGATAACGAGTTCTAT  AAAGACAGATGTAGAATTGGCTGGTGTCAAGACTCTAATAATAG  AGAACAAGACGATTCGTTGGTCTGGTGTGGCAAATTTCTGGGA  TATGGGAGAAATTTGTTATTTTGGAGAAGGAACAACAAGATTCA  TCGAAAACGCATTATTCATTGAATGAAAGCTTGAGGAACGAAGA  TACGAAATCAGCGGGTGAGCCCACCAGATGGGAGTTGGTGAGAG  AATCATGGAGAGAGCTT</p>
3' UTR	<p>TAACTCGAG</p>



**References**

- [1] T. Yorimitsu and D. J. Klionsky, "Autophagy: molecular machinery for self-eating," *Cell Death Differ*, vol. 12 Suppl 2, pp. 1542–52, 2005. 1, 2, 3
- [2] N. Mizushima, T. Yoshimori, and Y. Ohsumi, "The role of atg proteins in autophagosome formation," *Annu Rev Cell Dev Biol*, vol. 27, pp. 107–32, 2011. 1, 3
- [3] S. L. Clark, "Cellular differentiation in the kidneys of newborn mice studied with the electron microscope," *Journal of Biophysical and Biochemical Cytology*, vol. 3, no. 3, pp. 349–, 1957. 1
- [4] M. Thumm, R. Egner, B. Koch, M. Schlumpberger, M. Straub, M. Veenhuis, and D. H. Wolf, "Isolation of autophagocytosis mutants of *saccharomyces cerevisiae*," *FEBS Lett*, vol. 349, no. 2, pp. 275–80, 1994. 1
- [5] T. M. Harding, K. A. Morano, S. V. Scott, and D. J. Klionsky, "Isolation and characterization of yeast mutants in the cytoplasm to vacuole protein targeting pathway," *Journal of Cell Biology*, vol. 131, no. 3, pp. 591–602, 1995. 1
- [6] K. Takeshige, M. Baba, S. Tsuboi, T. Noda, and Y. Ohsumi, "Autophagy in yeast demonstrated with proteinase-deficient mutants and conditions for its induction," *Journal of Cell Biology*, vol. 119, no. 2, pp. 301–311, 1992. 1
- [7] M. Tsukada and Y. Ohsumi, "Isolation and characterization of autophagy-defective mutants of *saccharomyces-cerevisiae*," *FEBS Lett*, vol. 333, no. 1-2, pp. 169–174, 1993. 1
- [8] A. M. Motley, J. M. Nuttall, and E. H. Hettema, "Pex3-anchored atg36 tags peroxisomes for degradation in *saccharomyces cerevisiae*," *EMBO J*, vol. 31, no. 13, pp. 2852–68, 2012. 1
- [9] N. Mizushima, "Autophagy in protein and organelle turnover," *Cold Spring Harb Symp Quant Biol*, vol. 76, pp. 397–402, 2011. 1, 2
- [10] A. S. Rambold and J. Lippincott-Schwartz, "Mechanisms of mitochondria and autophagy crosstalk," *Cell Cycle*, vol. 10, no. 23, pp. 4032–4038, 2011. 2
- [11] C. Kraft, A. Deplazes, M. Sohrmann, and M. Peter, "Mature ribosomes are selectively degraded upon starvation by an autophagy pathway requiring the

- ubp3p/bre5p ubiquitin protease,” *Nat Cell Biol*, vol. 10, no. 5, pp. 602–610, 2008. 2
- [12] J. C. Farre, R. Krick, S. Subramani, and M. Thumm, “Turnover of organelles by autophagy in yeast,” *Curr Opin Cell Biol*, vol. 21, no. 4, pp. 522–530, 2009. 2
- [13] W. W. Li, J. Li, and J. K. Bao, “Microautophagy: lesser-known self-eating,” *Cell Mol Life Sci*, vol. 69, no. 7, pp. 1125–36, 2012. 2
- [14] M. A. Lynch-Day and D. J. Klionsky, “The cvt pathway as a model for selective autophagy,” *FEBS Lett*, vol. 584, no. 7, pp. 1359–1366, 2010. 2
- [15] A. Massey, R. Kiffin, and A. M. Cuervo, “Pathophysiology of chaperone-mediated autophagy,” *Int J Biochem Cell Biol*, vol. 36, no. 12, pp. 2420–34, 2004. 2
- [16] L. A. Knodler and J. Celli, “Eating the strangers within: host control of intracellular bacteria via xenophagy,” *Cellular Microbiology*, vol. 13, no. 9, pp. 1319–1327, 2011. 2
- [17] T. Johansen and T. Lamark, “Selective autophagy mediated by autophagic adapter proteins,” *Autophagy*, vol. 7, no. 3, pp. 279–96, 2011. 2
- [18] H. Cheong, U. Nair, J. F. Geng, and D. J. Klionsky, “The atg1 kinase complex is involved in the regulation of protein recruitment to initiate sequestering vesicle formation for nonspecific autophagy in *saccharomyces cerevisiae*,” *Mol Biol Cell*, vol. 19, no. 2, pp. 668–681, 2008. 3, 69
- [19] A. Kihara, T. Noda, N. Ishihara, and Y. Ohsumi, “Two distinct vps34 phosphatidylinositol 3-kinase complexes function in autophagy and carboxypeptidase y sorting in *saccharomyces cerevisiae*,” *J Cell Biol*, vol. 152, no. 3, pp. 519–30, 2001. 3, 69, 72
- [20] J. M. Backer, “The regulation and function of class iii pi3ks: novel roles for vps34,” *Biochem J*, vol. 410, no. 1, pp. 1–17, 2008. 3, 69
- [21] K. Obara, T. Sekito, K. Niimi, and Y. Ohsumi, “The atg18-atg2 complex is recruited to autophagic membranes via phosphatidylinositol 3-phosphate and exerts an essential function,” *Journal of Biological Chemistry*, vol. 283, no. 35, pp. 23972–23980, 2008. 3, 73, 135

- [22] Y. Fujioka, N. N. Noda, K. Fujii, K. Yoshimoto, Y. Ohsumi, and F. Inagaki, "In vitro reconstitution of plant atg8 and atg12 conjugation systems essential for autophagy," *J Biol Chem*, vol. 283, no. 4, pp. 1921–8, 2008. 3, 66, 69
- [23] N. Mizushima, T. Noda, T. Yoshimori, Y. Tanaka, T. Ishii, M. D. George, D. J. Klionsky, M. Ohsumi, and Y. Ohsumi, "A protein conjugation system essential for autophagy," *Nature*, vol. 395, no. 6700, pp. 395–8, 1998. 3, 49, 51, 52, 69
- [24] R. Krick, R. A. Busse, A. Scacioc, M. Stephan, A. Janshoff, M. Thumm, and K. Kuhnel, "Structural and functional characterization of the two phosphoinositide binding sites of proppins, a beta-propeller protein family," *Proc Natl Acad Sci U S A*, vol. 109, no. 30, pp. E2042–9, 2012. 4, 70, 72, 74, 75, 112, 130, 131, 132, 134, 136, 138
- [25] S. Baskaran, M. J. Ragusa, E. Boura, and J. H. Hurley, "Two-site recognition of phosphatidylinositol 3-phosphate by proppins in autophagy," *Mol Cell*, vol. 47, no. 3, pp. 339–48, 2012. 4, 70, 72, 74, 131, 132, 133, 134, 138
- [26] Y. Watanabe, T. Kobayashi, H. Yamamoto, H. Hoshida, R. Akada, F. Inagaki, Y. Ohsumi, and N. N. Noda, "Structure-based analyses reveal distinct binding sites for atg2 and phosphoinositides in atg18," *J Biol Chem*, vol. 287, no. 38, pp. 31681–90, 2012. 4, 70, 72, 74, 135, 138
- [27] K. Sugawara, N. N. Suzuki, Y. Fujioka, N. Mizushima, Y. Ohsumi, and F. Inagaki, "The crystal structure of microtubule-associated protein light chain 3, a mammalian homologue of *saccharomyces cerevisiae* atg8," *Genes Cells*, vol. 9, no. 7, pp. 611–8, 2004. 4, 52, 137
- [28] K. Sugawara, N. N. Suzuki, Y. Fujioka, N. Mizushima, Y. Ohsumi, and F. Inagaki, "Structural basis for the specificity and catalysis of human atg4b responsible for mammalian autophagy," *J Biol Chem*, vol. 280, no. 48, pp. 40058–65, 2005. 4, 137
- [29] Y. Yamada, N. N. Suzuki, T. Hanada, Y. Ichimura, H. Kumeta, Y. Fujioka, Y. Ohsumi, and F. Inagaki, "The crystal structure of atg3, an autophagy-related ubiquitin carrier protein (e2) enzyme that mediates atg8 lipidation," *J Biol Chem*, vol. 282, no. 11, pp. 8036–43, 2007. 4, 137

- [30] N. N. Noda, K. Satoo, Y. Fujioka, H. Kumeta, K. Ogura, H. Nakatogawa, Y. Ohsumi, and F. Inagaki, "Structural basis of atg8 activation by a homodimeric e1, atg7," *Mol Cell*, vol. 44, no. 3, pp. 462–75, 2011. 4, 138
- [31] N. N. Suzuki, K. Yoshimoto, Y. Fujioka, Y. Ohsumi, and F. Inagaki, "The crystal structure of plant atg12 and its biological implication in autophagy," *Autophagy*, vol. 1, no. 2, pp. 119–26, 2005. 4, 51, 137
- [32] M. Yamaguchi, N. N. Noda, H. Yamamoto, T. Shima, H. Kumeta, Y. Kobashigawa, R. Akada, Y. Ohsumi, and F. Inagaki, "Structural insights into atg10-mediated formation of the autophagy-essential atg12-atg5 conjugate," *Structure*, vol. 20, no. 7, pp. 1244–54, 2012. 4, 138
- [33] Y. Fujioka, N. N. Noda, H. Nakatogawa, Y. Ohsumi, and F. Inagaki, "Dimeric coiled-coil structure of *saccharomyces cerevisiae* atg16 and its functional significance in autophagy," *J Biol Chem*, vol. 285, no. 2, pp. 1508–15, 2010. 4, 68, 69, 137
- [34] X. Li, L. He, K. H. Che, S. F. Funderburk, L. Pan, N. Pan, M. Zhang, Z. Yue, and Y. Zhao, "Imperfect interface of beclin1 coiled-coil domain regulates homodimer and heterodimer formation with atg14l and uvrag," *Nat Commun*, vol. 3, p. 662, 2012. 4, 138
- [35] W. Huang, W. Choi, W. Hu, N. Mi, Q. Guo, M. Ma, M. Liu, Y. Tian, P. Lu, F. L. Wang, H. Deng, L. Liu, N. Gao, L. Yu, and Y. Shi, "Crystal structure and biochemical analyses reveal beclin 1 as a novel membrane binding protein," *Cell Res*, vol. 22, no. 3, pp. 473–89, 2012. 4, 138
- [36] S. Miller, B. Tavshanjian, A. Oleksy, O. Perisic, B. T. Houseman, K. M. Shokat, and R. L. Williams, "Shaping development of autophagy inhibitors with the structure of the lipid kinase vps34," *Science*, vol. 327, no. 5973, pp. 1638–42, 2010. 4, 138
- [37] T. Shintani and D. J. Klionsky, "Autophagy in health and disease: a double-edged sword," *Science*, vol. 306, no. 5698, pp. 990–5, 2004. 5
- [38] D. C. Rubinsztein, P. Codogno, and B. Levine, "Autophagy modulation as a potential therapeutic target for diverse diseases," *Nature Reviews Drug Discovery*, vol. 11, no. 9, pp. 709–U84, 2012. 5

- [39] A. Fleming, T. Noda, T. Yoshimori, and D. C. Rubinsztein, "Chemical modulators of autophagy as biological probes and potential therapeutics," *Nature Chemical Biology*, vol. 7, no. 1, pp. 9–17, 2011. 5
- [40] M. Komatsu and Y. Ichimura, "Selective autophagy regulates various cellular functions," *Genes to Cells*, vol. 15, no. 9, pp. 923–933, 2010. 5
- [41] F. W. Studier, "Protein production by auto-induction in high density shaking cultures," *Protein Expr Purif*, vol. 41, no. 1, pp. 207–34, 2005. 12
- [42] G. D. Van Duyne, R. F. Standaert, P. A. Karplus, S. L. Schreiber, and J. Clardy, "Atomic structures of the human immunophilin fkbp-12 complexes with fk506 and rapamycin," *J Mol Biol*, vol. 229, no. 1, pp. 105–24, 1993. 13
- [43] D. Hanahan, "Studies on transformation of escherichia coli with plasmids," *J Mol Biol*, vol. 166, no. 4, pp. 557–80, 1983. 22
- [44] W. J. Dower, J. F. Miller, and C. W. Ragsdale, "High efficiency transformation of e. coli by high voltage electroporation," *Nucleic Acids Res*, vol. 16, no. 13, pp. 6127–45, 1988. 22
- [45] D. J. Fitzgerald, P. Berger, C. Schaffitzel, K. Yamada, T. J. Richmond, and I. Berger, "Protein complex expression by using multigene baculoviral vectors," *Nat Methods*, vol. 3, no. 12, pp. 1021–32, 2006. 23, 53, 76
- [46] C. Bieniossek, Y. Nie, D. Frey, N. Olieric, C. Schaffitzel, I. Collinson, C. Romier, P. Berger, T. J. Richmond, M. O. Steinmetz, and I. Berger, "Automated unrestricted multigene recombineering for multiprotein complex production," *Nat Methods*, vol. 6, no. 6, pp. 447–50, 2009. 29, 120
- [47] U. K. Laemmli, "Cleavage of structural proteins during the assembly of the head of bacteriophage t4," *Nature*, vol. 227, no. 5259, pp. 680–5, 1970. 36
- [48] H. Towbin, T. Staehelin, and J. Gordon, "Electrophoretic transfer of proteins from polyacrylamide gels to nitrocellulose sheets: procedure and some applications," *Proc Natl Acad Sci U S A*, vol. 76, no. 9, pp. 4350–4, 1979. 36
- [49] H. Towbin, T. Staehelin, and J. Gordon, "Immunoblotting in the clinical laboratory," *J Clin Chem Clin Biochem*, vol. 27, no. 8, pp. 495–501, 1989. 36

- [50] F. H. Niesen, H. Berglund, and M. Vedadi, “The use of differential scanning fluorimetry to detect ligand interactions that promote protein stability,” *Nat Protoc*, vol. 2, no. 9, pp. 2212–21, 2007. 37
- [51] S. M. Kelly, T. J. Jess, and N. C. Price, “How to study proteins by circular dichroism,” *Biochim Biophys Acta*, vol. 1751, no. 2, pp. 119–39, 2005. 38
- [52] A. Dong, X. Xu, A. M. Edwards, C. Chang, M. Chruszcz, M. Cuff, M. Cymborowski, R. Di Leo, O. Egorova, E. Evdokimova, E. Filippova, J. Gu, J. Guthrie, A. Ignatchenko, A. Joachimiak, N. Klostermann, Y. Kim, Y. Korniyenko, W. Minor, Q. Que, A. Savchenko, T. Skarina, K. Tan, A. Yakunin, A. Yee, V. Yim, R. Zhang, H. Zheng, M. Akutsu, C. Arrowsmith, G. V. Avvakumov, A. Bochkarev, L. G. Dahlgren, S. Dhe-Paganon, S. Dimov, L. Dombrowski, J. Finerty, P., S. Flodin, A. Flores, S. Graslund, M. Hammerstrom, M. D. Herman, B. S. Hong, R. Hui, I. Johansson, Y. Liu, M. Nilsson, L. Nedyalkova, P. Nordlund, T. Nyman, J. Min, H. Ouyang, H. W. Park, C. Qi, W. Rabeh, L. Shen, Y. Shen, D. Sukumard, W. Tempel, Y. Tong, L. Tresagues, M. Vedadi, J. R. Walker, J. Weigelt, M. Welin, H. Wu, T. Xiao, H. Zeng, and H. Zhu, “In situ proteolysis for protein crystallization and structure determination,” *Nat Methods*, vol. 4, no. 12, pp. 1019–21, 2007. 39
- [53] P. Edman, “A method for the determination of amino acid sequence in peptides,” *Arch Biochem*, vol. 22, no. 3, p. 475, 1949. 39
- [54] C. G. Schuette, K. Hatsuzawa, M. Margittai, A. Stein, D. Riedel, P. Kuster, M. Konig, C. Seidel, and R. Jahn, “Determinants of liposome fusion mediated by synaptic snare proteins,” *Proc Natl Acad Sci U S A*, vol. 101, no. 9, pp. 2858–63, 2004. 40
- [55] K. Matsuoka, L. Orci, M. Amherdt, S. Y. Bednarek, S. Hamamoto, R. Schekman, and T. Yeung, “CoppII-coated vesicle formation reconstituted with purified coat proteins and chemically defined liposomes,” *Cell*, vol. 93, no. 2, pp. 263–75, 1998. 40
- [56] H. Eibl and W. E. Lands, “A new, sensitive determination of phosphate,” *Anal Biochem*, vol. 30, no. 1, pp. 51–7, 1969. 41
- [57] S. Castorph, S. Schwarz Henriques, M. Holt, D. Riedel, R. Jahn, and T. Salditt, “Synaptic vesicles studied by dynamic light scattering,” *Eur Phys J E Soft Matter*, vol. 34, no. 6, pp. 1–11, 2011. 41

- [58] J. M. Hernandez, A. Stein, E. Behrmann, D. Riedel, A. Cypionka, Z. Farsi, P. J. Walla, S. Raunser, and R. Jahn, "Membrane fusion intermediates via directional and full assembly of the snare complex," *Science*, vol. 336, no. 6088, pp. 1581–4, 2012. 41
- [59] E. Saridakis, S. Khurshid, L. Govada, Q. Phan, D. Hawkins, G. V. Crichlow, E. Lolis, S. M. Reddy, and N. E. Chayen, "Protein crystallization facilitated by molecularly imprinted polymers," *Proc Natl Acad Sci U S A*, vol. 108, no. 27, pp. 11081–6, 2011. 47, 99
- [60] J. Kim, W. P. Huang, and D. J. Klionsky, "Membrane recruitment of aut7p in the autophagy and cytoplasm to vacuole targeting pathways requires aut1p, aut2p, and the autophagy conjugation complex," *J Cell Biol*, vol. 152, no. 1, pp. 51–64, 2001. 49, 52, 59
- [61] K. Suzuki, T. Kirisako, Y. Kamada, N. Mizushima, T. Noda, and Y. Ohsumi, "The pre-autophagosomal structure organized by concerted functions of apg genes is essential for autophagosome formation," *EMBO J*, vol. 20, no. 21, pp. 5971–81, 2001. 49, 52, 67
- [62] N. N. Noda, Y. Ohsumi, and F. Inagaki, "Atg systems from the protein structural point of view," *Chem Rev*, vol. 109, no. 4, pp. 1587–98, 2009. 49
- [63] M. Komatsu, I. Tanida, T. Ueno, M. Ohsumi, Y. Ohsumi, and E. Kominami, "The c-terminal region of an apg7p/cvt2p is required for homodimerization and is essential for its e1 activity and e1-e2 complex formation," *J Biol Chem*, vol. 276, no. 13, pp. 9846–54, 2001. 49
- [64] N. Mizushima, T. Noda, and Y. Ohsumi, "Apg16p is required for the function of the apg12p-apg5p conjugate in the yeast autophagy pathway," *EMBO J*, vol. 18, no. 14, pp. 3888–96, 1999. 49, 53, 59
- [65] N. Mizushima, A. Kuma, Y. Kobayashi, A. Yamamoto, M. Matsubae, T. Takao, T. Natsume, Y. Ohsumi, and T. Yoshimori, "Mouse apg16l, a novel wd-repeat protein, targets to the autophagic isolation membrane with the apg12-apg5 conjugate," *J Cell Sci*, vol. 116, no. Pt 9, pp. 1679–88, 2003. 49, 53, 68, 74
- [66] Y. Ichimura, T. Kirisako, T. Takao, Y. Satomi, Y. Shimonishi, N. Ishihara, N. Mizushima, I. Tanida, E. Kominami, M. Ohsumi, T. Noda, and Y. Ohsumi,

- “A ubiquitin-like system mediates protein lipidation,” *Nature*, vol. 408, no. 6811, pp. 488–92, 2000. 49, 52, 61
- [67] T. Kirisako, Y. Ichimura, H. Okada, Y. Kabeya, N. Mizushima, T. Yoshimori, M. Ohsumi, T. Takao, T. Noda, and Y. Ohsumi, “The reversible modification regulates the membrane-binding state of apg8/aut7 essential for autophagy and the cytoplasm to vacuole targeting pathway,” *J Cell Biol*, vol. 151, no. 2, pp. 263–76, 2000. 50
- [68] I. Tanida, N. Mizushima, M. Kiyooka, M. Ohsumi, T. Ueno, Y. Ohsumi, and E. Kominami, “Apg7p/cvt2p: A novel protein-activating enzyme essential for autophagy,” *Mol Biol Cell*, vol. 10, no. 5, pp. 1367–79, 1999. 50
- [69] T. Hanada, N. N. Noda, Y. Satomi, Y. Ichimura, Y. Fujioka, T. Takao, F. Inagaki, and Y. Ohsumi, “The atg12-atg5 conjugate has a novel e3-like activity for protein lipidation in autophagy,” *J Biol Chem*, vol. 282, no. 52, pp. 37298–302, 2007. 50, 64, 66, 67, 68
- [70] N. Fujita, T. Itoh, H. Omori, M. Fukuda, T. Noda, and T. Yoshimori, “The atg16l complex specifies the site of lc3 lipidation for membrane biogenesis in autophagy,” *Mol Biol Cell*, vol. 19, no. 5, pp. 2092–100, 2008. 50
- [71] L. Radoshevich, L. Murrow, N. Chen, E. Fernandez, S. Roy, C. Fung, and J. Debnath, “Atg12 conjugation to atg3 regulates mitochondrial homeostasis and cell death,” *Cell*, vol. 142, no. 4, pp. 590–600, 2010. 50
- [72] J. Romanov, M. Walczak, I. Ibricu, S. Schuchner, E. Ogris, C. Kraft, and S. Martens, “Mechanism and functions of membrane binding by the atg5-atg12/atg16 complex during autophagosome formation,” *EMBO J*, 2012. 51
- [73] H. Nakatogawa, Y. Ichimura, and Y. Ohsumi, “Atg8, a ubiquitin-like protein required for autophagosome formation, mediates membrane tethering and hemifusion,” *Cell*, vol. 130, no. 1, pp. 165–78, 2007. 51
- [74] Y. Xin, L. Yu, Z. Chen, L. Zheng, Q. Fu, J. Jiang, P. Zhang, R. Gong, and S. Zhao, “Cloning, expression patterns, and chromosome localization of three human and two mouse homologues of gaba(a) receptor-associated protein,” *Genomics*, vol. 74, no. 3, pp. 408–13, 2001. 52
- [75] H. He, Y. Dang, F. Dai, Z. Guo, J. Wu, X. She, Y. Pei, Y. Chen, W. Ling, C. Wu, S. Zhao, J. O. Liu, and L. Yu, “Post-translational modifications of three members



- of the human map1lc3 family and detection of a novel type of modification for map1lc3b,” *J Biol Chem*, vol. 278, no. 31, pp. 29278–87, 2003. 52
- [76] G. Bjorkoy, T. Lamark, A. Brech, H. Outzen, M. Perander, A. Overvatn, H. Stenmark, and T. Johansen, “p62/sqstm1 forms protein aggregates degraded by autophagy and has a protective effect on huntingtin-induced cell death,” *J Cell Biol*, vol. 171, no. 4, pp. 603–14, 2005. 52
- [77] V. Kirkin, T. Lamark, Y. S. Sou, G. Bjorkoy, J. L. Nunn, J. A. Bruun, E. Shvets, D. G. McEwan, T. H. Clausen, P. Wild, I. Bilusic, J. P. Theurillat, A. Overvatn, T. Ishii, Z. Elazar, M. Komatsu, I. Dikic, and T. Johansen, “A role for nbr1 in autophagosomal degradation of ubiquitinated substrates,” *Mol Cell*, vol. 33, no. 4, pp. 505–16, 2009. 52
- [78] Y. Sagiv, A. Legesse-Miller, A. Porat, and Z. Elazar, “Gate-16, a membrane transport modulator, interacts with nsf and the golgi v-snare gos-28,” *EMBO J*, vol. 19, no. 7, pp. 1494–504, 2000. 52
- [79] J. T. Kittler, P. Rostaing, G. Schiavo, J. M. Fritschy, R. Olsen, A. Triller, and S. J. Moss, “The subcellular distribution of gabarap and its ability to interact with nsf suggest a role for this protein in the intracellular transport of gaba(a) receptors,” *Mol Cell Neurosci*, vol. 18, no. 1, pp. 13–25, 2001. 52
- [80] Y. Kabeya, N. Mizushima, A. Yamamoto, S. Oshitani-Okamoto, Y. Ohsumi, and T. Yoshimori, “Lc3, gabarap and gate16 localize to autophagosomal membrane depending on form-ii formation,” *J Cell Sci*, vol. 117, no. Pt 13, pp. 2805–12, 2004. 52, 69
- [81] Y. Paz, Z. Elazar, and D. Fass, “Structure of gate-16, membrane transport modulator and mammalian ortholog of autophagocytosis factor aut7p,” *J Biol Chem*, vol. 275, no. 33, pp. 25445–50, 2000. 52
- [82] M. Schwarten, M. Stoldt, J. Mohrluder, and D. Willbold, “Solution structure of atg8 reveals conformational polymorphism of the n-terminal domain,” *Biochem Biophys Res Commun*, vol. 395, no. 3, pp. 426–31, 2010. 52, 138
- [83] H. Kumeta, M. Watanabe, H. Nakatogawa, M. Yamaguchi, K. Ogura, W. Adachi, Y. Fujioka, N. N. Noda, Y. Ohsumi, and F. Inagaki, “The nmr structure of the autophagy-related protein atg8,” *J Biomol NMR*, vol. 47, no. 3, pp. 237–41, 2010. 52, 138

- [84] M. Matsushita, N. N. Suzuki, K. Obara, Y. Fujioka, Y. Ohsumi, and F. Inagaki, "Structure of atg5.atg16, a complex essential for autophagy," *J Biol Chem*, vol. 282, no. 9, pp. 6763–72, 2007. 53, 137
- [85] W. J. Netzer and F. U. Hartl, "Recombination of protein domains facilitated by co-translational folding in eukaryotes," *Nature*, vol. 388, no. 6640, pp. 343–9, 1997. 53
- [86] J. Fernandez and J. HÄuffler, *Gene Expression Systems - Using nature for the art of expression*. San Diego: Academic press, 1999. 53
- [87] I. Tanida, Y. S. Sou, J. Ezaki, N. Minematsu-Ikeguchi, T. Ueno, and E. Kominami, "Hsatg4b/hsapg4b/autophagin-1 cleaves the carboxyl termini of three human atg8 homologues and delipidates microtubule-associated protein light chain 3- and gabaa receptor-associated protein-phospholipid conjugates," *J Biol Chem*, vol. 279, no. 35, pp. 36268–76, 2004. 61
- [88] Y. Shao, Z. Gao, T. Feldman, and X. Jiang, "Stimulation of atg12-atg5 conjugation by ribonucleic acid," *Autophagy*, vol. 3, no. 1, pp. 10–6, 2007. 66
- [89] N. N. Noda, Y. Fujioka, Y. Ohsumi, and F. Inagaki, "Crystallization of the atg12-atg5 conjugate bound to atg16 by the free-interface diffusion method," *J Synchrotron Radiat*, vol. 15, no. Pt 3, pp. 266–8, 2008. 66
- [90] Y. Ichimura, Y. Imamura, K. Emoto, M. Umeda, T. Noda, and Y. Ohsumi, "In vivo and in vitro reconstitution of atg8 conjugation essential for autophagy," *J Biol Chem*, vol. 279, no. 39, pp. 40584–92, 2004. 67
- [91] Y. S. Sou, I. Tanida, M. Komatsu, T. Ueno, and E. Kominami, "Phosphatidylserine in addition to phosphatidylethanolamine is an in vitro target of the mammalian atg8 modifiers, lc3, gabarap, and gate-16," *J Biol Chem*, vol. 281, no. 6, pp. 3017–24, 2006. 67
- [92] N. Mizushima, A. Yamamoto, M. Hatano, Y. Kobayashi, Y. Kabeya, K. Suzuki, T. Tokuhiisa, Y. Ohsumi, and T. Yoshimori, "Dissection of autophagosome formation using apg5-deficient mouse embryonic stem cells," *Journal of Cell Biology*, vol. 152, no. 4, pp. 657–667, 2001. 67, 69
- [93] I. Tanida, T. Nishitani, T. Nemoto, T. Ueno, and E. Kominami, "Mammalian apg12p, but not the apg12p.apg5p conjugate, facilitates lc3 processing," *Biochem Biophys Res Commun*, vol. 296, no. 5, pp. 1164–70, 2002. 67

- [94] A. Kuma, N. Mizushima, N. Ishihara, and Y. Ohsumi, "Formation of the approximately 350-kda apg12-apg5.apg16 multimeric complex, mediated by apg16 oligomerization, is essential for autophagy in yeast," *J Biol Chem*, vol. 277, no. 21, pp. 18619–25, 2002. 68
- [95] E. L. Axe, S. A. Walker, M. Manifava, P. Chandra, H. L. Roderick, A. Habermann, G. Griffiths, and N. T. Ktistakis, "Autophagosome formation from membrane compartments enriched in phosphatidylinositol 3-phosphate and dynamically connected to the endoplasmic reticulum," *J Cell Biol*, vol. 182, no. 4, pp. 685–701, 2008. 69, 72
- [96] M. Hayashi-Nishino, N. Fujita, T. Noda, A. Yamaguchi, T. Yoshimori, and A. Yamamoto, "A subdomain of the endoplasmic reticulum forms a cradle for autophagosome formation," *Nat Cell Biol*, vol. 11, no. 12, pp. 1433–7, 2009. 69
- [97] P. Yla-Anttila, H. Vihinen, E. Jokita, and E. L. Eskelinen, "3d tomography reveals connections between the phagophore and endoplasmic reticulum," *Autophagy*, vol. 5, no. 8, pp. 1180–1185, 2009. 69
- [98] D. W. Hailey, A. S. Rambold, P. Satpute-Krishnan, K. Mitra, R. Sougrat, P. K. Kim, and J. Lippincott-Schwartz, "Mitochondria supply membranes for autophagosome biogenesis during starvation," *Cell*, vol. 141, no. 4, pp. 656–667, 2010. 69
- [99] B. Ravikumar, K. Moreau, L. Jahreiss, C. Puri, and D. C. Rubinsztein, "Plasma membrane contributes to the formation of pre-autophagosomal structures," *Nat Cell Biol*, vol. 12, no. 8, pp. 747–57, 2010. 69
- [100] K. Moreau, B. Ravikumar, M. Renna, C. Puri, and D. C. Rubinsztein, "Autophagosome precursor maturation requires homotypic fusion," *Cell*, vol. 146, no. 2, pp. 303–17, 2011. 69
- [101] A. R. J. Young, E. Y. W. Chan, X. W. Hu, R. Koch, S. G. Crawshaw, S. High, D. W. Hailey, J. Lippincott-Schwartz, and S. A. Tooze, "Starvation and ulk1-dependent cycling of mammalian atg9 between the tgn and endosomes," *J Cell Sci*, vol. 119, no. 18, pp. 3888–3900, 2006. 69
- [102] J. F. Geng, U. Nair, K. Yasumura-Yorimitsu, and D. J. Klionsky, "Post-golgi sec proteins are required for autophagy in *saccharomyces cerevisiae*," *Mol Biol Cell*, vol. 21, no. 13, pp. 2257–2269, 2010. 69

- [103] Y. Ohashi and S. Munro, "Membrane delivery to the yeast autophagosome from the golgi-endosomal system," *Mol Biol Cell*, vol. 21, no. 22, pp. 3998–4008, 2010. 69
- [104] S. A. Tooze and T. Yoshimori, "The origin of the autophagosomal membrane," *Nat Cell Biol*, vol. 12, no. 9, pp. 831–5, 2010. 69
- [105] A. van der Vaart, J. Griffith, and F. Reggiori, "Exit from the golgi is required for the expansion of the autophagosomal phagophore in yeast *saccharomyces cerevisiae*," *Mol Biol Cell*, vol. 21, no. 13, pp. 2270–84, 2010. 69
- [106] Y. Kamada, T. Funakoshi, T. Shintani, K. Nagano, M. Ohsumi, and Y. Ohsumi, "Tor-mediated induction of autophagy via an apg1 protein kinase complex," *J Cell Biol*, vol. 150, no. 6, pp. 1507–13, 2000. 69
- [107] T. Kawamata, Y. Kamada, Y. Kabeya, T. Sekito, and Y. Ohsumi, "Organization of the pre-autophagosomal structure responsible for autophagosome formation," *Mol Biol Cell*, vol. 19, no. 5, pp. 2039–2050, 2008. 69
- [108] I. G. Ganley, D. H. Lam, J. R. Wang, X. J. Ding, S. Chen, and X. J. Jiang, "Ulk1 center dot atg13 center dot fip200 complex mediates mtor signaling and is essential for autophagy," *Journal of Biological Chemistry*, vol. 284, no. 18, pp. 12297–12305, 2009. 69
- [109] C. H. Jung, C. B. Jun, S. H. Ro, Y. M. Kim, N. M. Otto, J. Cao, M. Kundu, and D. H. Kim, "Ulk-atg13-fip200 complexes mediate mtor signaling to the autophagy machinery," *Mol Biol Cell*, vol. 20, no. 7, pp. 1992–2003, 2009. 69
- [110] T. Lang, S. Reiche, M. Straub, M. Bredschneider, and M. Thumm, "Autophagy and the cvt pathway both depend on aut9," *J Bacteriol*, vol. 182, no. 8, pp. 2125–2133, 2000. 69
- [111] T. Noda, J. Kim, W. P. Huang, M. Baba, C. Tokunaga, Y. Ohsumi, and D. J. Klionsky, "Apg9p/cvt7p is an integral membrane protein required for transport vesicle formation in the cvt and autophagy pathways," *Journal of Cell Biology*, vol. 148, no. 3, pp. 465–479, 2000. 69
- [112] R. Krick, S. Henke, J. Tolstrup, and M. Thumm, "Dissecting the localization and function of atg18, atg21 and ygr223c," *Autophagy*, vol. 4, no. 7, pp. 896–910, 2008. 69, 72, 73

- [113] A. Petiot, E. Ogier-Denis, E. F. C. Blommaert, A. J. Meijer, and P. Codogno, "Distinct classes of phosphatidylinositol 3'-kinases are involved in signaling pathways that control macroautophagy in ht-29 cells," *Journal of Biological Chemistry*, vol. 275, no. 2, pp. 992–998, 2000. 70
- [114] H. Knaevelsrud and A. Simonsen, "Lipids in autophagy: Constituents, signaling molecules and cargo with relevance to disease," *Biochimica Et Biophysica Acta-Molecular and Cell Biology of Lipids*, vol. 1821, no. 8, pp. 1133–1145, 2012. 70
- [115] K. Obara and Y. Ohsumi, "Ptdins 3-kinase orchestrates autophagosome formation in yeast," *J Lipids*, vol. 2011, p. 498768, 2011. 70
- [116] K. Obara, T. Noda, K. Niimi, and Y. Ohsumi, "Transport of phosphatidylinositol 3-phosphate into the vacuole via autophagic membranes in *saccharomyces cerevisiae*," *Genes Cells*, vol. 13, no. 6, pp. 537–47, 2008. 70
- [117] E. Cebollero, A. van der Vaart, M. Zhao, E. Rieter, D. J. Klionsky, J. B. Helms, and F. Reggiori, "Phosphatidylinositol-3-phosphate clearance plays a key role in autophagosome completion," *Curr Biol*, vol. 22, no. 17, pp. 1545–53, 2012. 70
- [118] T. G. Kutateladze, "Translation of the phosphoinositide code by pi effectors," *Nature Chemical Biology*, vol. 6, no. 7, pp. 507–513, 2010. 70
- [119] T. J. Kubiseski, Y. M. Chook, W. E. Parris, M. Rozakis-Adcock, and T. Pawson, "High affinity binding of the pleckstrin homology domain of *msos1* to phosphatidylinositol (4,5)-bisphosphate," *J Biol Chem*, vol. 272, no. 3, pp. 1799–804, 1997. 70
- [120] M. A. Lemmon and K. M. Ferguson, "Signal-dependent membrane targeting by pleckstrin homology (ph) domains," *Biochem J*, vol. 350 Pt 1, pp. 1–18, 2000. 70
- [121] J. P. DiNitto and D. G. Lambright, "Membrane and juxtamembrane targeting by ph and ptb domains," *Biochim Biophys Acta*, vol. 1761, no. 8, pp. 850–67, 2006. 70
- [122] M. G. Ford, I. G. Mills, B. J. Peter, Y. Vallis, G. J. Praefcke, P. R. Evans, and H. T. McMahon, "Curvature of clathrin-coated pits driven by epsin," *Nature*, vol. 419, no. 6905, pp. 361–6, 2002. 70

- [123] M. G. Ford, B. M. Pearse, M. K. Higgins, Y. Vallis, D. J. Owen, A. Gibson, C. R. Hopkins, P. R. Evans, and H. T. McMahon, "Simultaneous binding of ptdins(4,5)p2 and clathrin by ap180 in the nucleation of clathrin lattices on membranes," *Science*, vol. 291, no. 5506, pp. 1051–5, 2001. 70
- [124] T. Itoh, S. Koshiba, T. Kigawa, A. Kikuchi, S. Yokoyama, and T. Takenawa, "Role of the enth domain in phosphatidylinositol-4,5-bisphosphate binding and endocytosis," *Science*, vol. 291, no. 5506, pp. 1047–51, 2001. 70
- [125] W. Cho and R. V. Stahelin, "Membrane binding and subcellular targeting of c2 domains," *Biochim Biophys Acta*, vol. 1761, no. 8, pp. 838–49, 2006. 70
- [126] T. Itoh and P. De Camilli, "Bar, f-bar (efc) and enth/anth domains in the regulation of membrane-cytosol interfaces and membrane curvature," *Biochim Biophys Acta*, vol. 1761, no. 8, pp. 897–912, 2006. 70
- [127] K. Hamada, T. Shimizu, T. Matsui, S. Tsukita, and T. Hakoshima, "Structural basis of the membrane-targeting and unmasking mechanisms of the radixin ferm domain," *EMBO J*, vol. 19, no. 17, pp. 4449–62, 2000. 70
- [128] T. G. Kutateladze, "Mechanistic similarities in docking of the fyve and px domains to phosphatidylinositol 3-phosphate containing membranes," *Progress in Lipid Research*, vol. 46, no. 6, pp. 315–327, 2007. 70, 133
- [129] T. G. Kutateladze, "Phosphatidylinositol 3-phosphate recognition and membrane docking by the fyve domain," *Biochimica Et Biophysica Acta-Molecular and Cell Biology of Lipids*, vol. 1761, no. 8, pp. 868–877, 2006. 70, 133
- [130] H. C. Dippold, M. M. Ng, S. E. Farber-Katz, S. K. Lee, M. L. Kerr, M. C. Peterman, R. Sim, P. A. Wiharto, K. A. Galbraith, S. Madhavarapu, G. J. Fuchs, T. Meerloo, M. G. Farquhar, H. Zhou, and S. J. Field, "Golp3 bridges phosphatidylinositol-4-phosphate and actomyosin to stretch and shape the golgi to promote budding," *Cell*, vol. 139, no. 2, pp. 337–51, 2009. 70
- [131] C. S. Wood, K. R. Schmitz, N. J. Bessman, T. G. Setty, K. M. Ferguson, and C. G. Burd, "Ptdins4p recognition by vps74/golph3 links ptdins 4-kinase signaling to retrograde golgi trafficking," *J Cell Biol*, vol. 187, no. 7, pp. 967–75, 2009. 70
- [132] P. Zimmermann, "The prevalence and significance of pdz domain-phosphoinositide interactions," *Biochim Biophys Acta*, vol. 1761, no. 8, pp. 947–56, 2006. 70

- [133] S. K. Dove, R. C. Piper, R. K. McEwen, J. W. Yu, M. C. King, D. C. Hughes, J. Thuring, A. B. Holmes, F. T. Cooke, R. H. Michell, P. J. Parker, and M. A. Lemmon, "Svp1p defines a family of phosphatidylinositol 3,5-bisphosphate effectors," *EMBO J*, vol. 23, no. 9, pp. 1922–33, 2004. 70, 72, 96, 99, 105, 106, 130, 132
- [134] L. F. Seet and W. J. Hong, "The phox (px) domain proteins and membrane traffic," *Biochimica Et Biophysica Acta-Molecular and Cell Biology of Lipids*, vol. 1761, no. 8, pp. 878–896, 2006. 70
- [135] C. P. Ponting, "Novel domains in nadph oxidase subunits, sorting nexins, and ptdins 3-kinases: Binding partners of sh3 domains?," *Protein Science*, vol. 5, no. 11, pp. 2353–2357, 1996. 70
- [136] J. W. Yu and M. A. Lemmon, "All phox homology (px) domains from *saccharomyces cerevisiae* specifically recognize phosphatidylinositol 3-phosphate," *Journal of Biological Chemistry*, vol. 276, no. 47, pp. 44179–44184, 2001. 70
- [137] S. Santagata, T. J. Boggon, C. L. Baird, C. A. Gomez, J. Zhao, W. S. Shan, D. G. Myszka, and L. Shapiro, "G-protein signaling through tubby proteins," *Science*, vol. 292, no. 5524, pp. 2041–2050, 2001. 70
- [138] Z. Szentpetery, A. Balla, Y. J. Kim, M. A. Lemmon, and T. Balla, "Live cell imaging with protein domains capable of recognizing phosphatidylinositol 4,5-bisphosphate; a comparative study," *Bmc Cell Biology*, vol. 10, 2009. 70
- [139] M. A. Lemmon, "Membrane recognition by phospholipid-binding domains," *Nature Reviews Molecular Cell Biology*, vol. 9, no. 2, pp. 99–111, 2008. 71, 135
- [140] W. Fan, A. Nassiri, and Q. Zhong, "Autophagosome targeting and membrane curvature sensing by barkor/atg14(1)," *Proc Natl Acad Sci U S A*, vol. 108, no. 19, pp. 7769–7774, 2011. 72
- [141] D. C. Nice, T. K. Sato, P. E. Stromhaug, S. D. Emr, and D. J. Klionsky, "Cooperative binding of the cytoplasm to vacuole targeting pathway proteins, cvt13 and cvt20, to phosphatidylinositol 3-phosphate at the pre-autophagosomal structure is required for selective autophagy," *Journal of Biological Chemistry*, vol. 277, no. 33, pp. 30198–30207, 2002. 72

- [142] F. Reggiori, K. A. Tucker, P. E. Stromhaug, and D. J. Klionsky, "The atg1-atg13 complex regulates atg9 and atg23 retrieval transport from the pre-autophagosomal structure," *Dev Cell*, vol. 6, no. 1, pp. 79–90, 2004. 72, 73, 135
- [143] J. A. Efe, R. J. Botelho, and S. D. Emr, "Atg18 regulates organelle morphology and fab1 kinase activity independent of its membrane recruitment by phosphatidylinositol 3,5-bisphosphate," *Mol Biol Cell*, vol. 18, no. 11, pp. 4232–44, 2007. 72, 73, 135
- [144] P. E. Stromhaug, F. Reggiori, J. Guan, C. W. Wang, and D. J. Klionsky, "Atg21 is a phosphoinositide binding protein required for efficient lipidation and localization of atg8 during uptake of aminopeptidase i by selective autophagy," *Mol Biol Cell*, vol. 15, no. 8, pp. 3553–66, 2004. 72, 73, 99, 105, 130, 135
- [145] S. I. Yamashita, M. Oku, and Y. Sakai, "Functions of pi4p and sterol glucoside are necessary for the synthesis of a nascent membrane structure during pexophagy," *Autophagy*, vol. 3, no. 1, pp. 35–37, 2007. 72
- [146] M. Asakura, S. Ninomiya, M. Sugimoto, M. Oku, S. Yamashita, T. Okuno, Y. Sakai, and Y. Takano, "Atg26-mediated pexophagy is required for host invasion by the plant pathogenic fungus *colletotrichum orbiculare*," *Plant Cell*, vol. 21, no. 4, pp. 1291–1304, 2009. 72
- [147] S. Yamashita, M. Oku, Y. Wasada, Y. Ano, and Y. Sakai, "Pi4p-signaling pathway for the synthesis of a nascent membrane structure in selective autophagy," *J Cell Biol*, vol. 173, no. 5, pp. 709–17, 2006. 72
- [148] A. E. Wurmser and S. D. Emr, "Novel ptdins(3)p-binding protein etf1 functions as an effector of the vps34 ptdins 3-kinase in autophagy," *Journal of Cell Biology*, vol. 158, no. 4, pp. 761–772, 2002. 72
- [149] P. Isakson, P. Holland, and A. Simonsen, "The role of alfy in selective autophagy," *Cell Death Differ*, 2012. 72, 74
- [150] S. Pankiv, E. A. Alemu, A. Brech, J. A. Bruun, T. Lamark, A. Overvatn, G. Bjorkoy, and T. Johansen, "Fyco1 is a rab7 effector that binds to lc3 and pi3p to mediate microtubule plus end-directed vesicle transport," *Journal of Cell Biology*, vol. 188, no. 2, pp. 253–269, 2010. 72
- [151] R. Krick, J. Tolstrup, A. Appelles, S. Henke, and M. Thumm, "The relevance of the phosphatidylinositolphosphat-binding motif frgt of atg18 and atg21 for the



- cvt pathway and autophagy,” *FEBS Lett*, vol. 580, no. 19, pp. 4632–8, 2006. 72, 73, 99, 105, 107, 130
- [152] T. Proikas-Cezanne, S. Waddell, A. Gaugel, T. Frickey, A. Lupas, and A. Nordheim, “Wipi-1alpha (wipi49), a member of the novel 7-bladed wipi protein family, is aberrantly expressed in human cancer and is linked to starvation-induced autophagy,” *Oncogene*, vol. 23, no. 58, pp. 9314–25, 2004. 73
- [153] H. E. Polson, J. de Lartigue, D. J. Rigden, M. Reedijk, S. Urbe, M. J. Clague, and S. A. Tooze, “Mammalian atg18 (wipi2) localizes to omegasome-anchored phagophores and positively regulates lc3 lipidation,” *Autophagy*, vol. 6, no. 4, 2010. 73
- [154] H. Barth, K. Meiling-Wesse, U. D. Epple, and M. Thumm, “Autophagy and the cytoplasm to vacuole targeting pathway both require aut10p,” *FEBS Lett*, vol. 508, no. 1, pp. 23–8, 2001. 73
- [155] J. Guan, P. E. Stromhaug, M. D. George, P. Habibzadegah-Tari, A. Bevan, J. Dunn, W. A., and D. J. Klionsky, “Cvt18/gsa12 is required for cytoplasm-to-vacuole transport, pexophagy, and autophagy in *saccharomyces cerevisiae* and *pichia pastoris*,” *Mol Biol Cell*, vol. 12, no. 12, pp. 3821–38, 2001. 73
- [156] K. Meiling-Wesse, H. Barth, C. Voss, E. L. Eskelinen, U. D. Epple, and M. Thumm, “Atg21 is required for effective recruitment of atg8 to the preautophagosomal structure during the cvt pathway,” *J Biol Chem*, vol. 279, no. 36, pp. 37741–50, 2004. 73, 135
- [157] C. U. Stirnimann, E. Petsalaki, R. B. Russell, and C. W. Muller, “Wd40 proteins propel cellular networks,” *Trends Biochem Sci*, vol. 35, no. 10, pp. 565–74, 2010. 73, 74, 76
- [158] L. Janda, P. Tichy, J. Spizek, and M. Petricek, “A deduced *thermomonospora curvata* protein containing serine/threonine protein kinase and wd-repeat domains,” *J Bacteriol*, vol. 178, no. 5, pp. 1487–9, 1996. 73
- [159] C. Xu and J. Min, “Structure and function of wd40 domain proteins,” *Protein Cell*, vol. 2, no. 3, pp. 202–14, 2011. 73, 74, 76
- [160] H. K. Fong, J. B. Hurley, R. S. Hopkins, R. Miake-Lye, M. S. Johnson, R. F. Doolittle, and M. I. Simon, “Repetitive segmental structure of the transducin

- beta subunit: homology with the *cdc4* gene and identification of related mrnas," *Proc Natl Acad Sci U S A*, vol. 83, no. 7, pp. 2162–6, 1986. 73
- [161] E. J. Neer, C. J. Schmidt, R. Nambudripad, and T. F. Smith, "The ancient regulatory-protein family of wd-repeat proteins," *Nature*, vol. 371, no. 6495, pp. 297–300, 1994. 73
- [162] T. F. Smith, C. Gaitatzes, K. Saxena, and E. J. Neer, "The wd repeat: a common architecture for diverse functions," *Trends Biochem Sci*, vol. 24, no. 5, pp. 181–5, 1999. 73
- [163] T. F. Smith, "Diversity of wd-repeat proteins," *Subcell Biochem*, vol. 48, pp. 20–30, 2008. 73
- [164] L. Yu, C. Gaitatzes, E. Neer, and T. F. Smith, "Thirty-plus functional families from a single motif," *Protein Sci*, vol. 9, no. 12, pp. 2470–6, 2000. 73
- [165] N. Pashkova, L. Gakhar, S. C. Winistorfer, L. P. Yu, S. Ramaswamy, and R. C. Piper, "Wd40 repeat propellers define a ubiquitin-binding domain that regulates turnover of f box proteins," *Mol Cell*, vol. 40, no. 3, pp. 433–443, 2010. 74
- [166] S. Biedermann and H. Hellmann, "Wd40 and cul4-based e3 ligases: lubricating all aspects of life," *Trends in Plant Science*, vol. 16, no. 1, pp. 38–46, 2011. 74
- [167] A. Simonsen, H. C. Birkeland, D. J. Gillooly, N. Mizushima, A. Kuma, T. Yoshimori, T. Slagsvold, A. Brech, and H. Stenmark, "Alfy, a novel fyve-domain-containing protein associated with protein granules and autophagic membranes," *J Cell Sci*, vol. 117, no. Pt 18, pp. 4239–51, 2004. 74
- [168] Q. Lu, P. Yang, X. Huang, W. Hu, B. Guo, F. Wu, L. Lin, A. L. Kovacs, L. Yu, and H. Zhang, "The wd40 repeat ptdins(3)p-binding protein epg-6 regulates progression of omegasomes to autophagosomes," *Dev Cell*, vol. 21, no. 2, pp. 343–57, 2011. 74
- [169] F. Cecconi, S. Di Bartolomeo, R. Nardacci, C. Fuoco, M. Corazzari, L. Giunta, A. Romagnoli, A. Stoykova, K. Chowdhury, G. M. Fimia, and M. Piacentini, "A novel role for autophagy in neurodevelopment," *Autophagy*, vol. 3, no. 5, pp. 506–8, 2007. 74
- [170] G. M. Fimia, A. Stoykova, A. Romagnoli, L. Giunta, S. Di Bartolomeo, R. Nardacci, M. Corazzari, C. Fuoco, A. Ucar, P. Schwartz, P. Gruss, M. Piacentini,

- K. Chowdhury, and F. Cecconi, "Ambra1 regulates autophagy and development of the nervous system," *Nature*, vol. 447, no. 7148, pp. 1121–5, 2007. 74
- [171] E. J. Neer and T. F. Smith, "G protein heterodimers: New structures propel new questions," *Cell*, vol. 84, no. 2, pp. 175–178, 1996. 74
- [172] D. Karathanassis, R. V. Stahelin, J. Bravo, O. Perisic, C. M. Pacold, W. W. Cho, and R. L. Williams, "Binding of the px domain of p47(phox) to phosphatidylinositol 3,4-bisphosphate and phosphatidic acid is masked by an intramolecular interaction," *Embo Journal*, vol. 21, no. 19, pp. 5057–5068, 2002. 75
- [173] O. Pylypenko, R. Lundmark, E. Rasmuson, S. R. Carlsson, and A. Rak, "The px-bar membrane-remodeling unit of sorting nexin 9," *Embo Journal*, vol. 26, no. 22, pp. 4788–4800, 2007. 75
- [174] S. Schoebel, W. Blankenfeldt, R. S. Goody, and A. Itzen, "High-affinity binding of phosphatidylinositol 4-phosphate by legionella pneumophila drpa," *EMBO Rep*, vol. 11, no. 8, pp. 598–604, 2010. 75
- [175] K. Narayan and M. A. Lemmon, "Determining selectivity of phosphoinositide-binding domains," *Methods*, vol. 39, no. 2, pp. 122–33, 2006. 99, 131
- [176] I. Mellman, R. Fuchs, and A. Helenius, "Acidification of the endocytic and exocytic pathways," *Annu Rev Biochem*, vol. 55, pp. 663–700, 1986. 113
- [177] I. Mellman, "The importance of being acid - the role of acidification in intracellular membrane traffic," *Journal of Experimental Biology*, vol. 172, pp. 39–45, 1992. 113
- [178] R. Oriij, J. Postmus, A. Ter Beek, S. Brul, and G. J. Smits, "In vivo measurement of cytosolic and mitochondrial ph using a ph-sensitive gfp derivative in saccharomyces cerevisiae reveals a relation between intracellular ph and growth," *Microbiology-Sgm*, vol. 155, pp. 268–278, 2009. 113
- [179] S. A. Lee, R. Eyeson, M. L. Cheever, J. M. Geng, V. V. Verkhusha, C. Burd, M. Overduin, and T. G. Kutateladze, "Targeting of the fyve domain to endosomal membranes is regulated by a histidine switch," *Proc Natl Acad Sci U S A*, vol. 102, no. 37, pp. 13052–13057, 2005. 133
- [180] S. A. Lee, J. Kovacs, R. V. Stahelin, M. L. Cheever, M. Overduin, T. G. Setty, C. G. Burd, W. Cho, and T. G. Kutateladze, "Molecular mechanism of membrane

- docking by the vam7p px domain,” *J Biol Chem*, vol. 281, no. 48, pp. 37091–101, 2006. 134
- [181] N. Jin, C. Y. Chow, L. Liu, S. N. Zolov, R. Bronson, M. Davisson, J. L. Petersen, Y. Zhang, S. Park, J. E. Duex, D. Goldowitz, M. H. Meisler, and L. S. Weisman, “Vac14 nucleates a protein complex essential for the acute interconversion of pi3p and pi(3,5)p(2) in yeast and mouse,” *EMBO J*, vol. 27, no. 24, pp. 3221–34, 2008. 135
- [182] T. Kumanomidou, T. Mizushima, M. Komatsu, A. Suzuki, I. Tanida, Y. S. Sou, T. Ueno, E. Kominami, K. Tanaka, and T. Yamane, “The crystal structure of human atg4b, a processing and de-conjugating enzyme for autophagosome-forming modifiers,” *J Mol Biol*, vol. 355, no. 4, pp. 612–8, 2006. 137
- [183] A. Oberstein, P. D. Jeffrey, and Y. Shi, “Crystal structure of the bcl-xl-beclin 1 peptide complex: Beclin 1 is a novel bh3-only protein,” *J Biol Chem*, vol. 282, no. 17, pp. 13123–32, 2007. 137
- [184] W. Feng, S. Huang, H. Wu, and M. Zhang, “Molecular basis of bcl-xl’s target recognition versatility revealed by the structure of bcl-xl in complex with the bh3 domain of beclin-1,” *J Mol Biol*, vol. 372, no. 1, pp. 223–35, 2007. 137
- [185] K. Satoo, N. N. Noda, H. Kumeta, Y. Fujioka, N. Mizushima, Y. Ohsumi, and F. Inagaki, “The structure of atg4b-lc3 complex reveals the mechanism of lc3 processing and delipidation during autophagy,” *EMBO J*, vol. 28, no. 9, pp. 1341–50, 2009. 137
- [186] B. Ku, J. S. Woo, C. Liang, K. H. Lee, H. S. Hong, X. E. K. S. Kim, J. U. Jung, and B. H. Oh, “Structural and biochemical bases for the inhibition of autophagy and apoptosis by viral bcl-2 of murine gamma-herpesvirus 68,” *PLoS Pathog*, vol. 4, no. 2, p. e25, 2008. 137
- [187] S. Sinha, C. L. Colbert, N. Becker, Y. Wei, and B. Levine, “Molecular basis of the regulation of beclin 1-dependent autophagy by the gamma-herpesvirus 68 bcl-2 homolog m11,” *Autophagy*, vol. 4, no. 8, pp. 989–97, 2008. 137
- [188] Y. Ichimura, T. Kumanomidou, Y. S. Sou, T. Mizushima, J. Ezaki, T. Ueno, E. Kominami, T. Yamane, K. Tanaka, and M. Komatsu, “Structural basis for sorting mechanism of p62 in selective autophagy,” *J Biol Chem*, vol. 283, no. 33, pp. 22847–57, 2008. 137

- [189] N. N. Noda, H. Kumeta, H. Nakatogawa, K. Satoo, W. Adachi, J. Ishii, Y. Fujioka, Y. Ohsumi, and F. Inagaki, "Structural basis of target recognition by atg8/lc3 during selective autophagy," *Genes Cells*, vol. 13, no. 12, pp. 1211–8, 2008. 137
- [190] T. Saio, M. Yokochi, and F. Inagaki, "The nmr structure of the p62 pb1 domain, a key protein in autophagy and nf-kappab signaling pathway," *J Biomol NMR*, vol. 45, no. 3, pp. 335–41, 2009. 137
- [191] R. Koopmann, K. Muhammad, M. Perbandt, C. Betzel, and M. Duszenko, "Trypanosoma brucei atg8: structural insights into autophagic-like mechanisms in protozoa," *Autophagy*, vol. 5, no. 8, pp. 1085–91, 2009. 137
- [192] M. Komatsu, H. Kurokawa, S. Waguri, K. Taguchi, A. Kobayashi, Y. Ichimura, Y. S. Sou, I. Ueno, A. Sakamoto, K. I. Tong, M. Kim, Y. Nishito, S. Iemura, T. Natsume, T. Ueno, E. Kominami, H. Motohashi, K. Tanaka, and M. Yamamoto, "The selective autophagy substrate p62 activates the stress responsive transcription factor nrf2 through inactivation of keap1," *Nat Cell Biol*, vol. 12, no. 3, pp. 213–23, 2010. 138
- [193] T. Saio, M. Yokochi, H. Kumeta, and F. Inagaki, "Pcs-based structure determination of protein-protein complexes," *J Biomol NMR*, vol. 46, no. 4, pp. 271–80, 2010. 138
- [194] Y. Watanabe, N. N. Noda, H. Kumeta, K. Suzuki, Y. Ohsumi, and F. Inagaki, "Selective transport of alpha-mannosidase by autophagic pathways: structural basis for cargo recognition by atg19 and atg34," *J Biol Chem*, vol. 285, no. 39, pp. 30026–33, 2010. 138
- [195] C. Hu, X. Zhang, Y. B. Teng, H. X. Hu, and W. F. Li, "Structure of autophagy-related protein atg8 from the silkworm bombyx mori," *Acta Crystallogr Sect F Struct Biol Cryst Commun*, vol. 66, no. Pt 7, pp. 787–90, 2010. 138
- [196] A. Rozenknop, V. V. Rogov, N. Y. Rogova, F. Lohr, P. Guntert, I. Dikic, and V. Dotsch, "Characterization of the interaction of gabarapl-1 with the lir motif of nbr1," *J Mol Biol*, vol. 410, no. 3, pp. 477–87, 2011. 138
- [197] S. Isogai, D. Morimoto, K. Arita, S. Unzai, T. Tenno, J. Hasegawa, Y. S. Sou, M. Komatsu, K. Tanaka, M. Shirakawa, and H. Tochio, "Crystal structure of the ubiquitin-associated (uba) domain of p62 and its interaction with ubiquitin," *J Biol Chem*, vol. 286, no. 36, pp. 31864–74, 2011. 138

- [198] S. B. Hong, B. W. Kim, K. E. Lee, S. W. Kim, H. Jeon, J. Kim, and H. K. Song, “Insights into noncanonical e1 enzyme activation from the structure of autophagic e1 atg7 with atg8,” *Nat Struct Mol Biol*, vol. 18, no. 12, pp. 1323–30, 2011. 138
- [199] A. M. Taherbhoy, S. W. Tait, S. E. Kaiser, A. H. Williams, A. Deng, A. Nourse, M. Hammel, I. Kurinov, C. O. Rock, D. R. Green, and B. A. Schulman, “Atg8 transfer from atg7 to atg3: a distinctive e1-e2 architecture and mechanism in the autophagy pathway,” *Mol Cell*, vol. 44, no. 3, pp. 451–61, 2011. 138
- [200] N. N. Noda, T. Kobayashi, W. Adachi, Y. Fujioka, Y. Ohsumi, and F. Inagaki, “Structure of the novel c-terminal domain of vacuolar protein sorting 30/autophagy-related protein 6 and its specific role in autophagy,” *J Biol Chem*, vol. 287, no. 20, pp. 16256–66, 2012. 138
- [201] N. Kondo-Okamoto, N. N. Noda, S. W. Suzuki, H. Nakatogawa, I. Takahashi, M. Matsunami, A. Hashimoto, F. Inagaki, Y. Ohsumi, and K. Okamoto, “Autophagy-related protein 32 acts as autophagic degron and directly initiates mitophagy,” *J Biol Chem*, vol. 287, no. 13, pp. 10631–8, 2012. 138
- [202] S. B. Hong, B. W. Kim, J. H. Kim, and H. K. Song, “Structure of the autophagic e2 enzyme atg10,” *Acta Crystallogr D Biol Crystallogr*, vol. 68, no. Pt 10, pp. 1409–17, 2012. 139

# Curriculum Vitae

## Personal Data

Ricarda Angela Busse

## Education

- 2009 - present      **PhD Student**  
Project: "Insights into membrane binding of PROPPINs and Reconstitution of mammalian autophagic conjugation systems"  
**Research group of Dr. Kühnel**, Department of Neurobiology headed by Prof. Dr. Jahn, Max-Planck-Institute for Biophysical Chemistry, Göttingen
- 2008 - 2009      **PhD Student**  
Project: "The role of E3 ubiquitin ligases in mammalian central nervous system development"  
**Research group of Dr. Stegmüller**, Department of Cellular and Molecular Neurobiology, Max-Planck-Institute for Experimental Medicine, Göttingen

- 2007 - 2008      **Diploma Student**  
 Project: "Functional analysis of the *yvcI-J-K-L-crh-yvcN*-operon in *Bacillus subtilis*"  
**Research group of Dr. Görke**, Department of General Microbiology headed by Prof. Dr. Stülke, Georg-August-University of Göttingen
- 2005 - 2007      **Student Assistant**  
 Projects: "Molecular evolution and phylogeny of calcarea" and "Phylogeny of deep porifera"  
**Research group of Junior-Prof. Dr. Wörheide**, Department of Geobiology, Georg-August-University of Göttingen
- 2003 - 2008      **Study of Biology** (Diploma) at the Georg-August-University of Göttingen  
 Subjects: Microbiology, Human Genetics, Phytology

## Teaching

- 2010 - 2011      **Tutor of method courses**  
 "Basic techniques in protein purification and characterization" within the Göttingen Graduate School for Neurosciences, Biophysic and Molecular Biosciences (GGNB)  
 "Basic Course: Biochemistry" within the Georg-August-University of Göttingen, Faculty of Biology
- 2010              **Supervisor of Labrotation student**  
 Danesh Moradi within the the International MSc/PhD Program "Molecular Biology" (GGNB)
- 2009              **Trainer for Journalists at the bench**  
 within EICOS - The European Initiative for Communicators of Science Initiative to improve communication between researchers and journalists



## Conferences

- 2012            **NeuroWISe** - Molecular Neurobiology  
Rehovot, Israel (poster presentation)
- 2011            **GBM** - Molecular Life Science  
Frankfurt, Germany (poster presentation)
- 2011            **Keystone Symposium** on Autophagy  
Whistler, Canada (poster presentation)
- 2011            "**Horizons** in Molecular Biology"  
Göttingen, Germany (poster presentation)
- 2010            "**Horizons** in Molecular Biology"  
Göttingen, Germany
- 2009            "**Horizons** in Molecular Biology"  
Göttingen, Germany

## Publications

- 2012            **Busse RA**, Scacioc A, Hernandez JM, Krick R, Stephan M, Janshoff A, Thumm M, Kühnel K.  
"Qualitative and quantitative characterization of protein-phosphoinositide interactions with liposome based methods"  
submitted to *Autophagy*
- 2012            Thumm M, **Busse RA**, Scacioc A, Stephan M, Janshoff A, Kühnel K, Krick R.  
"It takes two to tango: PROPPINs use two phosphoinositide-binding sites"  
*Autophagy* E-pub: 2012 Oct 9(1)

- 2012 Krick R, **Busse RA**, Scacioc A, Stephan M, Janshoff A, Thumm M, Kühnel K.  
 “Structural and functional characterization of the two phosphoinositide binding sites of PROPPINs, a beta-propeller protein family“  
*PNAS* 2012 Jul 109(30):E2042-9
- 2011 Landmann JJ, **Busse RA**, Latz JH, Singh KD, Stülke J, Görke B.  
 “Crh, the paralogue of the phosphocarrier protein HPr, controls the methylglyoxal bypass of glycolysis in *Bacillus subtilis*”  
*Mol Microbiol* 2011 Nov 82(3):770-87

## Co-Curricular Activities

- 2012 **Organization of the retreat for students of the “Biomolecules” program**  
 within the Göttingen Graduate School for Neurosciences, Biophysic and Molecular Biosciences (GGNB)
- 2012 **Organization of 2<sup>nd</sup> GGNB Summer Games**  
 within the Göttingen Graduate School for Neurosciences, Biophysic and Molecular Biosciences (GGNB)
- 2011 **Organization of 1<sup>st</sup> GGNB Summer Games**  
 within the Göttingen Graduate School for Neurosciences, Biophysic and Molecular Biosciences (GGNB)
- since 2011 **Student Representative in the “Dr-Rat”**  
 of the Georg-August-University School of Science (GAUSS)  
 - active in the working group for evaluating the “Quality of supervision of doctoral students in GAUSS”  
 - active in the working group for visa & insurances
- 2011 **Student Representative**  
 of the Göttingen Graduate School for Neuroscience, Biophysics and Molecular Biosciences (GGNB)